THE GENERAL DYNAMIC EQUATION FOR AEROSOLS

Thesis by

Fred Gelbard

In Partial Fulfillment of the Requirements

for the Degree of

Doctor of Philosophy

California Institute of Technology

Pasadena, California

1979

(Submitted October 24, 1978)

ACKNOWLEDGEMENTS

I would like to thank my advisor, Dr. John H. Seinfeld, for his guidance, interest, and encouragement throughout this work. Working with him was both an honor and a pleasure.

The discussions with other members of the faculty were also helpful. In particular, I would like to thank Dr. Sheldon K. Friedlander, Dr. T. E. Ramabhadran and Dr. Bruno Van den Bosch.

The open discussions with my friends and colleagues Arthur W. Stelson, Kenneth E. Bencala, Stanley P. Sanders, William S. Sargent and Edward K. Ruth were both enjoyable and informative.

Of my colleagues I would especially like to acknowledge Dr. Thomas W. Peterson for providing some of the exact solutions used in Chapter IV to test the numerical routines, and Dr. Peter H. McMurry for furnishing most of the experimental data used in Chapter V, and discussing experimental procedures.

Because swimming means so much to me, I would also like to thank Dr. Bradford Sturtevant, Dr. Paul E. Dimotakis, Dr. Daniel J. Kevles, Burt Kanner and Edwin V. Spencer for their coaching and the many enjoyable, yet demanding swimming workouts. I am most grateful to John L. Zyskind for his advice and coaching.

The financial support of the National Science Foundation is also appreciated.

ABSTRACT

This work focusses on developing and solving the conservation equations for a spatially homogeneous aerosol. We begin by developing the basic equations, and in doing so, a new form of the conservation equation or General Dynamic Equation (GDE), termed the discrete-continuous GDE, is presented. In this form, one has the ability to simulate aerosol dynamics in systems in which processes are occurring over a broad particle size spectrum, typical of those found in the atmosphere. All the necessary kinetic coefficients needed to solve the GDE are discussed and the mechanisms for gas-to-particle conversion are also elucidated.

Particle growth rates limited by gas phase diffusion, surface and volume reactions are discussed. In the absence of coagulation, analytic solutions for the above particle growth rates, arbitrary initial and boundary conditions, arbitrary sources, and first order removal mechanisms are developed.

To account for all processes, numerical solutions are required. Therefore, numerical techniques and the errors associated with the numerical solution of the GDE are discussed in detail. By comparing the numerical solution to both analytical solutions for simplified cases and smog chamber data, it is shown that the numerical techniques are highly accurate and efficient.

Techniques for simulating a sulfuric acid and water aerosol are presented. By application of the discrete-continuous GDE, the effect of neglecting cluster-cluster agglomeration, and the effect of a preexisting aerosol on the nucleation rate of a sulfuric acid and water aerosol are studied. The effects of coagulation are also elucidated by simulating the system with the full continuous GDE and the analytic solution to the continuous GDE in the absence of coagulation. Fairly good agreement between the predicted and experimentally observed distributions is obtained.

Finally, an exact solution to the continuous form of the GDE for a multicomponent aerosol for simplified cases is developed.

TABLE OF CONTENTS

	Page
ACKNOWLEDGEMENTS	ii
ABSTRACT	iii
LIST OF FIGURES	x
LIST OF TABLES	xv
CHAPTER I: INTRODUCTION	1
CHAPTER II: THEORETICAL DEVELOPMENT OF THE GENERAL DYNAMIC EQUATION FOR SPATIALLY HOMOGENOUS AEROSOLS	5
ABSTRACT	5
1. INTRODUCTION	6
2. GENERAL DYNAMIC EQUATIONS	9
2.1 Discrete General Dynamic Equation	9
2.2 Discrete-Continuous General Dynamic Equation	12
2.3 Continuous General Dynamic Equation	17
3. GENERAL ASPECTS OF AEROSOL FORMATION AND GROWTH	20
4. KINETIC COEFFICIENTS AND BOUNDARY CONDITION	28
4.1 Agglomeration Coefficient	28
4.2 Evaporation Coefficient	32
4.3 Growth Laws	33
4.3.1 Diffusion-Controlled Growth	34
4.3.2 Surface Reaction-Controlled Growth	38
4.3.3 Volume Reaction-Controlled Growth	39

TABLE OF CONTENTS
(continued)

	Page
4.4 Boundary Condition	41
5. LITERATURE REVIEW	43
NOTATION	52
REFERENCES	54
CHAPTER III: EXACT SOLUTION OF THE GENERAL DYNAMIC EQUATION FOR AEROSOL GROWTH BY CONDENSATION	59
ABSTRACT	59
1. INTRODUCTION	60
2. AEROSOL KINETIC COEFFICIENTS	63
2.1 Particle Growth	63
2.2 Coagulation	66
2.3 Sources and Sinks	69
3. NONDIMENSIONALIZATION AND SOLUTION OF THE GENERAL DYNAMIC EQUATION	70
4. CHARACTERISTIC GROWTH CURVES	74
5. SIZE DISTRIBUTION DYNAMICS	83
6. CONCLUSIONS	97
NOTATION	98
REFERENCES	101
APPENDIX	103
CHAPTER IV: NUMERICAL SOLUTION OF THE DYNAMIC EQUATION FOR PARTICULATE SYSTEMS	104

TABLE OF CONTENTS
(continued)

	Page
ABSTRACT	104
1. INTRODUCTION	105
2. SCALING OF THE EQUATIONS	109
3. COLLOCATION ON FINITE ELEMENTS	112
4. NUMERICAL IMPLEMENTATION	116
4.1 Finite Domain Error	118
4.2 Numerical Results	122
5. COAGULATION OF A LABORATORY AEROSOL	139
6. SUMMARY	142
NOTATION	144
REFERENCES	147
APPENDIX	149
CHAPTER V: APPLICATIONS OF THE GENERAL DYNAMIC EQUATION TO THE SIMULATION OF SULFURIC ACID/WATER AEROSOL FORMATION AND GROWTH	152
ABSTRACT	152
1. INTRODUCTION	153
2. DESCRIPTION OF THE EXPERIMENT	156
3. PHYSICAL PROPERTIES OF A H_2SO_4/H_2O AEROSOL PHOTOCHEMICALLY GENERATED IN THE PRESENCE OF A PREEXISTING URBAN AEROSOL	158

TABLE OF CONTENTS
(continued)

	Page
4. SIMULATION RESULTS USING THE DISCRETE-CONTINUOUS GDE	166
4.1 Establishment of the Steady State Molecular Cluster Profile in the Presence of a Preexisiting Aerosol	170
4.2 Determination of the Relative Importance of Condensation, Nucleation, and Scavenging for Gas-to-Particle Conversion	172
4.3 Determination of the Importance of Cluster-Cluster Agglomeration	178
5. USE OF THE CONTINUOUS GDE	189
6. SUMMARY	197
NOTATION	199
REFERENCES	200
CHAPTER VI: COAGULATION AND GROWTH OF A MULTICOMPONENT AEROSOL	203
ABSTRACT	203
1. INTRODUCTION	204
2. DYNAMICS OF MULTICOMPONENT AEROSOLS	206
3. MULTICOMPONENT COMPOSITION DISTRIBUTIONS	209
3.1 Pure Coagulation	209
3.2 Coagulation and Growth	211

TABLE OF CONTENTS
(continued)

	Page
4. SUMMARY	224
NOTATION	225
REFERENCES	226
APPENDIX	227
CHAPTER VII: SUMMARY AND CONCLUSIONS	229
REFERENCES	232
THESIS APPENDIX: A SECTIONAL APPROXIMATION TO THE DISCRETE GENERAL DYNAMIC EQUATION FOR AEROSOLS	233
1. INTRODUCTION	233
2. GOVERNING EQUATIONS FOR A SECTIONAL MODEL	237
3. CONCLUSION	245
REFERENCES	246

LIST OF FIGURES

Figure		Page
CHAPTER II		
1	Routes for gas-to-particle conversion	23
2	Agglomeration coefficient for spherical particles in air	31
3	Ratio of the agglomeration coefficient calculated from existing growth laws divided by the Fuchs-Phillips agglomeration coefficient	37
CHAPTER III		
1	Dimensionless Brownian coagulation coefficient	68
2	Characteristic growth curves for diffusion-limited growth (without the Kelvin effect)	76
3	Characteristic growth curves for diffusion-limited growth (with the Kelvin effect)	78
4	Characteristic growth curves for first order surface reaction-limited growth	79
5	Characteristic growth curves for first order volume reaction-limited growth	80
6	Characteristic growth curves for diffusion-limited, and zeroth order surface and volume reaction limited growth	82
7	Dimensionless particle growth rates for diffusion-limited growth	84
8	Dimensionless particle growth rates for half order surface reaction-limited growth	85
9	Dimensionless particle growth rates for first order surface reaction-limited growth	86
10	Dimensionless particle growth rates for second order surface reaction-limited growth	87

LIST OF FIGURES
(continued)

Figure		Page
11	Dimensionless particle growth rates for half order volume reaction-limited growth	88
12	Dimensionless particle growth rates for first order volume reaction-limited growth	89
13	Dimensionless particle growth rates for second order volume reaction-limited growth	90
14	Evolution of the dimensionless number distribution for diffusion-limited growth	92
15	Evolution of the dimensionless volume distribution for diffusion-limited growth	94
16	Evolution of the dimensionless number distribution for zeroth order volume reaction-limited growth	95
17	Evolution of the dimensionless volume distribution for zeroth order volume reaction-limited growth	96
CHAPTER IV		
1	Particle size spectra. $\beta_v=\beta_0$ and $\tau=N_0\beta_0 t$	126
2	Particle size spectra. $\beta_v=\beta_0$ and $\tau=N_0\beta_0 t$	128
3	Particle size spectra. $\beta_v=\beta_0$ and $\tau=N_0\beta_0 t$ (extended domain)	129
4	Particle size spectra. $\beta_v=\beta_1(v+\tilde{v})$ and $\tau=N_0\beta_1\nu_0 t$	130
5	Particle size spectra. $\beta_v = \beta_1(v+\tilde{v})$, $S_v = - R_0 n_v(v,t)$, $\tau = N_0\beta_1\nu_0 t$ and $\theta = R_0/\beta_1 N_0\nu_0 = 1$	132
6	Particle size spectra. $\beta_v = \beta_0$, $I_v = \sigma v$, $\tau = N_0\beta_0 t$ and $\Lambda = \sigma/N_0\beta_0 = 1$	134

LIST OF FIGURES
(continued)

Figure		Page
7	Particle size spectra. $\beta_v = \beta_0$, $S_v = S_0/v^* \exp(-v/v^*) - R_0 n_v(v,t)$, $\tau = N_0\beta_0 t$, $\theta = R_0/\beta_0 N_0 = 1$, $\Omega = S_0/\beta_0 N_0^2 = 1$ and $\Delta = v^*/v_0 = 0.01$	136
8	Particle size spectra for Husar's experiment using the Sitarski-Seinfeld coagulation coefficient	140
9	Particle size spectra for Husar's experiment using Fuchs' coagulation coefficient	141
CHAPTER V		
1	Equilibrium vapor pressure of H_2SO_4 in a mixture with water over a flat surface as a function of composition and temperature (15)	161
2	Equilibrium concentration of H_2SO_4 in a spherical droplet of H_2SO_4, as a function of the relative humidity and particle diameter	162
3	Equilibrium particle size as a function of the relative humidity and the number of H_2SO_4 molecules in the particle	163
4	Diffusivity for a H_2SO_4/H_2O particle at 37°C and 34% relative humidity	164
5	Number distribution evolution of the simulated experiment	167
6	Volume distribution evolution of the simulated experiment	169
7	Evolution of the concentration of molecular clusters in the discrete regime	171

LIST OF FIGURES
(continued)

Figure		Page
8	Evolution of the concentration profile of molecular clusters in the discrete regime when the initial concentrations are reduced by an order of magnitude	173
9	Comparison of cluster profiles in the discrete regime after 20 minutes of simulation	174
10	Total number of particles/cm^3 in the discrete and continuous regimes with and without cluster-cluster agglomeration	176
11	The net agglomeration rate of monomer with aerosol particles, monomer with clusters, and monomer with other monomer, for the simulated experiment	179
12	The net agglomeration rate of clusters with aerosol particles, clusters with other clusters, and aerosol particles with other aerosol particles, for the simulated experiment	180
13	The net rate of monomer condensation, monomer nucleation and nucleation, for the simulated experiment	181
14	Ratio of the nucleation rate to the condensation rate, for the simulated experiment	182
15	Fraction of the total flux of monomer entering the continuous regime by condensation, for the simulated experiment	183
16	Evolution of the concentration profile of molecular clusters in the discrete regime when cluster-cluster agglomerations are neglected	185
17	Number distribution evolution neglecting cluster-cluster agglomeration for the simulated experiment	186
18	Volume distribution evolution neglecting cluster-cluster agglomeration for the simulated experiment	187

LIST OF FIGURES
(continued)

Figure		Page
19	Number distribution evolution using the exact solution to the continuous GDE, neglecting coagulation for the simulated experiment	191
20	Volume distribution evolution using the exact solution to the continuous GDE,neglecting coagulation for the simulated experiment	192
21	Number distribution evolution using the numerical techniques of chapter IV to solve the continuous GDE with coagulation for the simulated experiment	194
22	Volume distribution evolution using the numerical techniques of chapter IV to solve the continuous GDE with coagulation for the simulated experiment	196
CHAPTER VI		
1	Initial two component composition distribution	218
2	Time evolution of the composition distribution when component 1 grows faster than component 2, $N_0\beta_0 t=0.1$	219
3	Time evolution of the composition distribution when component 1 grows faster that component 2, $N_0\beta_0 t=0.2$	220
4	Time evolution of the composition distribution when component 2 grows faster than component 1, $N_0\beta_0 t=0.1$	221
5	Time evolution of the composition distribution when component 2 grows faster than component 1, $N_0\beta_0 t=0.2$	222

LIST OF TABLES

Table		Page
CHAPTER II		
1	Brownian coagulation coefficients	29
2	Diffusion-controlled growth laws	35
3	Reaction-controlled growth laws	40
4	Reported solutions to the discrete GDE	44
5	Reported solutions to the continuous GDE	47
CHAPTER III		
1	Dimensionless growth laws	64
2	Characteristic growth curves	74
CHAPTER IV		
1	Summary of cases considered of the General Dynamic Equation for particulate systems	117
2	Dimensionless groups associated with the General Dynamic Equation for particulate systems	119
3	Analytical solutions to the General Dynamic Equation	120
4	Analytical expressions for the finite domain errors	123
5	Finite domain errors for cases 1-5	125
6	Finite domain error for case 6	138
CHAPTER VI		
1	Initial multicomponent distributions	208
2	Multidimensional Laplace transform pairs	210

LIST OF TABLES
(continued)

Table		Page
3	Composition density functions for coagulation of a multicomponent aerosol	212
4	Composition density functions for coagulation and growth of a multicomponent aerosol	215
THESIS APPENDIX		
1	Reported solutions to the discrete General Dynamic Equation	235

Chapter I

INTRODUCTION

Atmospheric pollutants are often classified as being either in the gaseous or particulate phase. Gaseous or particulate primary pollutants, which are emitted directly into the atmosphere, can undergo chemical or physical change resulting in what are called secondary pollutants. Much work has been devoted to modelling the kinetics of primary to secondary gaseous pollutants and the physical dynamics of aerosols. However, the evolution of atmospheric aerosols from primary emissions of both gaseous and particulate pollutants, and secondary sources is not completely understood.

For a spatially homogeneous system, one is interested in determining the temporal variation of gaseous pollutant concentrations and the particle size and chemical composition distribution function. Because of the various processes for gas-to-particle conversion, aerosol formation and growth can be intimately related to both the homogeneous and heterogeneous chemistry. In addition to chemical transformations within the particle and gas-to-particle conversion, the aerosol is also affected by physical processes such as particle removal and agglomeration.* Clearly, the coupling of chemical and physical processes adds to the complexity and difficulty of simulating aerosol dynamics.

*By agglomeration we mean the collision and subsequent coalescence of two particles of any size.

This work will be restricted to the dynamics of aerosol formation and growth by gas-to-particle conversion, physical processes and chemical reactions occurring in the particle phase. Thus the determination of the generation rate and concentration of gaseous pollutant by gas phase chemistry will not be of major concern. However, the effects of primary and secondary gaseous pollutants on the aerosol will be considered. Most of this work will be mainly concerned with determining the evolution of the size distribution, independent of the aerosol composition. The evolution of the chemical composition distribution function will be considered only in the last two chapters.

To establish a firm theoretical basis for simulating aerosol dynamics, the conservation equations or the so-called General Dynamic Equation (GDE) for a spatially homogeneous aerosol will be developed in Chapter II. As will be shown, the basic discrete representation of aerosol particles, although quite detailed, is impractical for most simulation purposes. Thus, a new form of the GDE, termed the discrete-continuous GDE will be developed. The relationship between the discrete-continuous GDE and the often used continuous GDE will also be discussed. Using the discrete-continuous GDE, the basic terminology and mechanisms for particle formation and growth will be clearly defined. The agglomeration and evaporation coefficients will be presented and the mechanisms for particle growth by gas phase diffusion and particle phase reaction will be discussed. A

review of previous approaches to simulating aerosol formation and growth will also be given in Chapter II.

In Chapter III the continuous GDE is cast into dimensionless form and solved analytically in the absence of coagulation.* The particle growth mechanisms considered are gas phase diffusion, and particle surface and volume reaction-limited growth. Arbitrary initial and boundary conditions, arbitrary sources and first order removal mechanisms are also considered.

For cases in which coagulation is also considered, numerical routines are required to solve the GDE . Thus in Chapter IV, the results of using two numerical techniques are discussed. It is shown that, due to the nature of agglomeration processes, larger particles are continually being formed and therefore any computational scheme which uses a finite particle size domain can introduce what will be called a finite domain error. This error results from particles that grow beyond the computational domain and are artificially lost in the computations. Thus, the influence of these large particles on the aerosol within the computational domain is inadvertently neglected. However, by expanding the computational domain, these errors can be reduced so that an acceptable solution can be obtained. Chapter IV concludes by showing that for a realistic aerosol undergoing coagulation, and a reasonable computational domain, the

---

*By coagulation we mean the agglomeration of particles larger than the critical size particle determined by classical nucleation theory.

finite domain error is negligible and that good qualitative agreement between the predicted and experimentally observed size distributions can be obtained.

In Chapter V techniques for simulating the formation and growth of a sulfuric acid and water aerosol in the presence of a preexisting urban aerosol will be discussed. Using the discrete-continuous or the continuous GDE, fairly good agreement between the predicted and experimentally observed distributions are obtained. More importantly, several of the often used assumptions in determining nucleation rates are scrutinized and it is shown that under certain conditions the effect of the preexisting aerosol and cluster-cluster agglomeration can be important.

In Chapter VI analytic solutions to the continuous GDE for a multicomponent aerosol are developed. It is shown that the different chemical nature of the aerosol constituents can greatly affect the evolution of the chemical composition distribution function.

Finally, in Chapter VII this work is summarized and placed in proper perspective relative to future work needed to simulate atmospheric aerosol dynamics.

Chapter II

THEORETICAL DEVELOPMENT OF THE GENERAL DYNAMIC EQUATION FOR SPATIALLY HOMOGENOUS AEROSOLS

ABSTRACT

Conservation equations for aerosol size distribution dynamics are derived and compared. A new discrete-continuous conservation equation is derived that overcomes the limitations of the purely discrete or continuous equations in simulating aerosol dynamics over a broad particle size spectrum. Several issues related to aerosol formation and growth not previously amenable to exact analysis are developed for detail study using the discrete-continuous equation: (1) the establishment of a steady state concentration profile of molecular clusters in the presence of a preexisting aerosol, (2) the relative importance of nucleation, condensation, and scavenging in gas-to-particle conversion, and (3) the importance of cluster-cluster agglomeration relative to other processes.

The necessary kinetic coefficients are discussed and a review of previous work on conservation equations for aerosol dynamics is also given.

1. INTRODUCTION

The dynamic behavior of an aerosol is described by a population balance equation. In its most general form the independent variables in the equation are particle size and composition (1), although in virtually all applications size is the only variable characterizing the aerosol. The population balance equation, which can be termed the General Dynamic Equation (GDE), can assume several forms depending on whether the aerosol size distribution is represented as discrete or continuous and on what physical and chemical phenomena are included. Because of the complex processes that an aerosol may undergo, simulation of the dynamics of an aerosol generally necessitates solution of some form of the GDE.

In the most fundamental approach to deriving the GDE, particles are represented as consisting of integer multiples of a single structural unit, typically a molecule. In these discrete equations particles differ only in the number of monomers they contain. The GDE consists then of an infinite set of nonlinear ordinary differential equations for the number densities of all particles. The discrete GDE, while rigorously valid, is impractical for simulation of aerosol behavior because of the typical wide range in particle size. A popular alternative to the discrete GDE is the continuous GDE, in which the particle size spectrum is taken to be continuous rather than discrete. Whereas the continuous GDE is more tractable than the discrete version, it suffers from the disadvantages of inaccurately representing processes

occurring among the very smallest particles, processes that are important in representing gas-to-particle conversion.

In this chapter a new form of the aerosol GDE which we term the discrete-continuous GDE is derived. In this form the discrete representation is used up to a certain multiplet number past which the particle size distribution is represented as continuous. The discrete-continuous GDE has the capability of representing the entire aerosol size distribution from single molecules to the largest particles, including all relevant physical phenomena occurring. A particular benefit of the discrete-continuous GDE is the ability to simulate for the first time the dynamics of molecular clusters in the presence of a preexisting aerosol. Because of this, the discrete-continuous GDE provides the opportunity to study theoretically a number of important questions related to aerosol formation and growth in reacting gas systems not previously amenable to exact analysis:

(1) Do the molecular clusters achieve a steady state, and if so, what are the relative concentrations of the particles and how large is the scavenging effect of a preexisting aerosol on the steady state concentrations?

(2) Can one estimate the relative importance of nucleation and condensation as routes for gas-to-particle conversion and will a particle burst be detected as a result of nucleation?

(3) How large is the error of neglecting cluster-cluster agglomeration?

Because in many cases the assumptions inherent in basic aerosol balance equations have not been clearly stated in the past, we hope additionally to clarify the limits of validity of commonly used aerosol equations.

In order to present a well organized and detailed discussion of the GDE and the processes it governs, this chapter is divided into five sections. We begin with the fundamental discrete representation of aerosol dynamics. Based on the discrete representation, the discrete-continuous GDE is derived. Next, the relationship between the discrete-continuous and the often used continuous GDE is elucidated. In the third section the discrete-continuous GDE is used to develop the theoretical framework needed to determine the relative importance of all physical processes, such as nucleation, condensation and scavenging for aerosol formation and growth. In the fourth section, the necessary kinetic coefficients for the GDE are presented, and growth laws based on surface and volume reaction-limited growth are developed. The boundary condition needed only for the continuous GDE is also developed in the fourth section. Having defined the assumptions inherent in each GDE, in the fifth section a review of previous work on the GDE is given. Because of the diversity of terminology used in the literature, the review is postponed until the final section.

2. GENERAL DYNAMIC EQUATIONS

2.1 Discrete General Dynamic Equation

We consider the following phenomena to be occurring: (1) agglomeration of two particles, (2) evaporation or escape of a monomer from a particle, and (3) homogeneous particle generation or removal processes apart from those that occur as a result of evaporation and agglomeration. As noted in the Introduction, we restrict our attention to size distribution dynamics and do not consider particle composition as an independent variable. Thus, the aerosol may be considered as chemically homogeneous for the purposes of deriving the governing dynamic equation.

For a spatially homogeneous aerosol the quantity of interest is the concentration of particles containing i monomers, where $i \geq 1$. Assuming an i-mer has a volume v_i, the concentration of i-mers, $N(v_i,t)$, will vary with time due to agglomeration, evaporation, generation and removal processes. The rate of agglomeration of i-mers with j-mers is equal to the rate of formation of (i+j)-mers, and is given by

$$\frac{\beta(v_i,v_j)N(v_i,t)N(v_j,t)}{1 + \delta_{i,j}} \qquad i,j \geq 1 \qquad [1]$$

where $\delta_{i,j}$ is the Kronecker delta and $\beta(v_i,v_j)$ is the kinetic coefficient of agglomeration of two particles of volumes v_i and v_j. The functional form of $\beta(v_i,v_j)$ will be discussed later. If i is equal to j, we must divide by 2, so as not to count the agglomeration twice (2,3,4). The rate of evaporation of i-mers is

$$E(v_i)N(v_i,t) \qquad i \geq 2 \qquad [2]$$

where $E(v_i)$ is the evaporation coefficient. The rate of formation of i-mers by agglomeration is the sum of all agglomerations resulting in an i-mer and is given by

$$\frac{1}{2} \sum_{j=1}^{i-1} \beta(v_{i-j},v_j)N(v_{i-j},t)N(v_j,t) \qquad i \geq 2 \qquad [3]$$

The factor of one-half is introduced because β is a symmetric function of its arguments and therefore the summation counts each agglomeration twice for i-j not equal to i. However, if i is an even integer, the term $\beta(v_{i/2},v_{i/2})N(v_{i/2},t)N(v_{i/2},t)$ is only counted once in the summation, but the factor of one-half is still required as given in Eq. [1]. The rate of depletion of i-mers by agglomeration with all other particles is given by

$$N(v_i,t) \sum_{j=1}^{\infty} \beta(v_i,v_j)N(v_j,t) \qquad i \geq 1 \qquad [4]$$

For j equal to i, the agglomeration rate is divided by 2 as given in Eq. [1], but because each agglomeration removes two i-mers, the rate is

also multiplied by 2, thereby cancelling the factor of one-half. The rate of formation of i-mers by evaporation from (i+1)-mers is

$$(1+\delta_{1,i})E(v_{i+1})N(v_{i+1},t) \quad i \geq 1 \qquad [5]$$

For i = 1, the dissociation of a dimer leads to the formation of two monomers, therefore the Kronecker delta is used in Eq. [5]. The rate of depletion of i-mers due to evaporation is given by,

$$E(v_i)N(v_i,t) \quad i \geq 2 \qquad [6]$$

combining Eqs. [3]-[5], and [6] the net rate of formation of monomers is

$$\frac{dN(v_1,t)}{dt} = - N(v_1,t)\sum_{j=1}^{\infty} \beta(v_1,v_j)N(v_j,t) + \sum_{j=2}^{\infty} (1+\delta_{2,j})E(v_j)N(v_j,t) + S_0(v_1,t) - S_1[v_1,t,N(v_1,t)] \qquad [7]$$

and the net rate of formation of i-mers for $i \geq 2$ is

$$\frac{dN(v_i,t)}{dt} = \frac{1}{2}\sum_{j=1}^{i-1} \beta(v_{i-j},v_j)N(v_{i-j},t)N(v_j,t) - N(v_i,t)\sum_{j=1}^{\infty} \beta(v_i,v_j)N(v_j,t) + E(v_{i+1})N(v_{i+1},t) - E(v_i)N(v_i,t) + S_0(v_i,t) - S_1[v_i,t,N(v_i,t)] \qquad [8]$$

where S_0 and S_1 represent all homogeneous generation and removal processes, respectively. Combined with the appropriate initial conditions, (i.e. $N(v_i,0)$, $i \geq 1$), Eqs. [7] and [8] constitute the discrete GDE for a spatially homogeneous aerosol. Because agglomeration constantly produces larger particles, Eqs. [7] and [8] are an infinite set of coupled ordinary differential equations.

2.2 Discrete-Continuous General Dynamic Equation

Although the discrete GDE is an accurate description of aerosol dynamics, the number of equations needed to simulate actual aerosols can be immense. For large particles the difference in size between an i-mer and an (i+1)-mer is relatively small. Thus, for particles that contain k+1 or more monomers, where k>>1, the discrete concentrations can be represented by n(v,t), which is a continuous function in the limit as $v_1/v_k \to 0$, defined by

$$N(v_i,t) = \int_{v_i-v_1/2}^{v_i+v_1/2} n(v,t)\, dv \qquad i \geq k+1 \qquad [9]$$

We now divide the distribution into two regimes. For particle volumes smaller than or equal to v_k the discrete representation is used, and for particle volumes greater than or equal to v_{k+1} a continuous representation is used. Using Eq. [9], Eq. [7] becomes

$$\frac{dN(v_1,t)}{dt} = - N(v_1,t) \left[\sum_{j=1}^{k} \beta(v_1,v_j)N(v_j,t) + \int_{v_{k+1}-v_1/2}^{\infty} \beta(v_1,v)n(v,t)\, dv \right]$$

$$+ \sum_{j=2}^{k} (1 + \delta_{2,j})E(v_j)N(v_j,t) + \int_{v_{k+1}-v_1/2}^{\infty} E(v)n(v,t)\, dv$$

$$+ S_0(v_1,t) - S_1[v_1,t,N(v_1,t)], \qquad [10]$$

and for $2 \leq i \leq k$, Eq. [8] becomes

$$\frac{dN(v_i,t)}{dt} = \frac{1}{2} \sum_{j=1}^{i-1} \beta(v_{i-j},v_j)N(v_{i-j},t)N(v_j,t)$$

$$- N(v_i,t) \left[\sum_{j=1}^{k} \beta(v_i,v_j)N(v_j,t) + \int_{v_{k+1}-v_1/2}^{\infty} \beta(v_i,v)n(v,t)\, dv \right]$$

$$+ \begin{cases} E(v_{i+1})N(v_{i+1},t) & 2 \leq i \leq k-1 \\ \displaystyle\int_{v_{k+1}-v_1/2}^{v_{k+1}+v_1/2} E(v)n(v,t)\, dv & i = k \end{cases}$$

$$- E(v_i)N(v_i,t) + S_0(v_i,t) - S_1[v_i,t,N(v_i,t)]. \qquad [11]$$

To derive the governing equation for $n(v,t)$ in the continuous regime, substitute $n(v,t)dv$ for $N(v,t)$ in Eq. [8], for $v \geq v_{k+1} - v_1/2$. Assuming conservation of volume, such that $v_j = jv_1$, for $v_{k+1} \leq v_i \leq v_{2k}$,

$$\frac{d[n(v_i,t)dv]}{dt} = \sum_{j=1}^{i-k-1} \beta(v_i-v_j,v_j)N(v_j,t)n(v_i-v_j,t)\,dv \quad i \geq k+2$$

$$+ \frac{1}{2} \sum_{j=i-k}^{k} \beta(v_i-v_j,v_j)N(v_i-v_j,t)N(v_j,t)$$

$$- n(v_i,t)dv \left[\sum_{j=1}^{k} \beta(v_i,v_j)N(v_j,t) + \int_{v_{k+1}-v_1/2}^{\infty} \beta(v_i,u)n(u,t)\,du \right]$$

$$+ E(v_i+v_1)n(v_i+v_1,t)\,dv - E(v_i)n(v_i,t)\,dv$$

$$+ S_0(v_i,t) - S_1'[v_i,t,n(v_i,t)]. \qquad [12]$$

For $v > v_{2k} + v_1/2$,

$$\frac{\partial[n(v,t)dv]}{\partial t} = \sum_{j=1}^{k} \beta(v-v_j,v_j)N(v_j,t)n(v-v_j,t)\,dv$$

$$+ \frac{1}{2} \int_{v_{k+1}-v_1/2}^{v-v_{k+1}+v_1/2} \beta(v-u,u)n(v-u,t)d(v-u)n(u,t)\,du$$

$$- \sum_{j=1}^{k} \beta(v,v_j)N(v_j,t)n(v,t)\,dv$$

$$- \quad n(v,t)\,dv \int_{v_{k+1}-v_1/2}^{\infty} \beta(v,u)n(u,t)\,du$$

$$+ E(v+v_1)n(v+v_1,t)\,dv - E(v)n(v,t)\,dv$$

$$+ S_0(v,t) - S_1'[v,t,n(v,t)], \qquad [13]$$

where

$$S_1'[v,t,n(v,t)] = S_1[v,t,N(v,t)]. \qquad [14]$$

Note that the Jacobian for the transformation from (v-u,u) coordinates to (v,u) coordinates is unity, and therefore du d(v-u) = du dv in the first integral on the right hand side of Eq. [13]. Substituting this expression into Eq. [13] and dividing both Eqs. [12] and [13] by dv results in

$$\frac{dn(v_i,t)}{dt} = \sum_{j=1}^{i-k-1} \beta(v_i-v_j,v_j)N(v_j,t)n(v_i-v_j,t) \quad i \geq k+2$$

$$+ \frac{1}{2} \sum_{j=i-k}^{k} \frac{\beta(v_i-v_j,v_j)N(v_i-v_j,t)N(v_j,t)}{v_1}$$

$$- n(v_i,t) \left[\sum_{j=1}^{k} \beta(v_i,v_j)N(v_j,t) + \int_{v_{k+1}-v_1/2}^{\infty} \beta(v_i,u)n(u,t)\,du \right]$$

$$+ E(v_i+v_1)n(v_i+v_1,t) - E(v_i)n(v_i,t)$$

$$+ \bar{S}_0(v_i,t) - \bar{S}_1[v_i,t,n(v_i,t)] \qquad [15]$$

for $v_{k+1} \leq v_i \leq v_{2k}$, $\bar{S}_0 = S_0/v_1$, and $\bar{S}_1 = S_1'/v_1$. For $v > v_{2k} + v_1/2$

$$\frac{\partial n(v,t)}{\partial t} = \sum_{j=1}^{k} \beta(v-v_j,v_j)N(v_j,t)n(v-v_j,t)$$

$$+ \frac{1}{2} \int_{v_{k+1}-v_1/2}^{v-v_{k+1}+v_1/2} \beta(v-u,u)n(v-u,t)n(u,t)\, du$$

$$- n(v,t) \sum_{j=1}^{k} \beta(v,v_j)N(v_j,t)$$

$$- n(v,t) \int_{v_{k+1}-v_1/2}^{\infty} \beta(v,u)n(u,t)\, du + E(v+v_1)n(v+v_1,t)$$

$$- E(v)n(v,t) + \bar{S}_0(v,t) - \bar{S}_1[v,t,n(v,t)] \qquad [16]$$

Because agglomeration of two particles from the discrete regime can only introduce new particles in the continuous regime smaller than or equal to v_{2k}, the continuous regime is divided into two sections. The first section contains particles of volume v, where $v_{k+1}-v_1/2 \leq v \leq v_{2k} + v_1/2$, and the second section contains particles larger than

$v_{2k} + v_1/2$. In the first section $n(v,t)$ is governed by Eq. [15], which is at most a system of k equations. Note that the second term of Eq. [16] is evaluated only for $v > 2v_{k+1} - v_1$. Combined with the appropriate initial conditions, Eqs. [10], [11], [15] and [16] constitute the discrete-continuous GDE.

2.3 Continuous General Dynamic Equation

If $N(v_i,t)$ is neglected for $2 \leq i \leq k$, Eqs. [15] and [16] become

$$\frac{\partial n(v,t)}{\partial t} = \frac{1}{2}\int_{v_{k+1}-v_1/2}^{v-v_{k+1}+v_{1/2}} \beta(v-u,u)n(v-u,t)n(u,t)\,du$$

$$- n(v,t)\int_{v_{k+1}-v_1/2}^{\infty} \beta(v,u)n(u,t)\,du + \bar{S}_0(v,t) - \bar{S}_1[v,t,n(v,t)]$$

$$+ n(v-v_1,t)\beta(v-v_1,v_1)N(v_1,t)$$

$$- n(v,t)[\beta(v,v_1)N(v_1,t) + E(v)]$$

$$+ E(v+v_1)n(v+v_1,t). \qquad [17]$$

In the limit as $v_1/v \to 0$, the last three terms of Eq. [17] reduce to

$$- \frac{\partial}{\partial v} \left\{ [\beta(v,v_1)N(v_1,t) - E(v)]v_1 n(v,t) \right\}$$
$$+ \frac{\partial^2}{\partial v^2} \left\{ [\beta(v,v_1)N(v_1,t) + E(v)] \frac{v_1^2 n(v,t)}{2} \right\} \qquad [18]$$

For most aerosols it has been shown (5) that the second term of [18] can be neglected. Therefore Eq. [17] becomes

$$\frac{\partial n(v,t)}{\partial t} = \frac{1}{2} \int_{v_{k+1}-v_1/2}^{v-v_{k+1}+v_1/2} \beta(v-u,u)n(v-u,t)n(u,t)\, du$$
$$- n(v,t) \int_{v_{k+1}-v_1/2}^{\infty} \beta(v,u)n(u,t)\, du + \bar{S}_0(v,t)$$
$$- \bar{S}_1[v,t,n(v,t)]$$
$$- \frac{\partial [I(v,t)n(v,t)]}{\partial v} \qquad [19]$$

where $I(v,t) = [\beta(v,v_1)N(v_1,t) - E(v)]v_1$. As shown elsewhere (5), $I(v,t)$ is the net growth rate of a particle of volume v due to condensation and evaporation of monomers, and is commonly called the condensation growth rate or the growth law (6-9). Notice that Eq. [19] is defined only over the domain $v \geq v_{k+1}-v_1/2$, and all information on

the distribution below this size is lost. One usually resorts to nucleation theory (10-12) to provide the generation rate of particles at $v = v_{k+1}$, thus supplying the boundary condition for Eq. [19]. A detailed discussion of the boundary condition will be given later.

Notice that the first integral on the right hand side of Eq. [19] is not evaluated in the region $[v_{k+1}-v_1/2, 2v_k+1]$. This is because agglomerations that form new particles in this region are neglected, (except for the agglomeration of monomers with k-mers, which is accounted for in the boundary condition.)

3. GENERAL ASPECTS OF AEROSOL FORMATION AND GROWTH

A major current problem in atmospheric science is developing a fundamental understanding of the dynamic behavior of air pollution aerosols. The qualitative picture of polluted tropospheric aerosols that has emerged is that primary aerosols, both natural and anthropogenic, provide the surface upon which secondary species ultimately condense. The principal source of secondary aerosol constituents is the primary gaseous pollutants, such as SO_2, NO_x and hydrocarbons. A major route for formation of secondary aerosol species is conversion of primary pollutant species to secondary gaseous species, followed by condensation of the secondary vapors on existing particles or nucleation to form fresh particles. It is still under debate whether nucleation or condensation is the dominant mechanism for gas-to-particle conversion in the atmosphere. To determine the nucleation rate one can supposedly measure the total number concentration of particles above the detectable size range of an instrument. (Although in reality the detection limit is probably not so precise as to be able to distinguish particles differing by only a single molecule, one can assume that for the ideal instrument only particles larger than a fixed size can be detected.) After correcting for the coagulation, generation and removal of particles larger than the detectable limit, the net observed increase in number concentration can be attributed to the flux of particles into the detectable size range.

However, the observed flux can be the result of the growth of small preexisting particles initially below the detectable limit or by the growth of particles formed by nucleation. Since current instrumentation (13,14), is probably not capable of detecting a typical critical size particle, no measurements have been reported in which the two mechanisms can be distinguished.

Because we wish to be precise in our definitions of condensation and nucleation as routes for gas-to-particle conversion, we will define clusters as particles containing i monomers, where $2 \leq i \leq k$, and aerosol particles as particles containing k+1 or more monomers. In developing the discrete-continuous GDE, the only constraint on k is that it be a large number. Thus, one can consider a k-mer to be the critical size particle for nucleation or that just below the lower size limit of detection. In either case the discrete-continuous GDE can be used to determine the net rate of formation of particles smaller and larger than k-mer. Thus, condensation will be defined as the net agglomeration rate of monomer and clusters with aerosol particles. Nucleation will be defined as the net formation rate of aerosol particles by the agglomeration of two particles from the discrete regime. Classical nucleation is then a special case of nucleation, in which the k-mer is the critical size particle. (However, classical nucleation theory neglects cluster-cluster agglomerations in determining the nucleation rate.) When we speak of the scavenging of an

i-mer by a j-mer, we mean the net agglomeration rate of the two particles where j>>i.

The general aspects of the gas-to-particle conversion process are depicted in Figure 1. Monomer, the secondary gaseous species, may either condense on aerosol particles or agglomerate with another monomer to enter the path involving molecular cluster dynamics. The molecular clusters may themselves be scavenged by aerosol particles or continue to grow to the point at which an aerosol particle is formed, the nucleation route. It is of interest to be able to estimate the relative importance of the two gas-to-particle conversion paths, direct condensation and nucleation, as a function of the generation rate of monomer and the quantity and size distribution of preexisting aerosol. In fact, there are several questions that arise in considering the general gas-to-particle conversion process:

(1) Is a steady state concentration profile of molecular clusters achieved, and, if so, how does the profile differ in the absence and presence of a preexisting aerosol?

(2) Can the relative importance of condensation, nucleation, and scavenging be estimated to determine the qualitative evolution of the aerosol, given knowledge of the monomer generation rate and the quantity and size distribution of preexisting aerosol?

(3) What is the importance of cluster-cluster agglomeration relative to the other processes influencing the cluster concentrations and the evolving aerosol size distribution?

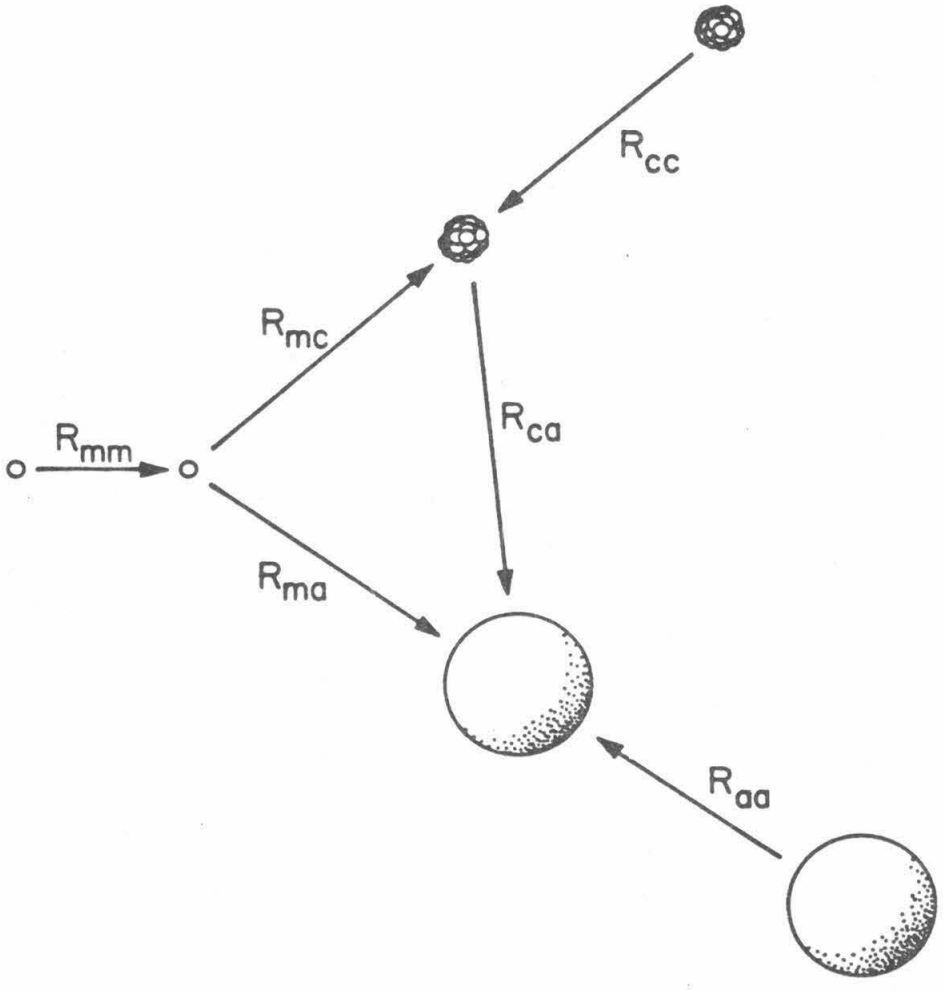

Figure 1

Routes for gas-to-particle conversion. R_{ij} is the net agglomeration rate of particle type i with particle type j where m is monomer, c is cluster and a is aerosol.

The discrete-continuous GDE implicitly accounts for all the processes referred to in these questions, and, on that basis, its solution provides quantitative answers to them. In this section the theoretical analysis needed to address these questions for general gas-to-particle conversion systems will be presented. Subsequently, in Chapter V, the analysis developed in this section will be used to answer the above questions for the particular experiment simulated.

For the six agglomeration processes (1) monomer-monomer (mm), (2) monomer-clusters (mc), (3) monomer-aerosol (ma), (4) cluster-aerosol (ca), (5) cluster-cluster (cc), and (6) aerosol-aerosol (aa), shown in Figure 1, the net rate of agglomeration of particle types i and j, R_{ij} is,

$$R_{mm} = \frac{1}{2}\beta(v_1,v_1)[N(v_1,t)]^2 - E(v_2)N(v_2,t) \qquad [20]$$

$$R_{mc} = \beta(v_1,v_2)N(v_1,t)N(v_2,t) - \int_{v_{k+1}-v_1/2}^{v_{k+1}+v_1/2} E(v)n(v,t)\,dv + \sum_{j=3}^{k} [\beta(v_1,v_j)N(v_1,t) - E(v_j)]N(v_j,t) \qquad [21]$$

$$R_{ma} = \int_{v_{k+1}-v_1/2}^{\infty} [\beta(u,v_1)N(v_1,t)n(u,t) - E(u+v_1)n(u+v_1,t)]du \qquad [22]$$

$$R_{ca} = \sum_{j=2}^{k} N(v_j,t) \int_{v_{k+1}-v_1/2}^{\infty} \beta(v_j,u)n(u,t)\, du \qquad [23]$$

$$R_{cc} = \frac{1}{2} \sum_{j=2}^{k} \sum_{j=2}^{k} \beta(v_i,v_j)N(v_i,t)N(v_j,t) \qquad [24]$$

$$R_{aa} = \frac{1}{2} \int_{v_{k+1}-v_1/2}^{\infty} \int_{v_{k+1}-v_1/2}^{\infty} \beta(v,u)n(u,t)n(v,t)\, dudv. \qquad [25]$$

The net nucleation rate is,

$$R_{nuc} = \sum_{i=k+1}^{2k} \left\{ \frac{1}{2} \sum_{j=i-k}^{k} \beta(v_i-v_j,v_j)N(v_i-v_j,t)N(v_j,t) \right\}$$

$$- \int_{v_{k+1}-v_1/2}^{v_{k+1}+v_1/2} E(u)n(u,t)\, du \qquad [26]$$

If a k-mer corresponds to the critical size particle, then R_{nuc} is the classical nucleation rate, generalized to include cluster-cluster agglomeration. The net nucleation rate divided by the net condensation rate of particles in the discrete regime is

$$\xi = \frac{R_{nuc}}{R_{ma}+R_{ca}} \qquad [27]$$

If $\xi << 1$ and $\xi >> 1$, condensation and nucleation, respectively, are the dominant mechanisms.

It is also of interest to determine the net number of monomers nucleating, given by

$$R_{m\text{-}nuc} = \sum_{i=k+1}^{2k} \frac{i}{2} \left\{ \sum_{j=i-k}^{k} \beta(v_i - v_j, v_j) N(v_i - v_j, t) N(v_j, t) \right\}$$

$$- (k+1) \int_{v_{k+1}-v_1/2}^{v_{k+1}+v_1/2} E(u) n(u,t)\, du \qquad [28]$$

The net number of monomers from the discrete regime condensing on aerosol particles is

$$R_{m\text{-}cond} = \sum_{j=1}^{k} jN(v_j,t) \int_{v_{k+1}-v_1/2}^{\infty} \beta(v_j,u) n(u,t)\, du$$

$$- \int_{v_{k+1}+v_1/2}^{\infty} E(u) n(u,t)\, du \qquad [29]$$

Thus the fraction of the total flux of monomer entering the continuous regime by condensation is

$$\bar{\alpha} = \frac{R_{m\text{-cond}}}{R_{m\text{-nuc}}+R_{m\text{-cond}}} \qquad [30]$$

Although the nucleation rate may be comparable to the monomer and cluster condensation rate, due to the scavenging of the small aerosol particles, no significant particle formation may be observed just above the detection limit. Since it has been experimentally observed (15,16), and theoretically predicted in Chapter V, that after a short time lag a burst of new particles should form just above the detection limit, it is also important to determine if such a phenomenon will occur in general. Because nucleation can only introduce new particles of size v_i, where $k+1 \leq i \leq 2k$, for a burst of new particles to be detected $dn(v_i,t)/dt$ must be positive as given by Eq. [15] for some $k+1 \leq i \leq 2k$, $t \geq 0$, and a detectable limit of v_{k+1}.

Techniques for obtaining a priori estimates of the rates discussed in this section will be presented in the analysis of the experimental simulation discussed in Chapter V.

4. KINETIC COEFFICIENTS AND BOUNDARY CONDITION

4.1 Agglomeration Coefficient

For typical atmospheric aerosols the dominant mechanism for agglomeration is Brownian motion. Usually when the agglomerating particles are larger than the critical size particle, the process is termed Brownian coagulation. (The term agglomeration is used here for the collision and subsequent coalescence of any size particles, and thus coagulation and condensation are special cases of agglomeration.) The functional form of β for Brownian coagulation is highly dependent on the sizes of the coagulating particles, relative to the mean free path of the medium, λ. The Knudsen number, is defined as $Kn = 2\lambda/D$, where D is the particle diameter.* For particles with $Kn \gg 1$ or $Kn \ll 1$ the coagulation processes is said to be in the free molecule or continuum regime, respectively. If, for one particle $Kn \ll 1$ and the other $Kn \gg 1$, the coagulation process is essentially classical diffusion or condensation. For these three limiting cases the functional form of β is well known and is given in Table 1 (17), where $\beta_D(D_i,D_j) = \beta(v_i,v_j)$, $\mathscr{D}$ is the particle diffusivity usually determined from the Stokes-Einstein expression (18), k is the Boltzmann constant, T is the absolute temperature, η is the viscosity of the medium and m is the mass of the particle. For $Kn_i \gg 1$ and $Kn_j \ll 1$ the continuum expression reduces to the correct form since $\mathscr{D}_j \ll \mathscr{D}_i$ and $D_i \ll D_j$. In the transition regime,

*It is usually assumed that the particles are spherical.

Table 1. Brownian Coagulation Coefficients, $\beta_D(D_i,D_j)$* (17)

Continuum $Kn_i \ll 1$ $Kn_j \ll 1$	Transition $Kn_i,\ Kn_j \sim O(1)$ $Kn_i = 2\lambda/D_i$	Free Molecule $Kn_i,\ Kn_j \gg 1$
$2\pi(\mathscr{D}_i+\mathscr{D}_j)(D_i+D_j)$	$2\pi(\mathscr{D}_i+\mathscr{D}_j)(D_i+D_j)\left[\frac{D_i+D_j}{D_i+D_j+2g_{ij}} + \frac{8(\mathscr{D}_i+\mathscr{D}_j)}{\bar{v}_{ij}(D_i+D_j)}\right]^{-1}$	$\frac{\pi}{4}(D_i+D_j)^2\,\bar{v}_{ij}$
$\mathscr{D}_i = \frac{kT}{3\pi D_i \eta}$	$\mathscr{D}_i = \begin{cases} \frac{kT}{3\pi D_i \eta}\left[1+Kn_i(1.257+0.4\exp(-1.1/Kn_i))\right] & \text{(Millikan)} \\ \frac{kT}{3\pi D_i \eta}\left[\frac{5+4Kn_i+6Kn_i^2+18Kn_i^3}{5-Kn_i+(8+\pi)Kn_i^2}\right] & \text{(Phillips)} \end{cases}$ $g_{ij} = (g_i^2 + g_j^2)^{1/2}$ $g_i = \frac{1}{3D_i\ell_i}\left\{(D_i+\ell_i)^3 - (D_i^2+\ell_i^2)^{3/2}\right\} - D_i$ $\ell_i = 8\mathscr{D}_i/(\pi\bar{v}_i)$	$\bar{v}_{ij} = (\bar{v}_i^2+\bar{v}_j^2)^{1/2}$ $\bar{v}_i = (8kT/(\pi m_i))^{1/2}$

*In using the expressions in this table, one assumes that each collision results in coalescence.

where Kn is of order one, the slip correction for the particle diffusivity can be based on either Millikan's (19) or Phillips' (20) correction. Both expressions are similar and are given in Table 1. Since Phillips' expression is more recent, it was used in this work. For determining β in the transition regime the interpolation formula of either Fuchs (21) or Sitarski and Seinfeld (17) can be used. As shown in Figure 2, both formulae are very similar but since Fuchs' formula with either slip correction goes to the correct limits for all three cases it will be used in this work unless stated otherwise. Fuchs' formula is given in Table 1 for the transition regime. In plotting Figure 2, Phillips' expression was used, and thus the plotted Fuchs formula is called the Fuchs-Phillips interpolation formula. Note that β_D is a symmetric function of its arguments, (i.e. $\beta_D(D_i,D_j) = \beta_D(D_j,D_i)$.)

If the particles are the size of a molecule it would probably be better to determine the diffusivity from kinetic theory (22), and thus*

$$\mathscr{D} = (1 + \Lambda) \frac{3}{8} \left(\frac{\pi}{2}\right)^{\frac{1}{2}} \frac{kT}{PS} \left[\frac{(m_1+m_b)kT}{m_1 m_b}\right]^{\frac{1}{2}} \qquad [31]$$

where P is the total pressure, $S = \frac{\pi}{4}(D_1+D_b)^2$, m_1, m_b and D_1, D_b are the masses and diameters of the diffusing particle and the background gas respectively, and $0 \leq \Lambda \leq 0.132$, (the maximum value of Λ is attained for hard spheres with greatly different masses.) As will be shown in

*It should be noted that Eq. [31] is only an approximation for $\mathscr{D}$ and one often uses a simpler expression which will be given in Eq. [34].

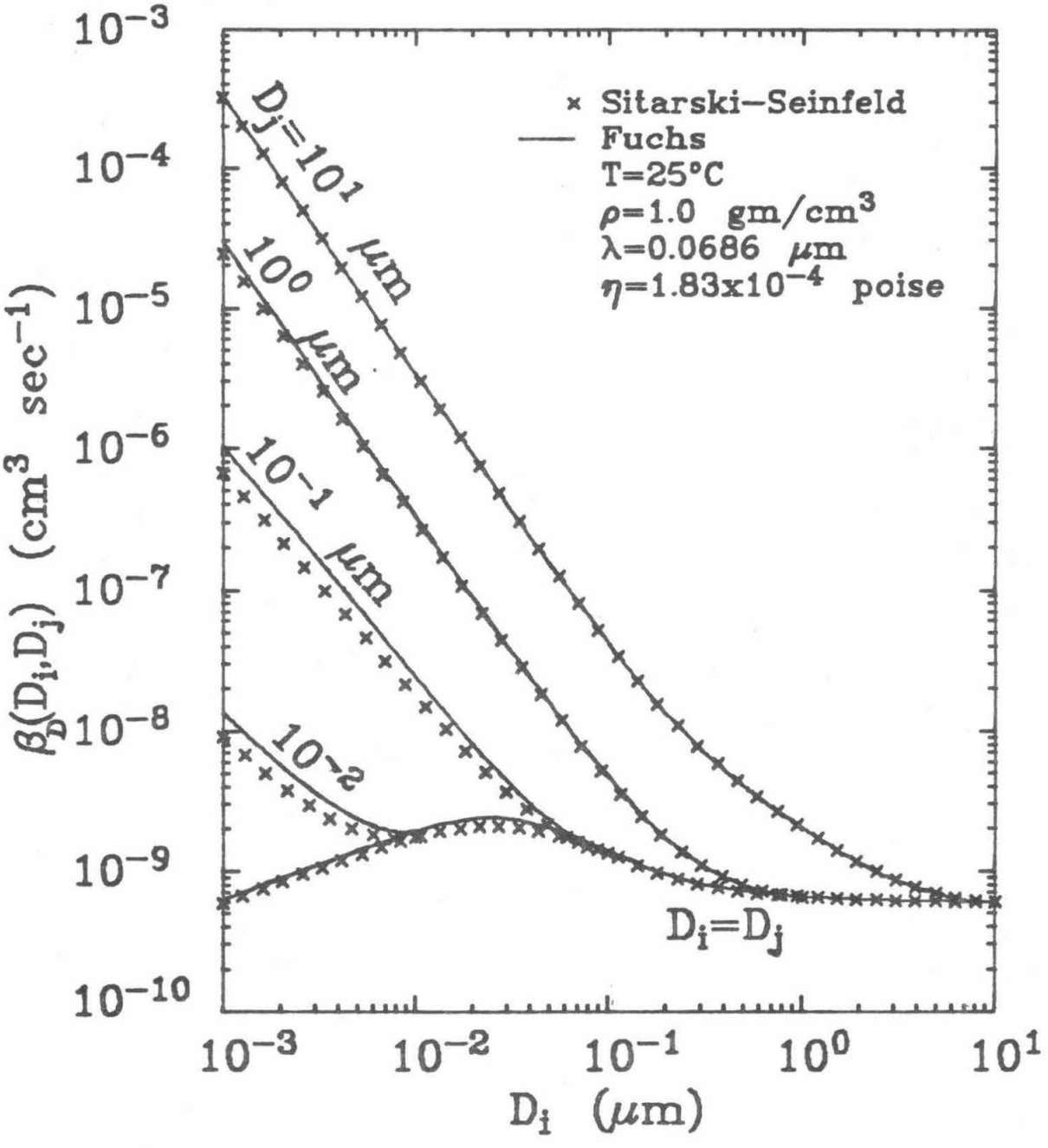

Figure 2

Agglomeration coefficient for spherical particles in air using Phillips' slip correction.

Chapter V the diffusivity as a function of particle size, determined from kinetic theory and the Stokes-Einstein expression intersect. Thus one can construct a diffusivity which is continuous with particle size and reduces to the correct limits.

4.2 Evaporation Coefficient

The evaporation coefficient is usually determined from the agglomeration coefficient at equilibrium conditions (10,23), and is given by,

$$E(v) = \beta(v,v_1)\, N_+ \left[\frac{v-v_1}{v}\right]^{2/3} \exp\left\{\frac{3^{2/3}(4\pi)^{1/3}\left[v^{2/3}-(v-v_1)^{2/3}\right]\sigma}{kT}\right\} \qquad [32]$$

where N_+ is the gas phase concentration of condensible species in equilibrium over a flat surface and σ is the surface tension. A major difficulty with this formulation arises in using bulk properties such as surface tension for particles containing only a few molecules. Hill (24) reports that work has been presented in the literature on the variation of surface tension with particle size, but there is even disagreement whether the surface tension increases or decreases with decreasing particle size. Unfortunately, for small particles the evaporation coefficient is highly dependent on the surface tension. For $v \gg v_1$, one often uses a two term expansion for $(v-v_1)^{2/3}$ in the

exponential to obtain

$$E(v) = \beta(v,v_1)\, N_+ \exp\left(\frac{4\sigma v_1}{DkT}\right) \qquad [33]$$

The exponential factor is then interpreted as the pressure rise due to curvature effects and the phenomena is often called the Kelvin effect (8,9).

4.3 Growth Laws

For most atmospheric aerosols, gas-phase diffusion is believed to be the rate determining step for particle growth (7). However, there is also evidence that heterogeneous chemical reactions involving gaseous species and the surface or interior of particles may serve as the rate determining step in gas-to-particle conversion (25-28). The particular mechanism of growth has an important influence on the rate at which particles of a certain size grow. Since temperature changes resulting from condensational growth of atmospheric aerosols are considered to be negligible (8,29), it will be assumed that isothermal conditions prevail. In this part of section 4, growth law expressions for $I(v,t)$ in the cases of diffusion-, surface-, and volume reaction-controlled growth are presented.

We consider the growth of a particle resulting from condensation of a single species A on the particle. In the case of diffusion-controlled growth, we restrict ourselves to the case in which A is

condensing on a particle of pure A or on a particle consisting of several species but for which the vapor pressure of A is independent of the particle's composition. In the cases of surface reaction- and volume reaction-controlled growth, A is presumably converted to another species B. It is assumed that in these two cases the equilibrium concentration of A above the particle surface is linearly related to the concentration of A in the particle. This condition can probably be expected to be valid as long as the concentration of A in the particle is small.

Because comparisons of the various growth laws are best made in terms of dimensionless variables, a detailed discussion of the growth laws is postponed until Chapter III. The dimensional form of all growth laws and the derivation of all reaction-controlled growth laws will be given in this section.

4.3.1 Diffusion-Controlled Growth

As shown in section 2.3 the growth law, $I(v,t)$ for diffusion-controlled growth can be determined from the agglomeration and evaporation coefficients. Just as for the agglomeration coefficient, the functional form of $I(v,t)$ is highly dependent on the Knudsen number of the particle. For particles in the continuum and free molecule regime, $I(v,t)$ is given in Table 2 in terms of the particle diameter. Although in the transition regime, one can use the interpolation formula for $\beta(v,v_1)$ given in Table 1, it is more convenient to use

Table 2. Diffusion-Controlled Growth Laws, I(v,t)* (6)

Continuum Kn<<1	Transition Kn ~ O(1)	Free Molecule Kn>>1
$2\pi D\mathcal{D}\Delta v_1$	$\dfrac{2\pi(D+2\alpha\lambda)\mathcal{D}\Delta v_1 D^2}{D^2+2b\lambda D+4a\lambda^2}$	$\pi D^2\left[\dfrac{kT}{2\pi m}\right]^{1/2} v_1\Delta$

	Fuchs (30)	Fuchs and Sutugin (6)
a =	$\dfrac{\alpha\mathcal{D}}{\lambda}\left[\dfrac{2\pi m}{kT}\right]^{1/2}$	1.33
b =	a/α	1.71
α =	~O(1)	1.0

*Kn = $2\lambda/D$, $\Delta = N_\infty - N_+\exp[(4\sigma v_1)/(DkT)]$, $v = \frac{\pi}{6}D^3$, $N_\infty \approx N(v_1,t)$

one of two interpolation formula for I(v,t) as given by Fuchs' flux matching formula (30) or Sahni's formula (31), (for convenience, the curve fit of Fuchs and Sutugin (6) is used for Sahni's formula). As shown in Table 2, both formulae for I(v,t) are very similar. For Fuchs' growth law, α is the number of mean free paths from the particle surface at which the flux matching condition is imposed. If

$$\mathscr{D} = \frac{\lambda}{3}\left[\frac{8kT}{\pi m}\right]^{1/2} \qquad [34]$$

then a=b = 4/3 for Fuchs' growth law, which is close to values of a and b given by Fuchs and Sutugin. Fuchs' growth law reduces to the correct form for Kn<<1 and Kn>>1, and the growth law of Fuchs and Sutugin will reduce to the correct limiting form if $\mathscr{D}$ is given by Eq. [34]. However Fuchs' growth law has only a second order correction in Kn^{-1} as $Kn \to \infty$, (6,8).

Although both expressions are valid in the limits of Kn large and small, difficulties arise when applying the formulae to situations in which the monomer is condensing on a particle not much larger than the monomer itself. The growth laws can be corrected for monomer condensation on an i-mer by multiplying the expressions by the terms, $\{(1+i^{1/3})/i^{1/3}\}^2\{(1+i)/i\}^{1/2}$ (23). With this correction, $I(v,t)/N(v_1,t)$ approaches $\beta(v,v_1)$ for E(v)=0. Figure 3 shows $\beta(v,v_1)$ obtained from the growth law relative to the Fuchs-Phillips formula for Brownian coagulation. Particle diffusivities were calculated based on kinetic theory for small

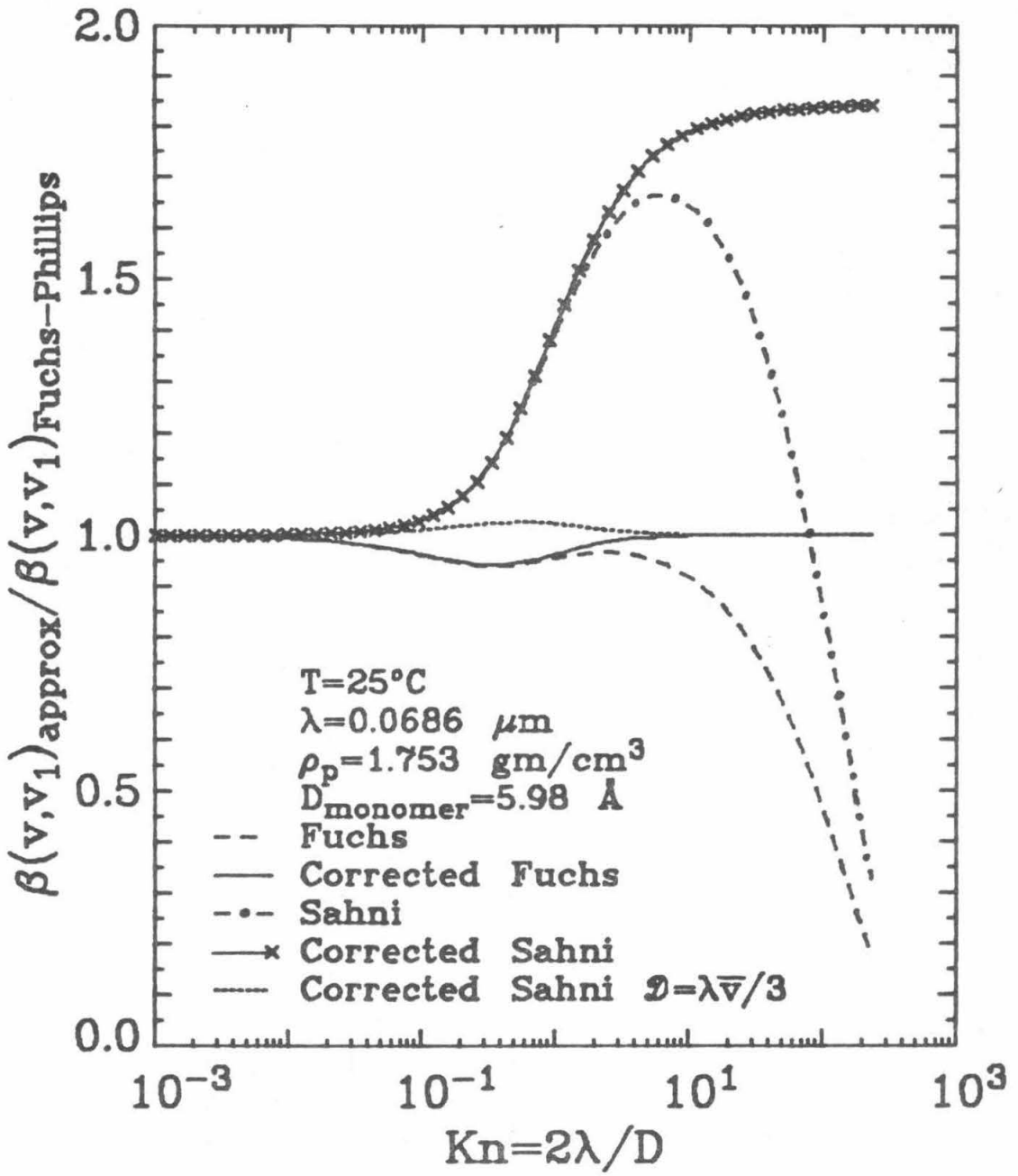

Figure 3

Ratio of the agglomeration coefficient between a monomer of volume v_1, with a particle of volume v, (assuming $v = \pi D^3/6$), calculated from existing growth laws divided by the Fuchs-Phillips agglomeration coefficient (17).

particles and the Stokes-Einstein expression for large particles. The transition point between the two theories was chosen such that the diffusivity is a continuous function of particle size as previously discussed. Notice that the approximate formulae are very poor for large Kn without the correction factor. Also notice that even the corrected Sahni expression significantly differs from the Fuchs-Phillips coefficient unless $\mathscr{D}$ is given by Eq. [34].

4.3.2 Surface Reaction-Controlled Growth

If surface chemical reaction is the rate-determining step for particle growth, then the rate at which reactants diffuse to the particle must equal the rate of reaction on the particle surface. Therefore, assuming the molecular volumes of the reactant and product to be identical,

$$\pi D^2 k_s N_s^{\gamma} = \frac{2\pi \mathscr{D}(D^3+2\alpha\lambda D^2)}{(D^2+2b\lambda D+4a\lambda^2)} \left[N_{\infty} - N_{+} \exp\left(\frac{4\sigma v_1}{DkT}\right) \right] \qquad [35]$$

where k_s is the surface reaction rate constant, N_s is the concentration of reactant on the surface of the particle, and γ is the order of the surface reaction. If

$$N_{+} = H_s N_s \qquad [36]$$

where H_s is constant, then by substituting Eq. [36] into Eq. [35] and

rearranging, we obtain the following equation for N_s,

$$N_s^{\gamma} + \frac{2N_s H_s (D+2\alpha\lambda)\mathcal{D} \exp\left(\frac{4\sigma v_1}{DkT}\right)}{k_s(D^2+2b\lambda D+4a\lambda^2)} - \frac{2N_\infty (D+2\alpha\lambda)\mathcal{D}}{k_s(D^2+2b\lambda D+4a\lambda^2)} = 0 \qquad [37]$$

For surface reactions of order γ,

$$I(v,t) = \pi D^2 v_1 k_s N_s^{\gamma}. \qquad [38]$$

The growth laws are given in terms of the particle diameter for γ = 0, 1/2, 1, and 2 in Table 3.

4.3.3 Volume Reaction-Controlled Growth

If chemical reaction occurring throughout the volume of particle is the rate-determining step for growth, then the equating of diffusion and reaction rates gives

$$\frac{\pi D^3}{6} k_v N_v^{\gamma} = \frac{2\pi\mathcal{D}(D^3+2\alpha\lambda D^2)}{(D^2+2b\lambda D+4a\lambda^2)} \left[N_\infty - N_+ \exp\left(\frac{4\sigma v_1}{DkT}\right)\right] \qquad [39]$$

where k_v is the volume reaction rate constant, and N_v is the concentration of reactant in the particle. Assuming

$$N_+ = H_v N_v \qquad [40]$$

where H_v is a constant, then by substituting Eq. [40] into Eq. [39]

Table 3. Reaction-Controlled Growth Laws, I(v,t)*

Reaction Order	Surface Reaction	Volume Reaction
$\gamma = 0$	ϕ_s	ϕ_v
$\gamma = 1/2$	$\phi_s \left[\frac{1+2\phi_1\phi_2 - (1+4\phi_1\phi_2)^{1/2}}{2\phi_1^2} \right]^{1/2}$	$\phi_v \left[\frac{1+2\phi_3\phi_4 - (1+4\phi_3\phi_4)^{1/2}}{2\phi_3^2} \right]^{1/2}$
$\gamma = 1$	$\frac{\phi_s\phi_2}{1+\phi_1}$	$\frac{\phi_v\phi_4}{1+\phi_3}$
$\gamma = 2$	$\frac{\phi_s}{4}\left[-\phi_1+(\phi_1^2+4\phi_2)^{1/2}\right]^2$	$\frac{\phi_v}{4}\left[-\phi_3+(\phi_3^2+4\phi_4)^{1/2}\right]^2$

*$\phi_s = \pi D^2 v_1 k_s$ $\quad \phi_1 = \frac{H_s\phi}{k_s}\exp\{(4\sigma v_1)/(DkT)\}$ $\quad \phi_4 = \frac{6N_\infty\phi}{k_v D}$

$\phi_v = \frac{\pi}{6} D^3 v_1 k_v$ $\quad \phi_2 = N_\infty\phi/k_s$

$\phi = \frac{2(D+2\alpha\lambda)\mathcal{D}}{D^2+2b\lambda D+4a\lambda^2}$ $\quad \phi_3 = \frac{6H_v\phi}{k_v D}\exp\{(4\sigma v_1)/(DkT)\}$

and rearranging, we obtain the following equation for N_v,

$$N_v^{\gamma} + \frac{12H_v(D+2\alpha\lambda)\mathscr{D}N_v\exp\left(\frac{4\sigma v_1}{DkT}\right)}{k_v D(D^2+2b\lambda D+4a\lambda^2)}$$

$$- \frac{12N_\infty(D+2\alpha\lambda)\mathscr{D}}{k_v D(D^2+2b\lambda D+4a\lambda^2)} = 0 \qquad [41]$$

For volume reactions of order γ the growth law is then

$$I(v,t) = \frac{\pi D^3}{6} v_1 k_v N_v^{\gamma}. \qquad [42]$$

The growth laws for γ = 0, 1/2, 1, and 2 are given in Table 3.

4.4 Boundary Condition

To determine the boundary condition at $v = v_{k+1}-v_1/2$, we note that implicit in Eq. [9] is constancy of $n(v,t)$ in the regions $[v_{k+1}-v_1/2 + \ell v_1, v_{k+1} + v_1/2 + \ell v_1]$, where ℓ is a positive integer or zero. (Although $n(v,t)$ is actually a series of step functions, because the spacing of the steps is so small relative to v, $n(v,t)$ can be used as a continuous function.) Thus, at the boundary, $n(v_{k+1}-v_1/2,t)$ is given by $N(v_{k+1},t)/v_1$. Using Eq. [15] and neglecting the clusters we have,

$$\frac{dN(v_{k+1},t)}{dt} = J - E(v_{k+1})N(v_{k+1},t)$$

$$- \beta(v_{k+1},v_1)N(v_{k+1},t)N(v_1,t) + E(v_{k+2})N(v_{k+2},t)$$

$$- N(v_{k+1},t) \int_{v_{k+1}-v_1/2}^{\infty} \beta(v_{k+1},u)n(u,t)\, du \qquad [43]$$

where J is equal to $\beta(v_1,v_k)N(v_1,t)N(v_k,t)$. Dividing Eq. [43] by v_1 results in the boundary condition

$$\frac{dn(v_{k+1}-v_1/2,t)}{dt} = \frac{J}{v_1} - n(v_{k+1},t)\left[E(v_{k+1}) + \beta(v_{k+1},v_1)N(v_1,t)\right]$$

$$+ E(v_{k+2})n(v_{k+2},t)$$

$$- n(v_{k+1},t) \int_{v_{k+1}-v_1/2}^{\infty} \beta(v_{k+1},u)n(u,t)\, du \qquad [44]$$

There are difficulties associated with determining J and hence the boundary condition. As will be shown in Chapter V, due to the scavenging by particles in the continuous regime, the discrete profile, and hence the nucleation rate is dependent on the continuous distribution. Therefore, if the profile in the discrete regime is affected by scavenging, J will vary as the continuous regime evolves and can not be determined in the absence of knowledge of the dynamics in the continuous regime.

5. LITERATURE REVIEW

Previous work on the General Dynamic Equation involved solutions to some form of either the discrete or continuous GDE. For the process of coagulation only, Drake (32) has given an extensive survey on the work of the so called Coagulation Equation in both the discrete and continuous form. Some of the more recent works on the full discrete and continuous GDE are listed in Tables 4 and 5, respectively.

For the discrete GDE to include all dynamic mechanisms, the number of differential equations must be equal to the largest multiplet number. As will be shown in Chapter V, if a single molecule is taken as the monomer, then a particle 1 μm in diameter contains approximately 10^{10} molecules. Clearly, 10^{10} differential equations are far beyond the capacity of modern computers. Based on the reported solutions given in Table 4, only several hundred differential equations are feasible.* Therefore, most discrete solutions are of limited value in simulating atmospheric aerosols.

Since particle size spacing differing by only a single monomer is not practical, solutions to approximate discrete equations, which will be called sectional approximations to the discrete equations have been reported. In these equations one usually breaks up the particle size domain into sections. Within each section all particle sizes are

*The work of McMurry (34) will be discussed in Chapter V.

Table 4. Reported Solutions to the Discrete GDE

	Investigator	Dynamics	Remarks
1.	Rice and Whitehead (33)	coagulation	exact solution
2.	McMurry (34)	condensation and removal	steady state assumption, several thousand particle sizes
3.	Courtney (35)	nucleation	~100 particle sizes
4.	Hidy (36)	coagulation	400-600 particle sizes, Runge-Kutta-Gill and Hamming's method for time integration
5.	Mockros, Quon, and Hjelmfelt (37)	coagulation and generation	100 particle sizes, Runge-Kutta and Adam's method for time integration
6.	Takahashi and Kasahara (38)	coagulation and removal	~100 particle sizes
7.	Suzuki, Ho, and Higuchi (39)	coagulation	100 particle sizes, Runge-Kutta and Hamming's method for time integration
8.	Abraham (40)	nucleation	~100 particle sizes, Fowler-Warten method for time integration
9.	Sutugin and Fuchs (41)	agglomeration and evaporation	126 unequally spaced particle sizes, Runge-Kutta method for time integration
10.	Gillette (42)	coagulation and removal	91 logarithmically spaced particle sizes, Runge-Kutta method for time integration

Table 4. Reported Solutions to the Discrete GDE (Continued)

	Investigator	Dynamics	Remarks
11.	Yoshida, Okuyama, Kousaka, and Kida (43)	coagulation	100 unequally spaced particle sizes, Runge-Kutta-Merson method for time integration
12.	Bauer and Frurip (44)	nucleation	80 particle sizes, Gear's method for time integration
13.	Hamill, Toon, and Kiang (45)	coagulation	

represented by a single particle size, taken as some mean size of the section. Since the initial sections for the smallest particles can contain very few particle sizes, reasonable representations of the smallest particle concentrations may be obtained. In order to span the larger sizes, the sections are usually progressively increased in extent. Thus one may not be obtaining a completely accurate and detailed description of the entire aerosol with these approximations. Since sectional approximations are hardly ever derived from the basic discrete equation, it is unclear what assumptions are made in using sectional approximations. In this thesis, the appendix presents a rigorous derivation of a proposed sectional approximation to the discrete GDE. As will be shown, two assumptions must be made, one on the concentration profile within a section and one on the appropriate agglomeration coefficient between particles of different sections. Further testing of sectional approximations by comparison to the discrete or discrete-continuous GDE is required before one can be confident that a reasonable approximate solution to the discrete GDE is obtained.

Probably because of its simplicity many solutions have been reported to the continuous GDE as given in Table 5. All analytic solutions which include coagulation, however, are only for simplified coagulation coefficients and thus cannot be used for most atmospheric aerosols. Their utility lies primarily in serving as test cases for numerical routines. If the coagulation integrals are neglected, exact *solutions* can be obtained for realistic growth laws, and particle

Table 5. Reported Solutions to the Continuous GDE

	Investigator	Dynamics	Remarks
1.	Golovin (46)	coagulation	exact solution
2.	Scott (47)	coagulation	exact solution
3.	Brock (48,49)	condensation, generation, and removal	exact solution
4.	Drake (50)	coagulation	exact solution
5.	Drake and Wright (51)	coagulation	exact solution
6.	Ramabhadran, Peterson, and Seinfeld (5)	coagulation and condensation	exact solution
7.	Peterson, Gelbard, and Seinfeld (52)	coagulation, condensation, generation, and removal	exact solution
8.	Gelbard and Seinfeld (9)	condensation, generation, and removal	exact solution
9.	Mulholland, Lee, and Baum (53)	coagulation	asymptotic solution, log-normal initial distribution
10.	Twomey (54)	coagulation and condensation	80-100 differential equations
11.	Spigler, Morgan, Greenfield, and Koontz (55)	coagulation, generation, and removal	80-100 differential equations

Table 5. Reported Solutions to the Continuous GDE (Continued)

	Investigator	Dynamics	Remarks
12.	Berry (56)	coagulation	logarithmic rescaling, Lagrangian 3-point interpolation
13.	Willis, Kerker, and Matijevic (57)	coagulation	
14.	Huang, Kerker, and Matijevic (58)	coagulation and removal	
15.	Cohen and Vaughan (59)	coagulation, generation, and removal	log-normal distribution, asymptotic and numerical solution
16.	Lindauer and Castleman (60)	coagulation and removal	5 point Newton-Cotes quadrature, Runge-Kutta and Adam's method for time integration
17.	Burgmeier, Blifford, and Gillette (61)	coagulation generation, and removal	trapezoidal rule, linear interpolation, finite differences for time integration
18.	Walter (62)	coagulation and constant generation rate	Simpson's rule, Euler-Cauchy polygon method
19.	Wadden, Quon, and Hulburt (63)	coagulation, condensation, and generation	logarithmic rescaling, overlapping parabolas, Runge-Kutta and Hamming's method for time integration
20.	Singh and Ramkrishna (64)	coagulation	weighted residuals; orthogonal collocation and the method of moments

Table 5. Reported Solutions to the Continuous GDE (Continued)

	Investigator	Dynamics	Remarks
21.	Middleton and Brock (65)	coagulation, condensation, generation by homogeneous nucleation	logarithmic rescaling, cubic spline interpolation Runge-Kutta method for time integration
22.	Gelbard and Seinfeld (66)	coagulation, condensation, generation and removal	logarithmic rescaling, cubic splines and orthogonal collocation on finite elements interpolations, Guass-Legendre quadrature, Adam's method for time integration

sources and sinks (9,48,49). The details of these solutions are given in Chapter III. For those cases in which the coagulation integrals are retained in the continuous GDE, numerical routines are required for realistic coagulation coefficients, growth laws, and initial and boundary conditions. Because the details of solving the continuous GDE numerically are given in Chapter IV, only a few brief statements on the various techniques reported by others will be given in this section.

Nearly all reported techniques employ the method of collocation (66), in which certain points in the particle size domain, called collocation points, are chosen at which the GDE is to be satisfied. One then proceeds to determine the temporal variations of the distribution at these points by evaluating the right hand side of Eq. [19] at the collocation points. Thus the partial-integrodifferential equation is converted to a system of coupled nonlinear ordinary differential equations. The major difference among the techniques is the method used to evaluate the right hand side of Eq. [19]. Assuming convergent integration techniques are used for both the coagulation integrals and the time integration, if a sufficient number of properly located collocation points are used, nearly all techniques should converge to the same solution. Therefore, the essential difference among the techniques appears to be the amount of computation needed for a convergent solution.

For numerical solution, Berry (56) was probably the first to report the success of using a logarithmic rescaling in particle size, which was later employed by Middleton and Brock (65) and then by Gelbard and Seinfeld (66). It was found that such a rescaling provided the so-called "stretching" of the particle size domain.

For nearly all techniques an interpolation method is needed to evaluate the coagulation integrals. As can be seen from Table 5, a wide variety of techniques have been reported, and as concluded in Chapter IV it is difficult to state conclusively which technique is best in all cases.

In special cases, for which one somehow has a priori knowledge of the shape of the resulting distribution, techniques to capitalize on this knowledge have been reported (59,64). In general such knowledge may not be available.

NOTATION

D	particle diameter, μm
$\mathscr{D}$	diffusivity, $cm^2\ sec^{-1}$
$E(v)$	evaporation coefficient, sec^{-1}
H_s	defined in Eq. [36], cm^{-1}
H_v	defined in Eq. [40]
$I(v,t)$	growth law, $\mu m^3\ sec^{-1}$
J	defined on page 42, $sec^{-1}\ cm^{-3}$
k	Boltzmann constant, $erg\ deg^{-1}$
k_s	surface reaction rate constant, $\mu m^{2\gamma-2}\ sec^{-1}$
k_v	volume reaction rate constant, $\mu m^{3\gamma-3}\ sec^{-1}$
Kn	Knudsen number
m	particle mass, gm
$N(v_i,t)$	number concentration, cm^{-3}
N_∞	gas phase concentration of condensible species, cm^{-3}
N_+	equilibrium gas phase concentration of condensible species, cm^{-3}
$n(v,t)$	number distribution function, $cm^{-3}\ \mu m^{-3}$
R_{ij}	net agglomeration rate of particle types i and j, $sec^{-1}\ cm^{-3}$
S_0	homogeneous particle generation rate, $sec^{-1}\ cm^{-3}$
S_1	homogeneous particle removal rate, $sec^{-1}\ cm^{-3}$
T	temperature, deg

t	time, sec
v	particle volume, μm^3
v_i	particle volume of a particle consisting of i monomers, μm^3

Greek Letters

$\bar{\alpha}$	fraction of the total flux of monomer entering the continuous regime by condensation
β	agglomeration coefficient, $cm^3\ sec^{-1}$
γ	reaction order
η	viscosity, poise
λ	mean free path, μm
ξ	net nucleation rate divided by the net condensation rate of particles in the discrete regime
ρ	density, $gm\ cm^{-3}$
σ	surface tension, $dyne\ cm^{-1}$

Subscripts

a	aerosol particle
c	cluster
cond	condensation
m	monomer
m-cond	monomer condensation
m-nuc	monomer nucleation
nuc	nucleation

REFERENCES

1. Chu, K. J. and Seinfeld, J. H., "Formulation and Initial Application of a Dynamic Model for Urban Aerosols," Atmos. Environ. 9, 375 (1975).

2. Chapman, S. and Cowling, T. G., "The Mathematical Theory of Non-Uniform Gases," p. 91. Cambridge Press, New York. 1964.

3. Fuchs, N. A., "The Mechanics of Aerosols," p. 290. Pergamon, New York, 1964.

4. Hidy, G. M. and Brock, J. R., "The Dynamics of Aerocolloidal Systems," pp. 298-299. Pergamon, Oxford, 1970.

5. Ramabhadran, T. E., Peterson, T. W., and Seinfeld, J. H., "Dynamics of Aerosol Coagulation and Condensation," A.I.Ch.E.J. 22, 840 (1976).

6. Fuchs, N. A. and Sutugin, A. G., in "Topics in Current Aerosol Research," (Hidy, G. M. and Brock, J. R., Eds.), Vol. 2, pp. 29-37. Pergamon, Oxford, 1971.

7. Heisler, S. L. and Friedlander, S. K., "Gas-to-Particle Conversion in Photochemical Smog," Atmos. Environ. 11, 156 (1977).

8. Peterson, T. W., "Aerosol Dynamics in an Urban Atmosphere," Ph.D. Thesis, California Institute of Technology, 1977.

9. Gelbard, F. and Seinfeld, J. H., "Exact Solution of the General Dynamic Equation for Aerosol Growth by Condensation," J. Colloid Interface Sci., in press.

10. Frenkel, J., "Kinetic Theory of Liquids," pp. 366-413. Dover, New York, 1955.

11. Zettlemoyer, A. C., (Ed.), "Nucleation." Marcel Dekker, New York, 1969.

12. Abraham, F. F., "Homogeneous Nucleation Theory." Academic, New York, 1974.

13. Thermo Systems Inc., Operating and Service Manual, Model 3030 Electrical Aerosol Analyzer, 500 Carigan Road, St. Paul, Minn. 55112.

14. Instrument Instruction Manual for Condensation Nuclei Monitor, Model Rich 100, Environment One Corp., 2773 Balltown Road, Schenectady, New York.

15. Evans, G. R. and Roddy, A.F ., "The Condensation Nuclei Formed in Polluted Air by Ultraviolet Radiation Whose Wavelengths are Longer than 2900 Å," Proc. 7-th Int'l. Conf. Condensation and Ice Nuclei, Prague and Vienna, p. 369 (1969).

16. Luria, M., Olszyna, K. J., De Pena, R. G., and Heicklen, J., "Kinetics of Particle Growth - V: Particle Formation in the Photolysis of SO_2-Allene Mixtures," J. Aerosol Sci. 5, 435 (1974).

17. Sitarski, M. and Seinfeld, J. H., "Brownian Coagulation in the Transition Regime," J. Colloid Interface Sci. 61, 261 (1977).

18. Friedlander, S. K., "Smoke, Dust and Haze," pp. 27-31. Wiley, New York, 1977.

19. Millikan, R. A., "The General Law of Fall of a Small Spherical Body Through a Gas, and its Bearing Upon the Nature of Molecular Reflection from Surfaces," Phys. Rev. 22, 1 (1923).

20. Phillips, W. F., "Drag on a Small Sphere Moving Through a Gas," Phys. Fluids 18, 1089 (1975).

21. Fuchs, N. A., "The Mechanics of Aerosols," pp. 291-294. Pergamon, New York, 1964.

22. Kennard, E. H., "Kinetic Theory of Gases," pp. 195-196. McGraw-Hill, New York,1938.

23. Friedlander, S. K., "On the Particle Size Spectrum of a Condensing Vapor," Phys. Fluids 3, 643 (1960).

24. Hill, P. G., "Condensation of Water Vapour During Supersonic Expansion in Nozzles," J. Fluid Mech. 25, 593 (1966).

25. Beilke, S. and Gravenhorst, G., "Heterogeneous SO_2-Oxidation in the Droplet Phase," Atmos. Environ. 12, 231 (1978).

26. Liberti, A., "The Nature of Particulate Matter," Pure and Appl. Chem. 24, 631 (1970).

27. Novakov, T., Chang, S.G.,and Harker, A. B., "Sulfates as Pollution Particulates: Catalytic Formation on Carbon (Soot) Particles," Science 186, 259 (1974).

28. Judeikis,H.S. and Siegel, S., "Particle-Catalyzed Oxidation of Atmospheric Pollutants," Atmos. Environ. 7, 619 (1973).

29. Heisler, S. L., "Gas-to-Particle Conversion in Photochemical Smog: Growth Laws and Mechanisms for Organics," Ph.D. Thesis, California Institute of Technology, 1976.

30. Fuchs, N. A., "Evaporation and Droplet Growth in Gaseous Media," p. 8. Pergamon, Oxford, 1959.

31. Sahni, D. C., "The Effect of a Black Sphere on the Flux Distribution in an Infinite Moderator," J. Nucl. Eng. A/B 20, 915 (1966).

32. Drake, R. L., in "Topics in Current Aerosol Research," (Hidy, G. M. and Brock, J. R., Eds.), Vol. 3, pp. 201-376. Pergamon, Oxford, 1972.

33. Rice, C. L. and Whitehead, R., "The Theory of the Coagulation of Emulsions," J. Colloid Interface Sci. 23, 174 (1967).

34. McMurry, P. H., "On the Relationship Between Aerosol Dynamics and the Rate of Gas-to-Particle Conversion," Ph.D. Thesis, California Institute of Technology, 1977.

35. Courtney, W. G., "Non-Steady-State Nucleation," J. Chem. Phys. 36, 2009 (1962).

36. Hidy,G.M., "On the Theory of Non-Interacting Particles in Brownian Motion," J. Colloid Sci. 20, 123 (1965).

37. Mockros, L. F., Quon, J. E., and Hjelmfelt, A. T., "Coagulation of a Continuously Reinforced Aerosol," J. Colloid Interface Sci. 23, 90 (1967).

38. Takahashi, K. and Kasahara, M., "A Theoretical Study of the Equilibrium Particle Size Distribution of Aerosols," Atmos. Environ. 2, 441 (1968).

39. Suzuki, A., Ho, N. F. H., and Higuchi, W. I., "Prediction of the Particle Size Distribution Changes in Emulsions and Suspensions by Digital Computation," J. Colloid Interface Sci. 29, 552 (1969).

40. Abraham, F. F., "Multistate Kinetics in Non-Steady-State Nucleation: A Numerical Solution," J. Chem. Phys. 51, 1632 (1969).

41. Sutugin, A. G. and Fuchs, N. A., "Formation of Condensation Aerosols Under Rapidly Changing Environmental Conditions," Aerosol Sci. 1, 287 (1970).

42. Gillette, D. A., "A Study of Aging of Lead Aerosols - II," Atmos. Environ. 6, 451 (1972).

43. Yoshida, T., Okuyama, K., Kousaka, Y., and Kida, Y., "Change in Particle Size Distributions of Polydisperse Aerosols Undergoing Brownian Coagulation," J. Chem. Eng. of Japan 8, 317 (1975).

44. Bauer, S. H. and Frurip, D. J., "Homogeneous Nucleation in Metal Vapors," J. Phys. Chem. 81, 1015 (1977).

45. Hamill, P., Toon, O. B., and Kiang, C. S., "Microphysical Processes Affecting Stratospheric Aerosol Particles," J. Atmos. Sci. 34, 1104 (1977).

46. Golovin, A. M., "The Solution of the Coagulation Equation for Raindrops, Taking Condensation Into Account," Sov. Phys. Dokl. 8, 191 (1963).

47. Scott, W. T., "Analytic Studies of Cloud Droplet Coalescence," J. Atmos. Sci. 25, 54 (1968).

48. Brock, J. R., "On Size Distributions of Atmospheric Aerosols," Atmos. Environ. 5, 833 (1971).

49. Brock, J. R., "Condensational Growth of Atmospheric Aerosols," J. Colloid Interface Sci. 39, 32 (1972).

50. Drake, R. L., "The Scalar Transport Equation of Coalescence Theory: Moments and Kernels," J. Atmos. Sci. 29, 537 (1972).

51. Drake, R. L. and Wright, T. J., "The Scalar Transport Equation of Coalescence Theory: New Families of Exact Solutions," J. Atmos. Sci. 29, 548 (1972).

52. Peterson, T. W., Gelbard, F., and Seinfeld, J. H., "Dynamics of Source-Reinforced, Coagulating, and Condensation Aerosols," J. Colloid Interface Sci. 63, 426 (1978).

53. Mulholland, G. W., Lee, T. G., and Baum, H. R., "Coagulation of Aerosols with Broad Initial Size Distributions," J. Colloid Interface Sci. 62, 406 (1977).

54. Twomey, S., "Computation of Rain Formation by Coalescence," J. Atmos. Sci. 23, 405 (1966).

55. Spigler, P., Morgan, J. G., Greenfield, M. A., and Koontz, R. L., "Evaluation of the Equation that Governs the Coagulation of an Aerosol," Proc. 9-th AEC Air Cleaning Conf., pp. 626-646. Boston, Massachusetts (1966).

56. Berry, E. X., "Cloud Droplet Growth by Collection," J. Atmos. Sci. 24, 688 (1967).

57. Willis, E., Kerker, M., and Matijevic, E., "Effect of Brownian Coagulation Upon Light Scattering of Colloidal Dispersions of Narrow Size Distribution," J. Colloid Sci. 23, 182 (1967).

58. Huang, C. M., Kerker, M., and Matijevic, E., "The Effect of Brownian Coagulation, Gradient Coagulation, Turbulent Coagulation, and Wall Losses Upon the Particle Size Distribution of an Aerosol," J. Colloid Interface Sci. 33, 529 (1970).

59. Cohen, E. R. and Vaughan, E. U., "Approximate Solution of the Equations for Aerosol Agglomeration," J. Colloid Interface Sci. 35, 612 (1971).

60. Lindauer, G. C. and Castleman, A. W., "Behavior of Aerosols Undergoing Brownian Coagulation and Gravitational Settling in Closed Systems," Aerosol Sci. 2, 85 (1971).

61. Burgmeir, J. W., Blifford, I. H., and Gillette, D. A., "A Reinforced Coagulation-Sedimentation Aerosol Model," Water, Air and Soil Pollution 2, 97 (1973).

62. Walter, H., "Coagulation and Size Distribution of Condensation Aerosols," Aerosol Sci. 4, 1 (1973).

63. Wadden, R. A., Quon, J. E., and Hulburt, H. M., "A Model of a Growing Coagulating Aerosol," Atmos. Environ. 8, 1009 (1974).

64. Singh, P. N. and Ramkrishna, D., "Transient Solution of the Brownian Coagulation Equation by Problem-Specific Polynomials," J. Colloid Interface Sci. 53, 214 (1975).

65. Middleton, P. and Brock, J., "Simulation of Aerosol Kinetics," J. Colloid Interface Sci. 54, 249 (1976).

66. Gelbard, F. and Seinfeld, J. H., "Numerical Solution of the Dynamic Equation for Particulate Systems," J. Comp. Phys. (1978) in press.

Chapter III

EXACT SOLUTION OF THE GENERAL DYNAMIC EQUATION FOR AEROSOL GROWTH BY CONDENSATION

ABSTRACT

Exact solution of the General Dynamic Equation for aerosol growth by condensation is obtained in dimensionless form for particle growth occurring by gas phase diffusion-, surface reaction- and volume reaction-controlled processes. Analytic expressions for the size distribution of an aerosol undergoing growth by gas-to-particle conversion and influenced by homogeneous source and removal processes are presented over the complete range of particle Knudsen number, Kn. Numerical results are presented to show the effect of the different growth mechanisms on size distribution dynamics.

1. INTRODUCTION

The dynamic behavior of a spatially homogeneous aerosol undergoing growth by condensation and coagulation is described by the General Dynamic Equation,

$$\frac{\partial n_D(D,t)}{\partial t} = \frac{-\partial[I_D(D,t)n_D(D,t)]}{\partial D}$$

$$+ D^2 \int_{D_a}^{D/2^{1/3}} \frac{\beta_D[(D^3-\tilde{D}^3)^{1/3},\tilde{D}]n_D[(D^3-\tilde{D}^3)^{1/3},t]n_D(\tilde{D},t)d\tilde{D}}{(D^3-\tilde{D}^3)^{2/3}}$$

$$- n_D(D,t) \int_{D_a}^{D_b} \beta_D(D,\tilde{D})n_D(\tilde{D},t)d\tilde{D}$$

$$+ S_D[n_D(D,t),D,t] \qquad [1]$$

where $n_D(D,t)$ is the size distribution density function at time t, D is the particle diameter, $\beta_D(D,\tilde{D})$ is the coagulation coefficient for particles with diameters D and $\tilde{D}$, $I_D(D,t) = dD/dt$, the rate of particle growth from condensation, $S_D[n_D(D,t), D,t]$ represents the net influx of particles in the size range [D, D+dD] from all homogeneous sources and sinks, and D_b and D_a are the upper and lower bounds of the size domain, respectively.

Although no exact solutions of Eq. [1] for physically realistic initial conditions and coefficients of coagulation and condensation have

been obtained, considerable progress in investigating the nature of solutions has been made by simplifying both the initial condition and the coefficients to the point that an exact solution can be obtained. If only the coagulation integrals are retained on the right hand side of Eq. [1], the so-called Coagulation Equation results which has been solved for simplified forms of β_D and initial conditions (1,2,3). If particle growth, sources and sinks are present, exact solutions for simplified forms of Eq. [1] have also been obtained (4,5). However, to solve the General Dynamic Equation, Eq. [1] for realistic coagulation and condensation coefficients, β_D and I_D, and initial conditions, numerical routines are required (6,7). Much of the difficulty in solving Eq. [1] either analytically or numerically is due to the coagulation integrals. For cases in which coagulation can be neglected, exact solutions of Eq. [1] have been reported for simplified forms of $I_D(D,t)$ (8,9).

The primary object of this chapter is to obtain exact solutions to Eq. [1] for situations in which coagulation can be neglected relative to the other phenomena influencing the size distribution. In particular, we will derive exact solutions to,

$$\frac{\partial n_D(D,t)}{\partial t} = - \frac{\partial}{\partial D} [I_D(D,t) n_D(D,t)] + S_D[n_D(D,t),D,t] \qquad [2]$$

for physically realistic forms of $I_D(D,t)$ and $S_D[n_D(D,t),D,t]$ for atmospheric aerosols. Previously, the only solutions to Eq. [2] available have been based on simplified forms of I_D and S_D (8,9). Expressions,

or growth laws, for $I_D(D,t)$ based on diffusion and surface and volume reactions are presented, i.e. we consider the particle growth to occur as a result of either gas-phase diffusion of condensing species, a surface reaction-controlled mechanism, or a particle volume reaction-controlled mechanism.

We begin by presenting the dimensionless forms of the growth laws, $I_D(D,t)$, for the three particle growth phenomena. Then, Eq. [1] is cast into dimensionless form for Brownian coagulation and for the three forms of $I_D(D,t)$. Next, for those situations in which coagulation can be neglected, Eq. [2] is solved in dimensionless form for arbitrary initial and boundary conditions, arbitrary sources and first-order removal mechanisms, and for the forms of $I_D(D,t)$ representing growth by diffusion-, surface-, and volume-controlled mechanisms. The nature of these solutions is discussed in detail, including aspects such as the time needed for the size distribution in a domain to become independent of the initial conditions and the role of the Kelvin effect in diffusion-controlled growth.

As a consequence of the solutions presented here, exact analytical expressions for the size distribution of an atmospheric aerosol undergoing growth by gas-to-particle conversion and influenced by homogeneous source and removal processes are now available.

2. AEROSOL KINETIC COEFFICIENTS

In this section we will present dimensionless forms of the growth law, $I_D(D,t)$, based on diffusion-, surface reaction-, and volume reaction-controlled mechanisms. We also introduce a dimensionless form of the coagulation coefficient $\beta_D(D,\tilde{D})$ for Brownian coagulation.

For a particle in a fluid the characteristic length scale that determines many of the transport properties of the particle is the mean free path of the medium λ. Thus, all aerosol kinetic coefficients will be expressed in terms of the Knudsen number, defined as $Kn = 2\lambda/D$.

2.1 Particle Growth

The dimensionless form of the growth laws given in Tables 2 and 3 of Chapter II are summarized in Table 1 of this chapter. The dimensionless groups C_i and E_i, $(i=0,1,2)$ are the ratios of characteristic rates of diffusion to the rate of reaction. For reaction-limited growth, which depends on the concentration of the reactant, the maximum growth rate occurs when the reaction rate is so fast relative to diffusion that all of the reactant that diffuses to the particle reacts immediately. Hence, the maximum growth rate must be given by the diffusion-limited growth law with no particle vapor pressure. Therefore, as C_i or $E_i \to 0$, $(i=0,1,2)$ for $\gamma = 1/2$, 1 and 2, $I_D(D,t)$

Table 1. Dimensionless Growth Laws, $I_D(D,t) = 2\phi\bar{I}(Kn)^*$

Controlling Mechanism	ϕ	$\bar{I}(Kn)$
Gas phase diffusion	$\frac{N_\infty v_1 \mathscr{D}}{\lambda}$	$[1-\bar{D}\exp(BKn)]f$
Surface reaction		
zeroth order ($\gamma=0$)	$v_1 k_s$	1
half order ($\gamma=1/2$)	$\frac{N_\infty v_1 \mathscr{D}}{\lambda}$	$\frac{\left[2+2C_0\exp(BKn)f^2-2(1+2C_0\exp(BKn)f^2)^{1/2}\right]^{1/2}}{C_0\exp(BKn)f}$
first order ($\gamma=1$)	$\frac{N_\infty v_1 \mathscr{D}}{\lambda}$	$\frac{Kn+\alpha Kn^2}{aKn^2+bKn+1+C_1(Kn+\alpha Kn^2)\exp(BKn)}$
second order ($\gamma=2$)	$\frac{N_\infty v_1 \mathscr{D}}{\lambda}$	$C_2\exp(2BKn)f^2\left[-1+(1+1/(C_2 f\exp(2BKn)))^{1/2}\right]^2$
Volume reaction		
zeroth order ($\gamma=0$)	$\frac{v_1 k_v \lambda}{3}$	Kn^{-1}

Table 1. Dimensionless Growth Laws, $I_D(D,t) = 2\phi\bar{I}(Kn)$* (Continued)

Controlling Mechanism	ϕ	$\bar{I}(Kn)$
half order (γ=1/2)	$\frac{N_\infty v_1 \mathscr{D}}{\lambda}$	$\frac{\left[2+2E_0\exp(BKn)f^2Kn^2-2(1+2E_0\exp(BKn)f^2Kn^2)^{1/2}\right]^{1/2}}{E_0\exp(BKn)fKn^2}$
first order (γ=1)	$\frac{N_\infty v_1 \mathscr{D}}{\lambda}$	$\frac{Kn+\alpha Kn^2}{aKn^2+bKn+1+E_1(Kn^2+\alpha Kn^3)\exp(BKn)}$
second order (γ=2)	$\frac{N_\infty v_1 \mathscr{D}}{\lambda}$	$E_2 Knf^2\exp(2BKn)\left[-1+(1+1/(E_2 f\exp(2BKn)Kn))^{1/2}\right]^2$

*$B = \frac{2\sigma v_1}{\lambda kT}$, $\bar{D} = \frac{N_+}{N_\infty}$, $f = (Kn+\alpha Kn^2)/(aKn^2+bKn+1)$

$C_0 = \frac{2H_s \mathscr{D}^2 N_\infty}{\lambda^2 k_s^2}$ $\quad C_1 = \frac{H_s \mathscr{D}}{k_s \lambda}$ $\quad C_2 = \frac{H_s^2 \mathscr{D}}{4k_s N_\infty \lambda}$

$E_0 = \frac{18H_v \mathscr{D}^2 N_\infty}{k_v^2 \lambda^4}$ $\quad E_1 = \frac{3H_v \mathscr{D}}{k_v \lambda^2}$ $\quad E_2 = \frac{3H_v^2 \mathscr{D}}{4N_\infty k_v \lambda^2}$

approaches the gas phase diffusion-limited growth law with $\bar{D} = 0$.* Conversely, as C_i or $E_i \to \infty$, the reaction rate is much slower than the diffusion rate. Since growth is reaction limited, $I_D \to 0$ in this case. For zeroth order kinetics the reaction rate is independent of the reactant concentration. In that case the growth rate is not constrained by diffusion.

2.2 Coagulation

Existing expressions for Brownian coagulation coefficients are tabulated in the literature (10). Because Fuchs' formula (11) has the correct limiting form for large and small values of Kn, it will be used here. In dimensionless form $\beta_D(D_i,D_j)n/kT$ is equal to,

$$\frac{\beta_{Kn}(Kn_i,Kn_j)n}{kT} = \frac{2Q(p_iKn_i+p_jKn_j)/3}{\frac{Q}{Q+(H_i^2+H_j^2)^{1/2}} + \frac{\pi A(p_iKn_i+p_jKn_j)}{2Q(Kn_i^3+Kn_j^3)^{1/2}}} \qquad [3]$$

where

$$Q = \frac{1}{Kn_i} + \frac{1}{Kn_j} \qquad [4]$$

---

*If however, the molecular volume of the product is greater than that for the diffusing species, reaction-limited growth for $\gamma>0$ may exceed the growth rate for diffusion-limited growth.

$$H_i = \frac{Kn_i^{3/2}}{6Ap_i}\left[\left(\frac{2}{Kn_i} + \frac{Ap_i}{Kn_i^{1/2}}\right)^3 - \left(\frac{4}{Kn_i^2} + \frac{A^2p_i^2}{Kn_i}\right)^{3/2}\right] - \frac{2}{Kn_i} \qquad [5]$$

$$A = \left[\frac{8\rho kT}{27\pi^2\eta^2\lambda}\right]^{1/2} \qquad [6]$$

$$p_i = \begin{cases} 1 + Kn_i[1.257 + 0.4\exp(-1.1/Kn_i)] & \text{(Millikan)} \quad [7] \\ \dfrac{5+4Kn_i+6Kn_i^2+18Kn_i^3}{5-Kn_i+(8+\pi)Kn_i^2} & \text{(Phillips)} \quad [8] \end{cases}$$

$$Kn_i = 2\lambda/D_i \qquad [9]$$

and where ρ is the particle density, η is the viscosity of the suspending medium, and T is the absolute temperature. Since there are two existing slip corrections to the particle diffusivity, Eq. [3] is written such that either Millikan's (12) or Phillips' (13) correction can be used, as given in Eqs. [6] and [7], respectively. Notice that the only parameter which is dependent on the physical properties of the medium or the particle is A. For typical atmospheric aerosols, A is approximately 0.075. In Figure 1, $\beta_{Kn}n/kT$ is shown, using Eq. [8] (using Eq. [7] similar results are obtained). The set of solid lines correspond to

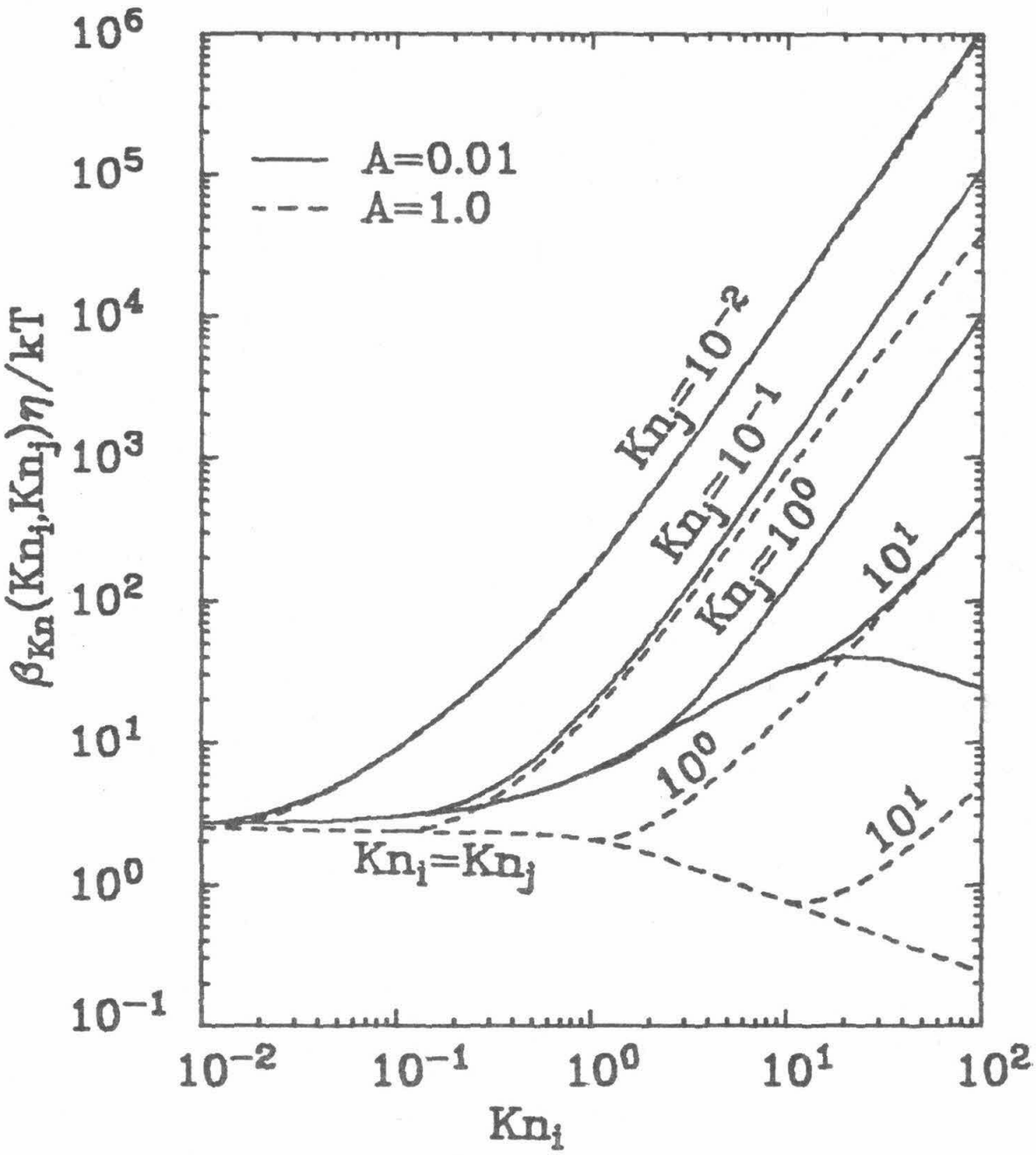

Figure 1

Dimensionless Brownian coagulation coefficient, using Fuchs-Phillips formula, $A = (8\rho kT/27\pi^2\eta^2\lambda)^{1/2}$.

A =0.01 and the set of broken lines correspond to A = 1.0. Since β_{Kn} is a symmetric function of its arguments, only values of $Kn_j \leq Kn_i$ are shown. The lower envelope corresponds to the coagulation coefficient of two particles with identical Knudsen numbers. In the continuum regime, where $Kn_j \ll 1$, β_{Kn} is proportional to kT/η, therefore Figure 1 shows that $\beta_{Kn}\eta/kT$ is insensitive to large variations in A in this regime. However, in the free molecule regime, where $Kn_i \gg 1$ and $Kn_j \gg 1$, $\beta_{Kn}\eta/kT$ is very sensitive to variations in A.

2.3 Sources and Sinks

For a typical atmospheric aerosol there are many sources of particles with varying production rates and sizes. For the solutions presented here to be as general as possible, Eq. [2] will be solved for an arbitrary source term $S_0(D,t)$.

Particle losses are generally represented as a first order removal process, and a review of the so-called "wall loss constant" is available in the literature (14). Since the exact functional form of the wall loss constant varies with the particular system we will assume the general removal term, $S_1(D,t)n_D(D,t)$.

3. NONDIMENSIONALIZATION AND SOLUTION OF THE GENERAL DYNAMIC EQUATION

To nondimensionalize Eq. [1] characteristic length and time scales must be chosen. As discussed previously, the mean free path of the medium, λ, is the appropriate length scale. The characteristic time scale can be based on coagulation, growth, source or sink mechanisms. For the solutions given, growth will always be present, and, since the mechanism for transport to the particle is diffusion, $\lambda^2/\mathscr{D}$ can be chosen as the characteristic time scale. Defining a dimensionless time, $\tau = \mathscr{D}t/\lambda^2$, and substituting into Eq. [1] results in the dimensionless form of the General Dynamic Equation,

$$\frac{\partial \bar{n}(Kn,\tau)}{\partial \tau} = \frac{\Lambda \zeta(\tau) \partial [\bar{n}(Kn,\tau) Kn^2 \bar{I}]}{\partial Kn}$$

$$+ \xi \int_{Kn_b}^{2^{1/3}Kn} \bar{\beta}(Kn'',Kn')\bar{n}(Kn'',\tau)\bar{n}(Kn',\tau)\left(\frac{Kn''}{Kn}\right)^4 dKn'$$

$$- \xi \int_{Kn_b}^{Kn_a} \bar{\beta}(Kn,Kn')\bar{n}(Kn',\tau)n(Kn,\tau)\ dKn' -$$

$$- \bar{S}_0(Kn,\tau) - \bar{S}_1(Kn,\tau)\bar{n}(Kn,\tau) \qquad [10]$$

where

$$\bar{n}(Kn,\tau) = \frac{-2\lambda n(2\lambda/Kn,\tau\lambda^2/\mathscr{D})}{N_\infty Kn^2} \qquad [11]$$

$$\bar{\beta}(Kn,Kn') = \beta_{Kn}(Kn,Kn')\eta/kT \qquad [12]$$

$$Kn'' = \left[\frac{1}{1/Kn^3 - 1/Kn'^3}\right]^{1/3} \qquad [13]$$

$$\bar{S}_0(Kn,\tau) = \frac{2S_0(2\lambda/Kn,\tau\lambda^2/\mathscr{D})\lambda^3}{\mathscr{D}N_\infty Kn^2} \qquad [14]$$

$$\bar{S}_1(Kn,\tau) = \frac{S_1(2\lambda/Kn,\tau\lambda^2/\mathscr{D})\lambda^2}{\mathscr{D}} \qquad [15]$$

$$\Lambda = \frac{\lambda\phi}{\mathscr{D}} \qquad \xi = \frac{N_\infty kT\lambda^2}{\mathscr{D}\eta} \qquad [16]$$

$$Kn_a = 2\lambda/D_b \qquad Kn_b = 2\lambda/D_a \qquad [17]$$

To account for any temporal variations in I_D,$\zeta(\tau)$ is introduced as an arbitrary positive function of τ. Notice that the definition of Λ will vary depending on the specific growth mechanism, and ϕ is defined in Table 1 for each mechanism.

At relatively small aerosol number densities, such as those frequently prevalent in ambient atmospheres, coagulation can often be neglected relative to condensation in influencing the temporal variations in $\bar{n}$. Brock (8) has termed particles with radii greater than 0.1μm as being in the "non-coagulating" size range. Thus, if other processes dominate one might be able to neglect coagulation. Even in situations in which coagulation cannot be neglected the pure condensation solution is useful to assess the effect of condensation alone on the distribution.

Neglecting the coagulation integrals in Eq. [10], we obtain

$$\frac{\partial \bar{n}(Kn,\tau)}{\partial \tau} = \Lambda\zeta(\tau)\frac{\partial}{\partial Kn}\left[\bar{n}(Kn,\tau)Kn^2\bar{I}\right] - \bar{S}_0(Kn,\tau) - \bar{S}_1(Kn,\tau)\bar{n}(Kn,\tau) \quad [18]$$

The characteristic equations for Eq. [18] are

$$\frac{dKn}{d\tau} = -\Lambda Kn^2\zeta(\tau)\bar{I} \quad [19]$$

$$\frac{d\bar{n}(Kn,\tau)}{d\tau} = \left[\Lambda\zeta(\tau)\frac{d(Kn^2\bar{I})}{dKn} - \bar{S}_1(Kn,\tau)\right]\bar{n}(Kn,\tau) - \bar{S}_0(Kn,\tau) \quad [20]$$

We note that Eq. [19] is simply the dimensionless growth law. Integrating Eq. [20] on the characteristic we have

$$\bar{n}(Kn,\tau) = \frac{-\int \bar{S}_0(Kn,\tau)Kn^2\bar{I}\exp[\int \bar{S}_1(Kn,\tau)d\tau]d\tau+C}{Kn^2\bar{I}\exp[\int \bar{S}_1(Kn,\tau)d\tau]} \qquad [21]$$

where C is determined from the initial or boundary condition, and Kn is given by Eq. [19]. Integrating Eq. [19] for some of the growth laws given in Table 1, we have the characteristic growth curves as given in Table 2.

For gas phase diffusion-limited growth a two term expansion of the exponential term for BKn<<1 is required, as originally pointed out by Davies (15), however if $\bar{D} = 0$ or $B = 0$, entry 1 of Table 2 is exact. For all other solutions given in Table 2 no approximations were required to evaluate the integral. Physically, the characteristics given in Table 2 represent the change in Knudsen number of a particle as a function of $\Lambda \int_{\tau_0}^{\tau} \zeta(\bar{\tau})d\bar{\tau}$. Given the Knudsen number, Kn_0 of a particle at $\tau_0 = 0$, the dimensionless time for a particle to grow to $Kn_1 < Kn_0$, can be determined for different mechanisms from Table 2.

Table 2. Characteristic Growth Curves*

Controlling Mechanism	$\int \frac{dKn}{Kn^2 \bar{I}(Kn)}$
Gas phase diffusion	$\psi_1 \ell n\ Kn + \psi_2 Kn^{-1} + \psi_3 Kn^{-2}$ $+ \psi_4 \ell n(1+\alpha Kn) + \psi_5 \ell n(1-\bar{D}-\bar{D}BKn)$
Surface reaction	
zeroth order ($\gamma=0$)	$-Kn^{-1}$
first order ($\gamma=1$)	$\frac{\alpha-b}{Kn} - \frac{1}{2} Kn^{-2} + (\alpha^2-b\alpha+a)\, \ell n\left(\frac{Kn}{1+\alpha Kn}\right)$ $-C_1 Kn^{-1} e^{BKn} + C_1 B \left[\ell n\ Kn + \sum_{j=1}^{\infty} \frac{(BKn)^j}{jj!}\right]$
Volume reaction	
zeroth order ($\gamma=0$)	$\ell n\ Kn$
first order ($\gamma=1$)	$\frac{\alpha-b}{Kn} - \frac{1}{2} Kn^{-2} + (\alpha^2-b\alpha+a)\, \ell n\left(\frac{Kn}{1+\alpha Kn}\right)$ $+ E_1 \left[\ell n\ Kn + \sum_{j=1}^{\infty} \frac{(BKn)^j}{jj!}\right]$

*$\psi_1 = \frac{[\bar{D}B+\alpha(\bar{D}-1)][\bar{D}B+b(1-\bar{D})]+(1-\bar{D})^2(\alpha^2+a)}{(1-\bar{D})^3}$ $\quad \psi_2 = \frac{(1-\bar{D})(\alpha-b)-\bar{D}B}{(1-\bar{D})^2}$

$\psi_3 = \frac{1}{2(\bar{D}-1)}$ $\quad \psi_4 = \frac{\alpha(a-b\alpha+\alpha^2)}{\alpha(\bar{D}-1)-\bar{D}B}$

$\psi_5 = \frac{\bar{D}B\{\bar{D}B[b(\bar{D}-1)-\bar{D}B]-a(\bar{D}-1)^2\}}{(1-\bar{D})^3[\bar{D}B+\alpha(1-\bar{D})]}$

4. CHARACTERISTIC GROWTH CURVES

In Figure 2 the characteristic growth curves for diffusion-limited growth, using the Fuchs and Sutugin coefficients, $\bar{D} = 0$, $\zeta(\tau) = 1$, and $Kn_b = 100$ are shown. The solid line characteristic originating from $Kn = Kn_b$ and $\Lambda\tau = 0$ divides the $\Lambda\tau$ - Kn plane into two major regions, and it will be called the major characteristic. The broken line characteristics all originate from the Kn axis, hence the solution $\bar{n}(Kn,\tau)$, below the major characteristic is determined from the initial condition $\bar{n}(Kn,0)$. The dot-dashed characteristics all originate from the $\Lambda\tau$ axis, hence $\bar{n}(Kn,\tau)$ above the major characteristic is determined from the boundary condition. Since the lower set of characteristics is a plot of entry 1 of Table 2, one can trace the growth of a particle as a function of dimensionless time. Note that the smaller particles that have large Knudsen numbers grow relatively fast, and hence their Knudsen numbers decrease with time. For all mechanisms, given a domain $[Kn_a, Kn_b]$, the dimensionless time required for the solution in that domain to be independent of the initial conditions is given by the intersection of the major characteristic with the line $Kn = Kn_a$.

For positive values of $\bar{D}$, a critical particle size, given by

$$Kn_{crit} = - \frac{\ell n(\bar{D})}{B} \qquad [22]$$

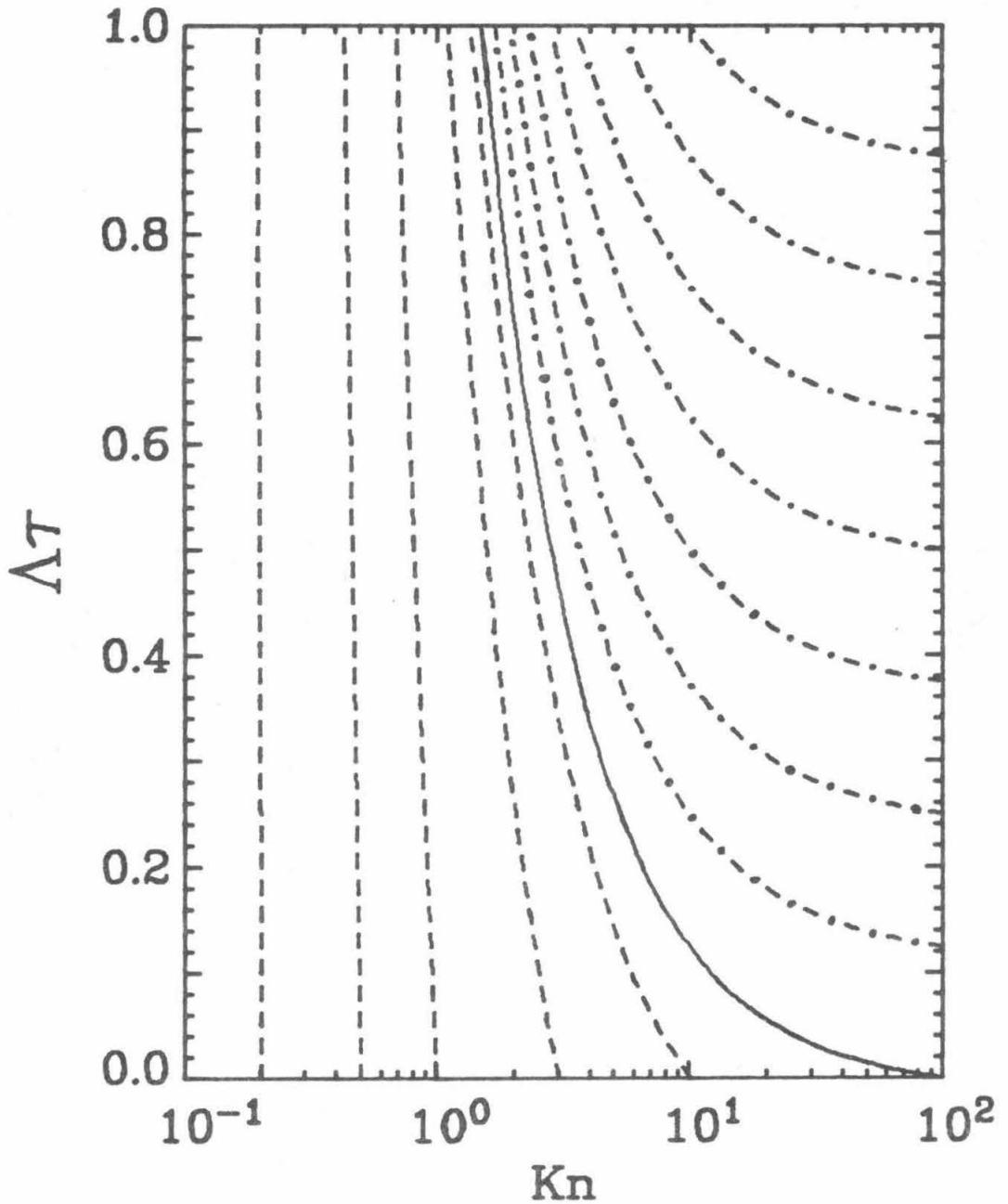

Figure 2

Characteristic growth curves for diffusion-limited growth, $\bar{D} = 0$, $a = 1.33$, $b = 1.71$, and $\alpha = 1.0$.

exists such that no growth occurs, i.e. $dKn/d\tau = 0$. For $Kn > Kn_{crit}$ the particle vaporizes due to the Kelvin effect, and for $Kn < Kn_{crit}$ the particle grows. Integrating entry 1 in Table 1 numerically for $\bar{D} = 0.1$ and $B = 0.1$, we obtain the rapid vaporization of particles with $Kn > Kn_{crit}$ in Figure 3. Note that in the region to the right the major characteristic, $\bar{n}(Kn,\tau)$ can be determined either from the boundary condition at $Kn_b = 1000$ or from the initial condition, but not from both conditions. Also note that due to the exponential term, Figure 3 shows that the time scale for vaporization is very short compared to growth as given in Figure 2.

Figures 4 and 5 show the characteristic growth curves for first order surface reaction- and volume reaction-limited growth, respectively. In these plots $B = 0.01$ and a,b and α are for the Fuchs and Sutugin coefficients. The solid lines correspond to maximum growth rate, that is $C_1 = 0$ for surface reaction and $E_1 = 0$ for volume reaction. As C_1 increases to 2 (as given by the broken lines) and 10 (as given by the dot-dashed lines), the growth rate decreases. Similarly, as E_1 increases from 0.2 (as given by the broken lines) and 0.6 (as given by the dot-dashed lines), the growth rate decreases.

For zeroth order kinetics the particle growth rate is independent of the concentration of reactant; therefore the growth rate is not limited by mass transfer, as in the case of first order kinetics. Using the Fuchs and Sutugin coefficients, the maximum value of $\bar{I}$ is less than 1. Therefore, the dimensionless growth rate for surface reactions and zeroth

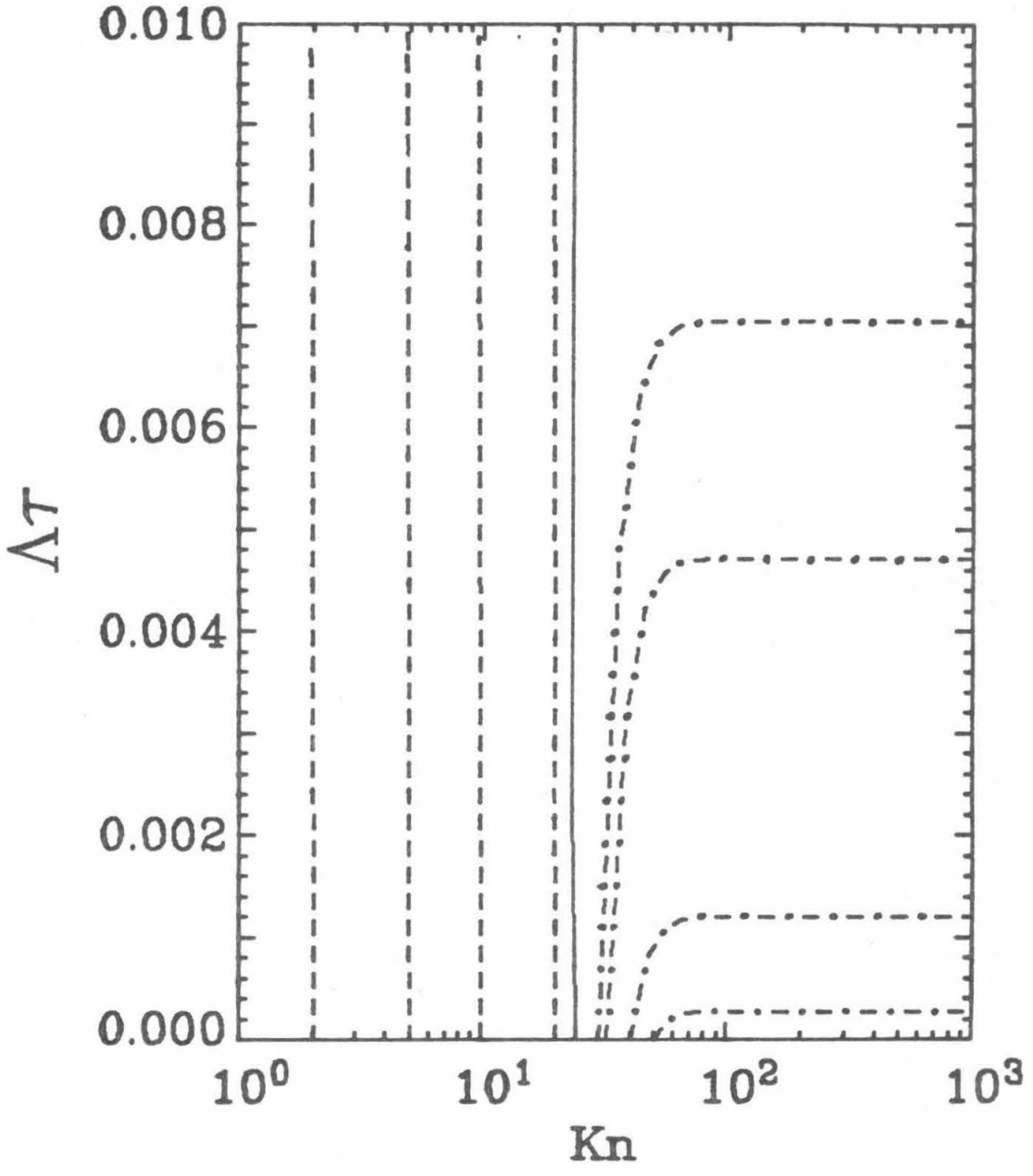

Figure 3

Characteristic growth curves for diffusion-limited growth, B = 0.1, $\bar{D}$ = 0.1, a = 1.33, b = 1.71, α = 1.0 and $Kn_{crit} \approx 23$.

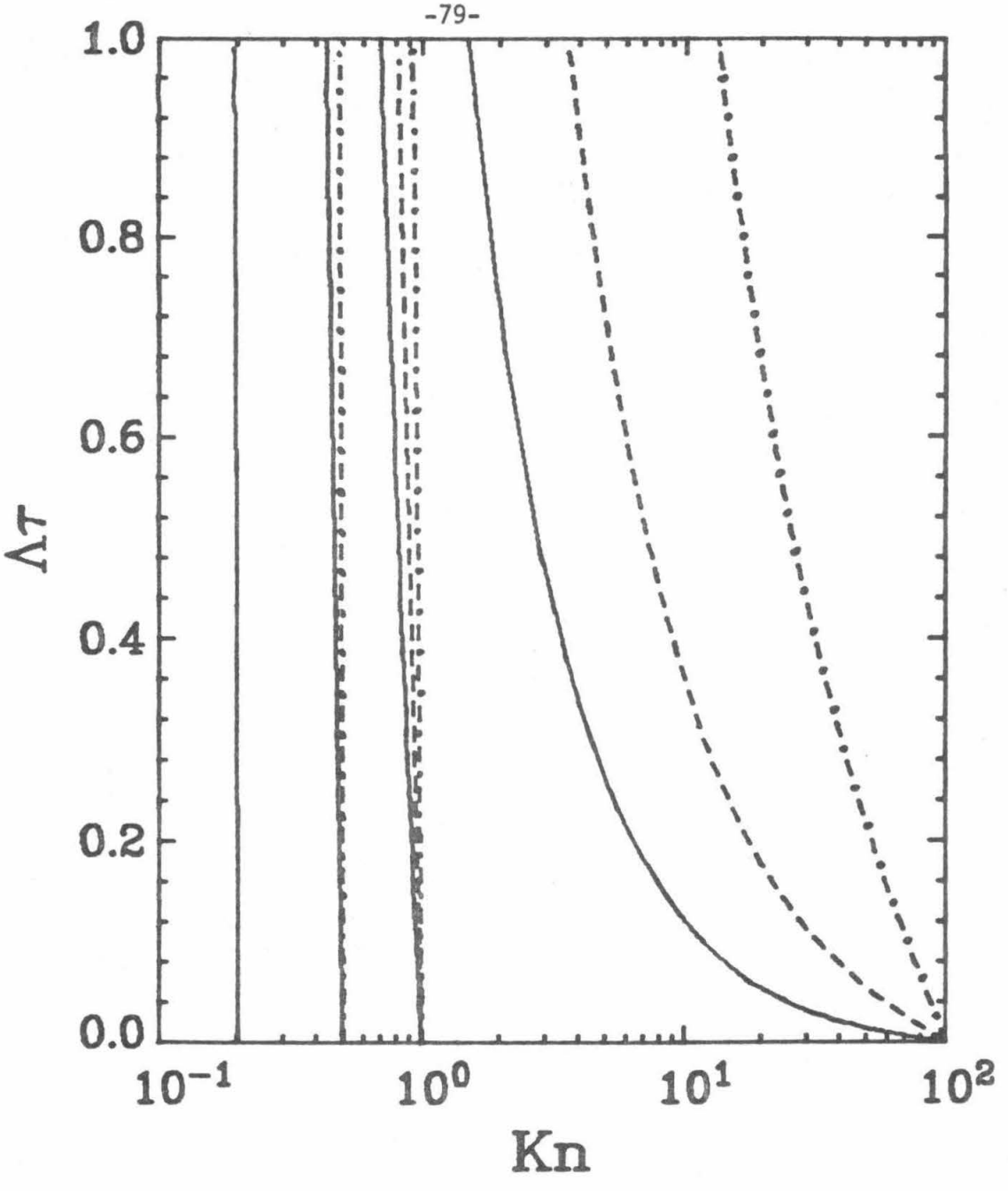

Figure 4

Characteristic growth curves for first order surface reaction-limited growth, —— C_1= 0, -- C_1= 2, — · — C_1= 10, B = 0.01, a = 1.33, b = 1.71, and α = 1.0.

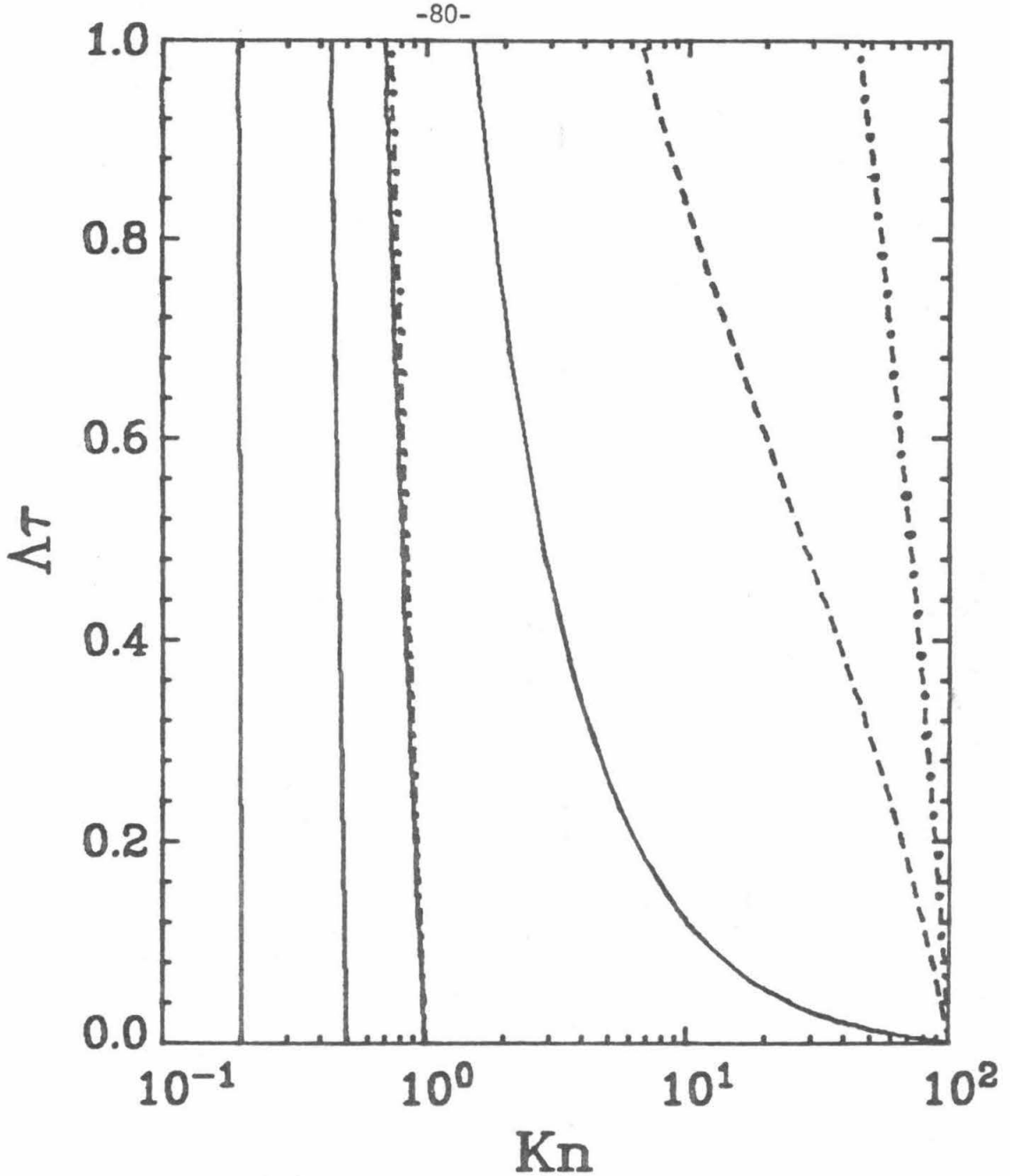

Figure 5

Characteristic growth curves for first order volume reaction-limited growth, —— $E_1 = 0$, -- $E_1 = 0.2$, —·— $E_1 = 0.6$, $B = 0.01$, $a = 1.33$, $b = 1.71$, and $\alpha = 1.0$.

order kinetics is always greater than diffusion-limited growth. For zeroth order volume reaction-limited growth, $\bar{I} \to 0$ as $Kn \to \infty$, and $\bar{I} \to \infty$ as $Kn \to 0$, therefore large particles will grow faster than small particles. Figure 6 shows the characteristic growth curves for diffusion-limited growth as solid lines, zeroth order surface reaction-limited growth as broken lines, and zeroth order volume reaction limited growth as dot-dashed lines. Notice that for large values of Kn, particle growth by volume reaction is slowest, but for small values of Kn, volume reaction is the fastest growth rate.

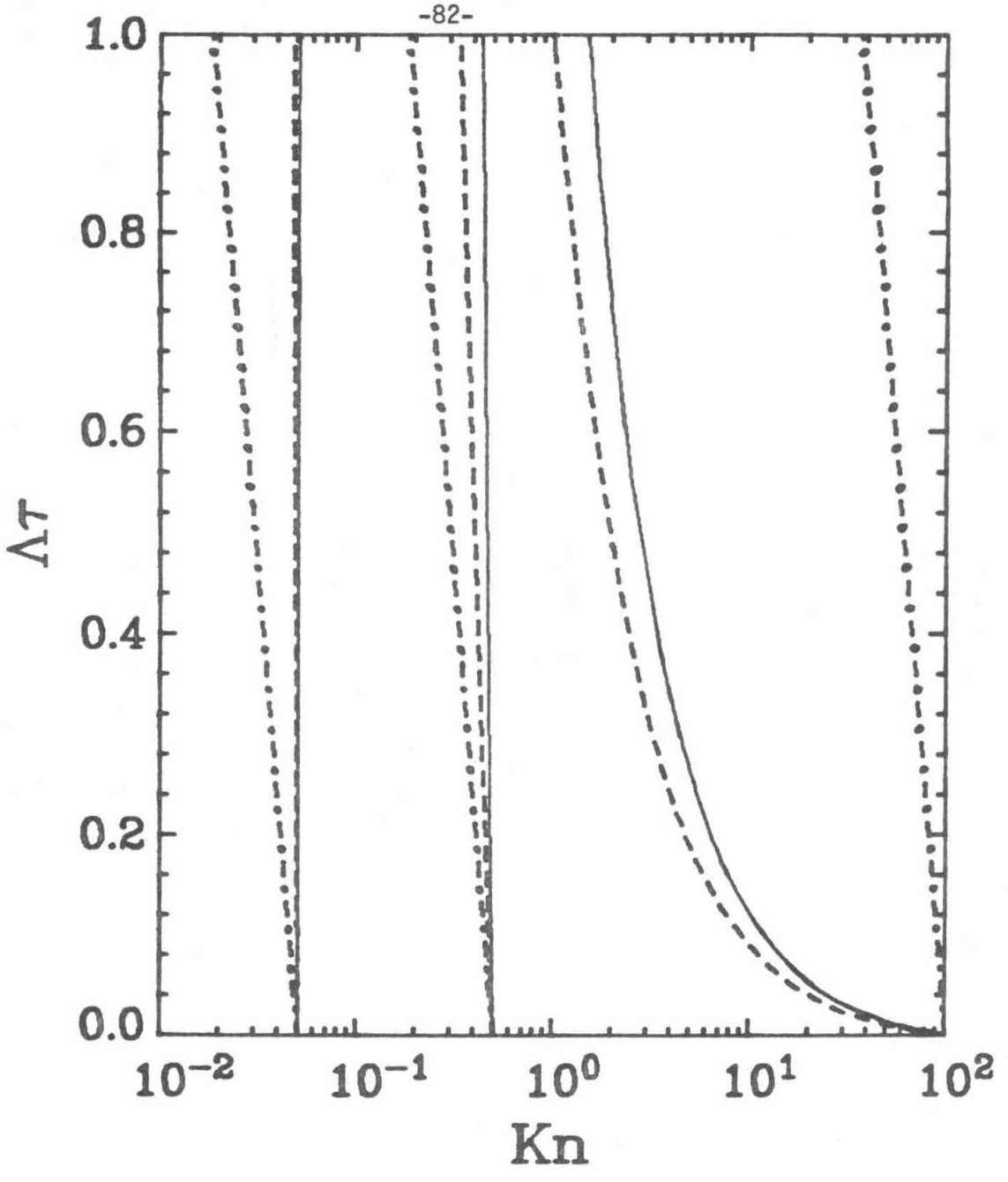

Figure 6

Characteristic growth curves for diffusion-limited growth (solid lines), zeroth order surface reaction-limited growth (broken lines), and zeroth order volume reaction-limited growth (dot-dashed lines).

5. SIZE DISTRIBUTION DYNAMICS

A common situation is $\bar{S}_1$ constant, $\bar{S}_0 = 0$ and $\zeta(\tau) = 1$. Then $\bar{n}(Kn,\tau)$ along the characteristic is given by

$$\bar{n}(Kn,\tau) = \bar{n}(Kn_0,\tau_0) \frac{Kn_0^2 \bar{I}(Kn_0)}{Kn^2 \bar{I}(Kn)} \exp[-\bar{S}_1(\tau-\tau_0)] \qquad [23]$$

Although Eq. [23] is valid for any $\bar{I}$, we will demonstrate the simplicity of the solution for diffusion-limited growth with the Fuchs and Sutugin coefficients and $\bar{D} = 0$. To determine $\bar{n}(Kn,\tau)$ we find the point $(Kn,\Delta\tau)$ in Figure 2. If this point is below the major characteristic, we trace the characteristic that crosses the point $(Kn,\Delta\tau)$ back to $\Delta\tau = 0$. The intersection with the Kn axis determines Kn_0. Entering Figure 7 with Kn and Kn_0 we read off the values of $\bar{I}(Kn)$ and $\bar{I}(Kn_0)$ for a = 1.33 and b = 1.71. Since the initial condition $\bar{n}(Kn_0,0)$ is known, we merely substitute into Eq. [23] to determine $\bar{n}(Kn,\tau)$. If the point $(Kn,\Delta\tau)$ is above the major characteristic, we trace the characteristic that crosses the point $(Kn,\Delta\tau)$ back to $Kn = Kn_b$ to determine $\Delta\tau_0$. Then we enter Figure 7 with Kn and $Kn_0 = Kn_b$ and read off the values of $\bar{I}(Kn)$ and $\bar{I}(Kn_0)$ for a = 1.33 and b = 1.71. Since the boundary condition, $\bar{n}(Kn_b,\tau_0)$ is known, we substitute into Eq. [23] to determine $\bar{n}(Kn,\tau)$. For reaction-limited growth, plots of $\bar{I}$ are given in Figures 8 - 13. Although a more accurate numerical technique (as given in the appendix) can be used, the graphical technique is useful for quick estimates of the solution.

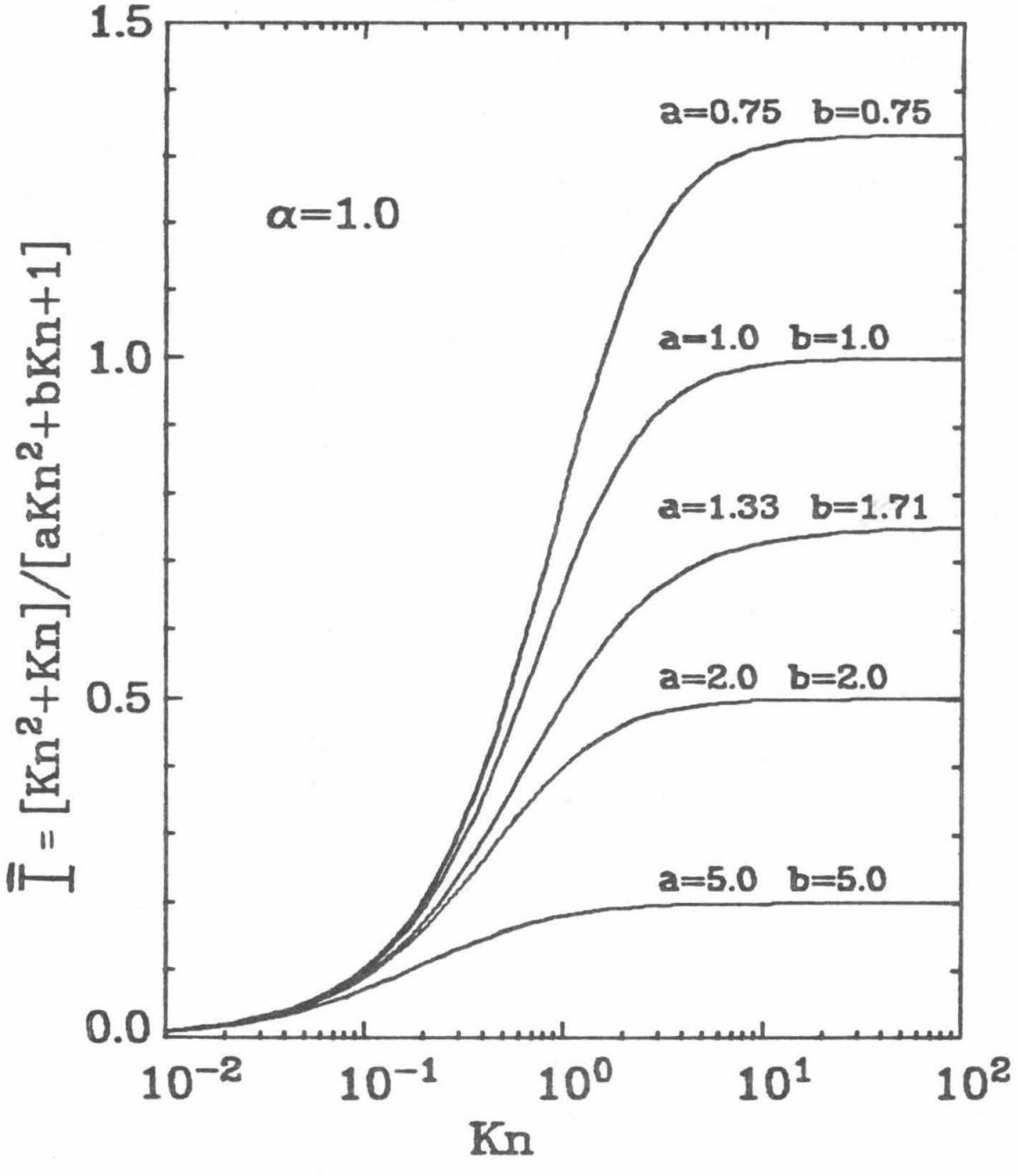

Figure 7

Dimensionless particle growth rates for diffusion-limited growth.

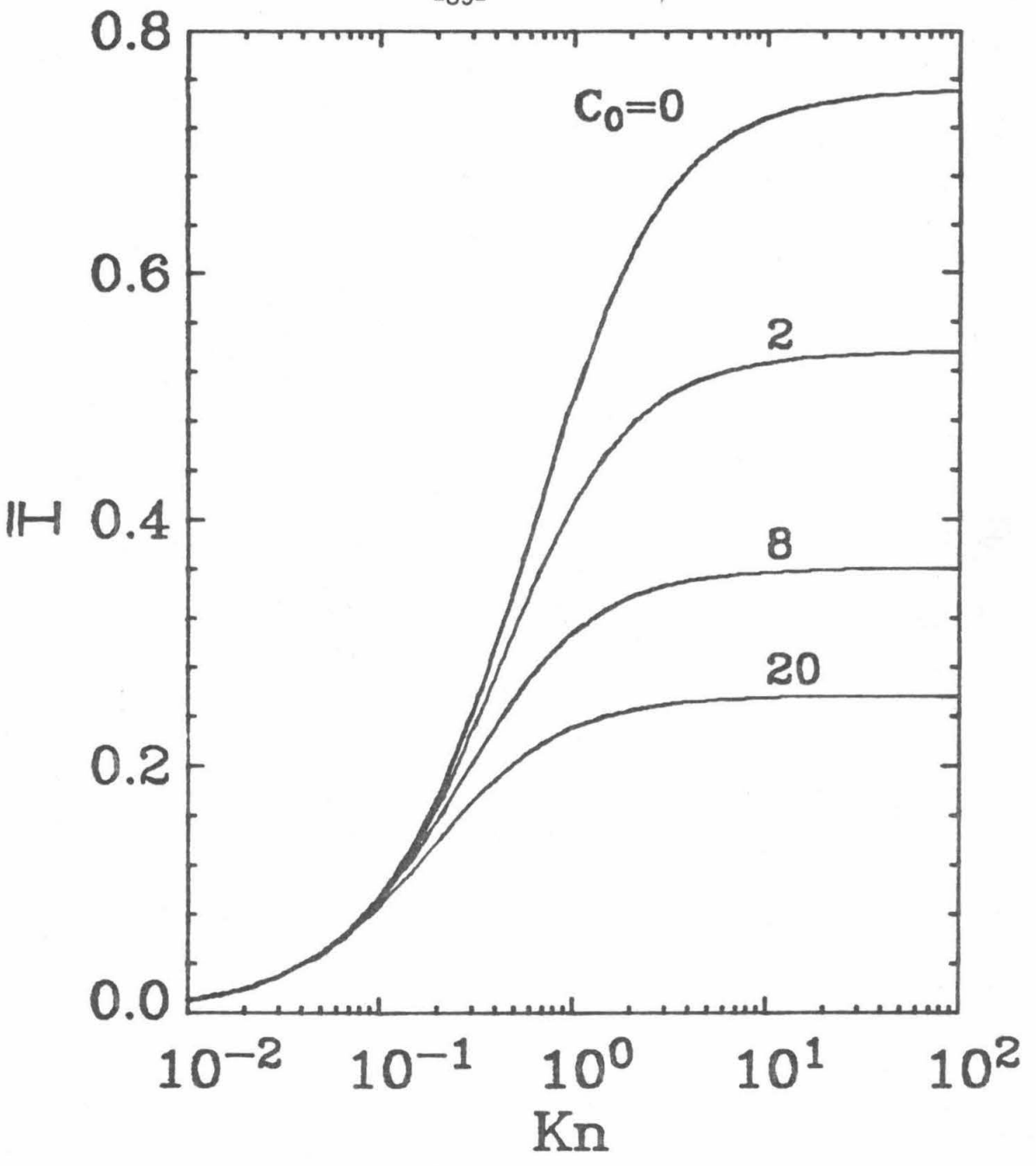

Figure 8

Dimensionless particle growth rates for half order surface reaction-limited growth, a = 1.33, b = 1.71, α =1.0 and B = 0.

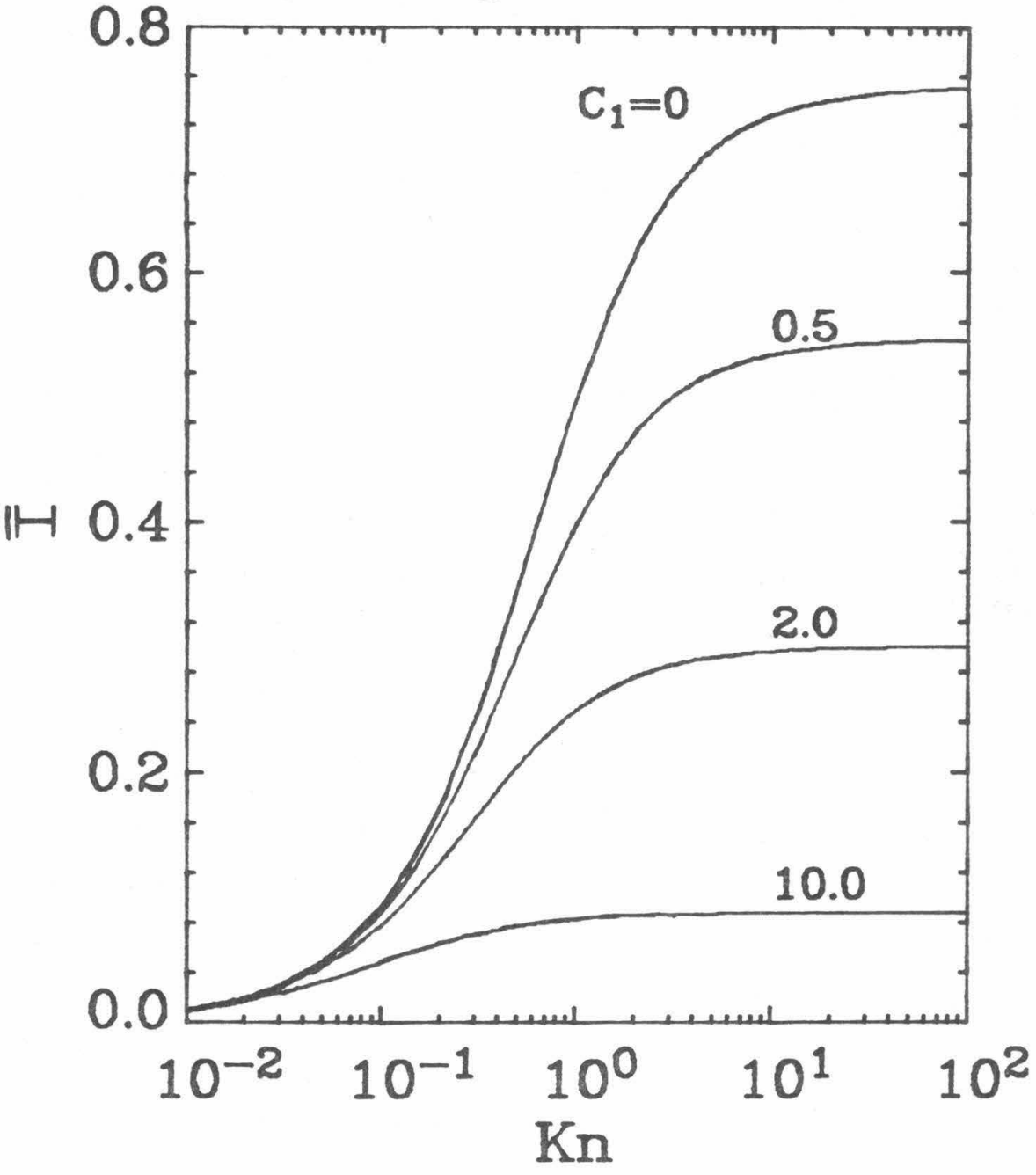

Figure 9

Dimensionless particle growth rates for first order surface reaction-limited growth, a = 1.33, b = 1.71, α = 1.0 and B = 0.

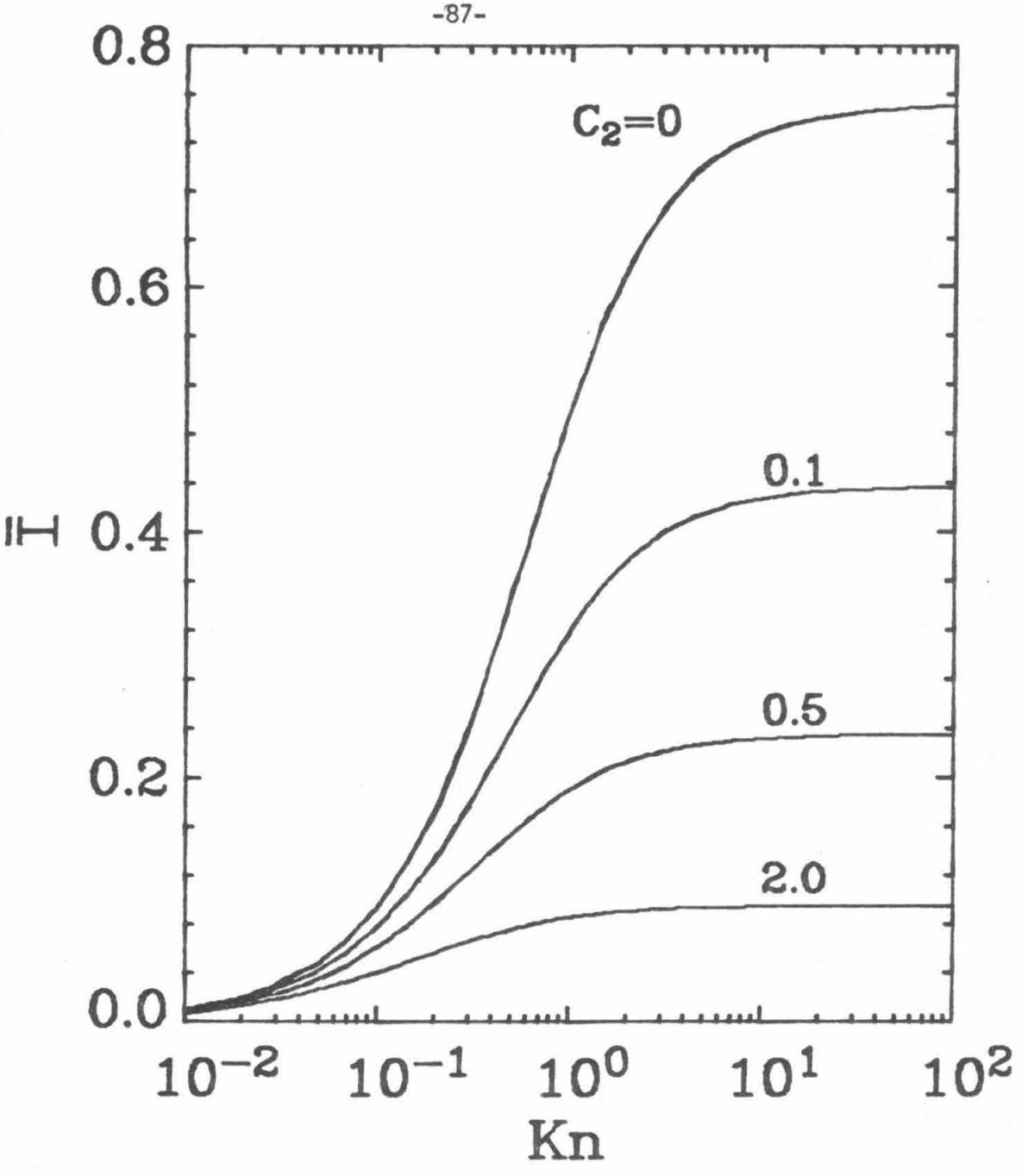

Figure 10

Dimensionless particle growth rates for second order surface reaction-limited growth, a = 1.33, b = 1.71, α =1.0 and B = 0.

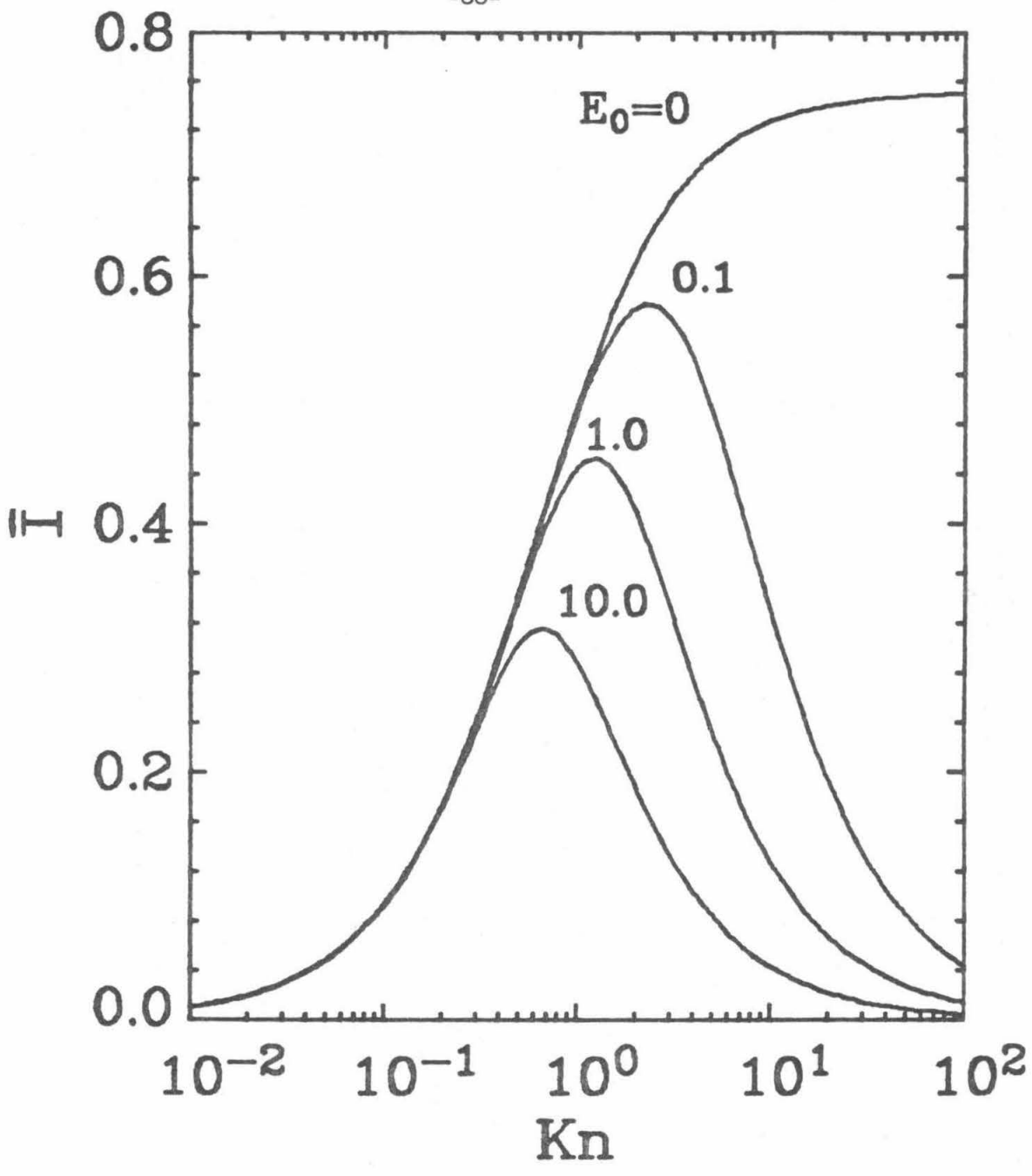

Figure 11

Dimensionless particle growth rates for half order volume reaction-limited growth, a = 1.33, b = 1.71, α =1.0 and B = 0.

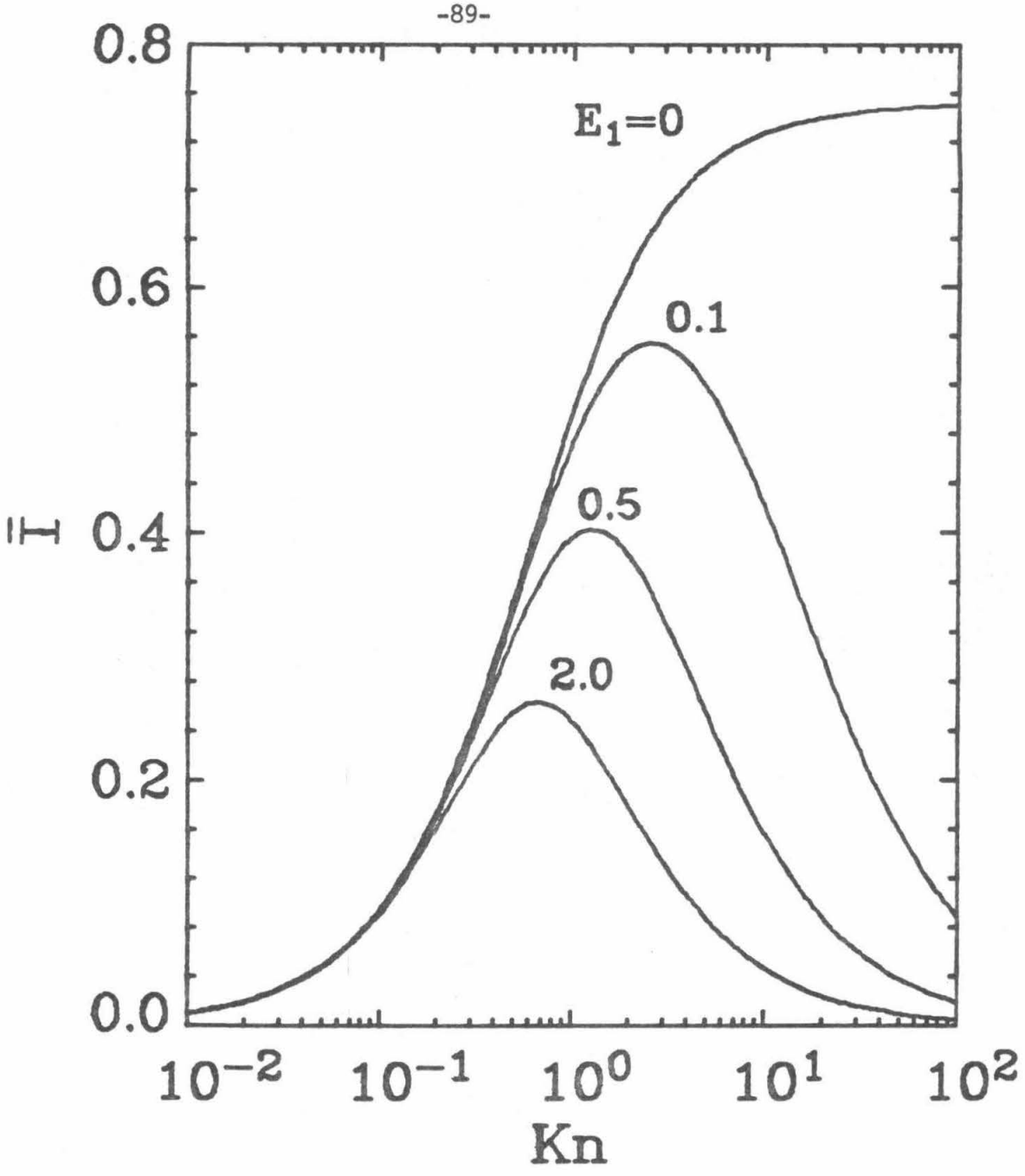

Figure 12

Dimensionless particle growth rates for first order volume reaction-limited growth, a = 1.33, b = 1.71, α =1.0 and B = 0.

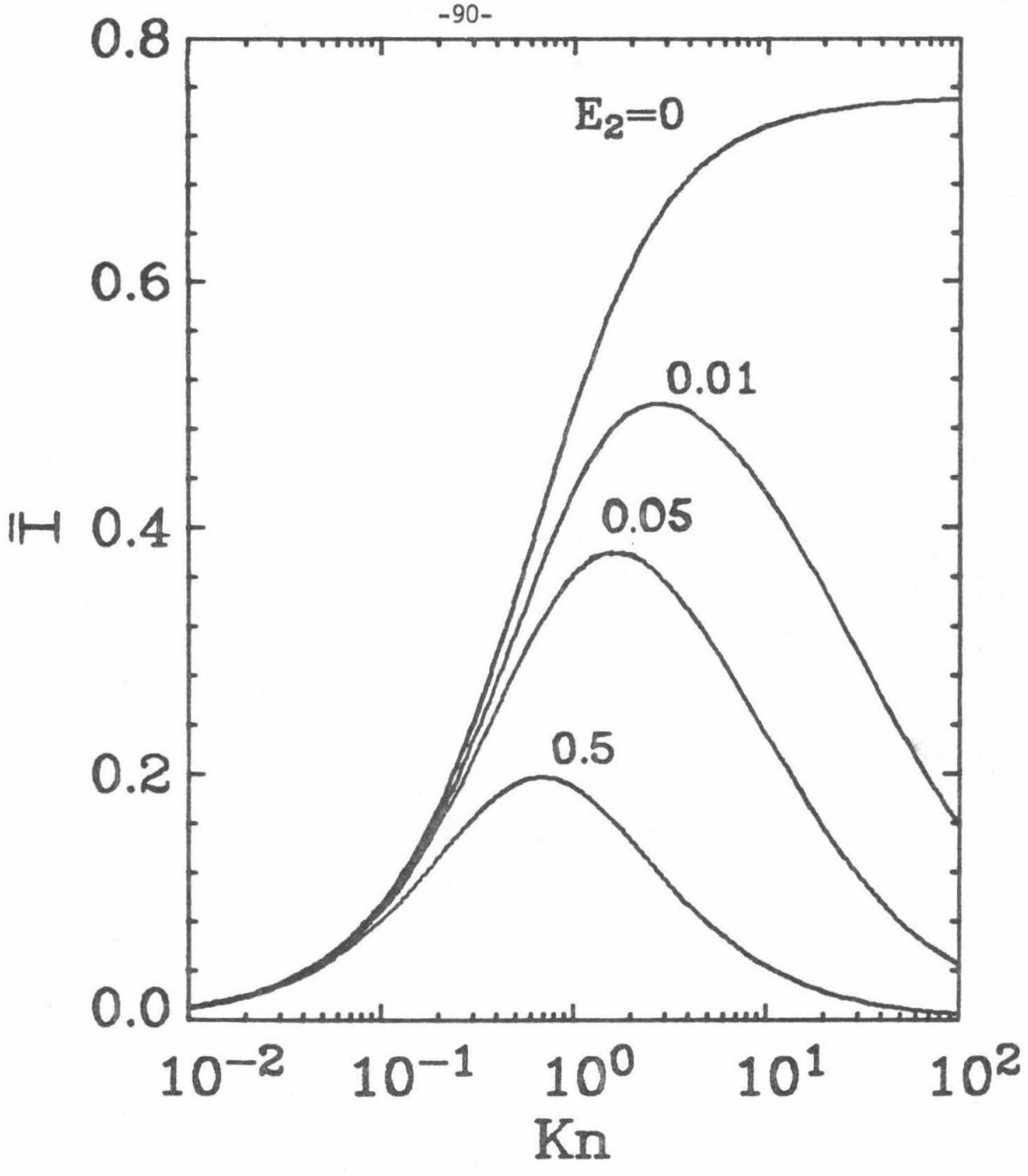

Figure 13

Dimensionless particle growth rates for second order volume reaction-limited growth, a = 1.33, b = 1.71, α =1.0 and B = 0.

An unlimited number of cases can be studied from the exact solution; for convenience we will limit ourselves to diffusion-controlled and zeroth order volume reaction-controlled growth. In both cases the same log-normal initial distribution with no sources or removal mechanisms will be used. Data are usually plotted so that the particle size increases along the x-axis. Therefore plots of the dimensionless number distribution, $\tilde{n}[\log_{10}(1/Kn),\tau]$ and dimensionless volume distribution $\tilde{V}[\log_{10}(1/Kn),\tau\ ]$ versus 1/Kn will be presented. In terms of the previously defined distribution,

$$\tilde{n}[\log_{10}(1/Kn),\tau] = \bar{n}(Kn,\tau)\ \frac{dKn}{d\ \log_{10}(1/Kn)} \qquad [24]$$

and

$$\tilde{V}[\log_{10}(1/Kn),\tau] = \frac{4\pi}{3Kn^3}\ \tilde{n}[\log_{10}(1/Kn),\tau] \qquad [25]$$

Data reported on particle growth usually show a decrease in the distribution for the smallest measurable particle size. Therefore we arbitrarily chose the boundary condition such that the distribution decays as $\exp(-5\Lambda\tau)$.

Figure 14 shows the evolution of the number distribution due to gas phase diffusion-limited growth for $\bar{D} = 0$. Based on Figure 2, we expect relatively rapid growth of small particles and hence their removal. Figure 14, therefore, shows the distribution decreasing for small values of Kn^{-1} and a corresponding increase for large values of

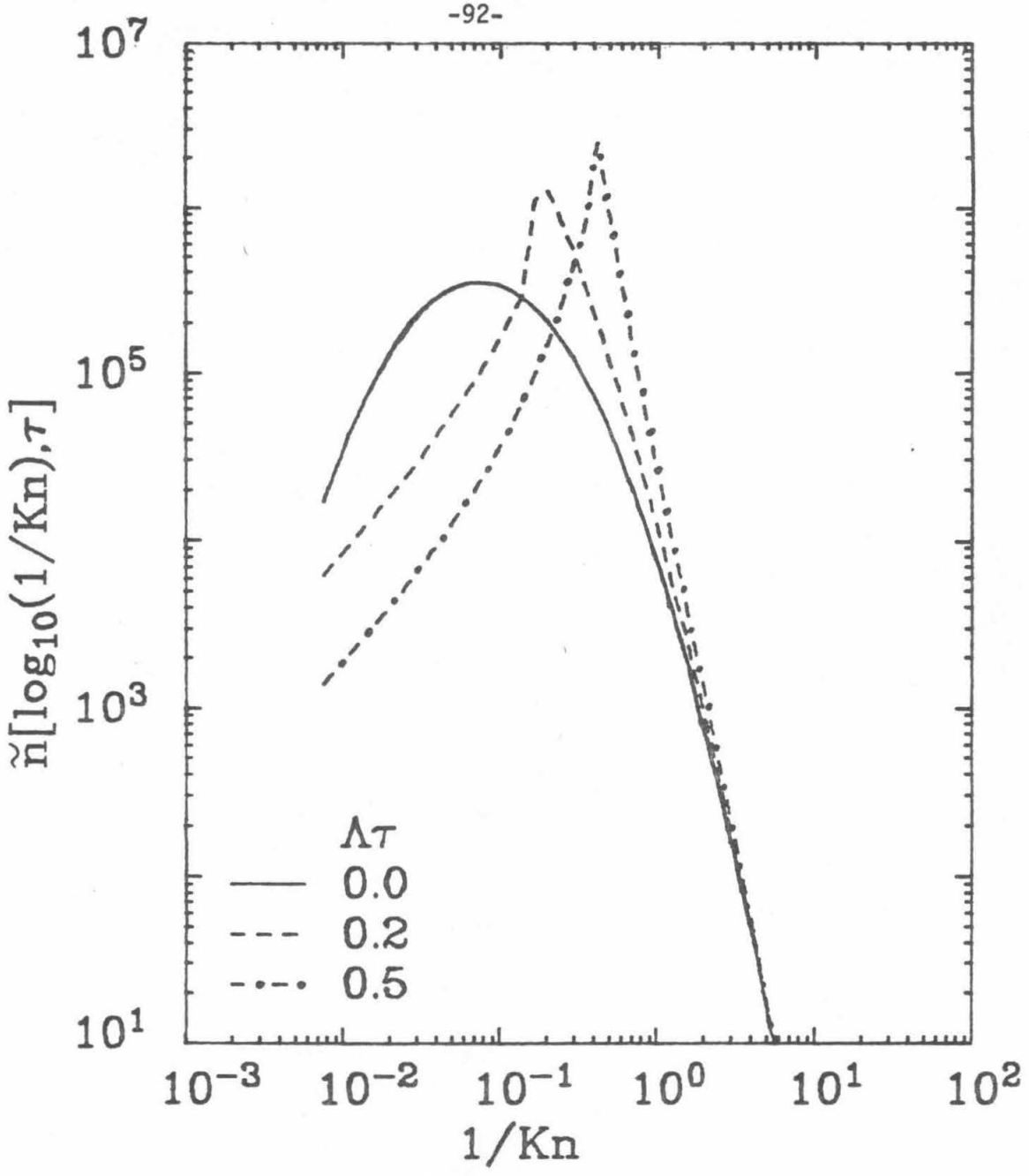

Figure 14

Evolution of the dimensionless number distribution for diffusion-limited growth, $\bar{D} = 0$, a = 1.33, b = 1.71, and $\alpha = 1.0$.

Kn^{-1}. The volume distribution plotted in Figure 15 shows the development of a sharp peak. This is a result of the large number of small particles growing to an appreciable size.

Figures 16 and 17 show the evolution of the number and volume distributions respectively, for zeroth order volume reaction-limited growth. From Figure 6 we see that the growth of large particles should be prevalent. Therefore, Figure 16 shows the shift in the number distributions for large values of Kn^{-1}. Figure 17 shows that the growth of large particles results in an increase and shift in the volume distribution to larger particles.

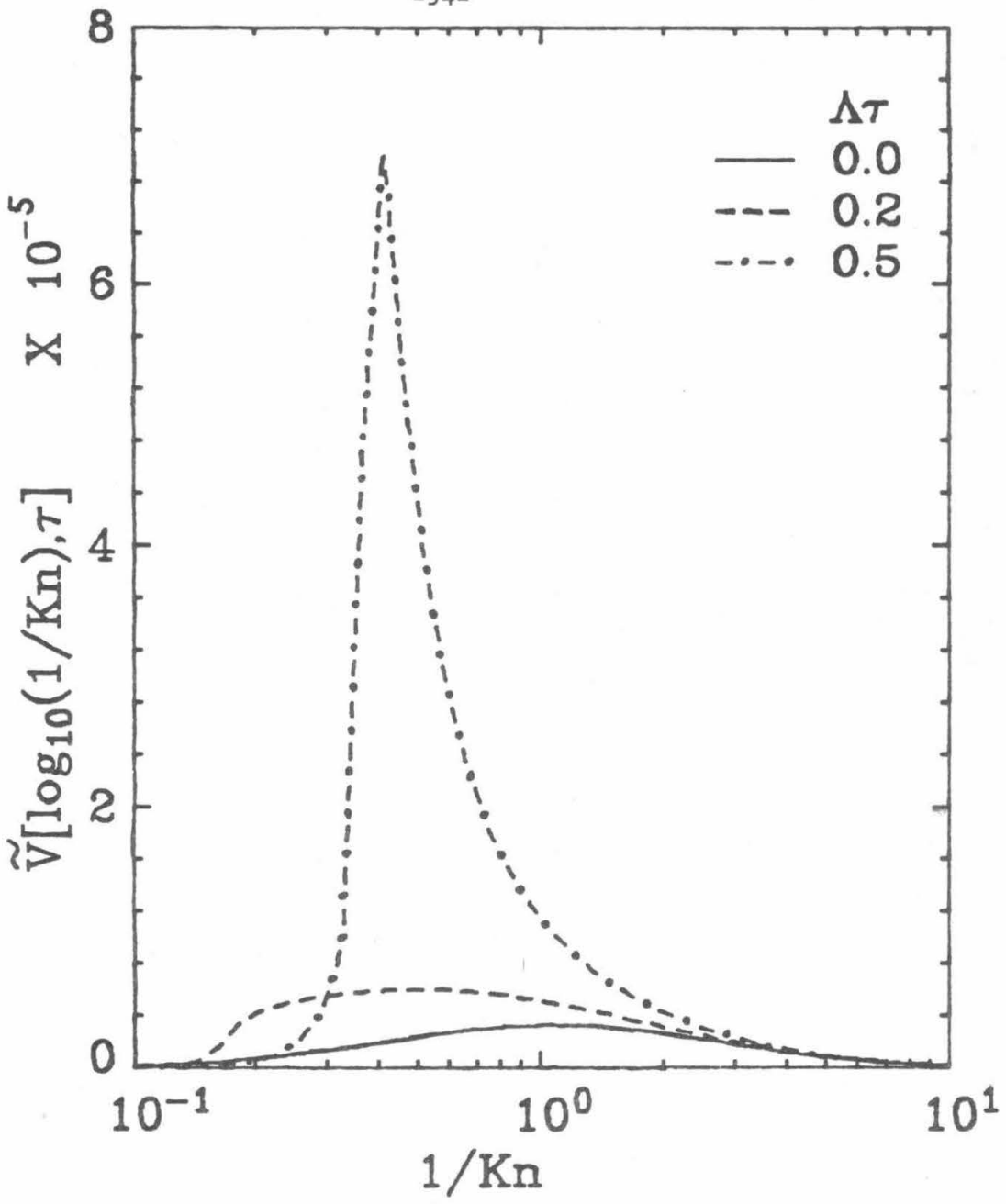

Figure 15

Evolution of the dimensionless volume distribution for diffusion-limited growth, $\bar{D}$ = 0, a = 1.33, b = 1.71, and α = 1.0.

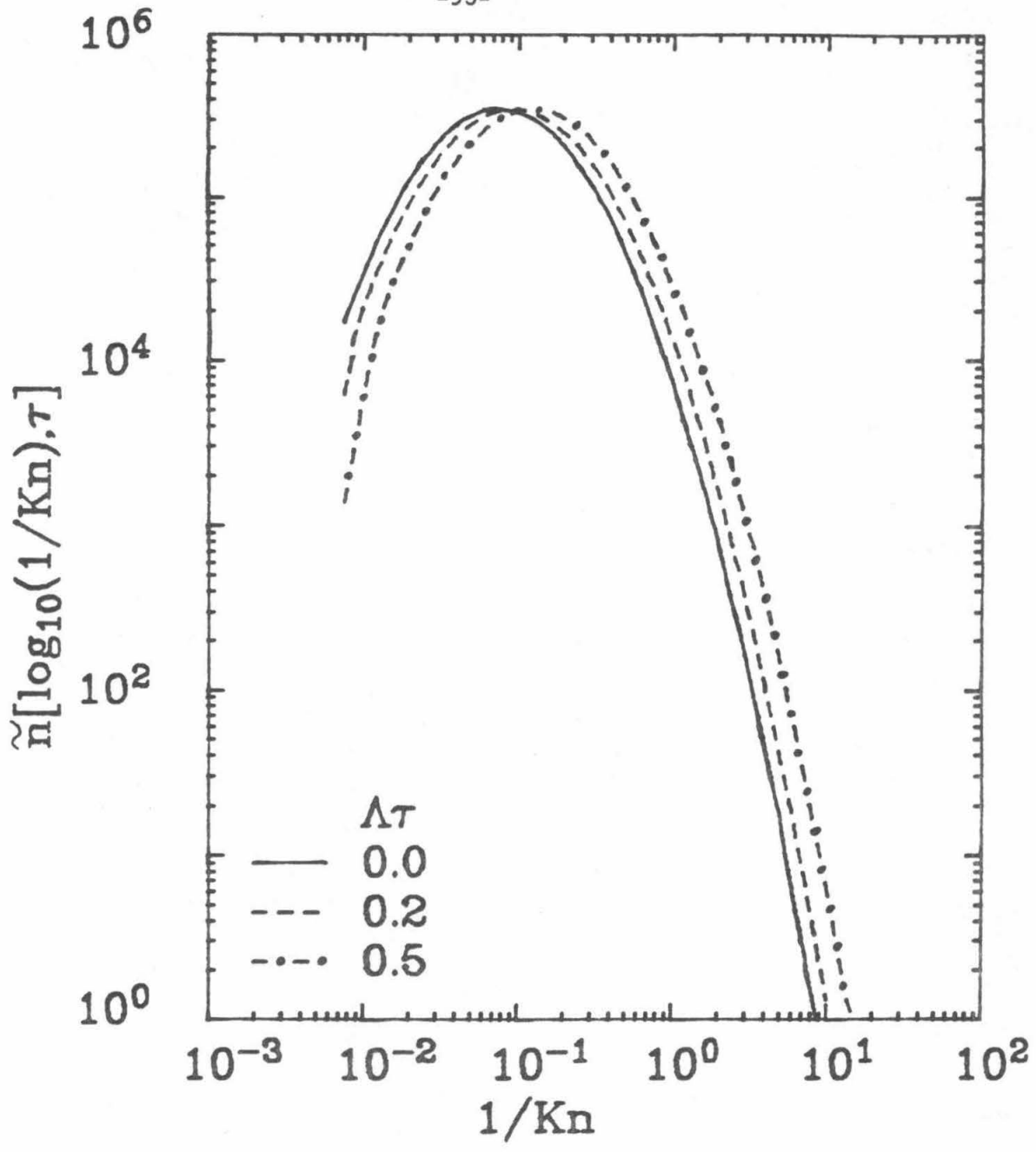

Figure 16

Evolution of the dimensionless number distribution for zeroth order volume reaction-limited growth.

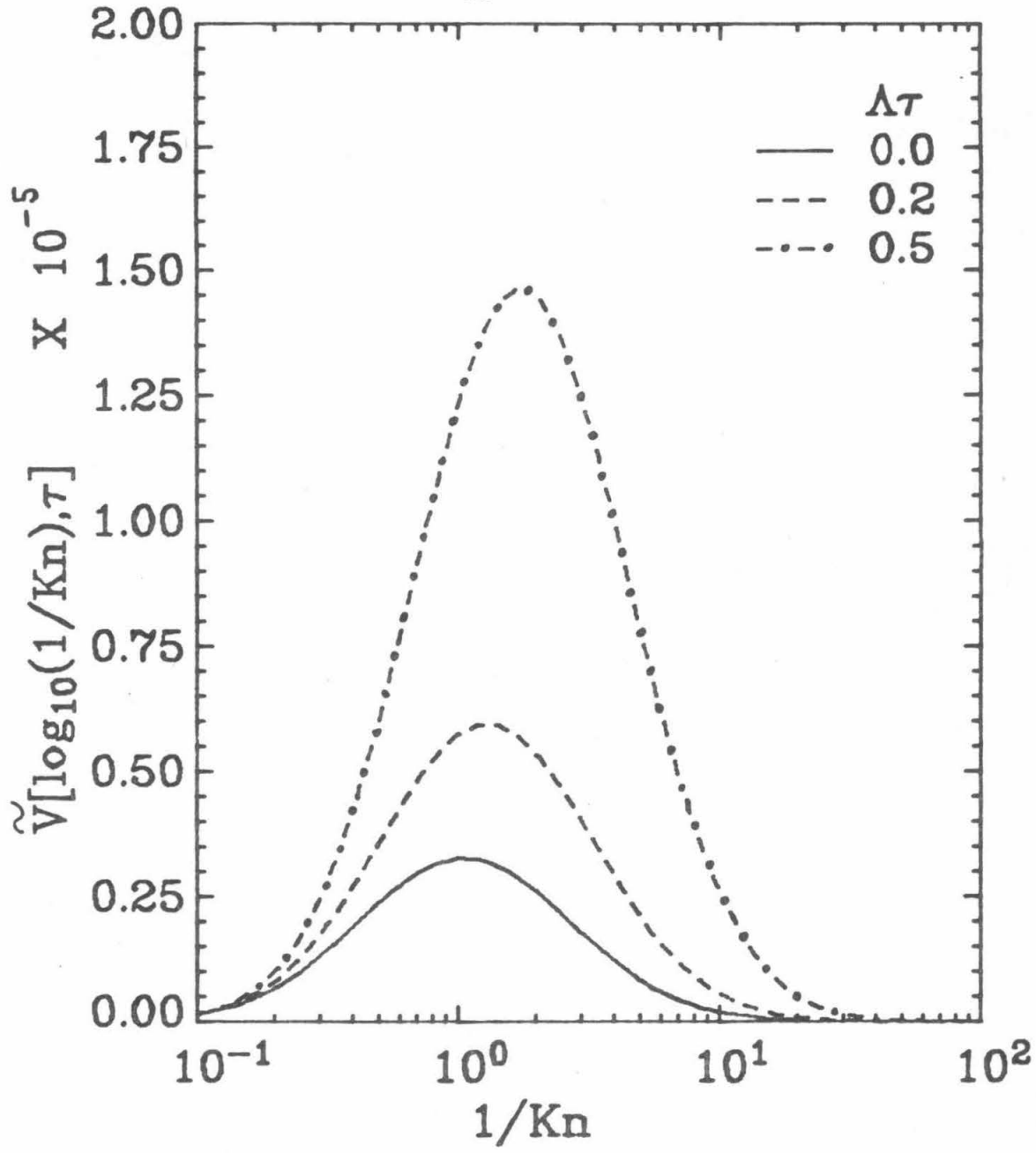

Figure 17

Evolution of the dimensionless volume distribution for zeroth order volume reaction-limited growth.

6. CONCLUSIONS

Exact solutions have been obtained for the size distributions of aerosols undergoing growth by condensation, enrichment by particle sources, and removal by first order mechanisms. The rate-limiting condensation growth mechanisms considered are: (1) gas phase diffusion; (2) chemical reaction on the particle surface, of orders 0, 1/2, 1 or 2 with respect to the concentration of condensed species on the particle surface; and (3) chemical reaction throughout the particle volume, of orders 0, 1/2, 1 or 2 with respect to the concentration of condensed species in the particle. It has been demonstrated that a positive order, reaction-limited growth, with either surface or volume reaction, is always slower than diffusion-limited growth with no particle vapor pressure. For cases of zeroth order surface or volume reaction, the particle growth rate may exceed that for diffusion-limited growth. The exact solutions presented here will enable, for the first time, analytical calculation of size distributions resulting from aerosol growth over the entire range of Knudsen numbers.

NOTATION

C_0 characteristic diffusion rate over the reaction rate for half order surface reaction-controlled growth

C_1 characteristic diffusion rate over the reaction rate for first order surface reaction-controlled growth

C_2 characteristic diffusion rate over the reaction rate for second order surface reaction-controlled growth

D particle diameter, μm

D_a smallest particle diameter, μm

D_b largest particle diameter, μm

$\mathscr{D}$ diffusivity, $cm^2\ sec^{-1}$

E_0 characteristic diffusion rate over the reaction rate for half order volume reaction-controlled growth

E_1 characteristic diffusion rate over the reaction rate for first order volume reaction-controlled growth

E_2 characteristic diffusion rate over the reaction rate for second order volume reaction-controlled growth

NOTATION (Continued)

$I_D(D,t)$	growth law, $\mu m\ sec^{-1}$
k	Boltzmann constant, $erg\ deg^{-1}$
k_s	surface reaction rate constant, $\mu m^{2\gamma-2}\ sec^{-1}$
k_v	volume reaction rate constant, $\mu m^{3\gamma-3}\ sec^{-1}$
Kn	Knudsen number
Kn_{crit}	critical Knudsen number
N_∞	gas phase concentration, cm^{-3}
N_+	equilibrium gas phase concentration, cm^{-3}
S_D	homogeneous particle sources and sinks, $\mu m^{-1}\ sec^{-1}\ cm^{-3}$
$S_0(D,t)$	homogeneous particle source, $\mu m^{-1}\ sec^{-1}\ cm^{-3}$
$S_1(D,t)$	homogeneous first order particle loss constant, sec^{-1}

Greek Letters

β_D	coagulation coefficient, $cm^3\ sec^{-1}$
γ	reaction order
η	viscosity, poise

Greek Letters (Continued)

λ	mean free path, μm
σ	surface tension, dyne cm^{-1}
τ	dimensionless time

REFERENCES

1. Golovin, A. M., "The Solution of the Coagulation Equation for Raindrops, Taking Condensation Into Account," Sov. Phys. Dokl. 8, 191 (1963).

2. Scott, W. T., "Analytic Studies of Cloud Droplet Coalescence," J. Atmos. Sci. 25, 54 (1968).

3. Drake, R. L., in "Topics in Current Aerosol Research" (Hidy, G. M. and Brock, J. R., Eds.), Pergamon, Oxford, 1972.

4. Peterson, T. W., Gelbard, F., and Seinfeld, J. H., "Dynamics of Source-Reinforced, Coagulating and Condensing Aerosols," J. Colloid Interface Sci. 63, 426 (1978).

5. Ramabhadran, T. E., Peterson, T. W., and Seinfeld, J. H., "Dynamics of Aerosol Coagulation and Condensation," A.I.Ch.E.J. 22, 840 (1976).

6. Middleton, P. and Brock, J., "Simulation of Aerosol Kinetics," J. Colloid Interface Sci. 54, 249 (1976).

7. Gelbard, F. and Seinfeld, J. H., "Numerical Solution of the Dynamic Equation for Particulate Systems," J. Comp. Phys., in press.

8. Brock, J. R., "On Size Distributions of Atmospheric Aerosols," Atmos. Environ. 5, 833 (1971).

9. Brock, J. R., "Condensational Growth of Atmospheric Aerosols," J. Colloid Interface Sci. 39, 32 (1972).

10. Sitarski, M. and Seinfeld, J. H., "Brownian Coagulation in the Transition Regime," J. Colloid Interface Sci. 61, 261 (1977).

11. Fuchs, N. A., "Mechanics of Aerosols," pp. 291-294. Pergamon, New York, 1964.

12. Millikan, R. A., "The General Law of Fall of a Small Spherical Body Through a Gas, and Its Bearing Upon the Nature of Molecular Reflection from Surfaces," Phys. Rev. 22, 1 (1923).

13. Phillips, W. F., "Drag on a Small Sphere Moving Through a Gas," Phys. Fluids 18, 1089 (1975).

14. Pich, J., "Simultaneous Brownian Coagulation and Diffusive Deposition of Monodisperse Particles," Atmos. Environ. 11, 989 (1977).

15. Davies, C. N., "Evaporation of Fine Atmospheric Particles," Faraday Symposia of the Chemical Society 7, 34 (1973).

APPENDIX

Let

$$g(Kn) = \int \frac{dKn}{Kn^2 \bar{I}(Kn)} \qquad [A1]$$

as given in Table 2. Then to find $\overline{Kn}$ for $\zeta(\tau) = 1$ such that

$$0 = g(\overline{Kn}) + \Lambda\tau - K_0 \qquad [A2]$$

where K_0 is an arbitrary constant, one can use a Newton iteration. Assuming Kn_i is obtained from the i-th iteration, then

$$Kn_{i+1} = Kn_i - Kn_i^2 \bar{I}(Kn_i)[g(Kn_i) - K_0]. \qquad [A3]$$

It was found that in most cases only three or four iterations are required to converge to $\overline{Kn}$.

Chapter IV

NUMERICAL SOLUTION OF THE DYNAMIC EQUATION FOR PARTICULATE SYSTEMS

ABSTRACT

The method of collocation using two finite element techniques is applied to the solution of the general population balance equation for particulate systems. Numerical solutions by both techniques are obtained in six cases for which analytical or asymptotic solutions are available. Errors associated with solving the equation on a finite particle size domain are analyzed. The techniques are also applied to the simulation of a smog chamber aerosol undergoing coagulation. The results indicate that, for simulating particulate system dynamics, both techniques are highly accurate and efficient.

1. INTRODUCTION

The state of a spatially and chemically homogeneous particulate system is described by its size distribution density function, $n_v(v,t)$ where $n_v(v,t)\,dv$ is the number of particles per unit volume of fluid having volumes in the range v to v + dv. The dynamics of such a system in which individual particles may grow through accretion of material from the fluid phase (or shrink by loss of material) and in which particles may collide and coagulate are described by the general particulate balance equation (1-2),

$$\frac{\partial n_v(v,t)}{\partial t} = -\frac{\partial}{\partial v}[I_v(v,t)n_v(v,t)] + \int_0^{v/2} \beta_v(v-\tilde{v},\tilde{v})n_v(v-\tilde{v},t)n_v(\tilde{v},t)\,d\tilde{v} - n_v(v,t)\int_0^{\infty} \beta_v(v,\tilde{v})n_v(\tilde{v},t)\,d\tilde{v} + S_v[n_v(v,t),v,t] \qquad [1]$$

where $I_v(v,t) = dv/dt$, the rate of change of the volume of a particle of volume v by transfer of material between the particle and the fluid phase, $\beta_v(v,\tilde{v})$ is the coagulation coefficient for particles of volumes v and $\tilde{v}$, and S_v is the net rate of addition of fresh particles into the

system. The initial and boundary conditions required for Eq. [1] are often stated as

$$n_v(v,0) = n_{v_0}(v) \qquad [2]$$

and

$$n_v(0,t) = 0 \qquad [3]$$

respectively. (The latter condition indicates that there are no particles of zero size.)

The first term on the right hand side of Eq. [1] represents the rate of growth of particles by transfer of material to individual particles. The second term represents the rate of accumulation of particles in the size range (v, v + dv) by collision of two particles of volumes v-$\tilde{v}$ and $\tilde{v}$ to form a particle of volume v (assuming conservation of volume during coagulation). The third term represents the rate of loss of particles in the size range (v, v + dv) by collision with all other particles. The last term represents all particle sources and sinks. Equation [1] arises in a wide variety of physical contexts, such as colloid chemistry, atmospheric aerosol dynamics, crystallization kinetics, and biological population dynamics.

Equation [1] can also be written in terms of particle diameter D (assuming spherical particles),

$$\frac{\partial n_D(D,t)}{\partial t} = - \frac{\partial}{\partial D} [I_D(D,t) n_D(D,t)]$$

$$+ D^2 \int_0^{D/\sqrt[3]{2}} \beta_D(\psi,\tilde{D}) n_D(\psi,t) n_D(\tilde{D},t) \frac{d\tilde{D}}{\psi^2}$$

$$- n_D(D,t) \int_0^{\infty} \beta_D(D,\tilde{D}) n_D(\tilde{D},t) \, d\tilde{D}$$

$$+ S_D[n_D(D,t),D,t] \qquad [4]$$

where $n_D(D,t) = (\pi D^2/2) n_v(v,t)$, $\psi = (D^3 - \tilde{D}^3)^{1/3}$, and $I_D = dD/dt$.

In spite of the great importance of Eqs. [1] and [4] to particulate system dynamics, solutions have been difficult to obtain. Analytical solutions are available only for a few simple forms of the initial conditions, $\beta_v(v,\tilde{v})$, $I_v(v,t)$ and $S_v[n(v,t), v,t]$ (2-5). Numerical solutions have been reported (6-16) but the optimum method for solving Eq. [1] has not been determined.

In this work we report on two collocation techniques used to solve the General Dynamic Equation. In Section 2 we discuss the proper scaling of the equation, in Section 3 we develop both methods and in Section 4 we describe the results of applying both methods to several test problems for which analytical or asymptotic solutions are available.

Finally, in Section 5 the general dynamic equation is solved for a coagulating aerosol, and comparisons are made with experiment. In the appendix to this chapter, techniques for reducing round off error are presented.

2. SCALING OF THE EQUATIONS

Equations [1] and [4] should be rescaled to a finite domain prior to numerical solution. We select a dimensionless finite particle size domain scaled from zero to one. Let us denote v_a, v_b and D_a,D_b as the chosen lower and upper limits on the volume and diameter, respectively, that will be employed in the numerical solution. Two possible transformations to a finite particle size domain (D_a,D_b) are linear and logarithmic (13),

$$u = \frac{D-D_a}{D_b-D_a} \qquad \text{or} \qquad u = \frac{v-v_a}{v_b-v_a} \qquad [5]$$

and

$$w = \frac{\ell n(D/D_a)}{\ell n(D_b/D_a)} = \frac{\ell n(v/v_a)}{\ell n(v_b/v_a)} \qquad [6]$$

For the representation of real systems, the logarithmic transformation given by Eq. [6] is preferred over the linear transformation given by Eq. [5]. Generally, the larger number of particles occur in in the smallest size range, and Eq. [6] more effectively expands that region. If significant effects occur equally over the entire particle size range, then a linear transformation is preferred. The use of a finite particle size domain introduces errors in that the General Dynamic Equation is based on an infinite particle size domain. For an actual particulate system, however, there are usually upper and lower bounds on the sizes of the particles that exist. In theory, D_a should

be chosen as the diameter of the smallest existing particle. (Although the general equations are written as if there exists a continuous spectrum of sizes down to zero, there is actually a lower cut-off in a real system.) D_b should be chosen large enough to include nearly all the particles in the system, yet small enough so that the region of major dynamic activity is not obscured. We will discuss the choice of D_a and D_b subsequently.

The analytical solutions of Eq. [1] currently available are based on rather idealized forms of the initial conditions, β_v, I_v, and S_v (2-5). For that reason, these solutions do not correspond directly to realistic physical conditions. Nevertheless, the use of available analytical solutions represents the only unambiguous way to ascertain the accuracy of the numerical solutions. Thus, in this chapter we will concentrate on obtaining numerical solutions for those cases for which analytical solutions are available.

Since aerosol data are usually given in terms of particle diameter, and the logarithmic transformation as given by Eq. [6] has the same form for either particle volume or diameter, we therefore choose to develop the numerical solution in terms of particle diameter.

Using Eq. [6], Eq. [4] becomes,

$$\frac{\partial m(w,t)}{\partial t} = - \frac{\partial}{\partial w} [I(w,t)m(w,t)]$$

$$+ \zeta^{3w} \int_0^{w-\frac{\ell n 2}{3\ell n\zeta}} \beta(x,z)m(x,t)m(z,t) \frac{dz}{\zeta^{3w}-\zeta^{3z}} - m(w,t) \int_0^1 \beta(w,z)m(z,t)\, dz$$

$$+ S[m(w,t),w,t] \qquad [7]$$

where I = dw/dt and

$$x = \frac{\ell n(\zeta^{3w}-\zeta^{3z})}{3\ell n\zeta} \qquad [8]$$

$$\zeta = D_b/D_a$$

and

$$m(w,t) = D(\ell n\ \zeta)n_D(D,t) \qquad [9]$$

$$S = D_a\zeta^w(\ell n\ \zeta)S_D \qquad [10]$$

From Eq. [9], we can relate m(w,t) and $n_v(v,t)$ as follows:

$$n_v(v,t) = \frac{2}{\pi(\ell n\zeta)D^3}\, m(w,t) \qquad [11]$$

3. COLLOCATION ON FINITE ELEMENTS

The most promising class of methods for solving Eq. [7] is that based on the methods of weighted residuals, in which the form of the solution is assumed in terms of a complete set of functions (generally polynomials) and substituted into the governing equation (17,18). To produce equations for the unknown coefficients of the expansion, the equation is multiplied by a weight factor, which is dependent on the method used, and integrated over the domain of interest. Among all the commonly used methods of weighted residuals, such as collocation, the Galerkin method and the method of moments, only collocation does not require extensive integral evaluations. Therefore, collocation emerges as the most attractive method of weighted residuals for solving Eq. [7].

In the traditional application of collocation a finite expansion of order $\overline{M}$ is forced to satisfy the differential equation at $\overline{M}+1$ predetermined collocation points, hence the residual is zero at these points. If the expansion satisfies the differential equation at all points in the region and at the boundary, then the expansion is by definition a representation of the exact solution. However, due to the large variations in magnitude of m(w,t) a single high order polynomial fit is not feasible. Therefore the finite element technique combined with collocation (19,20) represents a promising approach.

For both finite element techniques the domain of the independent variable is divided into elements within which the dependent variable is represented by a polynomial, often a cubic. At the grid points between elements the distributions and their derivatives are forced to be continuous. If the second derivative is forced to be continuous and collocation points are also taken at the grid points, then the finite element fit is actually a cubic spline. If within each element the independent variable is rescaled from 0 to 1 to avoid round off errors, and collocation points are taken as the roots of the shifted Legendre polynomial, then we have what has been called orthogonal collocation on finite elements (20). Since cubic splines are described in the literature (21,22), and they were originally reported in (16), only orthogonal collocation on finite elements will be described here. Because it is easier to write the code in terms of the distribution at the collocation points and not the expansion coefficients, the solution technique will be given in terms of the distribution at the collocation points.

Dividing the distribution, m(w,t) into M elements and using a cubic polynomial in each element results in the following representation of m(w,t) in the $\underline{i}$th element,

$$m(w,t) = A_{i,1}(t) + A_{i,2}(t)y_i + A_{i,3}(t)y_i^2 + A_{i,4}(t)y_i^3 \qquad [12]$$

$$i = 1,2,\ldots, M \ ,$$

where $A_{i,j}$ is the jth coefficient of the ith element, and $y_i = (w-w_{i-1})/(w_i-w_{i-1})$ for $w_{i-1}<w \leq w_i$. Imposing the condition of continuity of $m(w,t)$ and its first derivative at the grid points gives,

$$A_{i,1} + A_{i,2} + A_{i,3} + A_{i,4} = A_{i+1,1} \qquad [13]$$

$$A_{i,2} + 2A_{i,3} + 3A_{i,4} = \frac{(w_i-w_{i-1})}{(w_{i+1}-w_i)} A_{i+1,2} \qquad [14]$$

At each collocation point η within each element we have

$$A_{i,1} + \eta A_{i,2} + \eta^2 A_{i,3} + \eta^3 A_{i,4} = B_{i,k} \qquad [15]$$

and where $B_{i,k}$ represents the distribution, $m(w,t)$ at the kth collocation point in the ith element and $w = \eta(w_i - w_{i-1}) + w_{i-1}$. Using Eqs. [13] and [14] we can derive the following set of 2M+2 linear algebraic equations for $A_{i,j}$

$$(1 - 3\eta_k^2 + 2\eta_k^3)A_{i,1} + (\eta_k - 2\eta_k^2 + \eta_k^3)A_{i,2} + (3\eta_k^2 - 2\eta_k^3)A_{i+1,1}$$

$$\frac{(w_i-w_{i-1})}{(w_{i+1}-w_i)} (\eta_k^3 - \eta_k^2)A_{i+1,2} = B_{i,k} \qquad [16]$$

$$i = 2,\ldots, M-1; \quad k = 1,2$$

$$i = 1; \quad k = 1,2,3$$

and

$$A_{M,1} + \eta_k A_{M,2} + \eta_k^2 A_{M,3} + \eta_k^3 A_{M,4} = B_{M,k} \qquad [17]$$

$$k = 1,2,3$$

When placed in conventional matrix form, Eqs. [16] and [17] lead to a banded matrix of bandwidth 7 that can be inverted easily. Since the elements of the matrix are time independent, elimination need only be carried out once.

The final consideration is the location of the finite elements. In (20) is is suggested that the elements be located to minimize the residual. Although this is a reasonable criterion, it would require a costly iterative procedure in the present application. Without any prior knowledge of the behavior of m(w,t), the elements were equally spaced in w, or in terms of a dimensionless diameter.

4. NUMERICAL IMPLEMENTATION

We will consider the exponential initial volume distribution

$$n_{v_0}(v) = \frac{N_0}{\nu_0} e^{-\bar{v}} \qquad [18]$$

where N_0 is the total initial number of particles, ν_0 is the mean initial volume, and $\bar{v} = v/\nu_0$.

Because the mechanism of coagulation poses the greatest numerical difficulty, we will first consider the solution of Eq. [7] in the absence of growth and sources. In this case we will show the effect of using a finite particle size domain by studying two different collision mechanisms, $\beta_v = \beta_0$ and $\beta_v = \beta_1(v + \tilde{v})$. As mentioned previously, in actual particulate systems an upper limit to the particle size exists because of removal mechanisms, such as sedimentation or deposition. Therefore, the effects on the distribution of a first order removal mechanism will be studied. Then, the effect of simultaneous coagulation and growth will be studied. Finally, the numerical solution will be compared to an asymptotic solution for a system undergoing simultaneous coagulation and removal with a constant particle source. The cases considered are summarized in Table 1.

Particulate size distributions can be represented in a variety of ways. When the predominant number of particle occurs in the small size regime, we select a representation that expands the lower end of

Table 1. Summary of Cases Considered of the General Dynamic Equation for Particulate Systems†

$$\frac{\partial n_v}{\partial t} = -\frac{\partial}{\partial v}\left[I_v n_v\right] + \int_0^{v/2} \beta_v(v-\tilde{v},\tilde{v}) n_v(v-\tilde{v},t) n_v(\tilde{v},t)\, d\tilde{v}$$

$$- n_v(v,t) \int_0^{\infty} \beta_v(v,\tilde{v}) n(\tilde{v},t)\, d\tilde{v} + S_v(n_v,v,t)$$

Case	$\beta_v(v,\tilde{v})$	$I_v(v,t)$	$S_v(n_v,v,t)$	Analytical Solutions	Domain $[\bar{v}_a,\bar{v}_b]$
1	β_0	0	0	(4)	$[10^{-9}, 27]$
2	β_0	0	0	(4)	$[10^{-9}, 64]$
3	$\beta_1(v+\tilde{v})$	0	0	(3,4)	$[10^{-9}, 27]$
4	$\beta_1(v+\tilde{v})$	0	$-R_0 n_v$	(5)	$[10^{-9}, 27]$
5	β_0	σv	0	(2)	$[10^{-9}, 27]$
6	β_0	0	$\frac{S_0 e^{-v/v^*}}{v^*} - R_0 n_v$	(5)	$[10^{-9}, 27]$

†R_0, S_0, are σ are constant.

the spectrum. In such a case the distribution is usually represented versus a logarithmic size coordinate, e.g. Eq. [6]. When representing the analytical solutions to the cases listed in Table 1, however, it is most convenient to use, as the independent variable, $\bar{D}$ and, as the dependent variable, $\bar{n}_{\bar{D}}(\bar{D},t)/N_0$, where $\bar{D} = D/D_0$, $D_0 = (6\nu_0/\pi)^{1/3}$ and $\bar{n}_{\bar{D}}(\bar{D},t) = D_0 n_D(D,t)$.

All solutions will be expressed in terms of dimensionless groups, defined for each case in Table 2. Since all cases include coagulation, other mechanisms such as growth, removal, and sources will be expressed in terms of dimensionless groups scaled to coagulation. Although the definition of the dimensionless time τ, varies depending on the coagulation mechanism, for comparison purposes the same values of τ will be used in each case for which we present solutions. For convenience Λ, θ, and Ω will always be assumed to be unity. All analytical solutions will be shown as solid lines, and all numerical solutions will be represented by discrete points. Since both finite element techniques gave similar results both techniques are implied when numerical solutions are reported. The analytical solutions are given in Table 3.

4.1 Finite Domain Error

A major consideration in numerically solving an equation described over an infinite domain is the error incurred by the solution on a finite

Table 2. Dimensionless Groups Associated With the General Dynamic Equation for Particulate Systems

Group		Interpretation
$\tau = N_0\beta_0 t$	(Cases 1,2,5,6)	Dimensionless time
$= N_0\nu_0\beta_1 t$	(Cases 3,4)	
$\Lambda = \sigma/N_0\beta_0$	(Case 5)	$\frac{\text{Condensation rate}}{\text{Coagulation rate}}$
$\theta = R_0/N_0\nu_0\beta_1$	(Case 4)	$\frac{\text{Removal rate}}{\text{Coagulation rate}}$
$= R_0/N_0\beta_0$	(Case 6)	
$\Omega = S_0/N_0^2\beta_0$	(Case 6)	$\frac{\text{Source rate}}{\text{Coagulation rate}}$

Table 3. Analytical Solutions to Eq. [1] for the Initial Distribution given by Eq. [18]

Case	β_v	I_v	S_v	$n_v(v,t)$	Reference
1,2	β_0	0	0	$\frac{4N_0}{\nu_0(\tau+2)^2}\exp\left[-\frac{2\bar{v}}{\tau+2}\right]$	(4)
3*	$\beta_1(v+\tilde{v})$	0	0	$\frac{N_0(1-T)}{v\sqrt{T}}\exp\left[-(1+T)\bar{v}\right]I_1(2\bar{v}\sqrt{T})$	(3,4)
4†	$\beta_1(v+\tilde{v})$	0	$-R_0 n_v$	$\frac{N_0\tilde{T}\exp\left(\frac{\tilde{T}-1}{\theta}\right)}{\nu_0\sqrt{g}\,\bar{v}}\exp\left[-(1+g)\bar{v}\right]I_1(2\sqrt{g}\,\bar{v})$	(5)
5	β_0	σv	0	$\frac{4N_0}{\nu_0(\tau+2)^2}\exp\left[-\frac{2\bar{v}}{\tau+2}\exp(-\Lambda\tau) - \Lambda\tau\right]$	(2)

* $T = 1-e^{-\tau}$, I_1 is the modified Bessel function of the first kind of order one.

† $g(\tilde{T}) = 1 - \exp\left[\frac{T-1}{\theta}\right]$

$\tilde{T} = \exp(-\theta\tau)$

domain. To evaluate this so-called "finite-domain error," the fractions of the total number and volume of particles contained in the finite computational domain can be determined based on the analytical solutions. Thus,

$$M_0(t) = \frac{\int_{v_a}^{v_b} n_v(v,t)dv}{\int_0^{\infty} n_v(v,t)dv} \qquad [19]$$

and

$$M_1(t) = \frac{\int_{v_a}^{v_b} v n_v(v,t)dv}{\int_0^{\infty} v n_v(v,t)dv} \qquad [20]$$

represent these two fractions. Obviously, we desire to select v_a and v_b such that M_0 and M_1 do not differ appreciably from unity but not so close to 0 and ∞, respectively, that the computational requirements are excessive. Due to the processes of coagulation and particle growth, larger particles are continually being formed. Thus, by using any finite domain, M_0 and M_1 must eventually decrease from unity. The time

for which M_0 and M_1 differ significantly from unity can be delayed by extending the domain at the expense of increased computational requirements.

It is important to note that Eqs. [19] and [20] are evaluated based on the exact solution and therefore represent only the theoretical errors committed through the use of a finite computational domain. It is also important to distinguish the finite domain error from errors usually associated with numerical solutions, in that regardless of the numerical method or its accuracy, there will be an error incurred merely because the computation is carried out on a finite rather than an infinite domain. Due to the nature of Eq. [1], particles within any finite computational domain interact with particles outside the computational domain. Hence, as more particles form outside the computational domain, unavoidable errors are introduced into the distribution within the computational domain. Therefore, all mechanisms which form particles rapidly at the upper end of the size spectrum can lead to errors within the computational domain. For the cases given in Table 3 the analytical expressions for M_0 and M_1 are given in Table 4. Table 5 lists the finite domain errors for cases 1 to 5.

4.2 Numerical Results

The numerical and exact results for case 1 are shown in Figure 1. Using equally spaced elements in $\bar{D}$, Eq. [7] was solved numerically

Table 4. Analytical Expressions for the Finite Domain Errors*

Case	$M_0(t)$
1,2	$\exp\left[-\frac{2\bar{v}}{\tau+2}\right]$
3	$\sum_{k=0}^{\infty} \frac{(2k)!T^k}{k!(k+1)!} e^{-(1+T)\bar{v}} \sum_{r=0}^{2k} \frac{\bar{v}^{2k-r}}{(2k-r)!(1+T)^{r+1}}$
4	$\sum_{k=0}^{\infty} \frac{(2k)!g^k}{k!(k+1)!} \exp[-\bar{v}(1+g)] \sum_{r=0}^{2k} \frac{\bar{v}^{2k-r}}{(2k-r)!(1+g)^{r+1}}$
5	$\exp\left[-\frac{2\bar{v}}{\tau+2}\exp(-\Lambda\tau)\right]$

*Each expression is to be evaluated at $\bar{v}_a$ minus its value at $\bar{v}_b$. ($\bar{v}_a = \bar{D}_a^3$ and $\bar{v}_b = \bar{D}_b^3$)

Table 4. Analytical Expressions for the Finite Domain Errors* (Continued)

Case	$M_1(t)$
1,2	$\exp\left[-\frac{2\bar{v}}{\tau+2}\right]\left[\frac{2\bar{v}}{\tau+2}+1\right]$
3	$(1-T)\sum_{k=0}^{\infty}\frac{(2k+1)!T^k}{k!(k+1)!}e^{-(1+T)\bar{v}}\sum_{r=0}^{2k+1}\frac{\bar{v}^{2k+1-r}}{(2k+1-r)!(1+T)^{r+1}}$
4	$\exp\left[\frac{\tilde{T}-1}{\theta}\right]\sum_{k=0}^{\infty}\frac{(2k+1)!g^k}{k!(k+1)!}\exp\left[-\bar{v}(1+g)\right]\sum_{r=0}^{2k+1}\frac{\bar{v}^{2k+1-r}}{(2k+1-r)!(1+g)^{r+1}}$
5	$\exp\left[-\frac{2\bar{v}}{\tau+2}\exp(-\Lambda\tau)\right]\left[\frac{2\bar{v}}{\tau+2}\exp(-\Lambda\tau)+1\right]$

*Each expression is to be evaluated at $\bar{v}_a$ minus its value at $\bar{v}_b$.

($\bar{v}_a = \bar{D}_a^3$ and $\bar{v}_b = \bar{D}_b^3$)

Table 5. Finite Domain Errors for Cases 1-5

Case			
1	1.0	1.00	1.00
	3.0	1.00	1.00
	5.0	1.00	0.996
	7.0	0.998	0.983
	10.0	0.989	0.939
	20.0	0.914	0.703
2	5.0	1.00	1.00
	10.0	1.00	1.00
	20.0	0.997	0.980
	30.0	0.982	0.908
	50.0	0.915	0.705
3	0.5	0.999	0.988
	1.0	0.983	0.776
	1.5	0.950	0.483
	2.0	0.921	0.283
	3.0	0.887	0.0979
4	1.0	0.998	0.959
	2.0	0.990	0.856
	3.0	0.986	0.806
	5.0	0.983	0.780
	7.0	0.983	0.776
	10.0	0.983	0.776
5	1.0	0.999	0.990
	1.5	0.968	0.858
	2.0	0.839	0.545
	2.5	0.627	0.259
	3.0	0.416	0.102

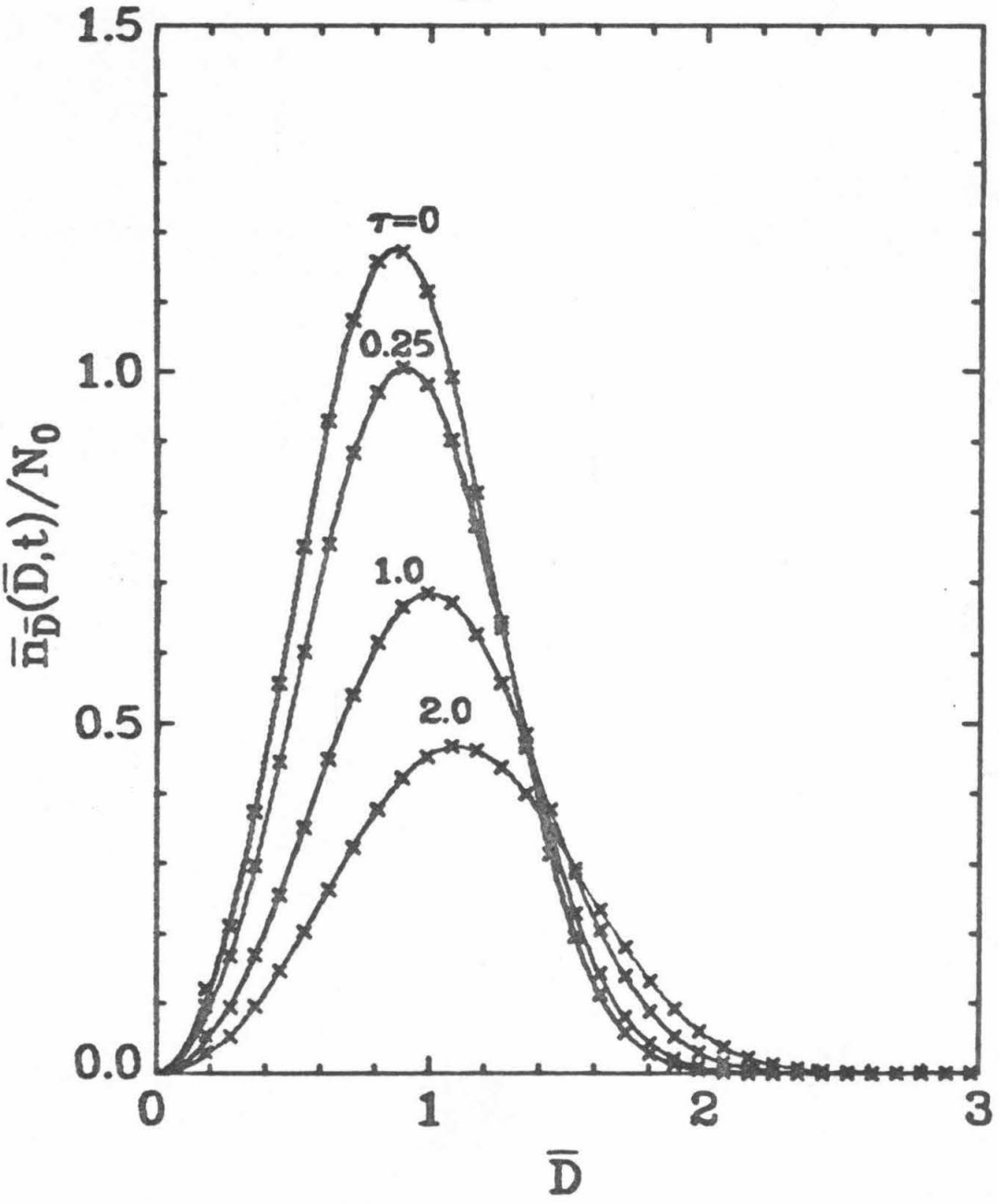

Figure 1

Particle size spectra. $\beta_v = \beta_o$ and $\tau = N_o\beta_o t$.

by both methods of Section 3. Excellent agreement between the numerical and exact solutions was obtained. From Table 5 we see that for the times considered in Figure 1 the finite domain errors are negligible. In fact, up to $\tau = 10$, no significant finite domain errors can be anticipated.

In order to demonstrate both the accuracy of both techniques for long dimensionless times and the effect of the finite domain error, case 1 was solved to $\tau = 20$. For the same domain as that in Figure 1, Table 5 indicates that this domain will lead to a substantial finite domain error. By multiplying the distribution by $(\tau+2)^2/4$, so as to emphasize the long time behavior of the solution, Figure 2 shows the numerical solution for $\bar{D}_b = 3.0$. At long times the numerical solution lies above the exact solution since the numerical solution does not account for collisions between particles inside the domain $[\bar{D}_a,\bar{D}_b]$ with those larger than $\bar{D}_b$. By increasing the computational domain, the finite domain errors are reduced, and hence an accurate solution can be obtained. From Table 5 for case 2, we see that if $\bar{D}_b$ is extended to 4.0 the finite domain errors are negligible for $\tau \leq 20$. As expected, Figure 3 shows the numerical solution in excellent agreement with the exact solution when $\bar{D}_b = 4.0$.

Figure 4 shows exact and numerical solutions for case 3. Consistent with Table 5, we see that as τ increases the deviation between the two solutions increases. The finite domain error is considerably

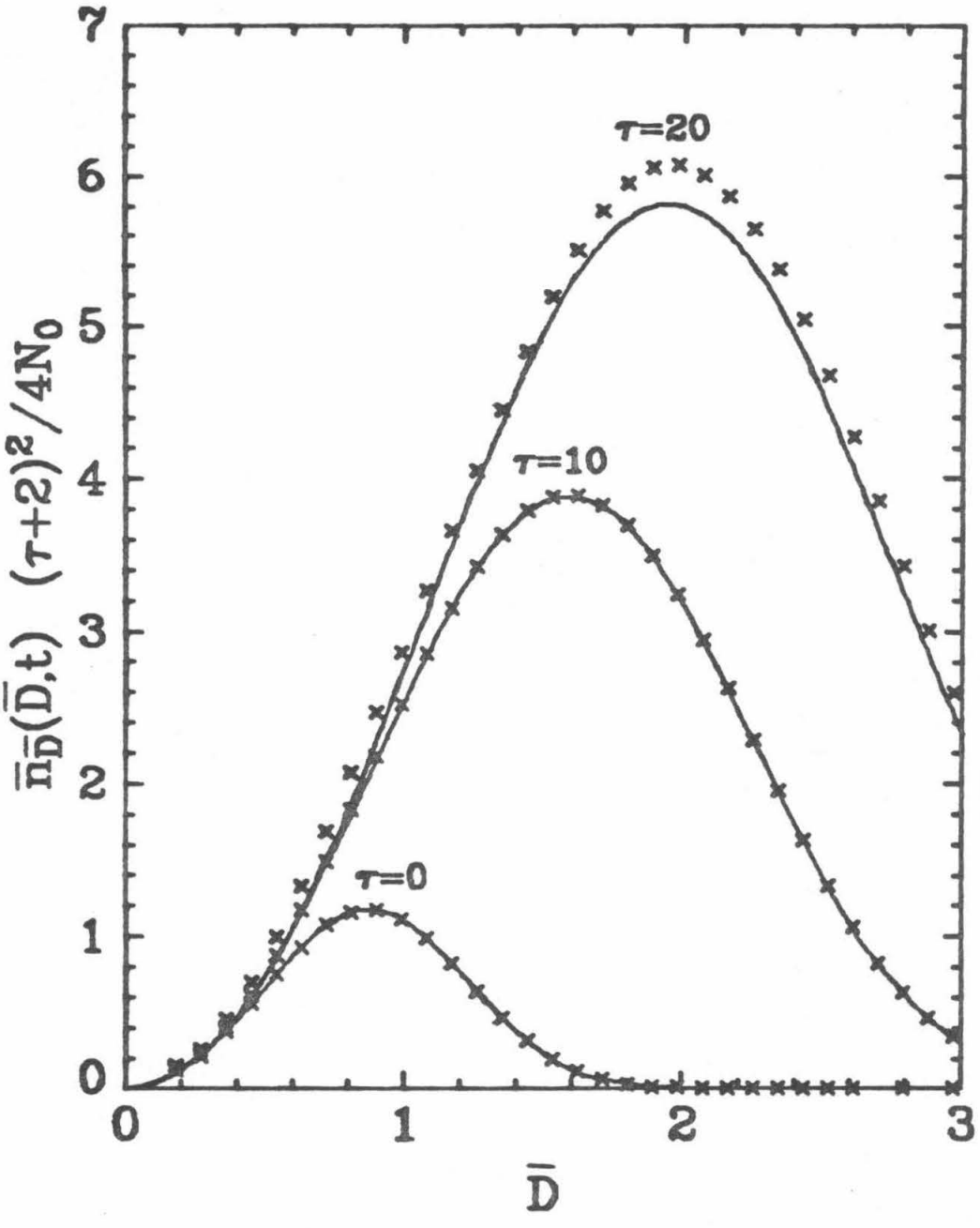

Figure 2

Particle size spectra. $\beta_v = \beta_0$ and $\tau = N_0\beta_0 t$.

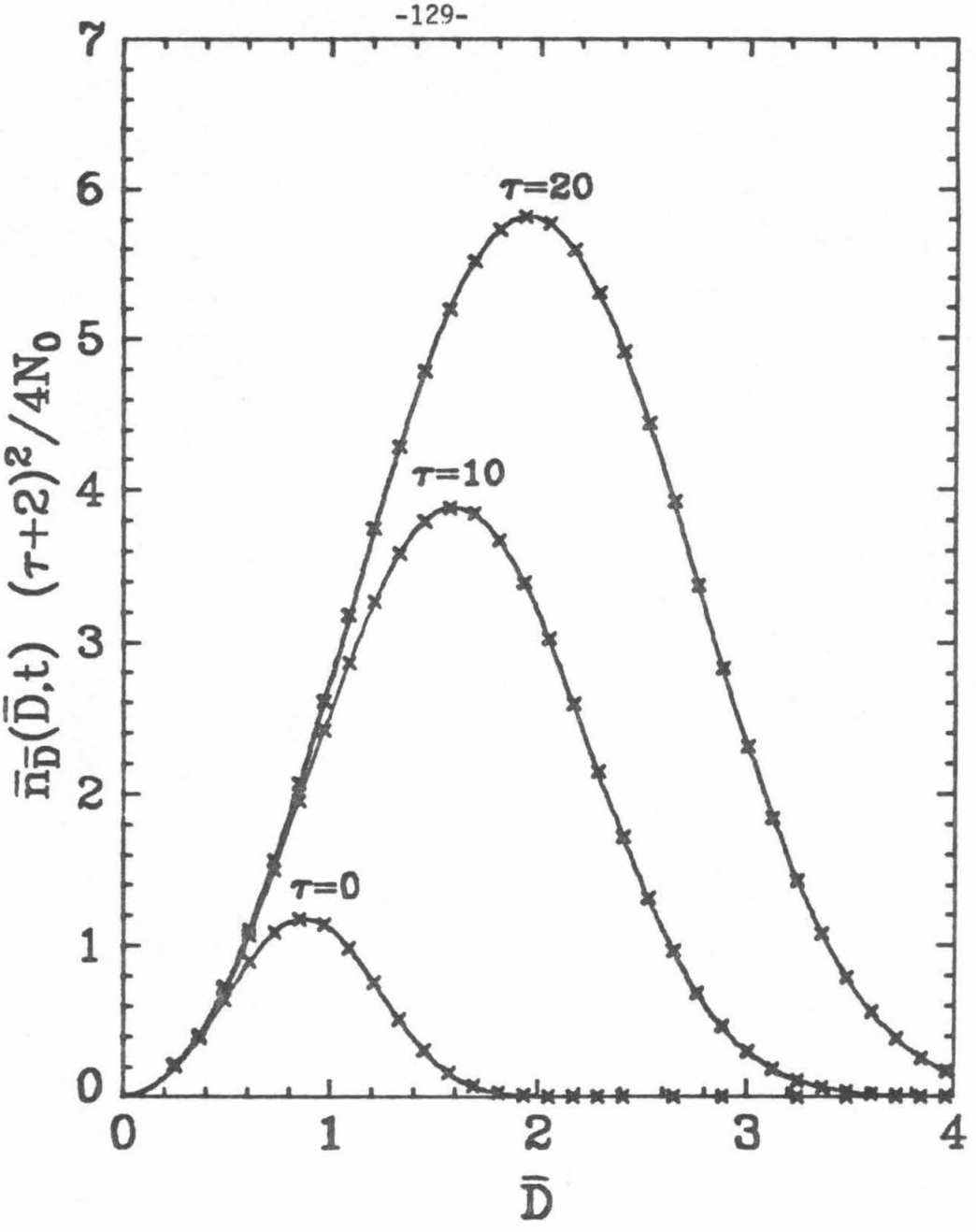

Figure 3

Particle size spectra. $\beta_v = \beta_o$ and $\tau = N_o\beta_o t$.

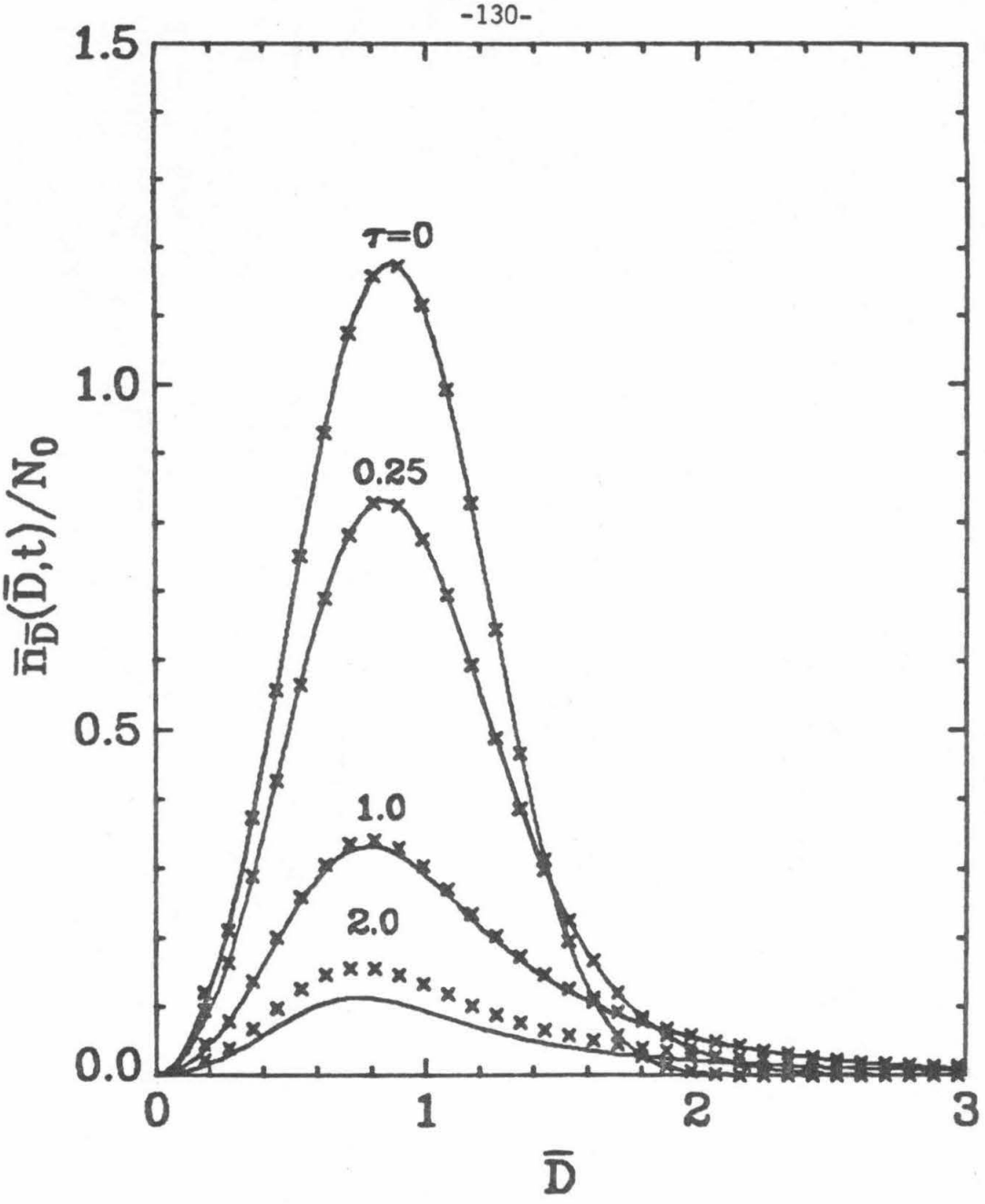

Figure 4

Particle size spectra. $\beta_v = \beta_1(v + \tilde{v})$ and $\tau = N_o\beta_1\nu_o t$.

more serious in case 3 than in case 1 because in case 3, β_v increases as the size of either particle increases, whereas in case 1, β_v is constant. Consequently, the shift of the spectrum to larger particle sizes is more rapid in case 3 at comparable values of the dimensionless time τ. At short times, $\tau < 1$, the numerical and exact solutions are very close. For longer times the numerical solution lies above the exact solution as in Figure 2 for case 1. We can of course, reduce the error by extending the computational domain. However, as mentioned previously in most particulate systems removal mechanisms are present. Therefore, in order to study the effect of removal on the finite domain error in case 4, we consider $\beta_v = \beta_1(v+\tilde{v})$, $S_v = -R_0\, n_v(v,t)$. From Table 5 we see a substantial decrease in the finite domain error with the addition of a first order removal mechanism. Since there are fewer particles greater than $\bar{v}_b$ in case 4 as compared to case 3, the effect of coagulation of particles within the domain with particles outside the domain is negligible. Hence, Figure 5 shows excellent agreement between the exact and numerical solutions.

Case 5 includes both coagulation and particle growth. Particle growth does not change the total number of particles; however, since only a finite domain is used in the numerical solution, particles will be artificially lost when they grow beyond the computational domain. From Table 5 we see that even greater finite domain errors in $M_0(t)$ exist for this case than for case 1. We see that particle growth is responsible for the additional error. Since the growth is independent

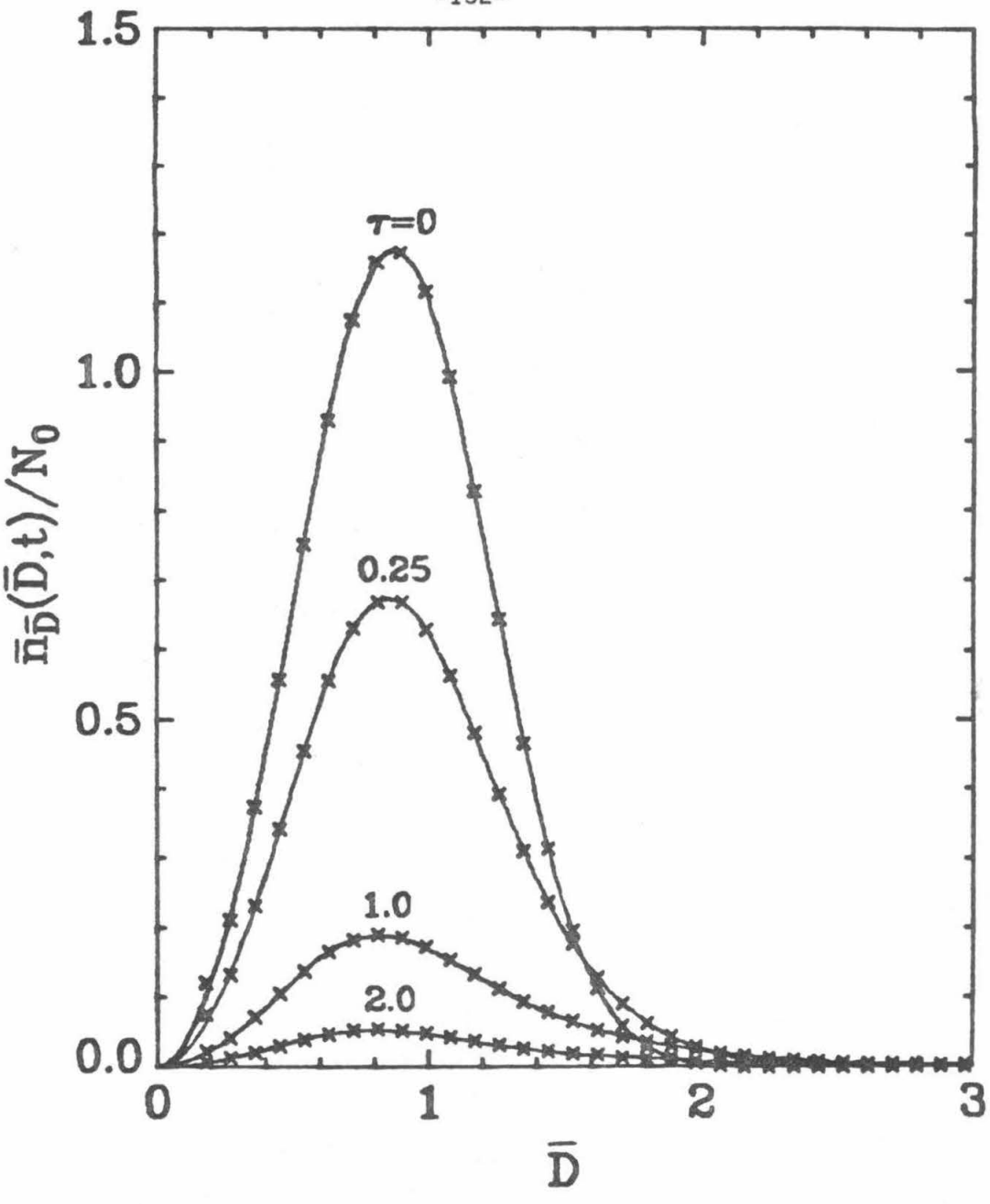

Figure 5

Particle size spectra. $\beta_v = \beta_1(v + \tilde{v})$, $S_v = - R_0 n_v(v,t)$, $\tau = N_0\beta_1\nu_0 t$ and $\theta = R_0/\beta_1 N_0 \nu_0 = 1$.

of the distribution at any point in the domain, even for an infinite domain, the finite domain errors shown in Table 5 do not lead to significant errors in the numerical solution. Thus, even though a substantial number of particles has been excluded, excellent agreement between the numerical and analytical solutions is still obtained, as shown in Figure 6.

In <u>case 6</u>, $\beta_v = \beta_0$ and $S_v = (S_0/v^*)\exp(-v/v^*) - R_0 n_v$, where v^* is a measure of the range of particle volumes over which particles are being generated. For the initial distribution given by Eq. [18] only an asymptotic solution for the large particle size end of the spectrum is available (5). Since the exact solution is not available, only the total number and volume of particles will be calculated for an infinite domain. Integrating Eq. [1] over v from 0 to ∞ leads to the following equation for N(t), the ratio of the number of particles present at time t to the initial number of particles,

$$\frac{dN}{d\tau} = -\frac{1}{2}N^2 - \theta N + \Omega \qquad [21]$$

where

$$N(t) = \frac{1}{N_0}\int_0^\infty n_v(v,t)dv \qquad [22]$$

Similarly, the ratio V of the total volume of particles at any time t to the initial volume of particles is described by

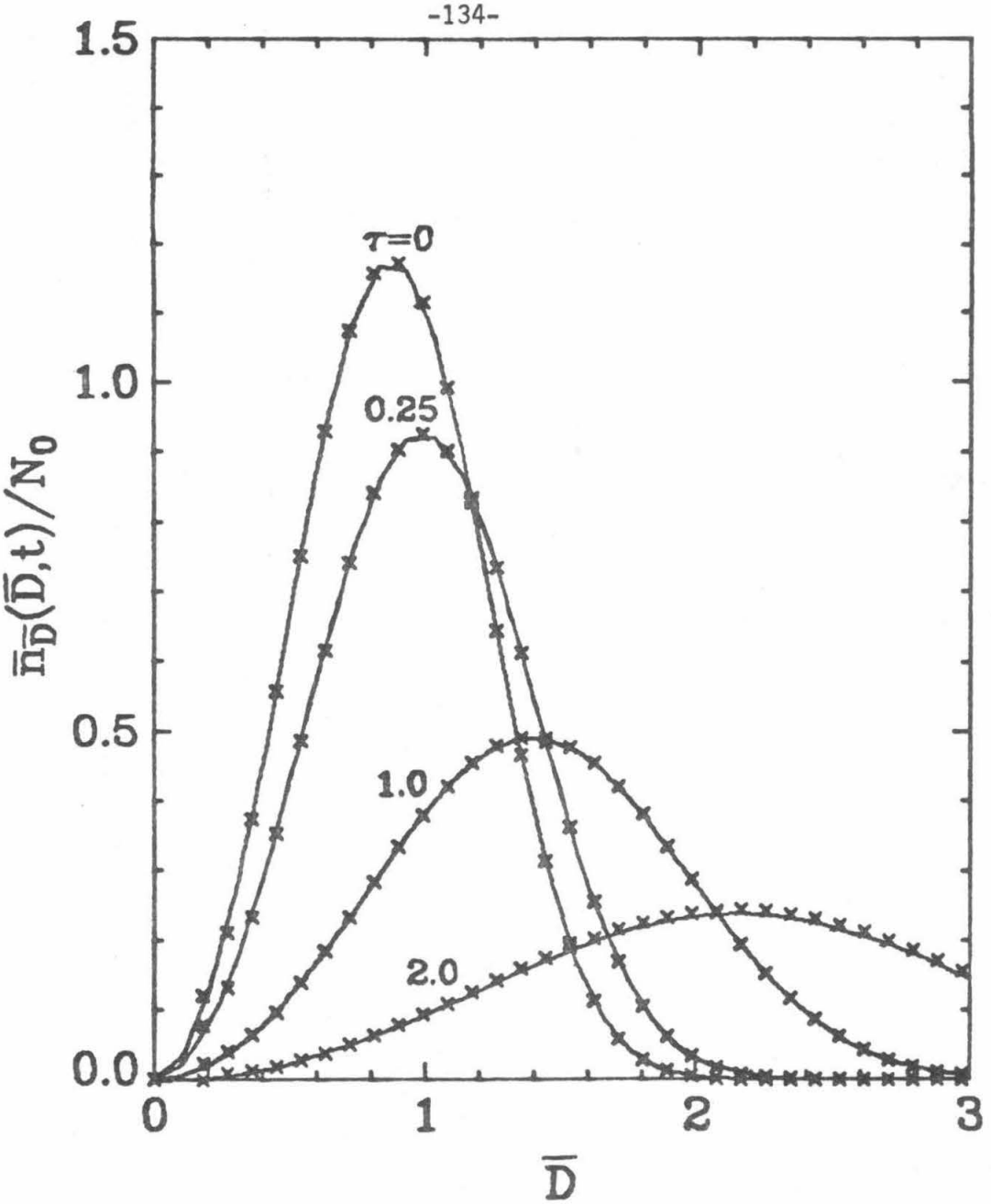

Figure 6

Particle size spectra. $\beta_v = \beta_o$, $I_v = \sigma v$, $\tau = N_o \beta_o t$ and $\Lambda = \sigma / N_o \beta_o = 1$.

$$\frac{dV}{d\tau} = - \theta V + \Delta\Omega \qquad [23]$$

where $\Delta = v^*/\nu_0$ and

$$V(t) = \frac{1}{N_0 \nu_0} \int_0^\infty v n_v(v,t)\, dv \qquad [24]$$

Solving Eqs. [21] and [23] yields

$$N(t) = \frac{r_1 - r_2\left(\frac{1-r_1}{1-r_2}\right)\exp\left[\frac{(r_2-r_1)\tau}{2}\right]}{1 - \left(\frac{1-r_1}{1-r_2}\right)\exp\left[\frac{(r_2-r_1)\tau}{2}\right]} \qquad [25]$$

and

$$V(t) = \left[\frac{\theta - \Delta\Omega}{\theta}\right]\exp(-\theta\tau) + \frac{\Delta\Omega}{\theta} \qquad [26]$$

where $r_1 = - \theta + \sqrt{\theta^2+2\Omega}$ and $r_2 = - \theta - \sqrt{\theta^2+2\Omega}$.

The numerical and asymptotic analytical solutions are shown in Figure 7 for $\Delta = 0.01$, $\theta = 1.0$, and $\Omega = 1.0$. In this case only, equally spaced elements in w, not $\bar{D}$, were used because of the large number of particles generated in the small size range. One reason for the deviation for the small particles is that the asymptotic solution does not hold. N(t) and V(t) were computed from Eqs. [25] and [26] and compared

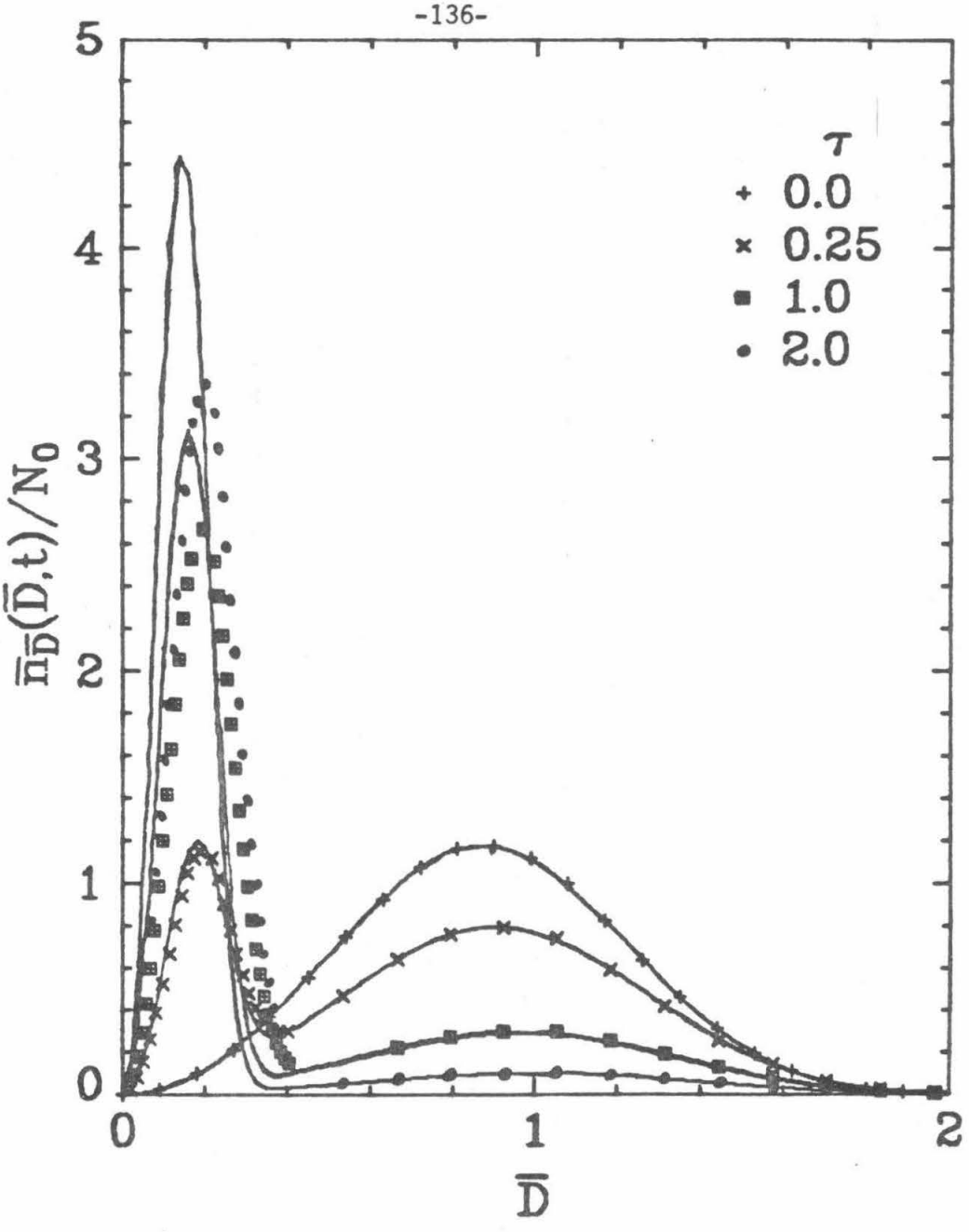

Figure 7

Particle size spectra. $\beta_v = \beta_o$, $S_v = S_o/v^* \exp(-v/v^*) - R_o n_v(v,t)$, $\tau = N_o\beta_o t$, $\theta = R_o/\beta_o N_o = 1$, $\Omega = S_o/\beta_o N_o^2 = 1$ and $\Delta = v^*/\nu_o = 0.01$. (Computations were carried out on $\bar{D}$ = [0.001, 3.0]. Only the region $\bar{D}$ = [0.001, 2.0] is shown.)

to the numerically computed values of N and V. The results are given in Table 6, where we see that, for the time considered, there is little finite domain error.

Table 6. Finite Domain Error for Case 6

$$\beta_v = \beta_0,\ S_v = \frac{S_0}{v^*} e^{v/v^*} - R_0 n_v \dagger$$

τ**	$\frac{N_{analytic}}{N_{numeric}}$	$\frac{V_{analytic}}{V_{numeric}}$
0.25	1.00	0.994
1.0	1.00	0.992
2.0	1.00	0.986

**$\tau = N_0 \beta_0 t$

† $\Omega = S_0/N_0^2\beta_0 = 1.0$, $\theta = R_0/N_0\beta_0 = 1.0$ and $\Delta = v^*/\nu_0 = 0.01$

5. COAGULATION OF A LABORATORY AEROSOL

As a test case for an actual aerosol, Husar's (23) 5th experiment for which there are ample data was simulated. In the experiment, approximately one gram of crystallized sodium chloride was vaporized in a slightly bent glass tube. The vapor was rapidly recondensed by the introduction of cool filtered air, thus forming an aerosol. Coagulation occurred in a 90 m^3 plastic bag from which samples were taken and analyzed. For the simulation, the initial distribution was curve fitted and it was assumed that only coagulation occurred at 293°K for spherical particles with a density of 2.165 gm/cc. In Figures 8 and 9 the measured size distributions are shown as discrete points and the theoretical results as lines, where $n'(\log_{10}D,t) = n_D(D,t)dD/d\log_{10}D$.* The Sitarski-Seinfeld (24) and Fuchs (25) coagulation coefficients were used in Figures 8 and 9 respectively. Because the Sitarski-Seinfeld coefficient is slightly less than Fuchs', the numerical solution of Figure 8 is slightly higher than that of Figure 9. Although both numerical and experimental size distributions are not in perfect agreement, their qualitative features are similar. Since coagulation is primarily a scavenging mechanism both the numerical and experimental distributions exhibit a rapid decrease for the smallest particles and a slight increase for the largest particles.

---

* Using 15 differential equations $\int_{v_a}^{v_b} vn_v(v,t)dv$ was conserved within 0.02%, thus indicating a negligible finite domain error.

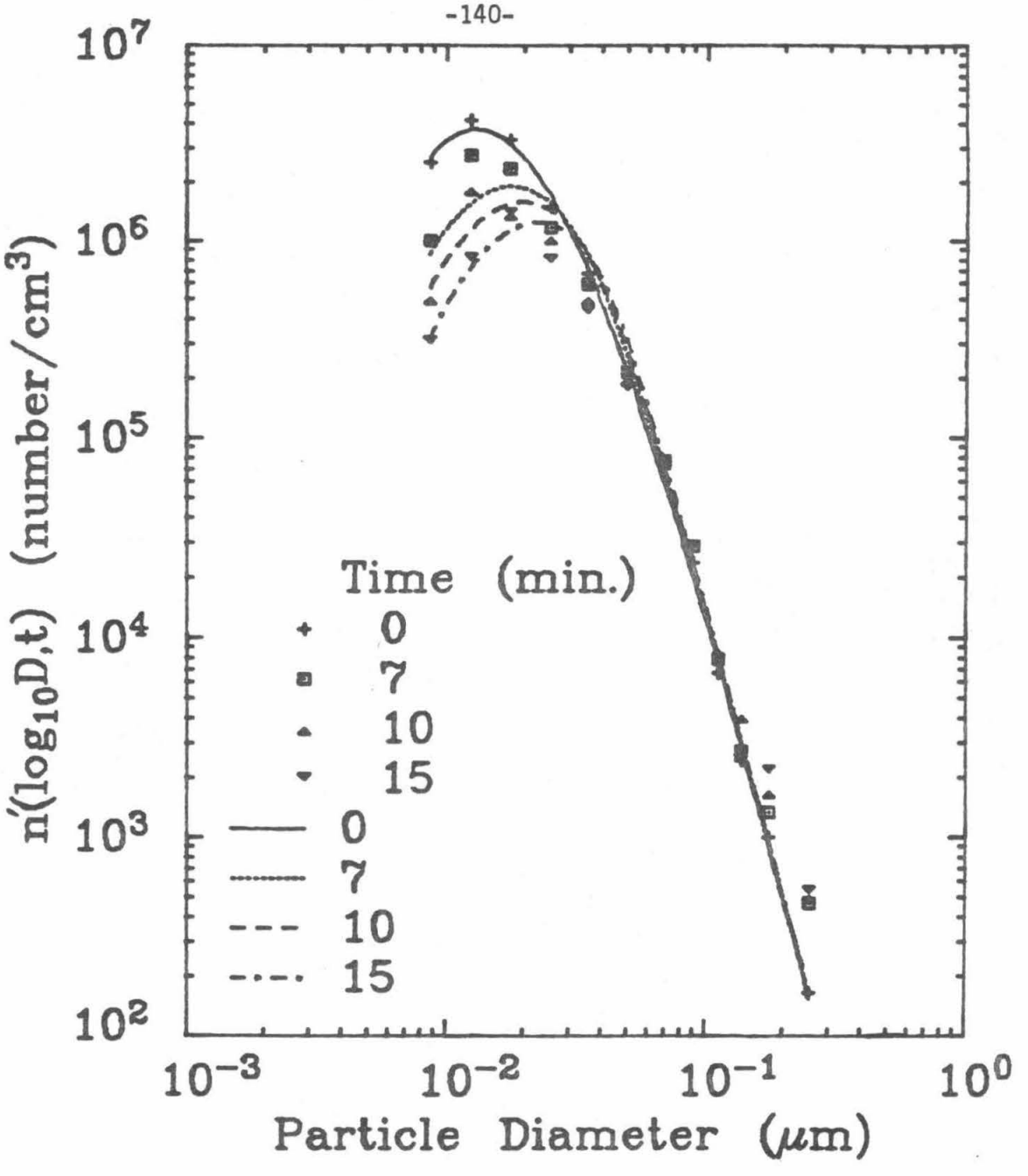

Figure 8

Particle size spectra for Husar's (23) experiment using the Sitarski-Seinfeld coagulation coefficient (24).

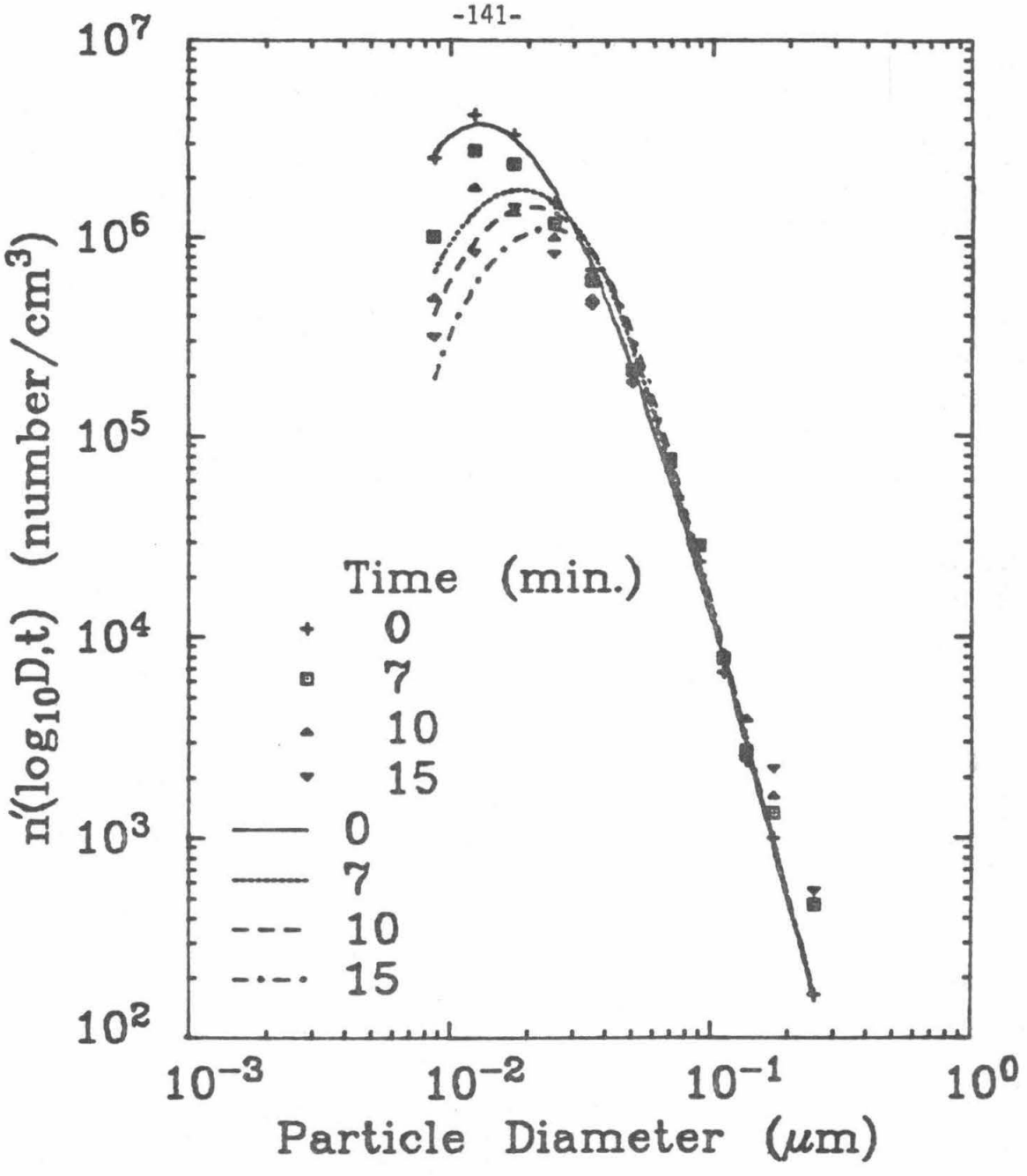

Figure 9

Particle size spectra for Husar's (23) experiment using Fuchs' coagulation coefficient (25).

6. SUMMARY

The principal alternatives to the method of weighted residuals for the solution of Eq. [1] either rely on assumptions on the expected shape of the solution (11,15), or employ discretization of particle sizes (6,8-10). The former class of methods, while computationally attractive, requires some prior knowledge of the solution. For a discrete or finite-difference solution to account for all possible particle sizes, the mesh spacing must, in principle, be equal to the size of the smallest particle. The number of particle sizes needed to represent exactly a distribution between particle volumes v_a and v_b is v_b/v_a; for atmospheric aerosols this ratio can be 10^{10}. Clearly, for a discrete solution to be computationally feasible the mesh spacing must be several orders of magnitude larger than the size of the smallest particle. In such a case substantial errors may be committed when representing the integral terms in Eq. [1]. For problems of the type considered here, the methods of weighted residuals, such as collocation on finite elements, appear to be more attractive and efficient than finite-difference methods.

Although no definite conclusions can be made on which finite element technique is best for all cases, the advantages and disadvantages of each technique should be pointed out. For $\bar{M}$ collocation points, cubic splines requires the solution of a $(\bar{M}-2)$-dimensional tridiagonal linear system, while orthogonal collocation on finite elements requires the solution to a linear system with a banded matrix of bandwidth 7.

However, to evaluate the distribution, orthogonal collocation on finite elements is considerably easier. The major difference between the two techniques is the location of the collocation points relative to the grid points. Orthogonal collocation of finite elements has the flexibility of locating the collocation points anywhere within the element, (although the roots of an orthogonal polynomial are considered optimal). In cubic splines the collocation points are fixed at the grid points, but twice as many elements can be used for the same number of collocation points and the fit has continuous second derivatives.

A major source of error in solving Eq. [1] by collocation on finite elements is the use of a finite computational domain. The cases considered here represent a severe test of the so-called finite domain error because the distributions for those cases for which analytical solutions can be obtained tend to have uncharacteristically large numbers of particles at the upper end of the size spectrum when compared with most actual particulate systems. As shown for an actual particulate system, the range of particle sizes is finite, and the finite domain error can be expected to be considerably less than that for cases such as those considered here. Hence time integrations can be performed for a longer time span.

NOTATION

$A_{i,j}(t)$	$\underline{j}$ th coefficient of the $\underline{i}$ th element, cm^{-3}
D	particle diameter, μm
$\bar{D}$	dimensionless particle diameter
D_a	smallest particle diameter, μm
D_b	largest particle diameter, μm
I_1	modified Bessel function of the first kind of order one
$I_D(D,t)$	particle diameter growth rate, $\mu m\ sec^{-1}$
$I_v(v,t)$	particle volume growth rate, $\mu m^3\ sec^{-1}$
$M_0(t)$	fraction of the total number of particles contained in the finite computational domain
$M_1(t)$	fraction of the total volume of particles contained in the finite computational domain
$m(w,t)$	rescaled number distribution function, cm^{-3}
N_0	initial particle concentration, cm^{-3}
$N(t)$	ratio of the number of particles present at time t to the initial number of particles
$n_D(D,t)$	number distribution function based on the particle diameter, $\mu m^{-1}\ cm^{-3}$
$n_v(v,t)$	number distribution function based on the particle volume, $\mu m^{-3}\ cm^{-3}$

NOTATION (Continued)

R_0	homogeneous particle loss constant, sec^{-1}
t	time, sec
v	particle volume, μm^3
$\bar{v}$	dimensionless particle volume
V(t)	ratio of the volume of particles present at time t to the initial volume of particles
w	rescaled dimensionless particle size
y	linear rescaled w

Greek Letters

β_0	constant coagulation coefficient, $cm^3\ sec^{-1}$
β_1	constant for the linear coagulation coefficient, sec^{-1}
$\beta_D(D,\tilde{D})$	coagulation coefficient based on the particle diameter, $cm^3\ sec^{-1}$
$\beta_V(v,\tilde{v})$	coagulation coefficient based on the particle volume, $cm^3\ sec^{-1}$
ζ	largest diameter over the smallest diameter
θ	removal rate over the coagulation rate
Λ	condensation rate over the coagulation rate

Greek Letters (Continued)

ν_0	mean initial particle volume, μm^3
σ	growth law coefficient, sec^{-1}
τ	dimensionless time
Ω	source rate over the coagulation rate

REFERENCES

1. Drake, R. L., in "Topics in Current Aerosol Research," (Hidy, G. M. and Brock, J. R. Eds.), Vol. 3, pp. 201-376. Pergamon, Oxford, 1972.

2. Ramabhadran, T. E., Peterson, T. W., and Seinfeld, J. H., "Dynamics of Aerosol Coagulation and Condensation," A.I.Ch.E.J. 22, 840 (1976).

3. Golovin, A. M., "The Solution of the Coagulation Equation for Raindrops, Taking Condensation Into Account," Sov. Phys. Dokl. 8, 191 (1963).

4. Scott, W. T., "Analytic Studies of Cloud Droplet Coalescence," J. Atmos. Sci. 25, 54 (1968).

5. Peterson, T. W., Gelbard, F., and Seinfeld, J. H., "Dynamics of Source-Reinforced, Coagulating, and Condensation Aerosols," J. Colloid Interface Sci. 63, 426 (1978).

6. Hidy,G.M.,"On the Theory of Non-Interacting Particles in Brownian Motion," J. Colloid Interface Sci. 20, 123 (1965).

7. Twomey, S., "Computation of Rain Formation by Coalescence," J. Atmos. Sci. 23, 405 (1966).

8. Mockros, L. F., Quon, J. E., and Hjelmfelt, A. T., "Coagulation of a Continuously Reinforced Aerosol," J. Colloid Interface Sci. 23, 90 (1967).

9. Takahashi, K. and Kasahara, M., "A Theoretical Study of the Equilibrium Particle Size Distribution of Aerosols," Atmos. Environ. 2, 441 (1968).

10. Suzuki, A., Ho, N. F.H., and Higuchi, W.I., "Prediction of the Particle Size Distribution Changes in Emulsions and Suspensions by Digital Computation," J. Colloid Interface Sci. 29, 552 (1969).

11. Cohen, E. R. and Vaughan, E. U., "Approximate Solution of the Equation for Aerosol Agglomeration," J. Colloid Interface Sci. 35, 612 (1971).

12. Gillette, D. A., "A Study of Aging of Lead Aerosols - II," Atmos. Environ. 6, 451 (1972).

13. Berry, E. X., "Cloud Droplet Growth by Collection," J. Atmos. Sci. 24, 688 (1967).

14. Burgmeir, J. W., Blifford, I. H., and Gillette, D. A., "A Reinforced Coagulation-Sedimentation Aerosol Model," Water, Air and Soil Pollution 2, 97 (1973).

15. Singh, P. N. and Ramkrishna, D., "Transient Solution of the Brownian Coagulation Equation by Problem-Specific Polynomials," J. Colloid Interface Sci. 53, 214 (1975).

16. Middleton, P. and Brock, J., "Simulation of Aerosol Kinetics," J. Colloid Interface Sci. 54, 249 (1976).

17. Finlayson, B. A., "The Method of Weighted Residuals and Variational Principles." Academic, New York, 1972.

18. Villadsen, J. V. and Stewart, W. E., "Solution of Boundary-Value Problems by Orthogonal Collocation," Chem. Eng. Sci. 22, 1483 (1967).

19. Martin, H. C. and Carey, G. F., "Introduction to Finite Element Analysis." McGraw-Hill, New York, 1973.

20. Carey, G. F. and Finlayson, B. A., "Orthogonal Collocation on Finite Elements," Chem. Eng. Sci. 30, 587 (1975).

21. Dahlquist, G. and Bjorck, A., "Numerical Methods," pp. 131-134. Prentice-Hall, Englewood Cliffs, New Jersey, 1974.

22. Carnahan, B., Luther, H. A., and Wilkes, J. O., "Applied Numerical Methods," p. 63. Wiley, New York, 1969.

23. Husar, R. B., "Coagulation of Knudsen Aerosols," Ph.D. Thesis, University of Minnesota, 1971.

24. Sitarski, M. and Seinfeld, J. H., "Brownian Coagulation in the Transition Regime," J. Colloid Interface Sci. 61, 261 (1977).

25. Fuchs, N. A., "The Mechanics of Aerosols," pp. 291-294. Pergamon, Oxford, 1964.

APPENDIX

In deriving the GDE in Chapter II, terms were grouped so that transformations from one GDE to the next would be simplified. However, Eqs. [7], [8], [10], [11], [15], [16], and [19] of Chapter II, are poorly arranged for numerical computation. Because computers represent a number by only a finite number of significant figures, the coding should be arranged to minimize round off errors. Since many of the processes represented in the GDE have very large, yet comparable rates associated with them, subtraction of these rates should result in a relatively small net rate, but due to machine round off, significant errors result. In general it is better to arrange the coding such that numbers with the smallest absolute value are added and subtracted first, with operations on the largest numbers performed last. If possible, terms should be factored before addition and subtraction. Therefore,

$$\frac{1}{2}\int_{v_{k+1}-v_1/2}^{v-v_{k+1}+v_1/2} \beta_v(v-u,u)n_v(v-u,t)n_v(u,t)\,du - n_v(v,t)\int_{v_{k+1}-v_1/2}^{\infty} \beta_v(v,u)n_v(u,t)\,du \qquad [A1]$$

should be evaluated as

$$\int_{v_{k+1} - v_1/2}^{v/2} [\beta_v(v-u,u)n_v(v-u,t) - \beta_v(v,u)n_v(v,t)]n_v(u,t)\,du - n_v(v,t)\int_{v/2}^{\infty} \beta_v(v,u)n_v(u,t)\,du \qquad [A2]$$

Because the number of clusters is expected to decrease very rapidly with cluster size

$$\sum_{j=1}^{i-1} \frac{1}{2}\,\beta_v(v_{i-j},v_j)N(v_j,t)N(v_{i-j},t) - N(v_i,t)\sum_{j=1}^{k} \beta_v(v_i,v_j)N(v_j,t) \qquad [A3]$$

should be evaluated as,

$$\sum_{j=i-1}^{1} \left[\frac{\beta_v(v_{i-j},v_j)N(v_{i-j},t)}{2} - \beta_v(v_i,v_j)N(v_i,t)\right]N(v_j,t) - N(v_i,t)\sum_{j=k}^{i} \beta_v(v_i,v_j)N(v_j,t). \qquad [A4]$$

For the monomer,

$$\int_{v-v_{k+1}+v_1/2}^{\infty} E(v)n_v(v,t)dv \quad - \quad N(v_1,t) \int_{v-v_{k+1}+v_1/2}^{\infty} \beta_v(v,v_1)n_v(v,t)\, dv \qquad [A5]$$

should be evaluated as,

$$\int_{v-v_{k+1}+v_1/2}^{\infty} \left[E(v) - \beta(v,v_1)N(v_1,t)\right] n_v(v,t)\, dv. \qquad [A6]$$

Finally,

$$\sum_{j=1}^{k} E(v_j)N(v_j,t) - N(v_1,t)\sum_{j=1}^{k} \beta(v_i,v_1)N(v_i,t) \qquad [A7]$$

should be evaluated as,

$$\sum_{j=k}^{1} \left[E(v_j) - N(v_1,t)\beta(v_i,v_1)\right] N(v_j,t). \qquad [A8]$$

It was found that not only was a more accurate solution obtained with these modifications to the coding, but also problems which were previously unstable achieved stability.

Chapter V

APPLICATIONS OF THE GENERAL DYNAMIC EQUATION TO THE SIMULATION OF SULFURIC ACID/WATER AEROSOL FORMATION AND GROWTH

ABSTRACT

The formation and growth of a sulfuric acid/water aerosol in a smog chamber is simulated using the discrete-continuous and continuous General Dynamic Equations, and the results are compared with recent experimental data. The following issues on aerosol formation and growth are investigated for the simulated experiment.

(1) The establishment of a steady state concentration profile of molecular clusters in the presence of a preexisting aerosol.

(2) The relative importance of nucleation, condensation, and scavenging in gas-to-particle conversion.

(3) The importance of cluster-cluster agglomeration relative to other processes.

1. INTRODUCTION

In the study of gaseous air pollutants, chemical reactions are isolated from transport processes by carrying out atmospheric chemical reactions in laboratory vessels, commonly referred to as smog chambers. Chemical mechanisms derived from analysis of the results of smog chamber experiments are then employed, together with descriptions of transport and diffusion, to produce mathematical models of atmospheric gaseous pollutant behavior. As in the study of gas phase air pollution chemistry, smog chambers have also been employed to elucidate aerosol formation and growth in an environment free of the complications of transport and diffusion. A key step in the process of developing a comprehensive mathematical model for atmospheric aerosols is careful analysis of the results of smog chamber experiments in which aerosol formation and growth accompanies the usual gaseous chemistry. These experiments must be analyzed to test our understanding of the gas-to-particle conversion process, to study the competition between condensation on existing particles and nucleation to form new particles, and to assess the importance of scavenging. A complication inherent in the performance and analysis of such experiments, not present in purely gaseous experiments, is that particle formation and growth is strongly influenced by the presence of existing aerosol. Thus, the initial conditions of aerosol number, size, and chemical composition in the reactor may substantially influence the ultimate

quantity and size distribution of aerosol achieved. Experiments of this type are ordinarily carried out with an initial charge that is either particle-free or consists of particles characteristic of primary sources or ambient air.

The discrete-continuous GDE is ideally suited for the simulation of aerosol formation and growth in smog chambers, and this chapter is devoted to the first simulation of actual experimental aerosol data in such a situation. Of all the existing smog chamber experiments involving aerosols, the photochemical oxidation of SO_2 to form a sulfate aerosol is the most common. Although several experimental investigations have been reported (1-8), the mechanisms by which the aerosol develops are not completely understood. Aerosol formation from SO_2 has been simulated previously using the continuous GDE (9,10). However, as previously discussed in Chapter II, the discrete-continuous GDE provides a more detailed description of the aerosol and does not rely on homogeneous nucleation theory to describe the molecular cluster dynamics. Because of the recent availability of experimental data (8), we are also able to make direct comparisons of the predicted and measured aerosol number and volume distributions for photochemical oxidation of SO_2.

We begin with a description of the experiment and the assumptions made on the physical properties of the aerosol. Then

using the discrete-continuous GDE, the predicted evolution of the distribution is compared with experiment. The discrete-continuous GDE is also used to study the relative importance of condensation, nucleation, scavenging and cluster-cluster agglomeration for gas-to-particle conversion. Finally, the results of using the continuous GDE are discussed.

2. DESCRIPTION OF THE EXPERIMENT

We have chosen to simulate one of the experiments of McMurry (8), a recent and comprehensive study of aerosol formation from the photochemical oxidation of SO_2. In the experiment a large teflon bag was filled with unfiltered ambient air, doped with measured amounts of NO, NO_2, SO_2 and C_3H_6, and exposed to solar radiation throughout the filling and data acquisition period. Based on the initial SO_2 concentration of 81 ppb, the initial bag volume was computed to be 49 m^3, (after correcting for the measured background SO_2 concentration of 15 ppb). Experiment P17 is simulated here because both the temperature and relative humidity remained almost constant at 37° C and 34%, respectively, throughout. The initial distribution was taken from the third reported size distribution, because it corresponded to the time that the observed SO_2 concentration began to decrease. Logarithmic interpolation was used to fit the initial size distribution, but due to instrument limitations the size distribution for particle diameters below 0.0133 μm was obtained by extrapolation. (The validity of the extrapolation will be discussed later.) Based on the initial curve fit, the total number, surface area, and volume of particles with diameters from 0.0133 μm to 1 μm are 1.65×10^5 cm^{-3}, 5.55×10^2 μm^2 cm^{-3} and 1.02×10^1 μm^3 cm^{-3}, respectively. It was assumed that all the SO_2 converted produced molecular H_2SO_4. The average loss rate of

SO_2 was used to compute a constant rate of H_2SO_4 generation of 4.84×10^7 molecules sec^{-1} cm^{-3}. (For comparison, in a different study of H_2SO_4/H_2O aerosol formation, a generation rate of 1.25×10^7 molecules sec^{-1} cm^{-3} was used (10.)

3. PHYSICAL PROPERTIES OF A H_2SO_4/H_2O AEROSOL PHOTOCHEMICALLY GENERATED IN THE PRESENCE OF A PREEXISTING URBAN AEROSOL

One of the major difficulties in simulating experimental data is determining the physical properties of the aerosol. In most cases, even if all the chemical constituents of the aerosol have been identified, the necessary thermodynamic data are not available. One is always confronted with the problem of determining particle properties such as diameter, vapor pressure, evaporation rate, and surface tension for a particle containing only a few molecules. Clearly, certain bulk concepts are meaningless for clusters containing several molecules, and the validity of extrapolating bulk values to molecular clusters is questionable.

We are faced here, therefore, with the problem of assuming the physical properties of the aerosol generated in the experiments of McMurry. In nearly all photochemical oxidation studies of SO_2 the assumed product is H_2SO_4 (8,10,11). Due to the presence of water vapor, it is also assumed that the particles consist of H_2SO_4/H_2O droplets. Unfortunately, in dealing with an urban atmosphere the matter is further complicated because the preexisting aerosol undoubtedly contains a complex mixture of salts and organics. We will assume that the only effect of the ambient aerosol and gaseous impurities is to reduce the H_2SO_4 vapor pressure over the droplets to the point that evaporation of H_2SO_4 can be neglected to a first

approximation. The reduction in particle vapor pressures due to impurities has recently been observed (12). The validity of neglecting evaporation of sulfuric acid will be discussed later.

For the bulk phase H_2SO_4/H_2O system all the necessary thermodynamic data are available (13-16). Except for the particle diffusivity, all physical properties were based on the bulk values. To account for the variation of composition with particle size it was assumed that for a particle containing a fixed number of H_2SO_4 molecules the number of H_2O molecules in the particle is determined by thermodynamic equilibrium. Due to the much higher concentration of H_2O in the gas phase, this is a valid assumption (17,18). As shown elsewhere (19-21), the free energy of formation of a particle as a function of the H_2SO_4 and H_2O in the particle for a fixed temperature, H_2SO_4 gas phase concentration, and relative humidity can be computed. Since the free energy surface is a saddle, there is a unique number of H_2O molecules associated with a fixed number of H_2SO_4 molecules for a minimum free energy of formation. Thus, for the conditions of the experiment, the particle density, surface tension, and acid concentration can be determined as a function of particle size. Because the operating temperatures of the experiment did not correspond to the temperature at which all the thermodynamic data are available, corrections were made to the thermodynamic data as described elsewhere (22). (The variation of the equilibrium

vapor pressure of H_2SO_4 in a mixture with water over a flat surface as a function of composition for ambient temperatures is shown in Fig. 1 (15).)

It is interesting to note the variation of physical properties with particle size as determined on the basis of the above assumptions. As shown in Fig. 2, the H_2SO_4 mole fraction in the particle is highly dependent on the particle size and relative humidity. Also notice that for a fixed particle size, the H_2O concentration increases as the relative humidity increases. Therefore, Fig. 3 shows that due to the additional H_2O molecules the particle size increases for a fixed number of H_2SO_4 molecules in the particle, as the relative humidity increases.

To calculate the particle diffusivity, kinetic theory (23) can be used for molecules and small molecular clusters. For larger particles the Stokes-Einstein expression (24) is more appropriate. Note from Fig. 4 that for the conditions of the experiment, at 37° C and 34% relative humidity, both expressions are not appreciably different over a wide range of particle diameters. Because the Stokes-Einstein expression (using Phillips' formula (25) for the drag), is considered valid for particles smaller than the mean free path of air (which is approximately 0.0714 μm at 37° C), the diffusivity for particle diameters larger than 0.00147 μm was calculated using the Stokes-Einstein expression, and for particle

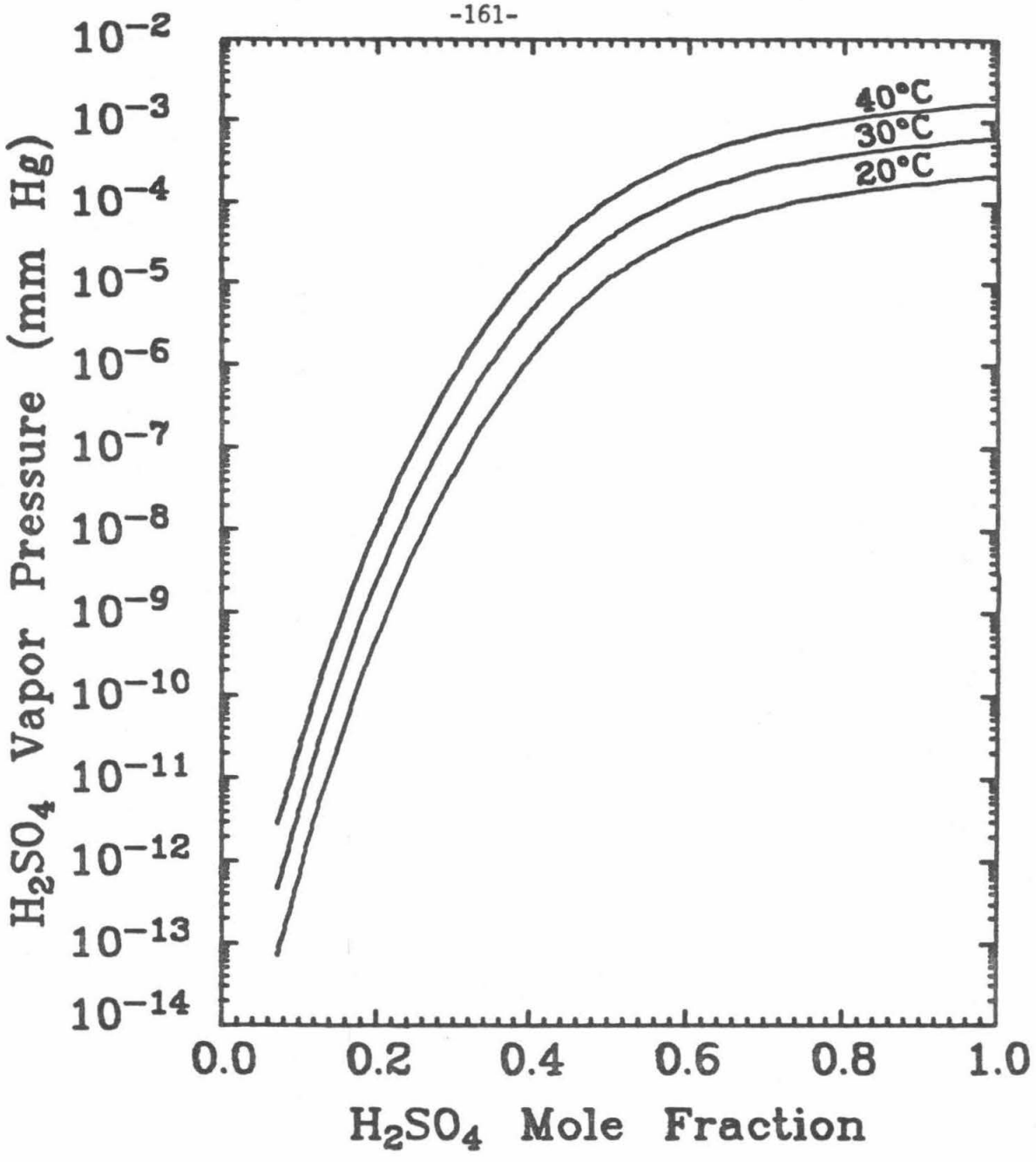

Figure 1

Equilibrium vapor pressure of H_2SO_4 in a mixture with water over a flat surface as a function of composition and temperature (15).

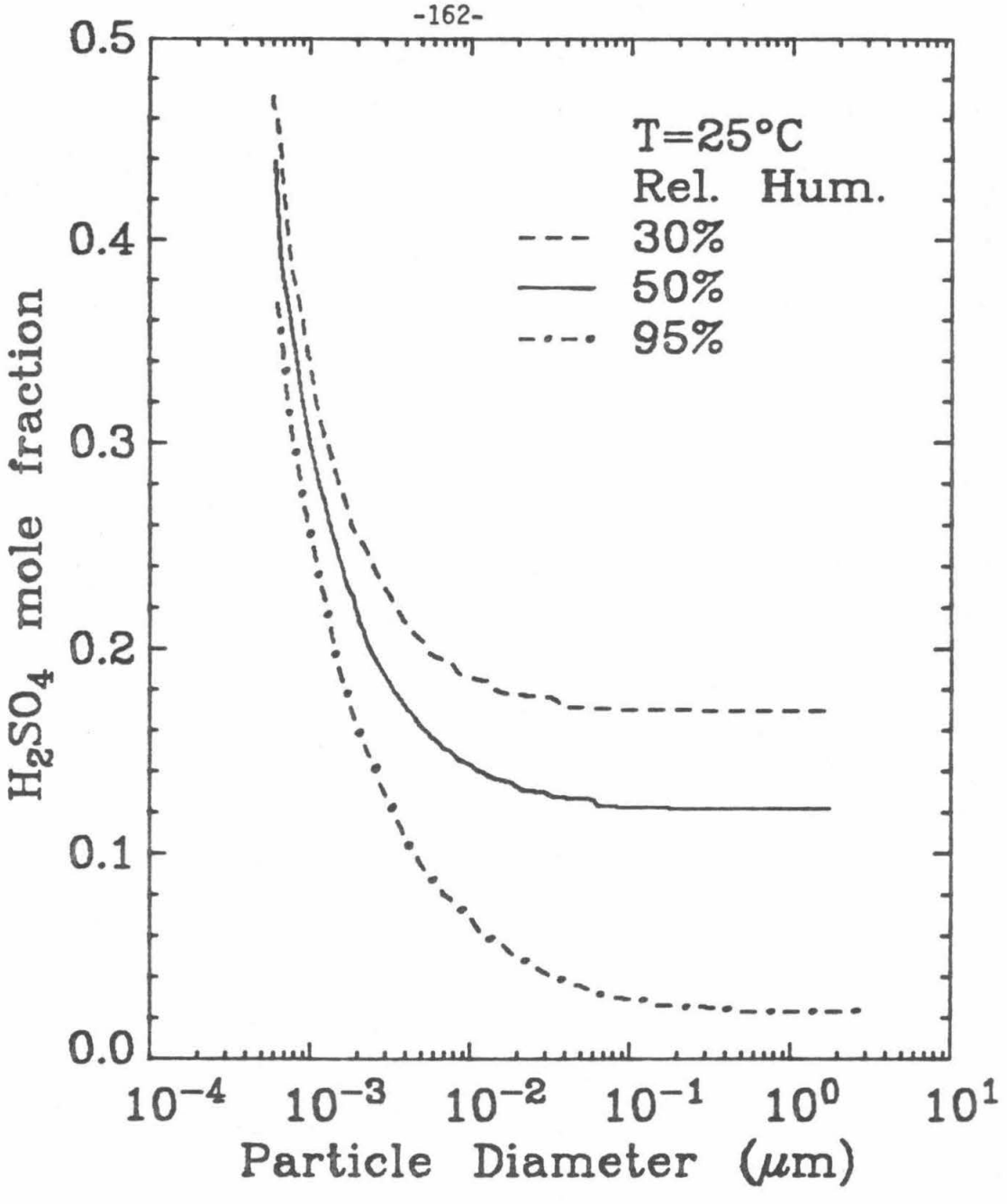

Figure 2

Equilibrium concentration of H_2SO_4 in a spherical droplet of H_2SO_4 and H_2O, as a function of the relative humidity and particle diameter.

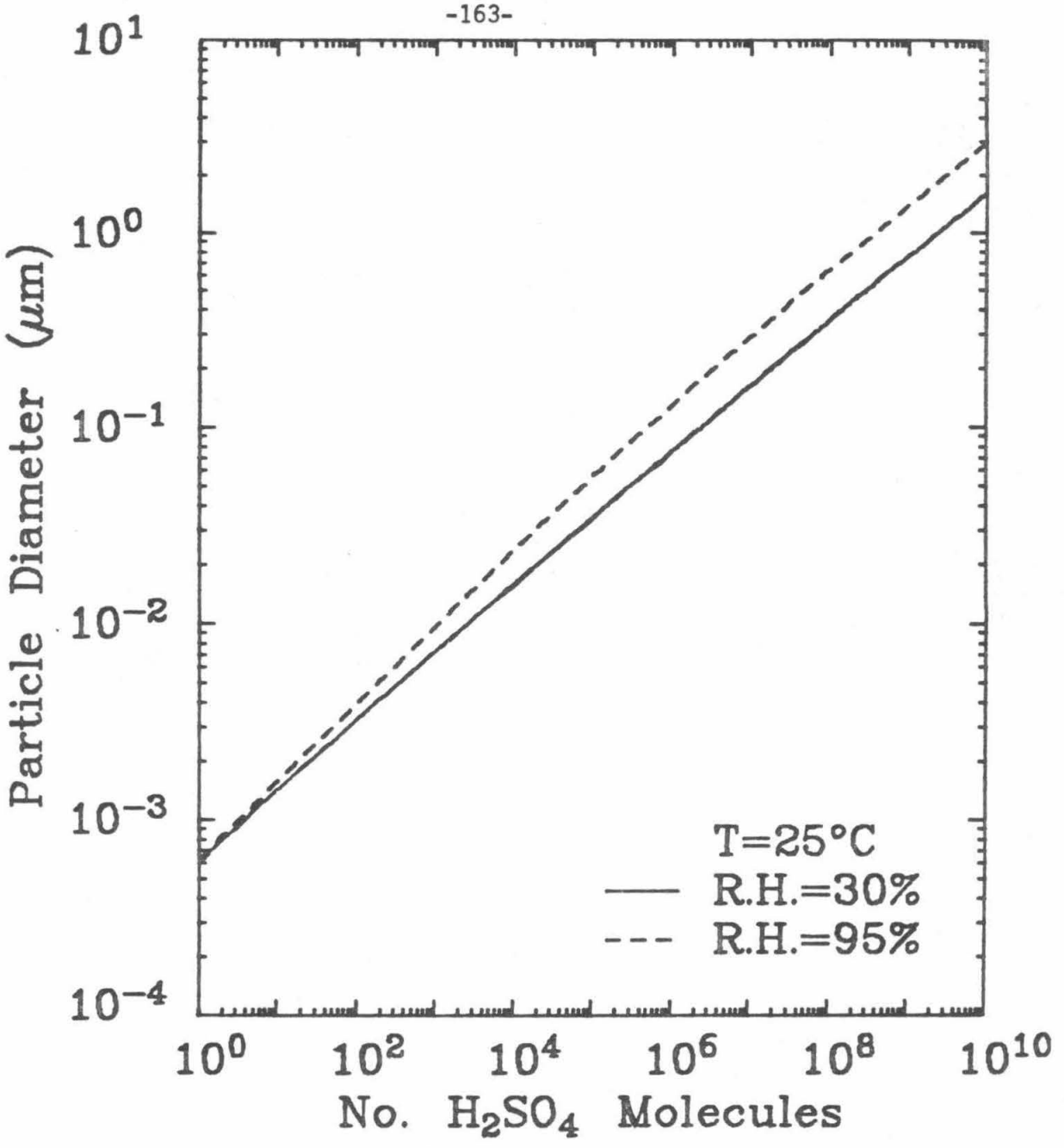

Figure 3

Equilibrium particle size as a function of the relative humidity and the number of H_2SO_4 molecules in the particle.

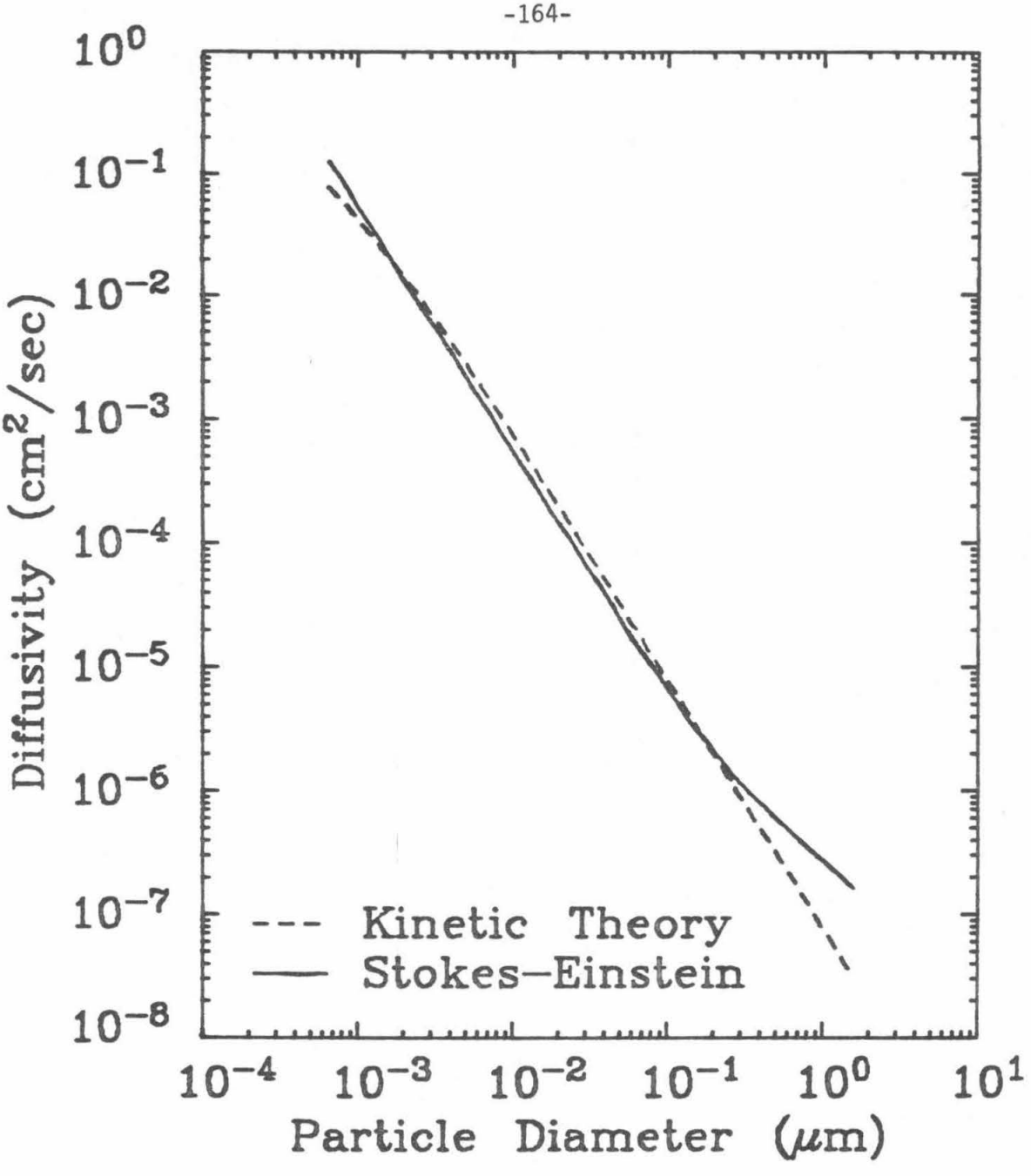

Figure 4

Diffusivity for a H_2SO_4/H_2O particle at 37° C and 34% relative humidity. Particle composition and density as a function of size were determined by thermodynamic equilibrium.

diameters smaller than 0.00147 μm by kinetic theory. As shown in Fig. 4, 0.00147 μm corresponds to the crossover point of the two expressions.

4. SIMULATION RESULTS USING THE DISCRETE-CONTINUOUS GDE

The aerosol is assumed to consist of sulfuric acid-water particles in thermodynamic equilibrium at the temperature and relative humidity of the experiment. The quantity conserved during particle agglomeration is the number of sulfuric acid molecules. Thus, the independent variable v in the GDE will be the number of sulfuric acid molecules rather than the particle volume. Since particle size is uniquely related to the number of sulfuric acid molecules in the particle at any relative humidity, v can be converted to particle volume. The details of solving the GDE numerically are given in Chapter IV.* In the computations the Fuchs-Phillips agglomeration coefficient (26) was used, and the upper limit on particle size was taken to be 1 μm diameter.

The computed and measured number distributions, in terms of $\bar{n}(\log_{10}D,t) = n(v,t)dv/d\log_{10}D$, are shown in Fig. 5. Agreement between the predicted and observed spectra below about 0.1 μm diameter is not as good as that above 0.1 μm. The discrepancy between predicted and observed size distributions in the lower end of the spectrum can be a result of the neglect of monomer evaporation from

*It is important to monitor the so-called "finite domain error," by checking that $\sum_{i=1}^{k} v_i N(v_i,t) + \int_{v_{k+1}-v_1/2}^{\infty} v\, n(v,t)\, dv$ is conserved during the computation. For the present application v represents the number of H_2SO_4 molecules, and for the times and the domain considered the error was less than 0.4%.

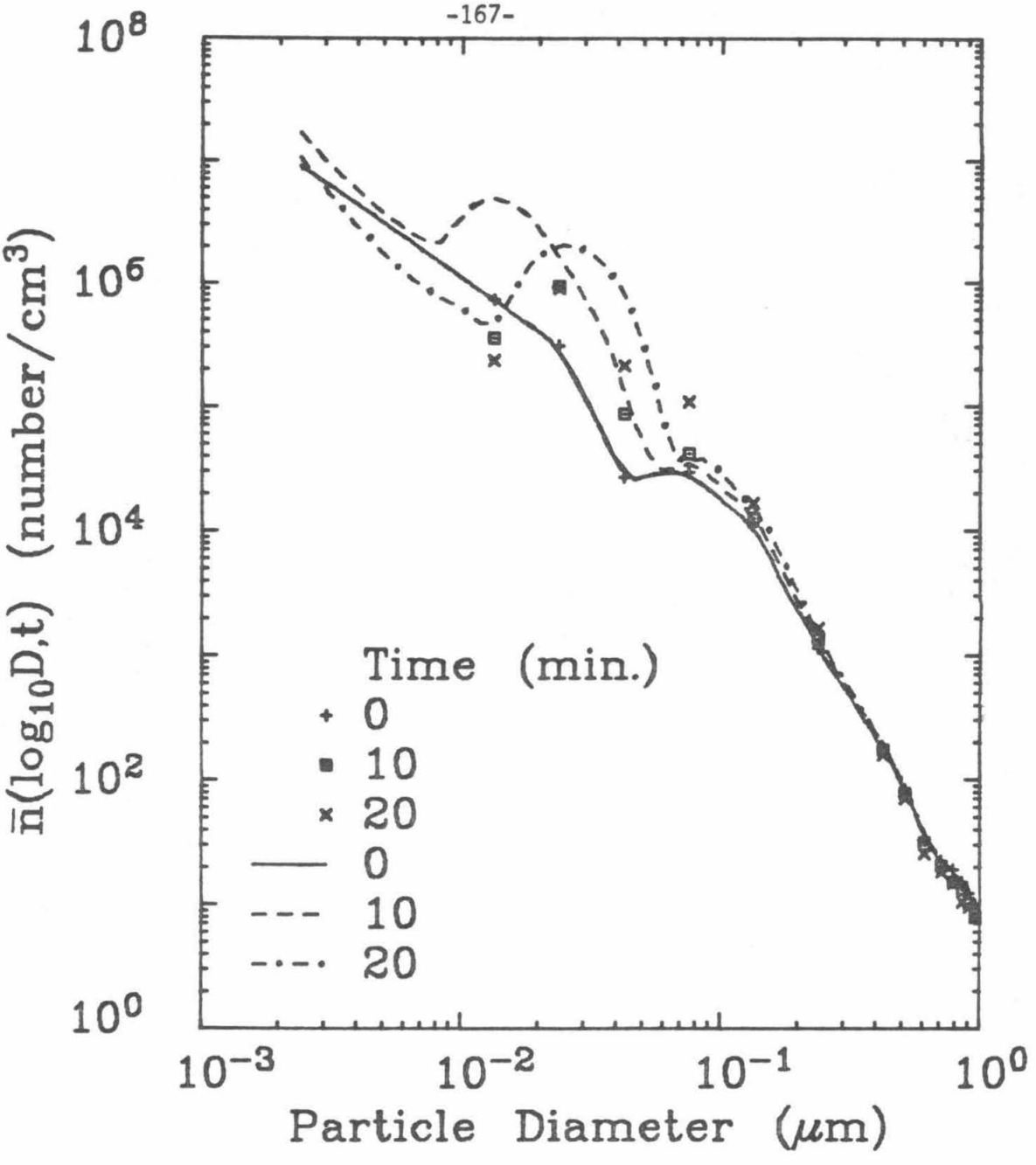

Figure 5

Number distribution evolution. Discrete points are the measured values and the lines are the computed results. The initial distribution for particle diameters below 0.0133 μm was obtained by extrapolation.

small particles, assuming each collision results in coalescence, or an inaccurate extrapolation of the initial size distribution into the non-detectable size regime. In addition, the accuracy of the data at the smallest particle sizes was estimated to be only within an order of magnitude (27). The actual evaporation rate probably lies somewhere between that of pure sulfuric acid/water and the assumed value of zero. Based on the assumption of no evaporation and each collision results in coalescence, the predicted number density represents that for a maximum particle growth rate. A second possible source of error arises in extrapolating the initial size distribution below the detectable limit down to the monomer. The particles below the detection limit grow by agglomeration and condensation, and may have a significant effect on the distribution in the detectable size range.

For large particles the errors committed by neglecting evaporation and extrapolating the initial distribution are smaller and thus better agreement between the predictions and the data is expected. The number distribution changes very little for large particles and comparisons are best made using the volume distribution $V(\log_{10}D,t)$, where $V(\log_{10}D,t) = \pi D^3\bar{n}(\log_{10}D,t)/6$. Fig. 6 shows that the predicted volume distribution agrees very well with the data for large particle sizes.

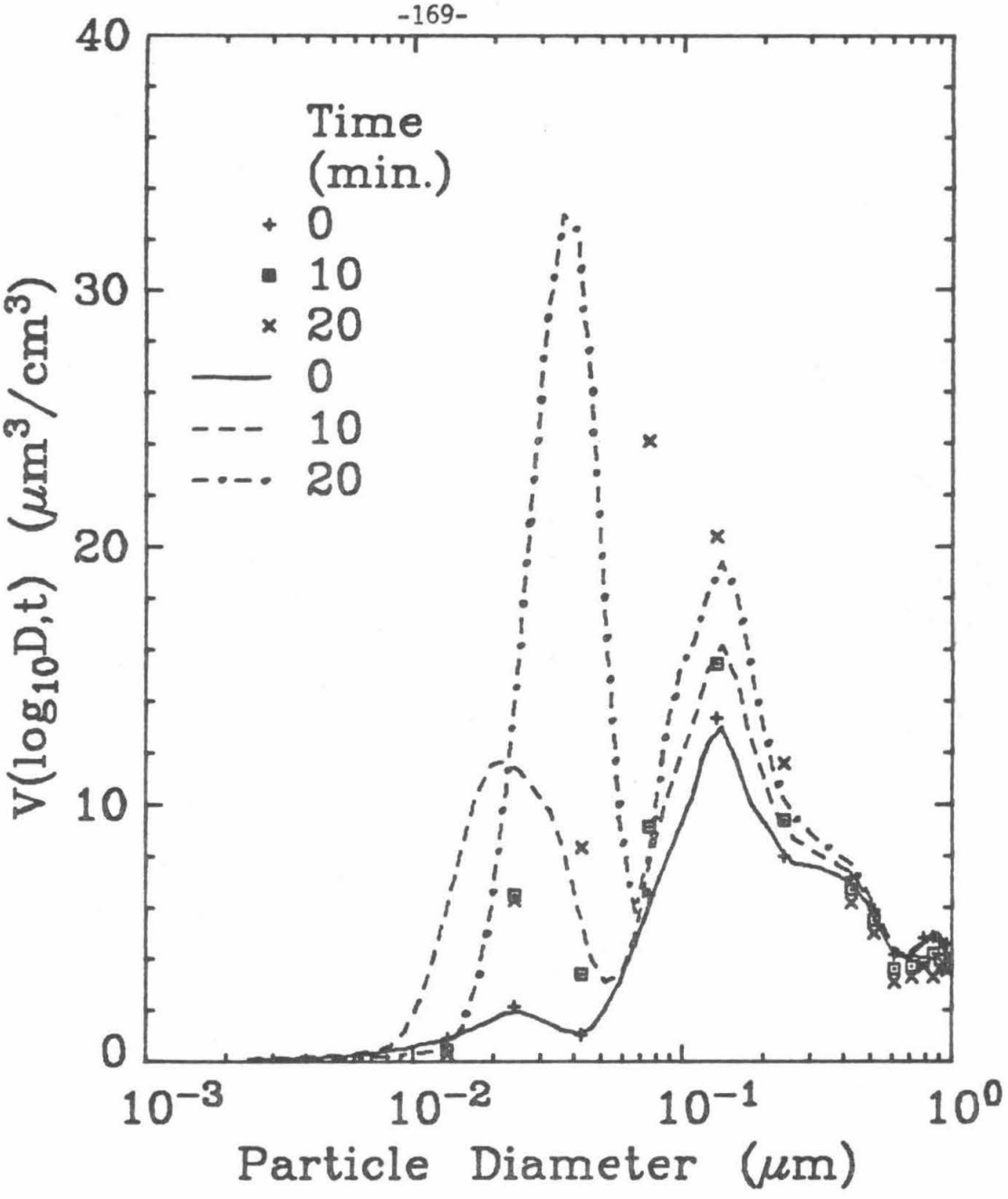

Figure 6

Volume distribution evolution. Discrete points are the measured values, and the lines are the computed results.

4.1 Establishment of the Steady State Molecular Cluster Profile in the Presence of a Preexisting Aerosol

A key assumption of classical nucleation theory is the existence of a steady state concentration profile of molecular clusters smaller than the critical size (28-31). According to the classical theory, the scavenging effect of any preexisting aerosol, which would reduce the nucleation rate, is neglected. However, using the discrete-continuous GDE it can be shown that due to scavenging a steady state profile different from that predicted by classical nucleation theory is rapidly established in the presence of a preexisting aerosol.

Figure 7 shows the computed concentration profile in the discrete regime for the conditions of the experiment of McMurry (8) in which evaporation was neglected. The profile first rapidly increases due to the generation of H_2SO_4 monomer. As monomers and clusters agglomerate, larger clusters are rapidly formed in the discrete regime. However, as larger particles are formed in the continuous regime, the scavenging of smaller particles increases, and the discrete concentration profile gradually decreases as shown. Since the steady state profile is independent of the initial cluster concentrations, it was found that if the initial cluster concentrations are reduced by an order of magnitude, the evolving discrete profile,

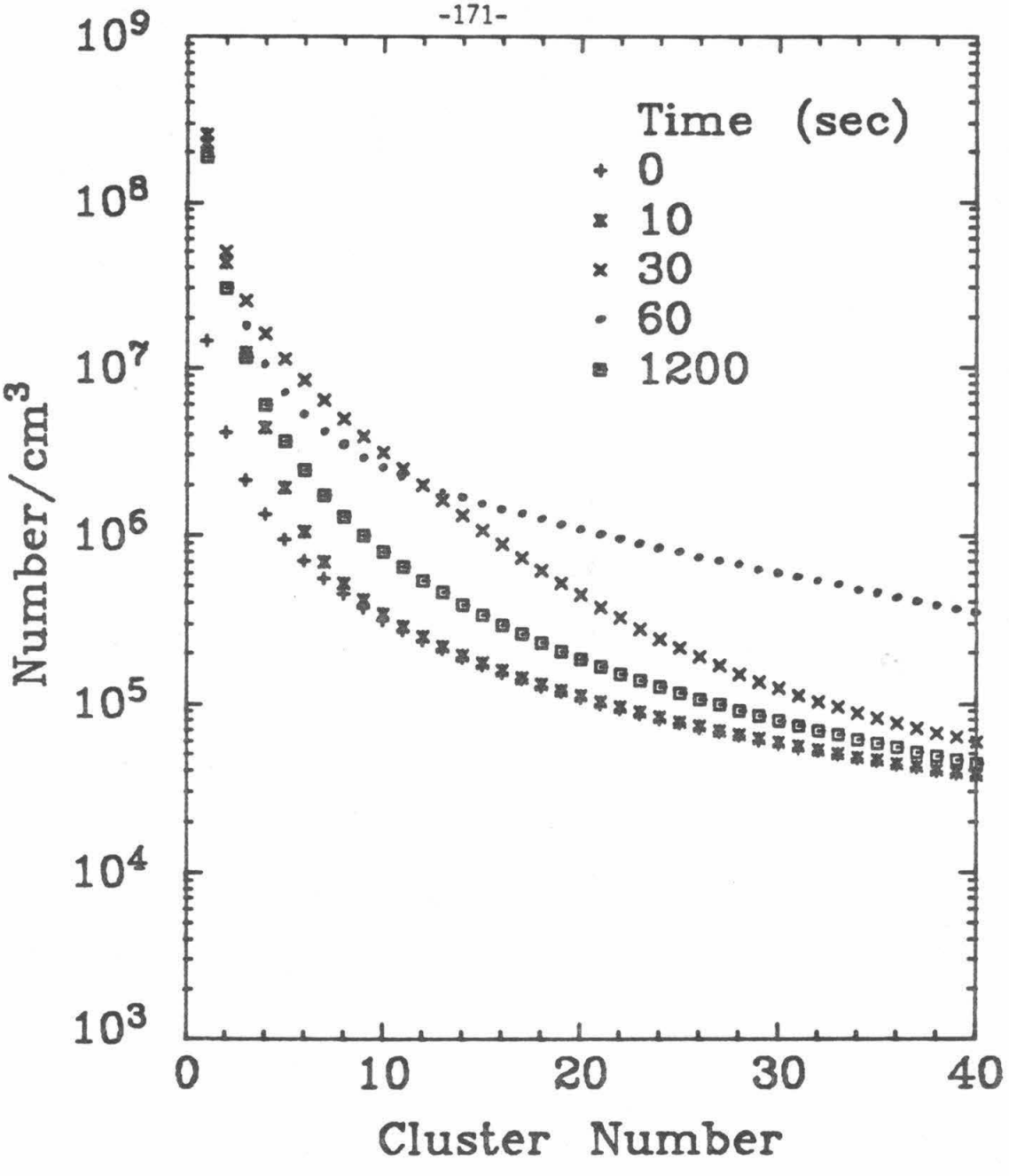

Figure 7

Evolution of the concentration profile of molecular clusters in the discrete regime.

shown in Fig. 8, is practically the same after 1 minute as that shown in Fig. 7, for a much higher initial profile. Similarly, the continuous distribution was not significantly affected by the choice of the initial cluster profile. Thus, time scales on the order of minutes were probably required to reach steady state. (However, we have not determined the exact time or largest cluster size for which the steady state approximation is valid.)

In the development of classical nucleation theory no account is made for the presence of particles much larger than the critical size. In the atmosphere, however, preexisting aerosol may have a significant effect on the nucleation rate. The preexisting aerosol serves as a condensation site for clusters and thus scavenges clusters before they reach the critical size for nucleation. If one neglects the scavenging effect, the resulting steady state profile is significantly higher as shown in Fig. 9. Hence, the classical theory predicts an aerosol independent nucleation rate greater than the aerosol dependent nucleation rate with scavenging.

4.2 Determination of the Relative Importance of Condensation, Nucleation, and Scavenging for Gas-to-Particle Conversion

Having previously developed the general expressions for the rates of processes in Chapter II, we would now like to apply the expressions in the analysis of the experiment just simulated.

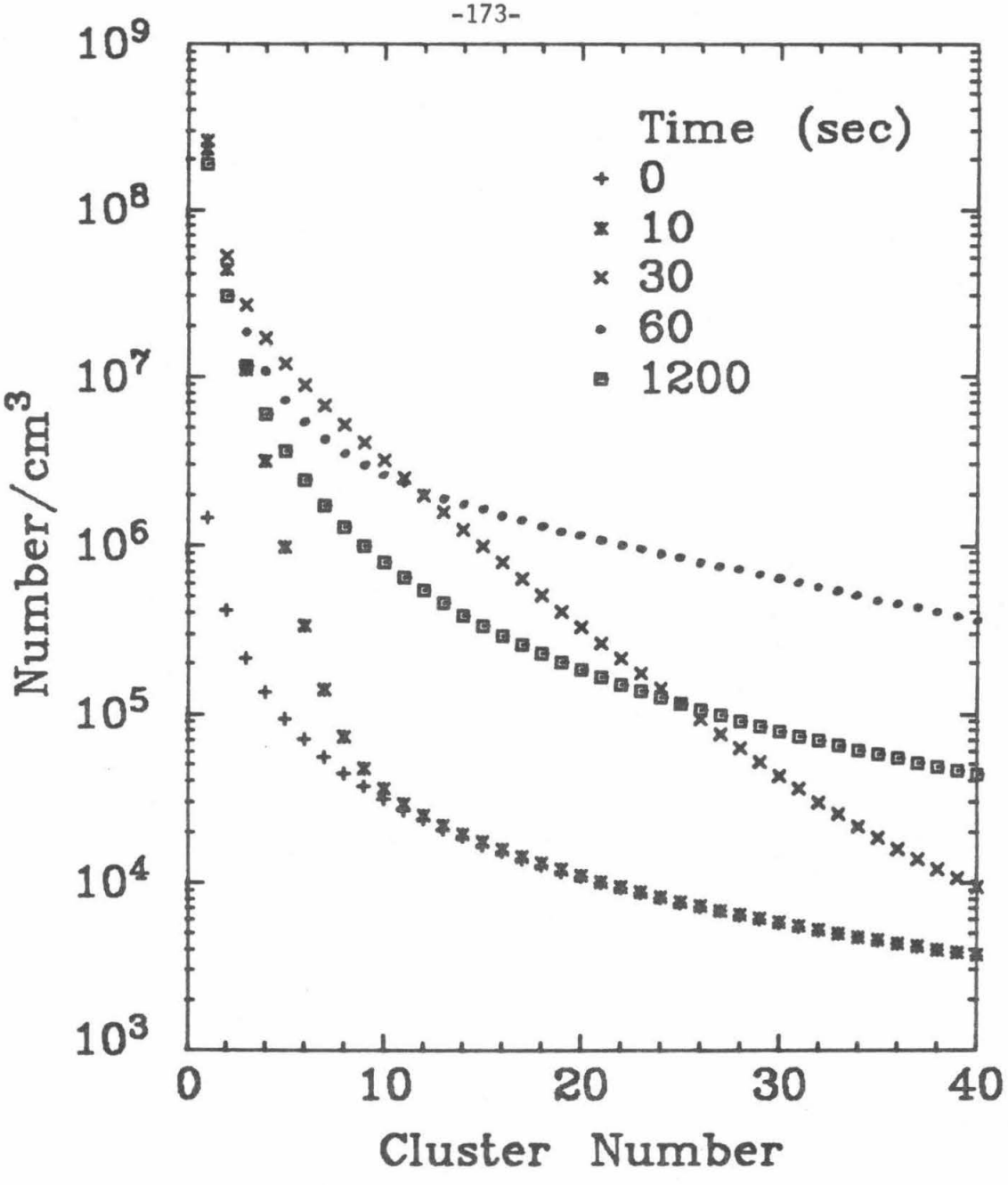

Figure 8

Evolution of the concentration profile of molecular clusters in the discrete regime when the initial concentrations are reduced by an order of magnitude.

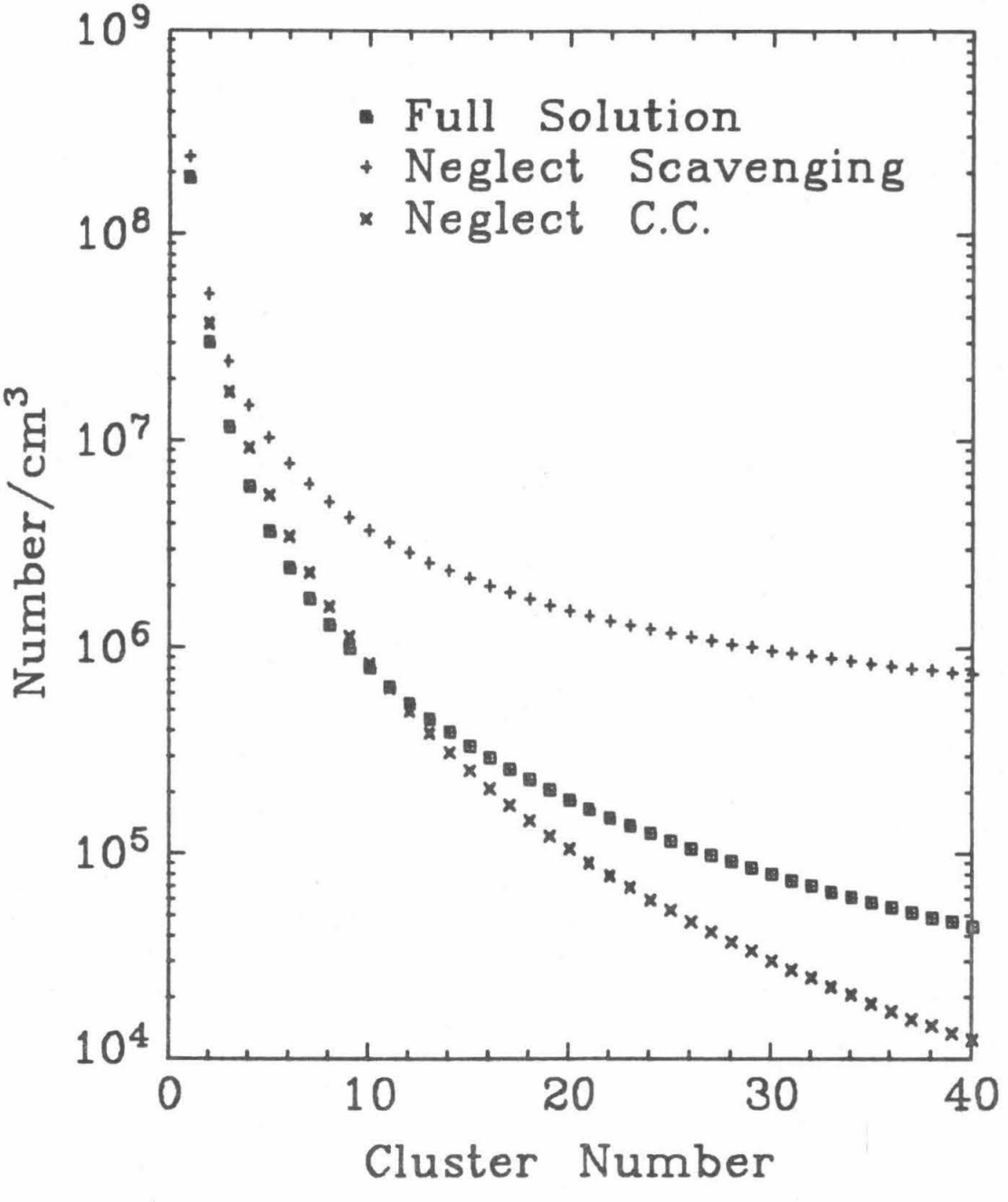

Figure 9

Comparison of cluster profiles in the discrete regime, after 20 minutes of simulation. (C.C. stands for cluster-cluster agglomeration.)

Unfortunately, in order to evaluate any of the rate expressions R_{ij}, the discrete-continuous GDE must be solved so that the distribution is known as a function of time. However, if one is interested only in a priori estimates, the steady state approximation can be used for the discrete regime as discussed in the previous section. Although the steady state profile changes as the aerosol evolves, the temporal variations are small and qualitatively predictable. As the aerosol grows, greater scavenging of the particles in the discrete regimes occurs. Thus, $N(v_i,t)$ for $1 \leq i \leq k$, will, in general, decrease after the steady state is established, as shown in Fig. 7.

The computed total number densities in the discrete and continuous regimes are shown as solid lines in Fig. 10 (the broken lines will be discussed later). During the first 30 seconds, a large number of small particles are predicted to form in the discrete regime. After 30 seconds these small clusters are predicted to nucleate at the boundary between the discrete and continuous regimes, and thus a burst of new particles occurs in the continuous regime. Since the 23.6 Å boundary between the two regimes is less than the present lower limit of detection of the condensation nuclei counter (32,33), it is clear why a time delay is often observed between the time of initiation of condensable species generation and the time of first aerosol detection. Time lags from 45 seconds to several

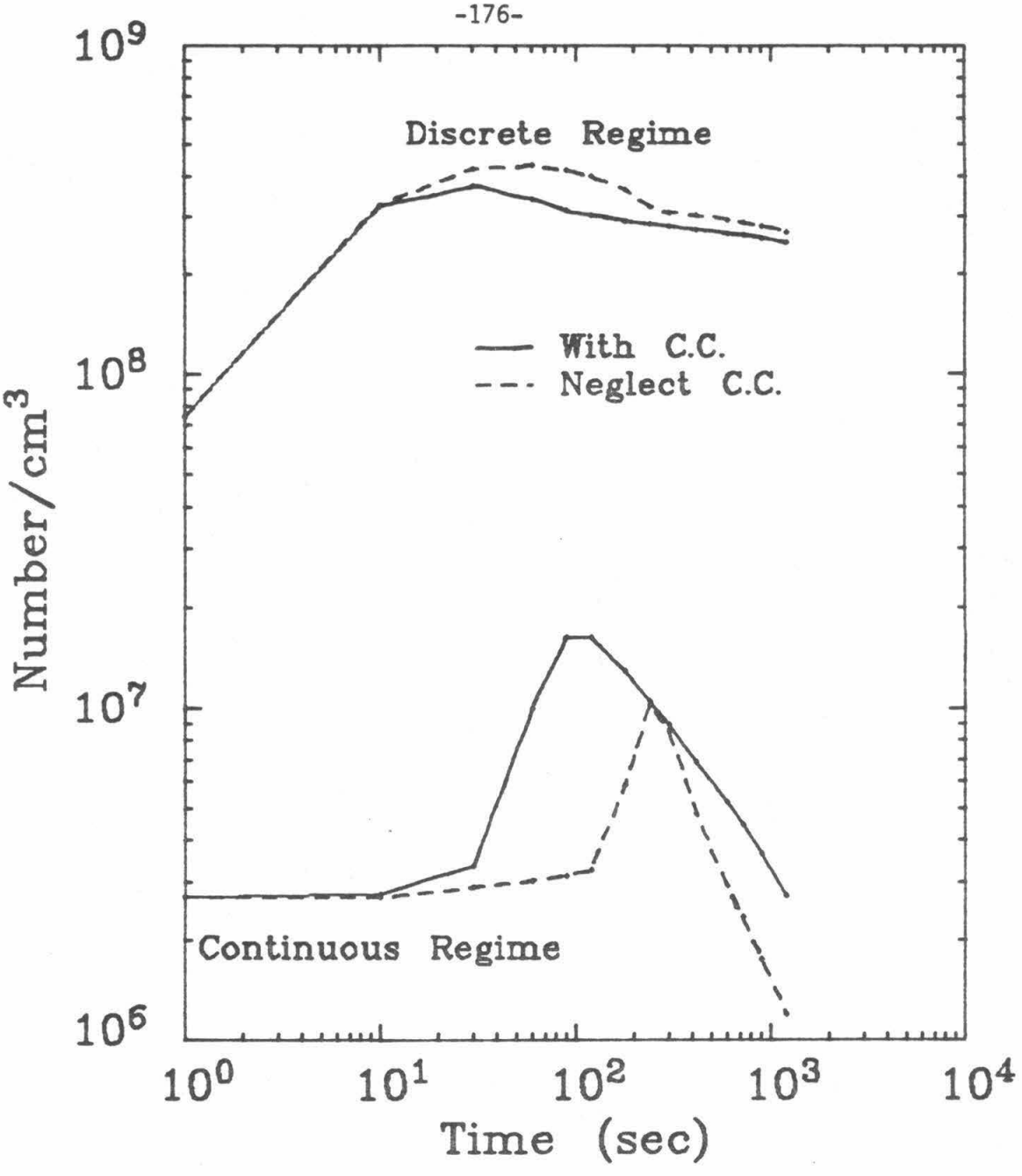

Figure 10

Total number of particles/cm^3 in the discrete and continuous regimes. The discrete regime is from 0.0006 to 0.00237 μm diameter and the continuous regime is from 0.00237 to 1.0 μm diameter. Broken lines calculated by neglecting cluster-cluster agglomeration.

minutes have been reported (1,2), although not all experiments have shown a significant time lag (4). After the particle burst, the newly formed particles in the continuous regime continued to grow, with the resulting wave formation in the distribution shown in Fig. 5.

In order to determine if a particle burst will occur in general, define $dn_0(v_i)/dt = dn(v_i,0)/dt$, and $dn_{ss}(v_i)/dt$ as the right hand side of Eq. [15] of Chapter II based on the initial cluster profile and the steady state profile, respectively. Then if $dn_{ss}(v_i)/dt > 0$ a particle burst should occur. If $dn_{ss}(v_i)/dt < 0$ but $dn_0(v_i)/dt > 0$, a very short burst should occur but once the transients have decayed, scavenging will dominate and no significant particle bursts should occur. (Clearly if $dn_0(v_i)/dt < 0$ and $dn_{ss}(v_i)/dt < 0$ no particle burst should occur.) One can also obtain an estimate of $n(v_{k+1}-v_1/2,t)$ by extrapolating the steady state profile to a (k+1)-mer. Then if $n(v_{k+1}-v_1/2,t) = N(v_{k+1},t)/v_1$, is much greater than $n(v_{k+1}-v_1/2,0)$, a particle burst may occur. To determine the movement of the wave in the distribution, as a result of condensational growth, the exact solution of Chapter III can be used.

In the experiment just simulated, R_{mm}, R_{mc}, R_{cc}, R_{nuc} and $R_{m\text{-}nuc}$ initially increased then decreased after about one minute due to the increased scavenging resulting from aerosol growth, as shown in

Figs. 11-13, where $\bar{R}_{ij} = R_{ij}/S_o(v_1,t)$. In Fig. 14 we see that $\xi << 1$; hence most of the monomer and clusters leave the discrete regime by condensation and not nucleation. Since there is a time lag from the initiation of monomer generation to nucleation, the initial accumulation of monomer and clusters results in a decrease in ξ, due to increased condensation. However, once the growing clusters pass into the continuous regime, ξ peaks, as shown in Fig. 14, and then continually decreases. Except for this short period, when the clusters enter the continuous regime, the dominant process for monomer conversion is condensation. Figure 15 shows that $\bar{\alpha} > 0.9$ throughout most of the simulation, indicating that more than 90% of the monomer is converted to aerosol by condensation.

4.3 Determination of the Importance of Cluster-Cluster Agglomeration

A second key assumption of classical nucleation theory is neglect of the agglomeration of molecular clusters. The validity of such an approximation can now be evaluated.

Define $N'(v_i,t)$ as the discrete concentration of i-mers computed without cluster-cluster agglomeration. Then $\varepsilon(v_i,t) = N'(v_i,t)/N(v_i,t)$ is an indication of the error committed in neglecting cluster-cluster agglomeration. If ε does not significantly differ from unity for $1 \leq i \leq k$, cluster-cluster agglomeration can be neglected. In simulating McMurry's experiment, possibly because evaporation was

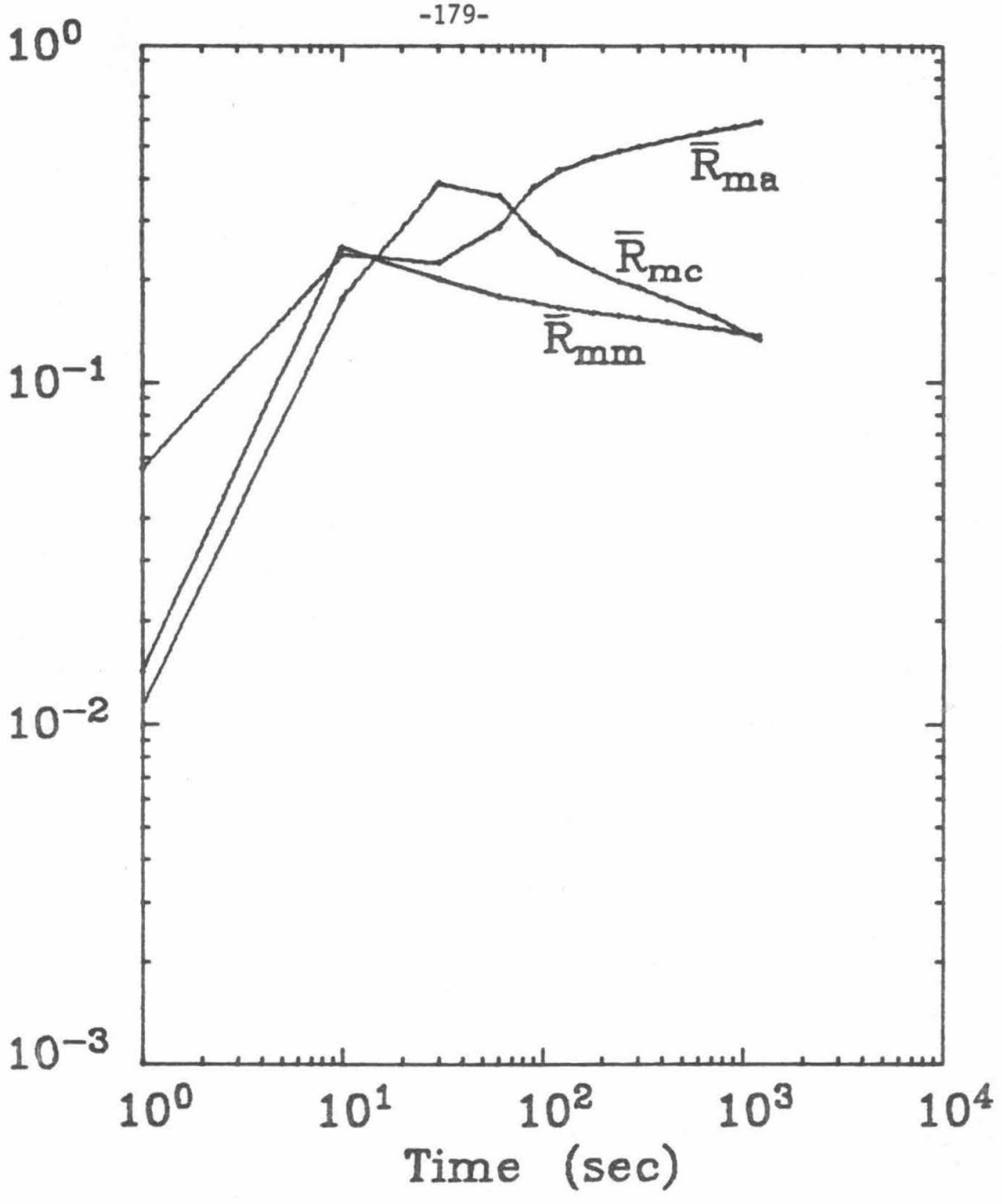

Figure 11

$\bar{R}_{ij}$ is the net rate of agglomeration of particle types i and j over the monomer generation rate of 4.84×10^7 cm^{-3}, for the simulated experiment, where m, c, and a represent monomer, clusters and aerosol particles, respectively.

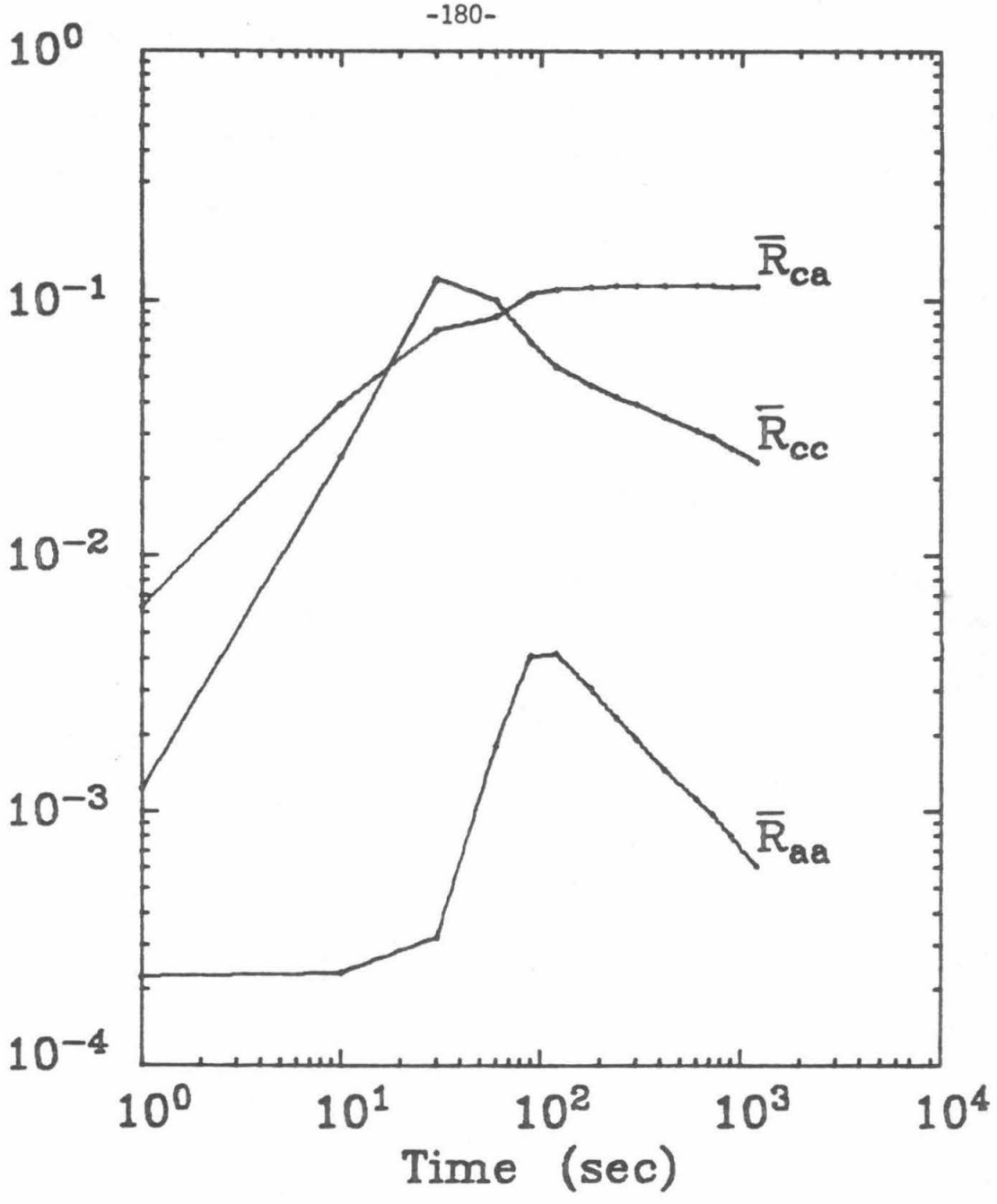

Figure 12

$\bar{R}_{ij}$ is the net rate of agglomeration of particle types i and j over the monomer generation rate of 4.84×10^7 cm^{-3} for the simulated experiment where c and a represent clusters and aerosol particles, respectively.

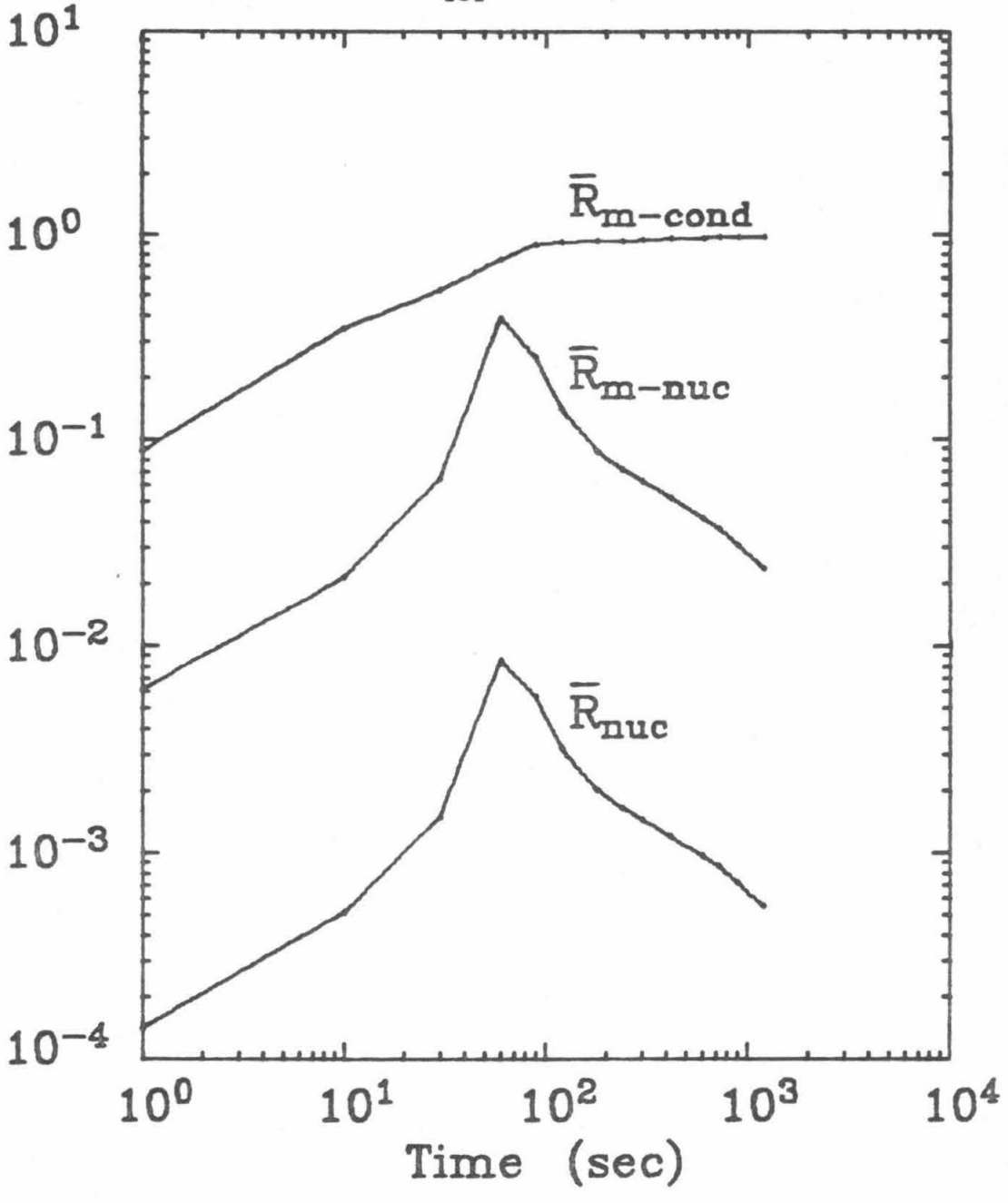

Figure 13

$\bar{R}_{m\text{-}cond}$, $\bar{R}_{m\text{-}nuc}$ and $\bar{R}_{nuc}$ are the net rate of monomer condensation, monomer nucleation and nucleation over the monomer generation rate of 4.84×10^7 cm^{-3}, respectively, for the simulated experiment.

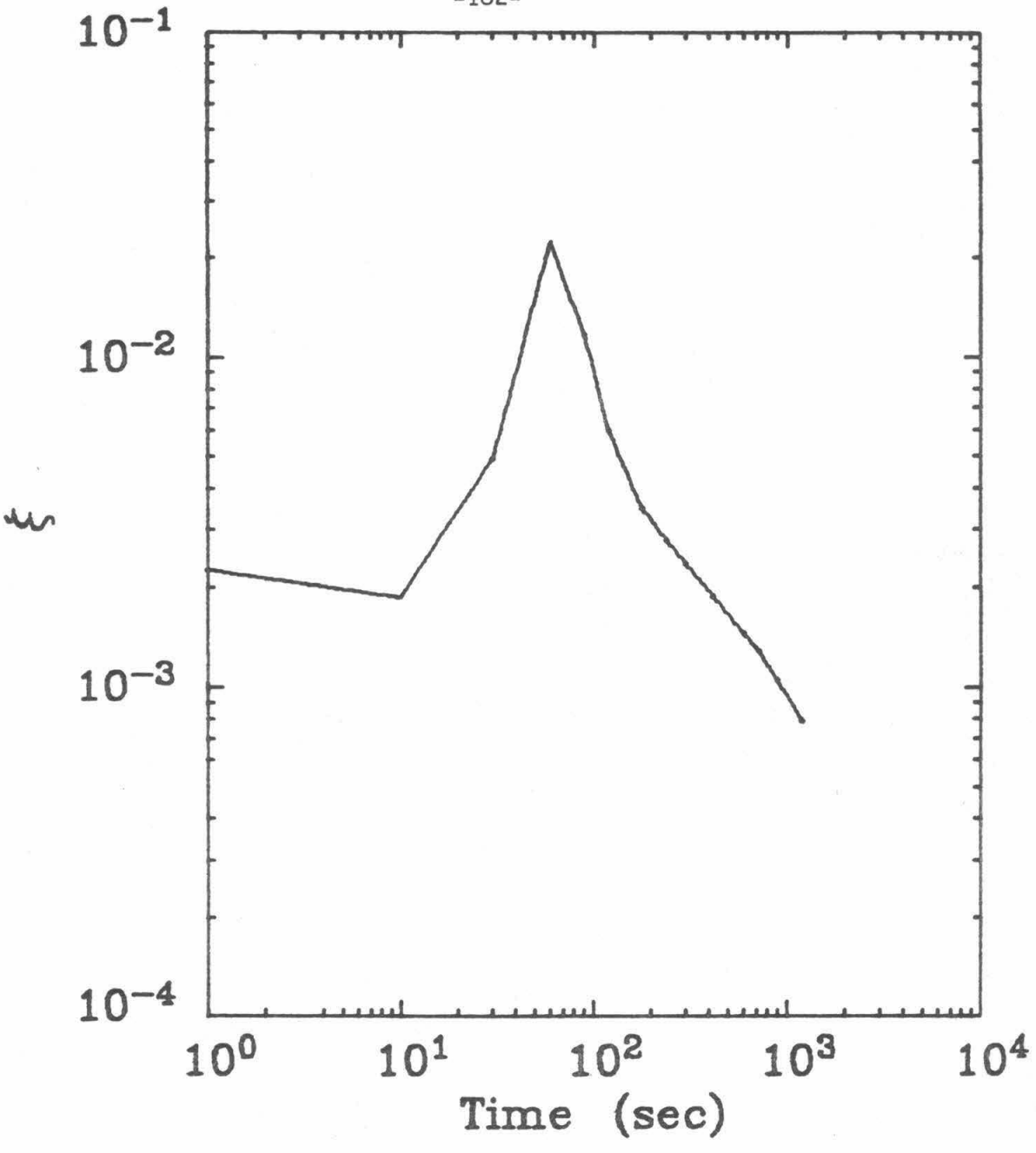

Figure 14

Ratio of the nucleation rate to the condensation rate for the simulated experiment.

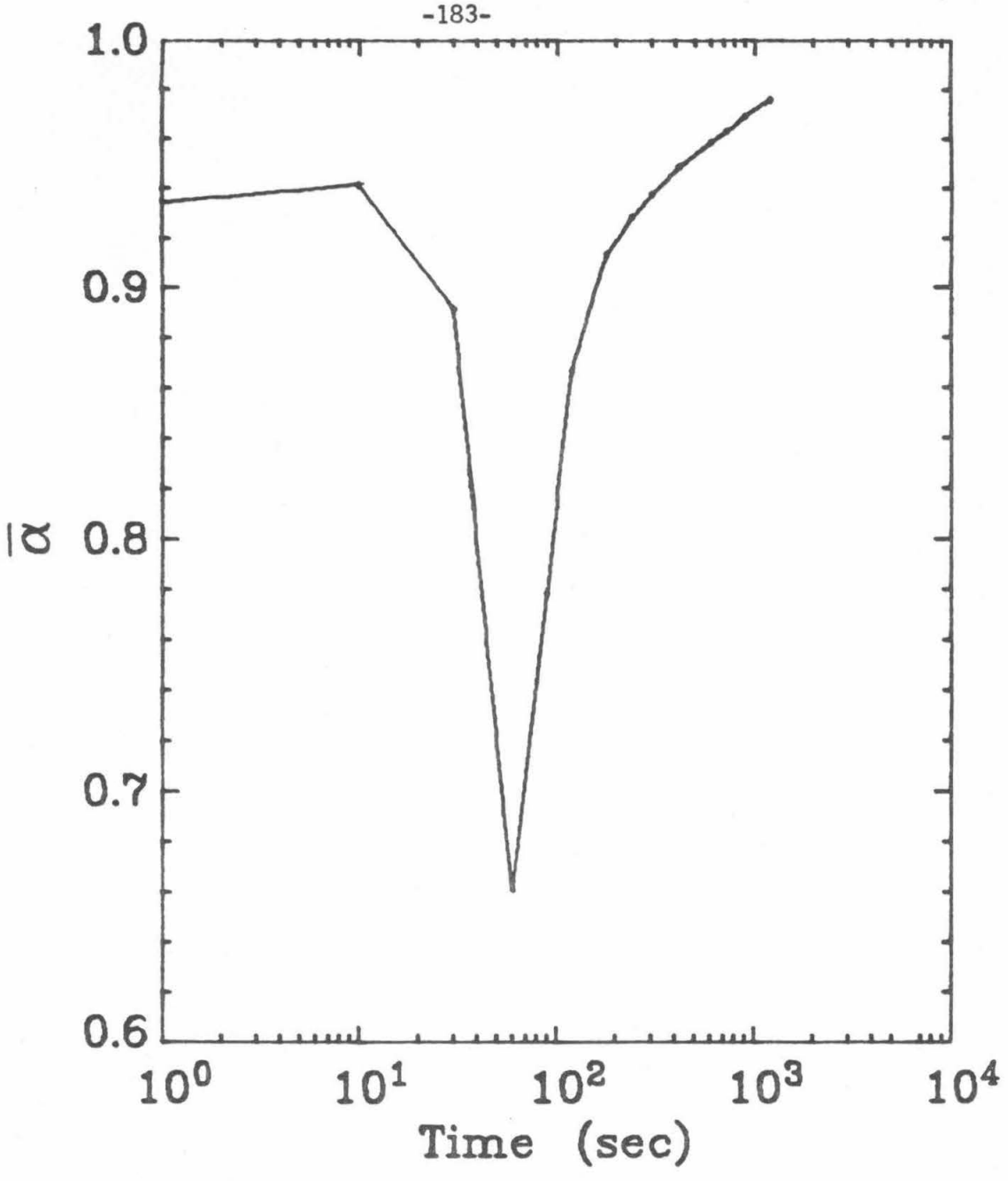

Figure 15

Fraction of the total flux of monomer entering the continuous regime by condensation for the simulated experiment.

neglected, a large number of clusters formed, and ε was generally significantly different than unity for the clusters. Errors committed in the cluster concentrations introduce errors in the continuous regime, due to the nucleation of the clusters. Figure 16 shows the evolution of the cluster profile neglecting cluster-cluster agglomerations. By comparing Figs. 7 and 16, notice that the evolution of the cluster profile has been artifically hampered by neglecting cluster-cluster agglomerations and the final cluster concentration profiles shown in Fig. 9 are significantly different. The error of neglecting cluster-cluster agglomerations also resulted in a deceptively low nucleation rate. Thus, the resulting distribution shown in Fig, 17 has a lower small particle concentration as compared to that shown in Fig. 5. Hence, Fig. 10 shows significant discrepancies for the total number of particles in the continuous regime computed with and without cluster-cluster agglomeration. Thus, cluster-cluster agglomeration apparently played an important role in the formation of new particles in the continuous regime. However, for condensational growth the details of the discrete regime are unimportant. Since Fig. 10 shows some agreement for the total concentration of particles in the discrete regime, with and without cluster-cluster agglomeration, the condensational growth mechanism should not have been affected by neglecting cluster-cluster agglomerations. Hence, Fig. 18 shows that agreement was obtained

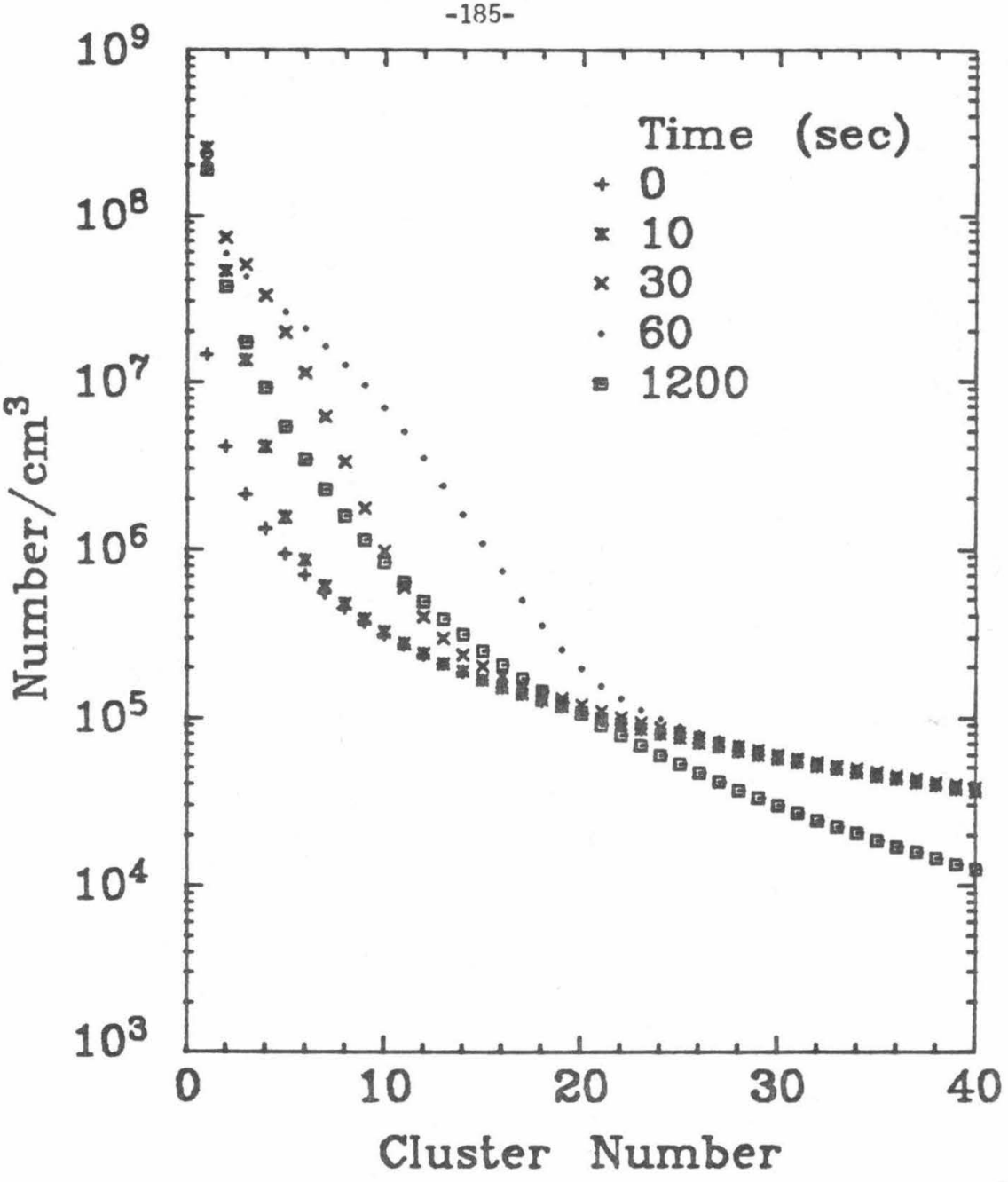

Figure 16

Evolution of the concentration profile of molecular clusters in the discrete regime when cluster-cluster agglomerations are neglected.

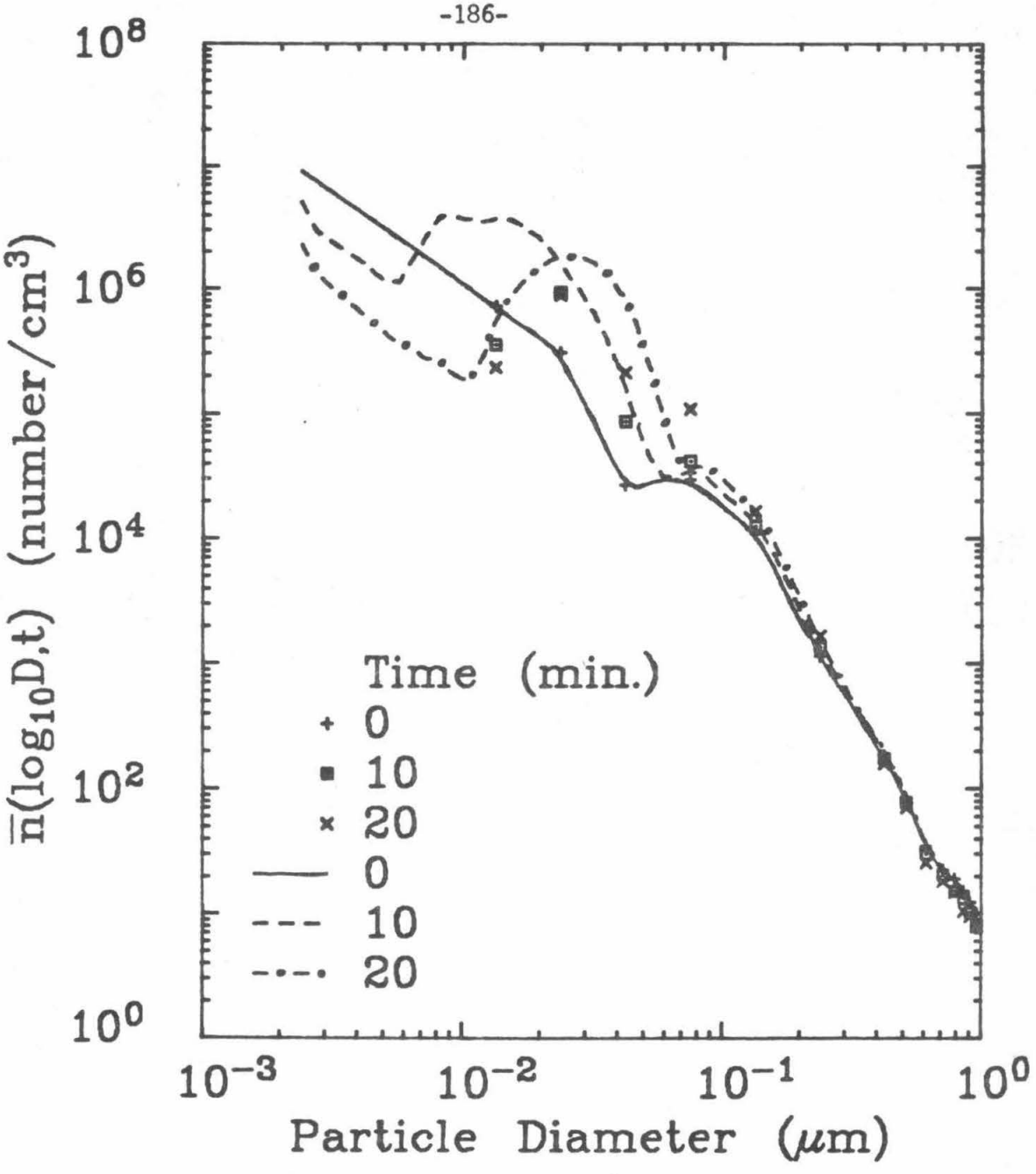

Figure 17

Number distribution evolution. Discrete points are the measured values and the lines are the computed results neglecting cluster-cluster agglomerations.

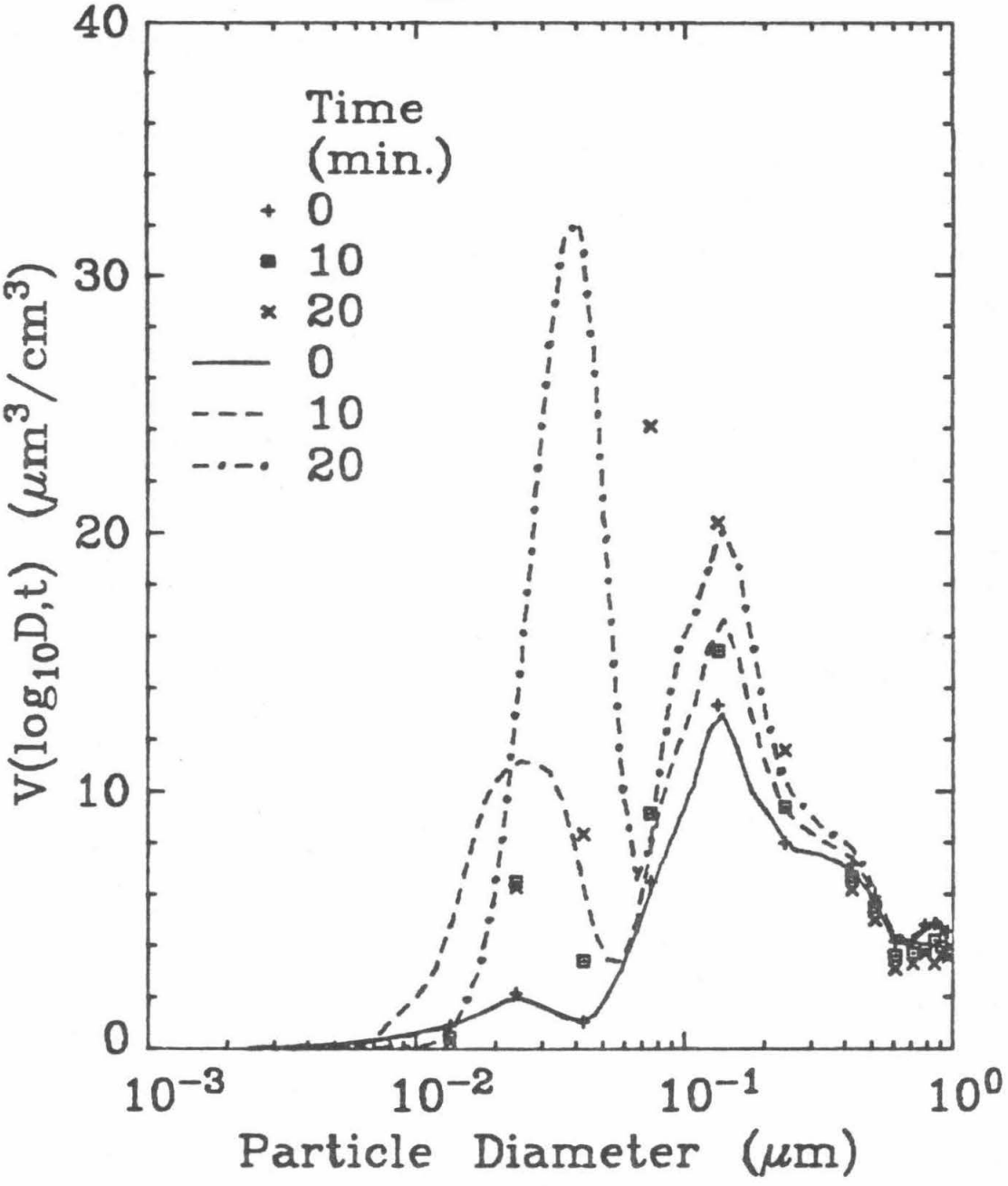

Figure 18

Volume distribution evolution. Discrete points are the measured values, and the lines are the computed results neglecting cluster-cluster agglomerations.

with the full solution, (shown in Fig. 6) for large particles which grow primarily by condensation.

One can compute the steady state cluster concentations if cluster-cluster agglomeration is negligible and evaporation is present, by iterating on the monomer concentration and solving a linear system of algebraic equations with a tridiagonal coefficient matrix. Although in the experiment simulated, both evaporation and cluster-cluster agglomeration cannot be neglected, if circumstances are such that both processes can be neglected, then McMurry (8) has shown that the cluster concentrations can be obtained directly.

5. USE OF THE CONTINUOUS GDE

Probably because of its simplicity, the solution to the continuous GDE is the approach usually taken to simulate aerosol dynamics. To apply the continuous GDE, $\beta(v,u)$, $I(v,t)$, and an initial and boundary condition must be specified. However, specifying the boundary condition on particle size makes application of the continuous GDE for simulating gas-to-particle conversion difficult, without solving for the complete distribution, including the clusters. Since it has been shown that the discrete profile can be affected by aerosol scavenging, the discrete profile and hence the nucleation rate is dependent on the continuous distribution. Thus, the boundary condition apparently cannot be determined in the absence of knowledge of the dynamics in the continuous regime.

It is still of interest to attempt to simulate the experiment of McMurry using the continuous GDE and to compare the results to those obtained using the discrete-continuous GDE. If coagulation can be neglected, the exact solutions of the continuous GDE is given in Chapter III for realistic growth laws and arbitrary initial and boundary conditions. If coagulation is not neglected, a numerical solution such as that given in Chapter IV is required. A comparison of the two solutions reveals the effect of coagulation on the size distribution.

To provide a meaningful comparison between the solutions of the discrete-continuous and continuous GDE's, the boundary condition for the continuous GDE will be taken so that it coincides with the solution of the discrete-continuous GDE. To calculate I(v,t) a monomer concentration equal to the concentration of the sum of the first few discrete clusters after 60 sec. was used. This procedure resulted in an H_2SO_4 concentration of 0.025 ppb. The first few clusters were used, because relative to a particle in the continuous regime they behave essentially as monomer molecules. The growth law of Fuchs was used in the calculations since it agreed with the Fuchs-Phillips β as shown in Chapter II. For the particle size domain considered, composition effects were small and thus neglected.

Using the exact solution, the calculated number and volume distributions are shown in Figs. 19 and 20, respectively. Recall that one of the assumptions used in deriving the continuous GDE in Chapter II is that $v >> v_1$. Therefore, calculations were only performed within the detection limits of the instrumentation. Because of this, the wave formation in the number distribution is not shown in Fig. 19. However, within the detectable range, the exact solution agrees with the solution to the discrete-continuous GDE shown in Fig. 5. On comparing the volume distributions plotted for the discrete-continuous GDE in Fig. 6 and for the exact solution to the continuous GDE in Fig. 20, we note that the growth

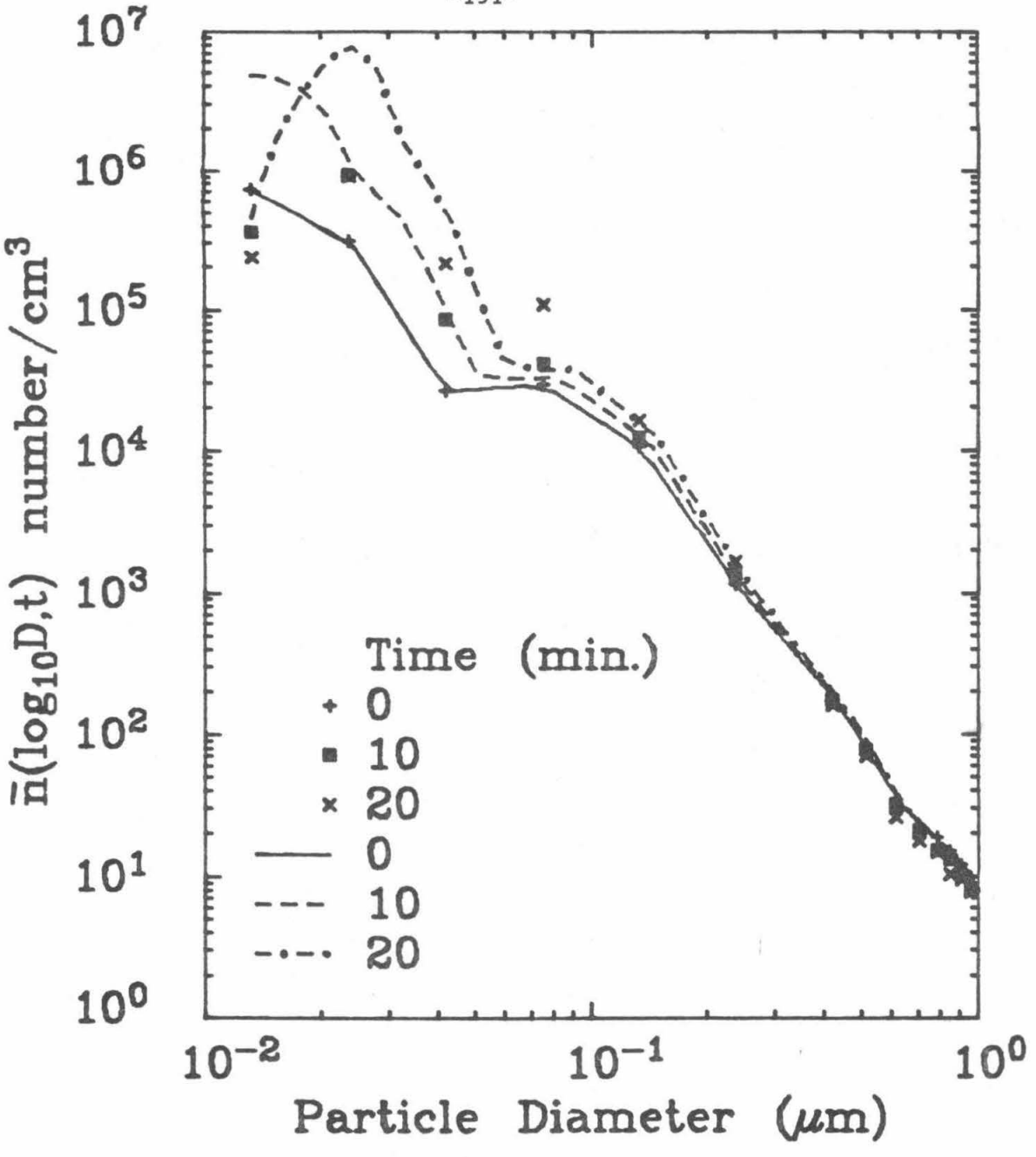

Figure 19

Number distribution evolution. Discrete points are the measured values and the lines are the results calculated using the exact solution to the continuous GDE neglecting coagulation.

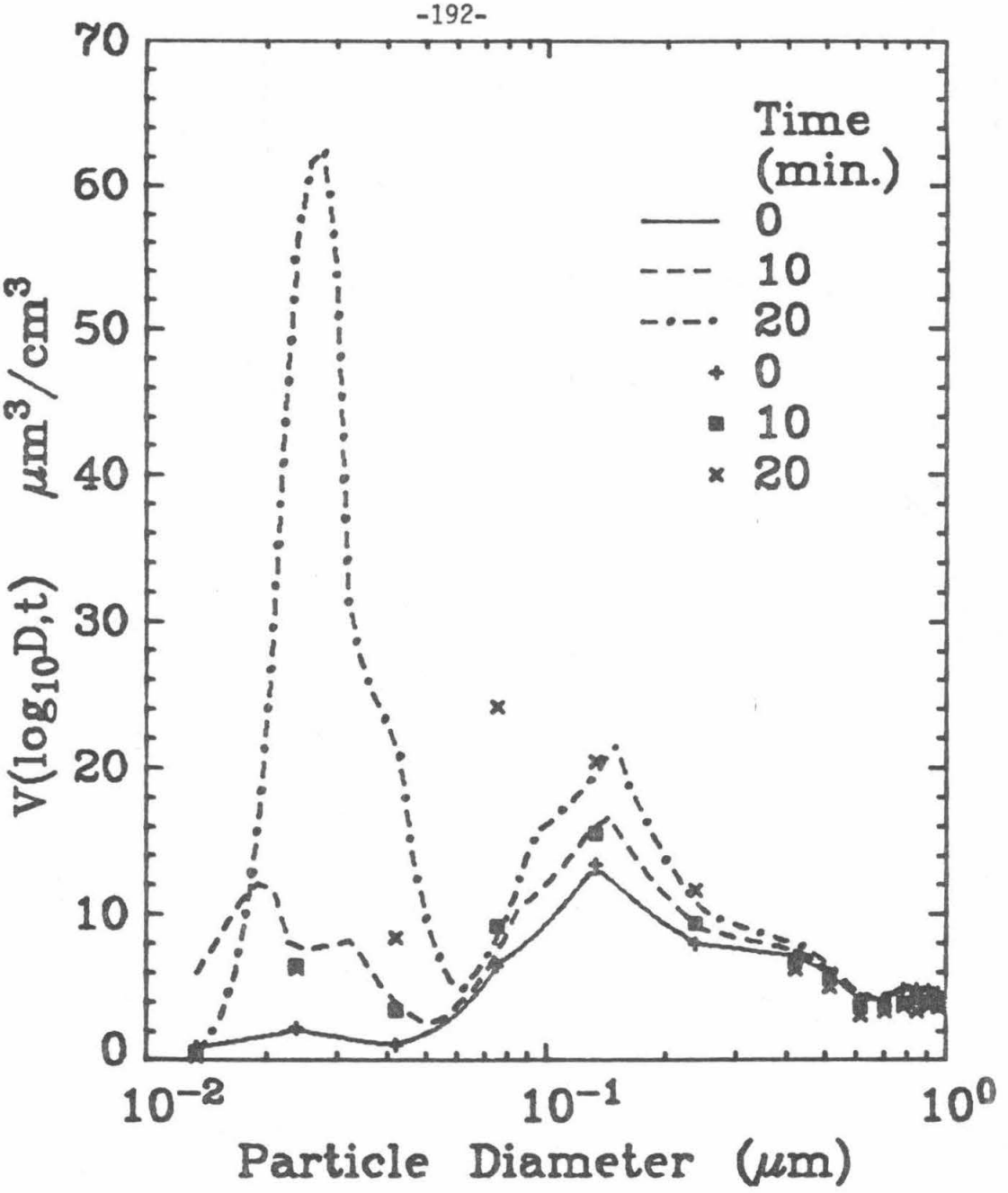

Figure 20

Volume distribution evolution. Discrete points are the measured values and the lines are the results calculated using the exact solution to the continuous GDE neglecting coagulation.

of small particles just below the detection limit, results in even a greater peak for particles just above the detection limit for the exact solution. This is because, not only was evaporation neglected and the boundary condition obtained from the solution to an equation with an extrapolated initial distribution, but also coagulation was neglected. For the large particle sizes the exact solution agrees with both the solution to the discrete-continuous GDE and the data. This is because the effect of coagulation is smaller for large particles, and the growth of large particles is mainly due to condensation. Thus, the exact solution is a very powerful yet relatively simple way to simulate certain classes of aerosol dynamics.

If coagulation is included in the continuous GDE, numerical solutions are necessary. Using the same boundary condition and gas phase concentration of condensible species as for the exact solution, the numerical solution was obtained by the techniques described in Chapter IV. Because coagulation scavenges small particles without significant effects on the large particles, Fig. 21 shows a significant decrease in the number distribution for small particles. Notice that the effect of using linear interpolation for the initial distribution is "smoothed out" by coagulation, which did not occur in Figs. 19 and 20. Also notice that Fig. 21 agrees with the solution to the discrete-continuous

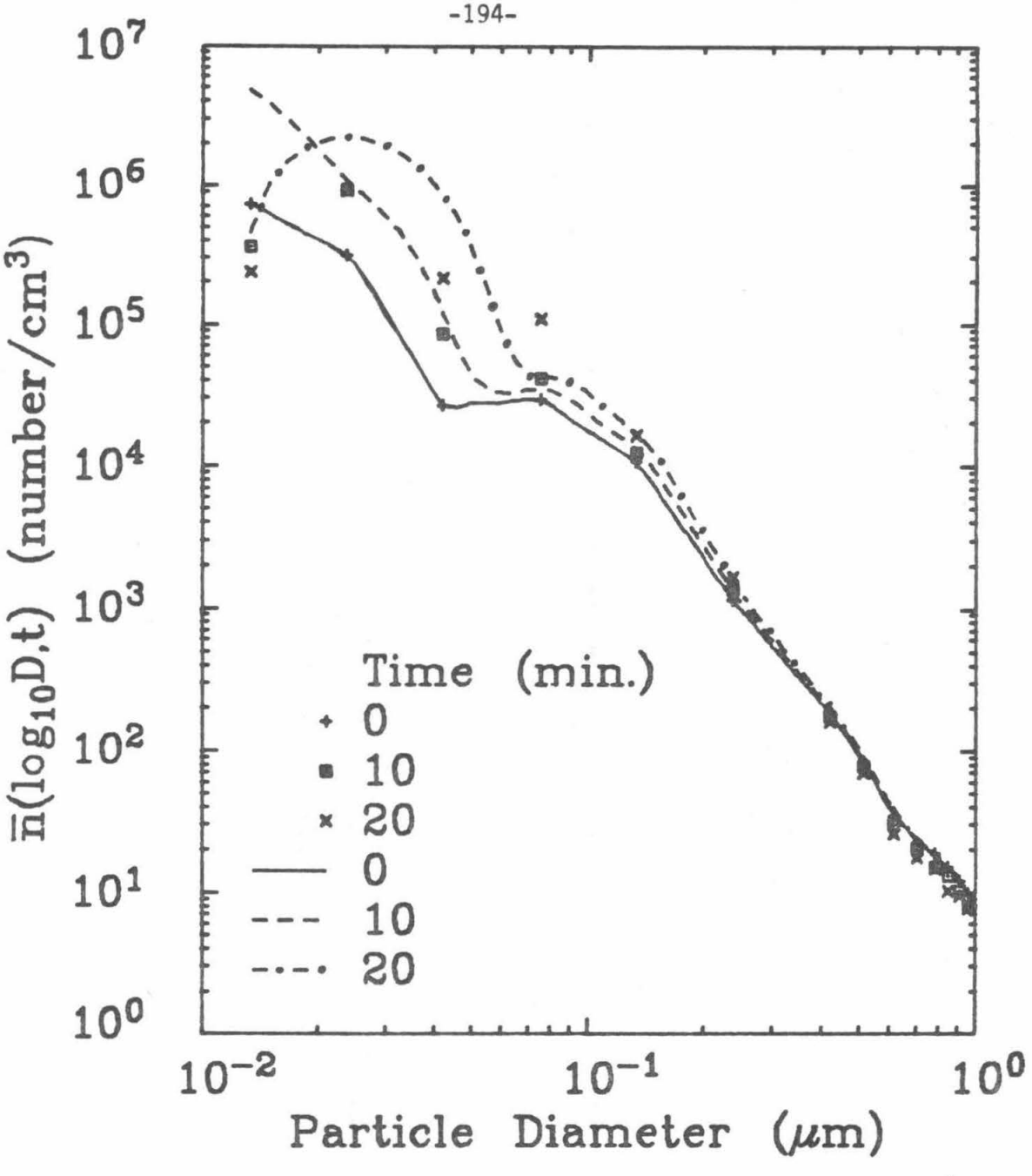

Figure 21

Number distribution evolution. Discrete points are the measured values and the lines are the computed results using the numerical techniques of Chapter IV to solve the continuous GDE with coagulation.

GDE shown in Fig. 5. Because of the scavenging effect of coagulation, one should also expect less aerosol volume for small particles than without coagulation. Thus, Fig. 22 shows that the volume distribution significantly drops for small particles due to coagulation, as compared to Fig. 20. Again we see agreement is obtained with the solution to the discrete-continuous GDE (shown in Fig. 6) for large particles.

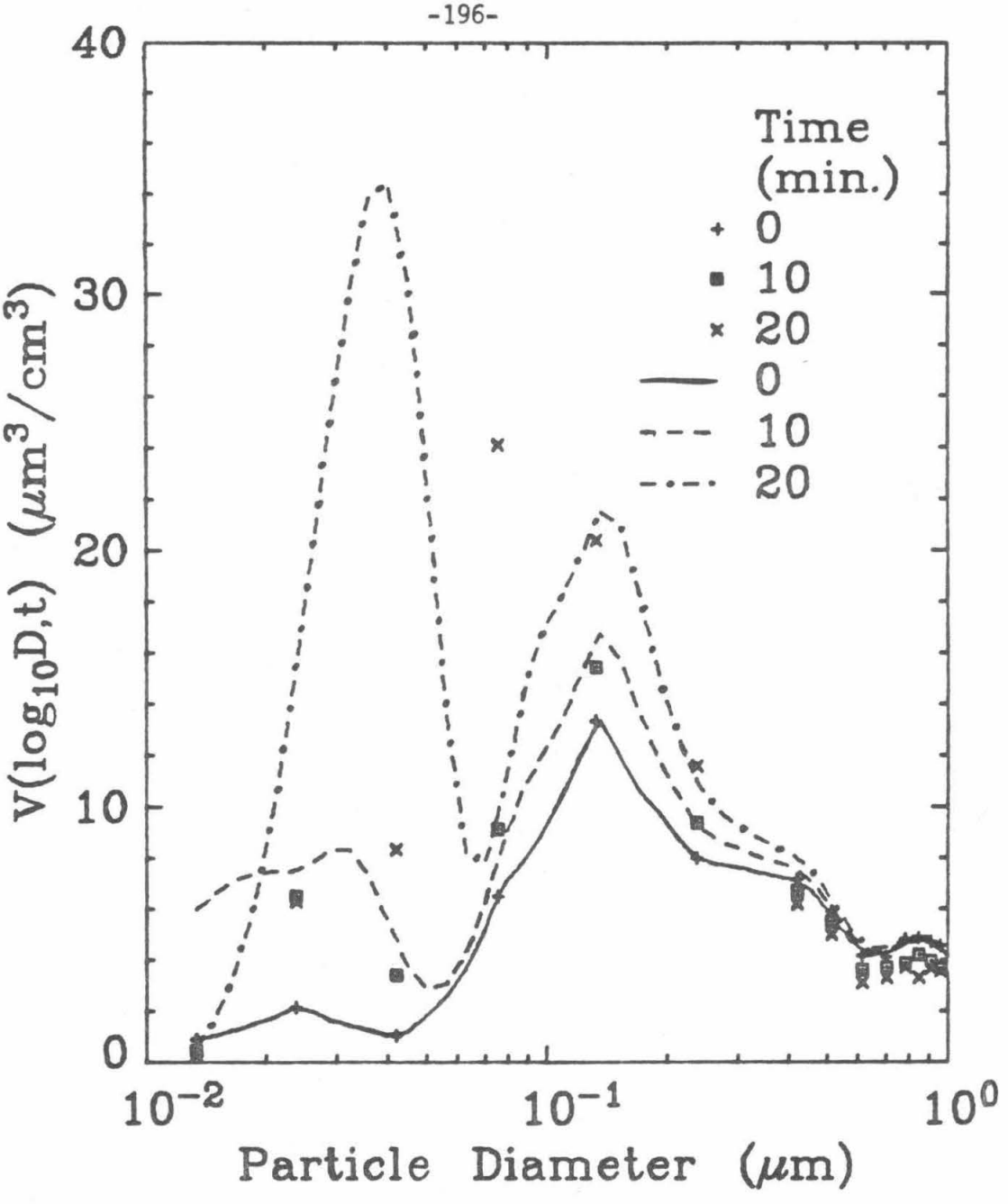

Figure 22

Volume distribution evolution. Discrete points are the measured values and the lines are the computed results using the numerical techniques of Chapter IV to solve the continuous GDE with coagulation.

6. SUMMARY*

Using bulk thermodynamic data, the physical properties of a sulfuric acid and water aerosol were determined as a function of temperature, relative humidity and particle size. For particles in thermodynamic equilibrium, it was shown that due to surface tension effects, the composition and hence the density and vapor pressure of the particle is size dependent. To account for these variations, the conservation equation, as expressed by the GDE, was used for the conservation of H_2SO_4 and not particle volume.

Since a preexisting urban aerosol was used in the simulated experiment, it was assumed that due to ambient impurities, the evaporation of H_2SO_4 can be neglected to a first approximation. Due to instrument limitations, extrapolation of the initial distribution was required. However, since it was shown that a steady state profile is rapidly established in the discrete regime, extrapolation in this regime probably did not introduce significant errors. Although some errors were probably introduced by extrapolating the initial distribution, neglecting evaporation and assuming that each particle collision results in coalescence, fairly good agreement was obtained with experiment in predicting the evolution of the size distribution.

---

*The conclusions on the issues listed in the abstract of this chapter are given in Chapter VII.

It has also been shown that the solution of the continuous GDE can produce results similar to that obtained from applications of the discrete-continuous GDE. However, it must be noted that the boundary condition for the continuous GDE was obtained from the solution to the discrete-continous GDE.

NOTATION

D	particle diameter, μm
$n(v,t)$	number distribution function, μm^{-3} cm^{-3}
$N(v_i,t)$	number concentration, cm^{-3}
$N'(v_i,t)$	number concentration computed neglecting cluster-cluster agglomerations, cm^{-3}
R_{ij}	net agglomeration rate of particle types i and j, sec^{-1} cm^{-3}
v	particle volume, μm^3

Greek Letters

$\bar{\alpha}$	fraction of the total flux of monomer entering the continuous regime by condensation
$\beta(v,u)$	agglomeration coefficient, cm^3 sec^{-1}
ξ	net nucleation rate divided by the net condensation rate of particles in the discrete regime

Subscripts

a	aerosol particle
c	cluster
cond	condensation
m	monomer
m-cond	monomer condensation
m-nuc	monomer nucleation
nuc	nucleation

REFERENCES

1. Evans, G. R. and Roddy, A. F., "The Condensation Nuclei Formed in Polluted Air by Ultraviolet Radiation Whose Wavelengths are Longer Than 2900 Å," Proc. 7th Int'l. Conf. Condensation and Ice Nuclei, Prague and Vienna, p. 369 (1969).

2. Luria, M., Olszyna, K. J., DePena, R. G., and Heicklen, J., "Kinetics of Particle Growth - V: Particle Formation in the Photolysis of SO_2-Allene Mixtures," J. Aerosol Sci. 5, 435 (1974).

3. Haury, G., Jordan, S., and Hofman, C., "Experimental Investigation of the Aerosol-Catalyzed Oxidation of SO_2 Under Atmospheric Conditions," Atmos. Environ. 12, 281 (1978).

4. Cox, R. A. and Penkett, S.A.,"Aerosol Formation from Sulphur Dioxide in the Presence of Ozone and Olefinic Hydrocarbons," J. Chem. Soc., Faraday Trans. 68, 1735 (1972).

5. Friend, J. P., Leifer, R., and Trichon, M., "On the Formation of Stratospheric Aerosols," J. Atmos. Sci. 30, 465 (1973).

6. Bricard, J., Cabane, M., Madelaine, G., and Vigla, D., "Formation and Properties of Neutral Ultrafine Particles and Small Ions Conditioned by Gaseous Impurities of the Air," J. Colloid Interface Sci. 39, 42 (1972).

7. Cox, R. A., "Some Experimental Observations of Aerosol Formation in the Photo-oxidation of Sulfur Dioxide," Aerosol Sci. 4, 473 (1973).

8. McMurry, P. H., "On the Relationship Between Aerosol Dynamics and the Rate of Gas-to-Particle Conversion," Ph.D. Thesis, California Institute of Technology, 1977.

9. Wadden, R. A., Quon, J. E., and Hulburt, H. M., "A Model of a Growing Coagulating Aerosol," Atmos. Environ. 8, 1009 (1974).

10. Kiang, C. S. and Middleton, P., "Formation of Secondary Sulfuric Acid Aerosols in Urban Atmosphere," Geophysical Research Letters, 4, 17 (1977).

11. Hamill, P., Kiang, C. S., and Cadle, R. D., "The Nucleation of H_2SO_4-H_2O Solution Aerosol Particles in the Stratosphere," J. Atmos. Sci. 34, 150 (1977).

12. Chang, D. P. Y. and Hill, R. C., "Retardation of Aqueous Droplet Evaporation by Air Pollutants," presented at 71st Annual Air Pollution Control Assoc. Meeting, Houston, Texas, June 1978.

13. Sebinina, L. and Terpugow, L., "Die Oberflächenspannung des Systems Schwefelsäure-wasser," Z. Phys. Chem. A173, 237 (1935).

14. Giauque, W. F., Hornung, E. W., Kunzler, J. E., and Rubin, T. R., "The Thermodynamic Properties of Aqueous Sulfuric Acid Solutions and Hydrates from 15 to 300° K," J. Am. Chem. Soc. 82, 62 (1960).

15. Gmitro, J. I. and Vermeulen, T., "Vapor-Liquid Equilibria for Aqueous Sulfuric Acid," UCRL-10886 (1963).

16. Perry, R. H. and Chilton, C. H., Eds., "Chemical Engineers Handbook." 3-80,81. McGraw-Hill, New York, 5th Ed., 1973.

17. Hamill, P., "The Time Dependent Growth of H_2O-H_2SO_4 Aerosols by Heteromolecular Condensation," J. Aerosol Sci. 6, 475 (1975).

18. Hamill, P., Toon, O. B., and Kiang, C. S., "Microphysical Processes Affecting Stratospheric Aerosol Particles," J. Atmos. Sci. 34, 1104 (1977).

19. Reiss, H., "The Kinetics of Phase Transitions in Binary Systems," J. Chem. Phys. 18, 840 (1950).

20. Doyle, G. J., "Self-Nucleation in the Sulfuric Acid Water System," J. Chem. Phys., 35, 795 (1961).

21. Mirabel, P. and Katz, J. L., "Binary Homogeneous Nucleation as a Mechanism for the Formation of Aerosols," J. Chem. Phys., 60, 1138 (1974).

22. Itoh, M., Takahashi, K., and Kasahara, M., "The Temperature Dependence of Nucleation of Sulfuric Acid-Water Mixture in Air," J. Aerosol Sci. 8, 183 (1977).

23. Kennard, E. H., "Kinetic Theory of Gases," pp. 195-196. McGraw-Hill, New York, 1938.

24. Friedlander, S. K., "Smoke, Dust and Haze," pp. 27-31. Wiley, New York, 1977.

25. Phillips, W. F., "Drag on a Small Sphere Moving Through a Gas," Phys. Fluids 18, 1089 (1975).

26. Sitarski, M. and Seinfeld, J. H., "Brownian Coagulation in the Transition Regime," J. Colloid Interface Sci. 61, 261 (1977).

27. McMurry, P. H., private communication.

28. Frenkel, J., "Kinetic Theory of Liquids," pp. 366-413. Dover, New York, 1955.

29. Zettlemoyer, A.C ., (Ed.), "Nucleation." Marcel Dekker, New York, 1969.

30. Abraham, F. F., "Homogeneous Nucleation Theory." Academic, New York, 1974.

31. Katz, J. L., "Condensation of a Supersaturated Vapor," J. Chem. Phys. 52, 4733 (1970).

32. Instrument Instruction Manual for Condensation Nuclei Monitor, Model Rich 100, Environment One Corp., 2773 Balltown Road, Schenectady, New York.

33. Liu, B. Y. H. and Kim, C. S., "On the Counting Efficiency of Condensation Nuclei Counters," Atmos. Environ. 11, 1097 (1977).

Chapter VI

COAGULATION AND GROWTH OF A MULTICOMPONENT AEROSOL

ABSTRACT

Analytical solutions to the coagulation equation in the absence and presence of particle growth for a multicomponent aerosol are presented. From the general solutions corresponding to a class of initial composition distributions, four cases are considered in an attempt to elucidate the effects of coagulation and growth on the evolving composition distribution.

1. INTRODUCTION

There has been considerable interest in obtaining solutions to the integro-differential equation describing the coagulation of an aerosol,

$$\frac{\partial n(v,t)}{\partial t} = \frac{1}{2}\int_0^v \beta(v-\tilde{v},\tilde{v})n(v-\tilde{v},t)n(\tilde{v},t)d\tilde{v} - n(v,t)\int_0^\infty \beta(v,\tilde{v})n(\tilde{v},t)d\tilde{v} \qquad [1]$$

where $n(v,t)$ is the aerosol size distribution density function based on particle volume v, and $\beta(v,\tilde{v})$ is the coagulation coefficient for particles of volumes v and $\tilde{v}$(1-3). In addition, recently solutions have been obtained, in certain special instances, to the equation describing the dynamics of $n(v,t)$ when coagulation is accompanied by particle growth,

$$\frac{\partial n(v,t)}{\partial t} + \frac{\partial}{\partial v}\left\{I(v,t)n(v,t)\right\} = \frac{1}{2}\int_0^v \beta(v-\tilde{v},\tilde{v})n(v-\tilde{v},t)n(\tilde{v},t)d\tilde{v} - n(v,t)\int_0^\infty \beta(v,\tilde{v})n(\tilde{v},t)d\tilde{v} \qquad [2]$$

where $I(v,t) = dv/dt$, the rate of growth of a particle of volume v (4,5).

Often we must deal with aerosols that consist of several chemical species, a notable example being atmospheric aerosols. We can define a composition density function for a multicomponent aerosol as $n(x_1,x_2,\ldots,x_m,t)$, such that $n(x_1,\ldots,x_m,t)\, dx_1 \ldots dx_m$ is the number of particles at time t in the mass ranges x_1 to $x_1 + dx_1$, x_2 to $x_2 + dx_2,\ldots,x_m$ to $x_m + dx_m$ and where x_i represents the mass of component i in the particle. There are virtually no studies of the balance equation for $n(x_1,x_2,\ldots,x_m,t)$ including both coagulation and growth. In the only previous study of this nature, Lushnikov (6) solved the coagulation equation for a two-component system. In this work we present the first analytical solutions of the multicomponent aerosol balance equation including coagulation and growth. We confine our attention to a coagulation coefficient independent of particle volume, i.e., $\beta(v,\tilde{v}) = \beta_o$, and growth rates that depend linearly on the mass of each species in the particle. The solutions, which, of necessity, are for special cases only, do provide a quantitative indication of the role of the initial distribution, coagulation, and the growth rates on the dynamics of a multicomponent aerosol.

2. DYNAMICS OF MULTICOMPONENT AEROSOLS

The equation governing $n(x_1,x_2,\ldots,x_m,t)$ in the presence of coagulation and growth is

$$\frac{\partial n(x_1,x_2,\ldots,x_m,t)}{\partial t} + \sum_{i=1}^{m} \frac{\partial}{\partial x_i} \left\{ I_i(x_1,x_2,\ldots,x_m,t)n \right\}$$

$$= \frac{\beta_o}{2} \int_0^{x_m} \cdots \int_0^{x_1} n(x_1-\tilde{x}_1,x_2-\tilde{x}_2,..,x_m-\tilde{x}_m,t)n(\tilde{x}_1,\tilde{x}_2,..,\tilde{x}_m,t)d\tilde{x}_1..d\tilde{x}_m$$

$$- \beta_o n(x_1,x_2,..,x_m,t) \int_0^{\infty} \cdots \int_0^{\infty} n(\tilde{x}_1,\tilde{x}_2,\ldots,\tilde{x}_m,t)d\tilde{x}_1 \ldots d\tilde{x}_m \qquad [3]$$

where $I_i = dx_i/dt$, and where, as noted above, we have assumed the coagulation coefficient β to be constant. The initial condition for Eq. [3] is

$$n(x_1,x_2,\ldots,x_m,0) = n_o(x_1,x_2,\ldots,x_m) \qquad [4]$$

The conditions under which β can be assumed constant have been discussed elsewhere (5,7). It is necessary to select functional forms for the I_i. We select the linear growth laws

$$I_i = \sigma_i x_i \qquad [5]$$

indicating that the rate of growth of the ith component fraction of each particle depends on the current mass of component i in the particle. The growth expression of Eq. [5], while simplified, is not a physically unrealistic form. For a one-component aerosol I usually assumes the form σx^{γ}, where $0<\gamma\leq 1$. The case of $\gamma=1$ corresponds to a growth mechanism in which homogeneous chemical reaction in the particle is rate controlling. Eq. [5] represents the extension of this concept to a multicomponent particle.

The initial distributions considered in this study are given in Table 1. Distributions 1 and 2 in Table 1 represent cases $p_i=0$ and $p_i=1$ for the general distribution labelled 0 and are multicomponent versions of the exponential and gamma distributions often used as initial conditions for one-component systems (2). Distribution 3 in Table 1 ($p_1=1$, $p_2=0$) is a mixed distribution for the case of m=2. Finally, distribution 4 represents two monodisperse populations, one consisting of N_1 particles, each containing mass x_1^* of component 1, and the other consisting of N_0-N_1 particles, each containing mass x_2^* of component 2.

Table 1. Initial Conditions $n_o(x_1,x_2,\ldots, x_m)^\dagger$

Distribution	$n_o(x_1,x_2,\ldots, x_m)$
0 ($p_i \geq 0$)	$N_o \prod_{i=1}^{m} \frac{(p_i+1)^{p_i+1} x_i^{p_i} \exp -\left[(p_i+1)\frac{x_i}{x_{i_o}}\right]}{\Gamma(p_i+1) x_{i_o}^{p_i+1}}$
1 ($p_i=0$)	$N_o \prod_{i=1}^{m} \frac{\exp}{x_{i_o}} \left[-\frac{x_i}{x_{i_o}}\right]$
2 ($p_i=1$)	$N_o \prod_{i=1}^{m} \frac{4 x_i}{x_{i_o}^2} \exp\left[-\frac{2 x_i}{x_{i_o}}\right]$
3 ($p_1=1$, $p_2=0$, $m=2$)	$\frac{4 N_o x_1}{x_{1_o}^2 x_{2_o}} \exp\left[-\frac{2 x_1}{x_{1_o}} - \frac{x_2}{x_{2_o}}\right]$
4 ($m=2$)	$N_1\delta(x_1-x_1^*,x_2)+(N_o-N_1)\delta(x_1,x_2-x_2^*)$

$^\dagger N_o$ = total initial number of particles

$$= \int_0^\infty \cdots \int_0^\infty n_o(x_1,x_2,\ldots,x_m)dx_1 \ldots dx_m$$

x_{i_o} = mean initial mass of component i

$$= \frac{1}{N_o} \int_0^\infty \cdots \int_0^\infty x_i n_o(x_1,x_2,\ldots,x_m)dx_1 \ldots dx_m$$

3. MULTICOMPONENT COMPOSITION DISTRIBUTIONS

The technique used to solve Eq. [3] is based on a multidimensional Laplace transform. For a function $f(x_1,x_2,\ldots,x_m)$, a multidimensional Laplace transform is defined by

$$\bar{f}(s_1,s_2,\ldots,s_m) = \int_0^\infty \cdots \int_0^\infty \exp\left\{ - \sum_{j=1}^{m} s_j x_j \right\} f(x_1,x_2,..,x_m)dx_1..dx_m \quad [6]$$

The inversion formula is

$$f(x_1,x_2,..,x_m) = \frac{1}{(2\pi i)^m} \int_{c_m-i\infty}^{c_m+i\infty} \cdots \int_{c_1-i\infty}^{c_1+i\infty} \exp\left\{\sum_{j=1}^{m} s_j x_j\right\} \bar{f}(s_1,s_2,..,s_m)ds_1..ds_m \quad [7]$$

An extensive treatment of the two-dimensional Laplace transforms can be found in (8). In this study it was necessary to develop a set of multidimensional transforms. The transforms required here are given in Table 2.

3.1 Pure Coagulation

We first consider the case in which only coagulation is occurring, i.e., $I_i=0$ for $i=1,2,\ldots,m$. If $N(t)$ is the total number of particles at time t, then in the case of pure coagulation,

Table 2. Multidimensional Laplace Transform Pairs[†]

$f(x_1,x_2,\ldots,x_m)$	$\bar{f}(s_1,s_2,\ldots,s_m)$
$\left\{\prod_{j=1}^{m} \frac{\exp}{a_j}\left[-\frac{b_j x_j}{a_j}\right]\right\} f\left(\frac{x_1}{a_1},\ldots,\frac{x_m}{a_m}\right)$	$\bar{f}\,(a_1 s_1 + b_1,\ldots, a_m s_m + b_m)$
$\int_0^{x_m}\cdots\int_0^{x_1} f(x_1-\tilde{x}_1,\ldots,x_m-\tilde{x}_m)\, g(\tilde{x}_1,\ldots,\tilde{x}_m)\,d\tilde{x}_1\cdots d\tilde{x}_m$	$\bar{f}(s_1,\ldots,s_m)\bar{g}(s_1,\ldots,s_m)$
$\frac{\partial}{\partial x_j}\left\{x_j f(x_1,\ldots,x_m)\right\}$	$-s_j \frac{\partial \bar{f}}{\partial s_j}$
$\sum_{k=0}^{\infty} a^k \prod_{i=1}^{m} \frac{x_i^{(k+1)R_i-1}}{\Gamma[(k+1)R_i]}$	$\frac{1}{\prod_{i=1}^{m} s_i^{R_i} - a}$ $(R_i>0)$
$\delta(x_1-x_1^*, x_2-x_2^*,\ldots,x_m-x_m^*)$	$\exp\left[-\sum_{i=1}^{m} s_i x_i^*\right]$

[†]The fourth transform pair is derived in the appendix.

$$N(t) = \frac{2N_o}{2 + \beta_o N_o t} \qquad [8]$$

Taking the $\underline{m}$th dimensional Laplace transform of Eq. [3], we obtain

$$\frac{d\bar{n}}{dt} = \frac{\beta_o}{2} (\bar{n})^2 - \beta_o \bar{n} N(t) \qquad [9]$$

the solution of which is

$$\bar{n} = \frac{4\bar{n}_o}{(2+\beta_o N_o t)^2 - \beta_o t(2+\beta_o N_o t)\bar{n}_o} \qquad [10]$$

Inversion of Eq. [10] for the initial conditions given in Table 1 produces the solutions for $n(x_1, x_2, .., x_m, t)$. (In cases 3 and 4 of Table 1, m=2). These solutions are given in Table 3. We note that for m=2, the solution corresponding to initial distribution 1 can be expressed in terms of a modified Bessel function of the first kind of zeroth order. This special case was solved in (6) for $\beta = 2\beta_o$.

3.2 Coagulation and Growth

With $I_i = \sigma_i x_i$, Eq. [3] can be transformed to

$$\frac{\partial \bar{p}}{\partial T} - \sum_{i=1}^{m} \frac{2\Lambda_i s_i}{(1-T)^2} \frac{\partial \bar{p}}{\partial s_i} = \frac{\bar{p}^2}{2N_o} \qquad [11]$$

Table 3. Composition Density Functions for Coagulation of a Multicomponent Aerosol

Initial distribution (see Table 1)†	$n(x_1,x_2,\ldots,x_m,t)$
0 ($p_i \geq 0$)	$\frac{4N_o}{(\tau+2)^2} \prod_{i=1}^{m} \frac{(p_i+1)^{p_i+1}}{x_{i_o}} \exp\left[\frac{-(p_i+1)x_i}{x_{i_o}}\right] \times \sum_{k=0}^{\infty} \left(\frac{\tau}{\tau+2}\right)^k \prod_{j=1}^{m} \frac{\left[(p_j+1)^{(p_j+1)}\right]^k \left(\frac{x_j}{x_{j_o}}\right)^{(k+1)(p_j+1)-1}}{\Gamma[(k+1)(p_j+1)]}$
1 ($p_i=0$)	$\frac{4N_o}{(\tau+2)^2} \prod_{i=1}^{m} \frac{\exp\left[-\frac{x_i}{x_{i_o}}\right]}{x_{i_o}} \sum_{k=0}^{\infty} \frac{\left[\frac{\tau}{\tau+2} \prod_{j=1}^{m} \frac{x_j}{x_{j_o}}\right]^k}{(k!)^m}$
1 ($p_i=0, m=2$)	$\frac{4N_o}{(\tau+2)^2} \frac{\exp\left[-\frac{x_1}{x_{1_o}} - \frac{x_2}{x_{2_o}}\right]}{x_{1_o}x_{2_o}} I_o\left\{2\sqrt{\frac{\tau x_1 x_2}{(\tau+2)x_{1_o}x_{2_o}}}\right\}$

Table 3. (Cont.)

2 (p_i=1)

$$\frac{4^{m+1}N_o}{(\tau+2)^2}\prod_{i=1}^{m}\frac{\exp\left[\frac{-2x_i}{x_{i_o}}\right]}{x_{i_o}}\sum_{k=0}^{\infty}\frac{\left(\frac{4^m\tau}{\tau+2}\right)^k\prod_{j=1}^{m}\left(\frac{x_j}{x_{j_o}}\right)^{2k+1}}{[(2k+1)!]^m}$$

3 (p_1=1,p_2=0,m=2)

$$\frac{16N_o\exp\left[-\frac{2x_1}{x_{1_o}}-\frac{x_2}{x_{2_o}}\right]}{(\tau+2)^2x_{1_o}x_{2_o}}\sum_{k=0}^{\infty}\frac{\left[\frac{4\tau x_2}{(\tau+2)x_{2_o}}\right]^k\left[\frac{x_1}{x_{1_o}}\right]^{2k+1}}{k!(2k+1)!}$$

4 (m=2)

$$\frac{4}{(\tau+2)^2}\sum_{k=0}^{\infty}\left(\frac{\beta_o t}{\tau+2}\right)^k\Bigg\{N_1^{k+1}\delta[x_1-(k+1)x_1^*,x_2]$$

$$+\binom{k+1}{1}N_1^{k}(N_o-N_1)\delta[x_1-kx_1^*,x_2-x_2^*]$$

$$+\binom{k+1}{2}N_1^{k-1}(N_o-N_1)^2\delta[x_1-(k-1)x_1^*,x_2-2x_2^*]+\ldots$$

$$+\binom{k+1}{k+1}(N_o-N_1)^{k+1}\delta[x_1,x_2-(k+1)x_2^*]\Bigg\}$$

---

†$\tau = \beta_o N_o t$

where $\bar{p} = 2\bar{n}/(1-T)^2$, $T = \beta_o N_o t/(2+\beta_o N_o t)$, and $\Lambda_i = \sigma_i/\beta_o N_o$. Physically, Λ_i is a dimensionless group that represents the ratio of the characteristic time for growth of the ith component of a particle to the characteristic time for coagulation. Eq. [11] is solved by the method of characteristics, and the Laplace inversion is carried out with the aid of Table 2. The solutions corresponding to the initial distributions in Table 1 are given in Table 4.

Figures 1 - 5 show the evolution of the composition distribution of a two-component aerosol in the presence of simultaneous coagulation and growth. Figure 1 corresponds to initial distribution 3 in Table 1. Figures 2 and 3 show the evolution of this initial distribution, when component 1 grows faster than component 2, (i.e., $\Lambda_1 > \Lambda_2$). Figures 4 and 5 show the evolution, for the same initial distribution, when component 2 grows faster than component 1, (i.e., $\Lambda_1 < \Lambda_2$). Because particle growth does not change the total number of particles, the total volume under the surface of the distribution is not influenced by growth. However, growth moves particles into larger mass ranges, thereby displacing the volume under the surface to larger mass ranges. The combination of growth and coagulation results in the movement of the volume under the surface, with a decrease in the total volume under the surface. In Figures 2 and 3, the values of $\Lambda_1 = 10.0$ and $\Lambda_2 = 0.1$ have been assumed. With these values of Λ_1 and Λ_2, there is a

Table 4. Composition Density Function for Coagulation and Growth of a Multicomponent Aerosol

Initial Distribution (see Table 1)†	$n(x_1, x_2, \ldots, x_m, t)$
0 ($p_i \geq 0$)	$\frac{4N_o}{(\tau+2)^2} \prod_{i=1}^{m} \frac{(p_i+1)^{p_i+1}}{x_{i_o}} \exp\left\{\frac{-(p_i+1)x_i \exp(-\Lambda_i\tau)-\Lambda_i\tau}{x_{i_o}}\right\} \times$ $\sum_{k=0}^{\infty}\left(\frac{\tau}{\tau+2}\right)^k \prod_{j=1}^{m} \frac{\left[(p_j+1)^{p_j+1}\right]^k\left[\frac{x_j}{x_{j_o}}\exp(-\Lambda_j\tau)\right]^{(k+1)(p_j+1)-1}}{\Gamma[(k+1)(p_j+1)]}$
1 ($p_i = 0$)	$\frac{4N_o}{(\tau+2)^2} \prod_{i=1}^{m} \frac{\exp}{x_{i_o}} -\left[\frac{x_i}{x_{i_o}}\exp(-\Lambda_i\tau)-\Lambda_i\tau\right]$ $\times \sum_{k=0}^{\infty} \frac{\left[\frac{\tau}{\tau+2}\prod_{j=1}^{m}\frac{x_j}{x_{j_o}}\exp(-\Lambda_j\tau)\right]^k}{(k!)^m}$

Table 4. (Cont.)

1 (p_i=0, m=2)

$$\frac{4N_o \exp}{(\tau+2)^2 x_{1_o} x_{2_o}} \left\{ \frac{-x_1 e^{-\Lambda_1 \tau}}{x_{1_o}} - \frac{x_2 e^{-\Lambda_2 \tau}}{x_{2_o}} \quad -(\Lambda_1+\Lambda_2)\tau \right\}$$

$$\times \quad I_o \left\{ 2 \sqrt{\frac{\tau x_1 x_2 \exp[-(\Lambda_1+\Lambda_2)\tau]}{(\tau+2) x_{1_o} x_{2_o}}} \right\}$$

2 (p_i=1)

$$\frac{4^{m+1} N_o}{(\tau+2)^2} \prod_{i=1}^{m} \frac{\exp}{x_{i_o}} \left[\frac{-2x_i}{x_{i_o}} e^{-\Lambda_i \tau} \quad -\Lambda_i \tau \right]$$

$$\times \quad \sum_{k=0}^{\infty} \frac{\left[\frac{4^m \tau}{\tau+2}\right]^k \prod_{j=1}^{m} \left[\frac{x_j \ e}{x_{j_o}} \right]^{-\Lambda_j \tau} \ ^{2k+1}}{[(2k+1)!]^m}$$

Table 4. (Cont.)

3 ($p_1=1$, $p_2=0$, $m=2$)

$$\frac{16N_o \exp}{(\tau+2)^2 x_{1_o} x_{2_o}} \left\{ \frac{-2x_1 e^{-\Lambda_1\tau}}{x_{1_o}} - \frac{x_2 e^{-\Lambda_2\tau}}{x_{2_o}} - (\Lambda_1+\Lambda_2)\tau \right\}$$

$$\times \sum_{k=0}^{\infty} \left[\frac{4\tau}{\tau+2}\right]^k \frac{\left[\frac{x_1 e^{-\Lambda_1\tau}}{x_{1_o}}\right]^{2k+1} \left[\frac{x_2 e^{-\Lambda_2\tau}}{x_{2_o}}\right]^k}{k!\ (2k+1)!}$$

4

$$\frac{4}{(\tau+2)^2} \sum_{k=0}^{\infty} \left(\frac{\beta_o t}{\tau+2}\right)^k \left\{ N_1^{k+1}\, \delta\,(x_1-(k+1)x_1^* e^{\Lambda_1\tau}, x_2^*) \right.$$

$$+ \binom{k+1}{1} N_1^k (N_o-N_1)\delta[x_1-kx_1^* e^{\Lambda_1\tau}, x_2-x_2^* e^{\Lambda_2\tau}]$$

$$\left. + \ldots + \binom{k+1}{k+1} (N_o-N_1)^{k+1}\delta[x_1, x_2-(k+1)x_2^* e^{\Lambda_2\tau}] \right\}$$

---

† $\Lambda_i = \frac{\sigma_i}{\beta_o N_o}$

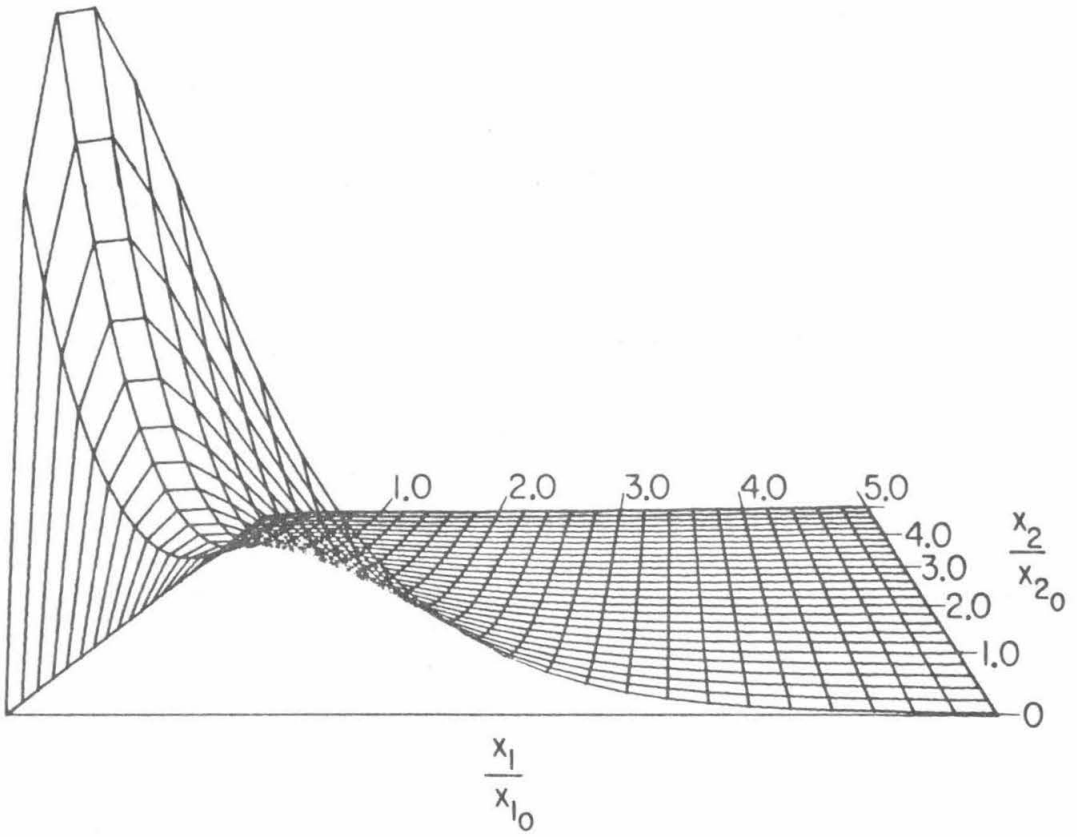

Figure 1

Initial composition distribution ($p_1=1$, $p_2=0$)

$$\frac{n_0 x_{1_0} x_{2_0}}{N_0} = \frac{4x_1}{x_{1_0}} \exp\left[- \frac{2x_1}{x_{1_0}} - \frac{x_2}{x_{2_0}} \right]$$

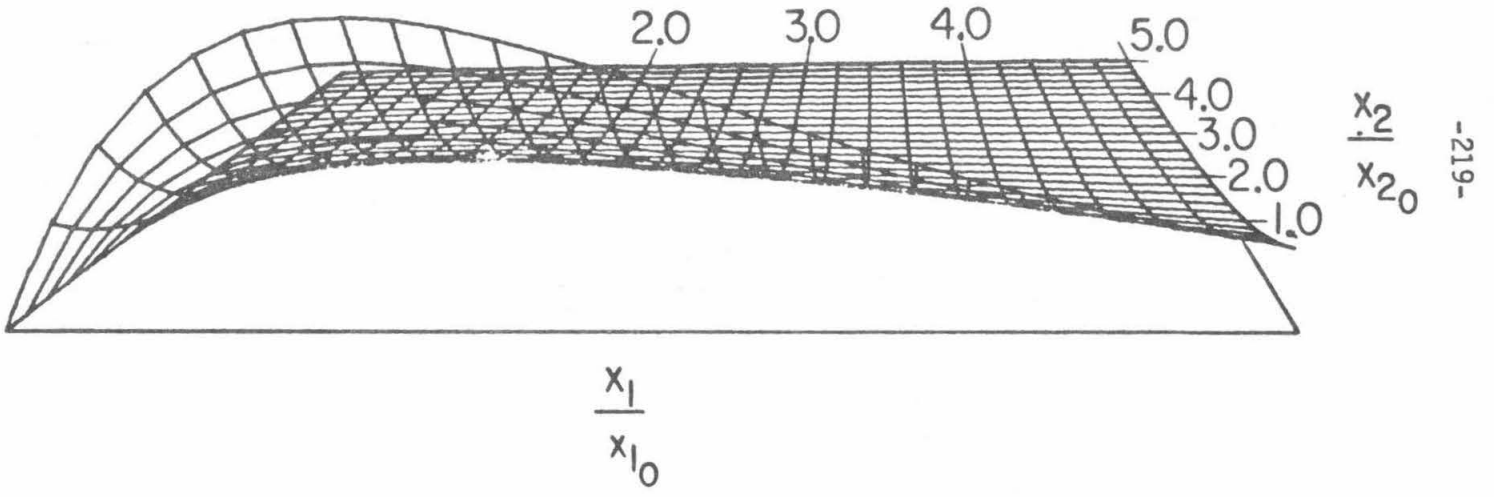

Figure 2

Time evolution of the composition distribution (p_1=1, p_2=0) for $\Lambda_1 = 10.0$, $\Lambda_2 = 0.1$ and $N_o\beta_o t = 0.1$.

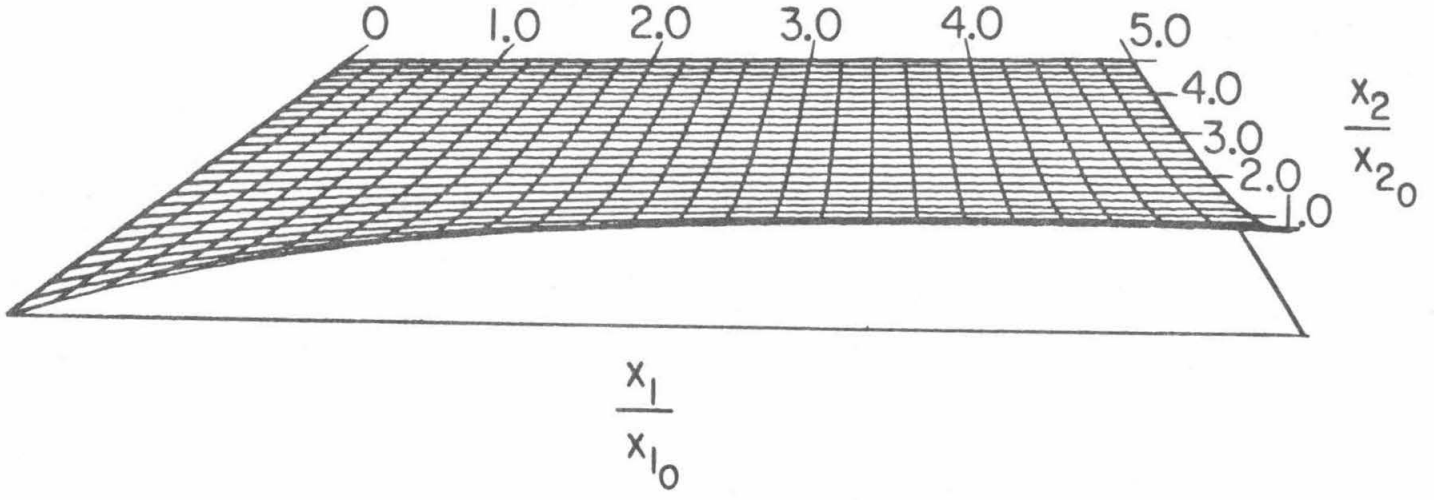

Figure 3

Time evolution of the composition distribution (p_1=1, p_2=0) for $\Lambda_1 = 10.0$, $\Lambda_2 = 0.1$ and $N_0\beta_0 t = 0.2$.

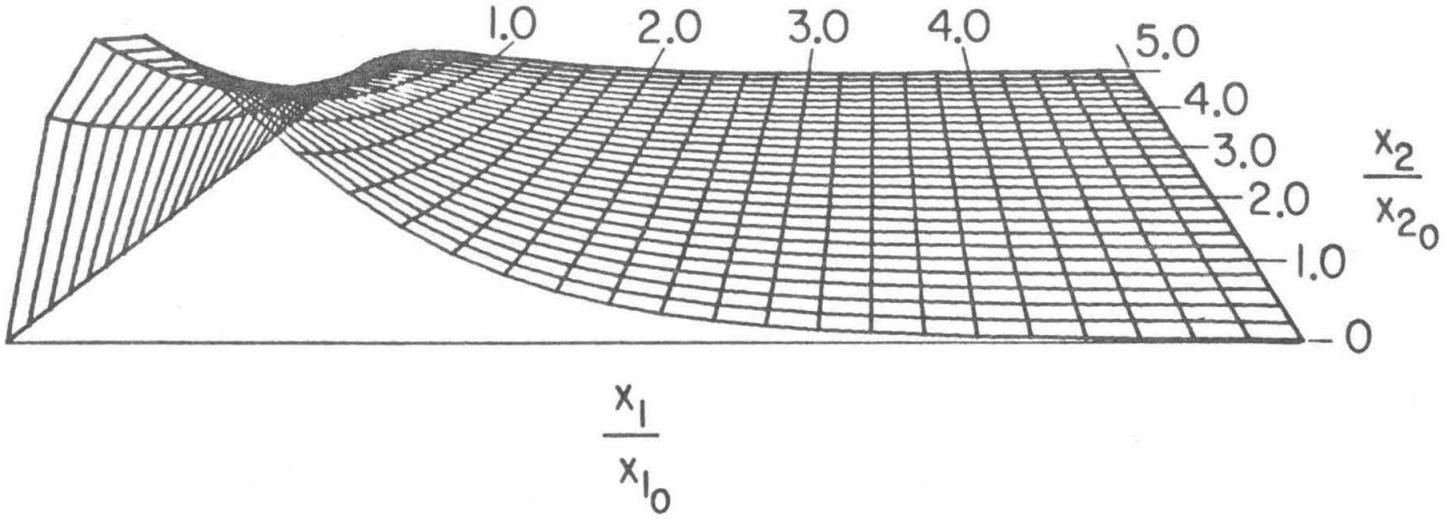

Figure 4

Time evolution of the composition distribution (p_1=1, p_2=0) for $\Lambda_1 = 0.1$, $\Lambda_2 = 10.0$ and $N_0\beta_0 t = 0.1$.

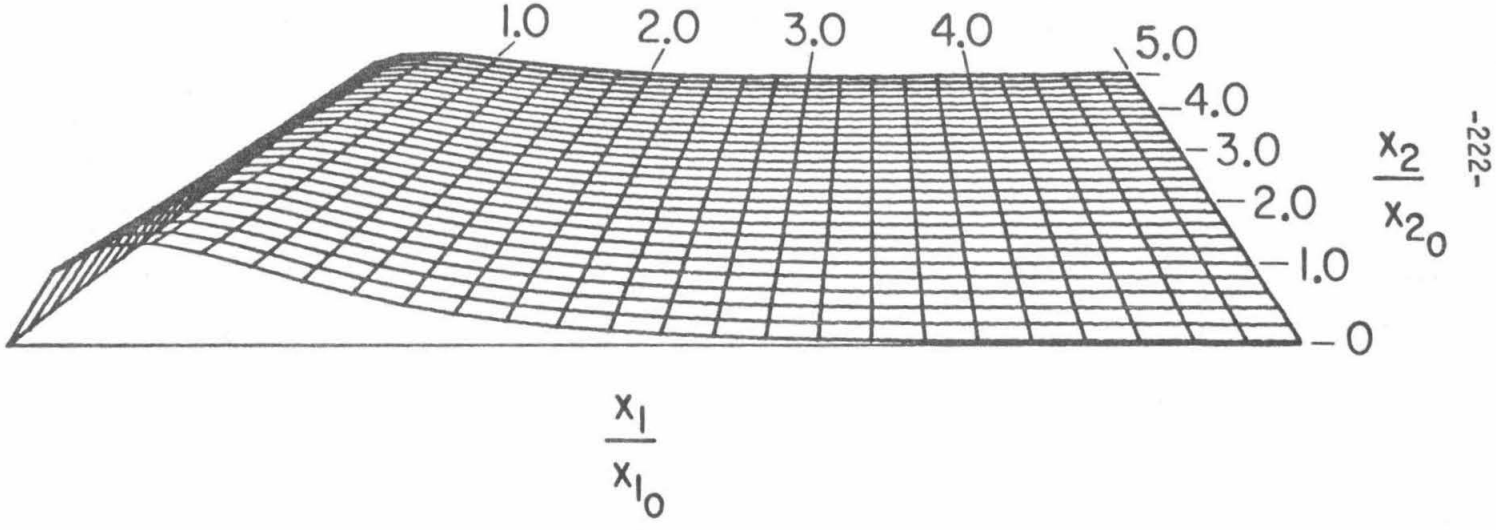

Figure 5

Time evolution of the composition distribution (p_1=1, p_2=0) for $\Lambda_1 = 0.1$, $\Lambda_2 = 10.0$ and $N_0\beta_0 t = 0.2$.

relatively more rapid growth of component 1 as compared to component 2. This effect is evident by the more rapid movement of the volume under the surface along the x_1-axis as compared to that along the x_2-axis. However, if component 2 grows faster, an entirely different surface evolves for the same initial condition. Using the values of $\Lambda_1 = 0.1$ and $\Lambda_2 = 10.0$, Figures 4 and 5 show the greater volume displacement under the surface along the x_2-axis. Thus, the different chemical nature of two components can have significant effects on the evolving distributions, even for identical initial conditions and total number of particles.

4. SUMMARY

New analytic solutions have been obtained for the dynamic composition distribution $n(x_1,x_2,\ldots,x_m,t)$ of a multicomponent aerosol undergoing coagulation with and without particle growth. The solutions have been obtained for a general class of initial distributions, including two monodisperse populations. Selected two-component composition distributions have been exhibited to illustrate the effect of simultaneous coagulation and growth on the aerosol. To obtain analytical solutions the choice of parameters, such as the coagulation coefficient and the particle growth law, is, by necessity, quite limited and simplified. Consequently, the solutions presented here do not simulate actual physical circumstances. Rather, the value of the solutions lies in their ability to elucidate in a concise manner the essential nature of multicomponent aerosol coagulation and growth. Furthermore, the solutions can serve as a standard against which one may wish to compare numerical solutions to multicomponent dynamic aerosol equations, should such techniques be developed in the future.

NOTATION

$I(v,t)$	particle growth rate, $\mu m\ sec^{-1}$
I_i	particle mass growth rate, $gm\ sec^{-1}$
m	number of components
$n(v,t)$	size distribution density function, $\mu m^{-3}\ cm^{-3}$
$n(x_1,x_2,\ldots,x_m,t)$	composition density function, $gm^{-m}\ cm^{-3}$
$n_o(x_1,x_2,\ldots,x_m)$	initial composition density function, $gm^{-m}\ cm^{-3}$
$N(t)$	total number concentration, cm^{-3}
N_o	initial number concentration, cm^{-3}
t	time, sec
v	particle volume, μm^3
x_i	mass of component i, gm

Greek Letters

β	coagulation coefficient, $cm^3\ sec^{-1}$
Λ_i	characteristic growth time over characteristic coagulation time of component i
σ	growth laws constant, sec^{-1}
τ	dimensionless time

REFERENCES

1. Golovin, A. M., "The Solution of the Coagulation Equation for Raindrops, Taking Condensation Into Account," Sov. Phys. Dokl. 8, 191 (1963).

2. Scott, W. T., "Analytic Studies of Cloud Droplet Coalescence," J. Atmos. Sci. 25, 54 (1968).

3. Drake, R. L., in "Topics in Current Aerosol Research," (Hidy, G. M. and Brock, J. R., Eds.), Vol. 3, pp. 201-376. Pergamon, Oxford, 1972.

4. Ramabhadran, T. E., Peterson, T. W., and Seinfeld, J. H., "Dynamics of Aerosol Coagulation and Condensation," A.I.Ch.E.J. 22, 840 (1976).

5. Peterson, T. W., Gelbard, F., and Seinfeld, J. H., "Dynamics of Source-Reinforced, Coagulating, and Condensing Aerosols," J. Colloid Interface Sci. 63, 426 (1978).

6. Lushnikov, A. A., "Evolution of Coagulating Systems III. Coagulating Mixtures," J. Colloid Interface Sci. 54, 94 (1976).

7. Hidy, G. M. and Brock, J. R., "The Dynamics of Aerocolloidal Systems." Pergamon, Oxford, 1970.

8. Ditkin, V. A. and Prudnikov, A. P., "Operational Calculus in Two Variables and Its Applications." Pergamon, Oxford, 1962.

APPENDIX

To invert

$$\frac{1}{\prod_{i=1}^{m} S_i^{R_i} - a} \qquad [A1]$$

rearrange [A1] to

$$\frac{1}{\prod_{i=1}^{m} S_i^{R_i}} \left[\frac{1}{1 - \frac{a}{\prod_{i=1}^{m} S_i^{R_i}}} \right] . \qquad [A2]$$

Then for $o \leq a / \prod_{i=1}^{m} S_i^{R_i} < 1$, [A2] becomes

$$\sum_{k=o}^{\infty} \frac{a^k}{\prod_{i=1}^{m} S_i^{R_i(k+1)}} . \qquad [A3]$$

Inverting [A3] term by term for $R_i > o$ results in the multidimensional inverse given in Table 2.

Chapter VII

SUMMARY AND CONCLUSIONS

A new form of the General Dynamic Equation (GDE) for aerosols, termed the discrete-continuous GDE, has been developed. The strength of the equation lies in the ability to simulate aerosol dynamics in systems in which processes are occurring over a broad particle size spectrum, such as aerosol formation and growth in reacting gas systems. Whereas the most fundamental, the discrete GDE is impractical for simulating aerosol processes involving more than a few hundred particle sizes. The continuous GDE is capable, in principle, of representing aerosol dynamics over the complete particle size spectrum, although, in practice, the dynamics of molecular clusters are not adequately represented by this equation. In addition, problems arise in properly specifying the boundary condition on the continuous GDE at the lower end of the size spectrum when fresh particles are being formed by gas-to-particle conversion. The desire to simulate aerosol dynamics in systems in which fresh particles are being formed from reacting gases in the presence of a preexisting aerosol, the typical urban atmospheric situation, in fact, prompted much of this work. Previous attempts to simulate this situation have been based on the use of the continuous GDE together with classical nucleation theory to specify the flux of fresh, stable particles into the system. We have shown here that

classical nucleation theory, however, may be inaccurate in predicting the flux of stable nuclei in this system, since the theory neglects the scavenging of molecular clusters by aerosol particles and cluster-cluster agglomeration.

With the discrete-continuous GDE it is now possible to simulate the detailed processes occuring during aerosol formation and growth in reacting gas systems. We have simulated the dynamics of sulfuric acid/water aerosols generated by photochemical oxidation of sulfur dioxide in a smog chamber in the presence of a preexisting aerosol, since this system has been one of the most frequently studied, and the experimental data of McMurry are available (1). Agreement between predictions and data were generally good, although uncertainties in the system, such as the exact composition of the aerosol and the complete initial distribution, precluded precise, quantitative comparisons. More importantly, we have been able to study for the first time two long-standing and important issues related to aerosol behavior in gas-to-particle conversion: (1) the establishment of a steady state concentration profile of molecular clusters in both the presence and absence of a preexisting aerosol and (2) the relative roles of condensation, nucleation, and cluster-cluster agglomeration in transferring mass to the larger particles in the spectrum. In particular, we found that a steady state is established for the molecular clusters and that under certain circumstances the profiles can differ in the absence and presence of a preexisting aerosol and cluster-cluster agglomeration can be important relative

to other processes influencing molecular clusters. Using the discrete-continuous GDE, dimensionless criteria were also developed to estimate the relative importance of nucleation, condensation, and cluster-cluster agglomeration for general gas-to-particle conversion processes.

Although the discrete-continuous GDE provided a detailed description of aerosol formation and growth, if an appropriate boundary condition and growth law is used, the simpler continuous GDE can be used to simulate aerosol dynamics for particles much larger than the monomer. It was shown in Chapter V that under the proper conditions, the continuous GDE will agree with the full solution. Similarly, in the absence of coagulation the analytic solution to the continuous GDE can provide a relatively simple yet powerful way to simulate certain classes of aerosol dynamics.

Having presented both numerical and analytical solutions for aerosols undergoing physical processes, atmospheric aerosol studies should be developed to include the chemistry. We have reported work in this direction with the development of chemical reaction-controlled growth laws given in Chapter II and the exact solutions to the continuous multicomponent GDE for simplified cases given in Chapter VI. However, to obtain the composition distribution function for a realistic aerosol, numerical techniques will probably be required. In the absence of coagulation, the resulting first-order hyperbolic partial differential equation for the composition distribution

function can probably be solved by the method of characteristics. However, for realistic aerosols, due to the expected interdependence and complexity of the growth and reaction mechanisms, in most cases one will not be able to obtain an analytic solution as was obtained in Chapter III for the size distribution. Also, the necessary thermodynamic data for multicomponent mixtures are generally not available. Much work is needed in determining the physical properties of aerosol constituents in the bulk phase and as a function of particle size. Future work on aerosol physics and chemistry, and aerosol interactions with gaseous chemistry should be very interesting. It is hoped that this work will provide some basis for future studies on atmospheric aerosols.

REFERENCES

1. McMurry, P. H., "On the Relationship Between Aerosol Dynamics and the Rate of Gas-To-Particle Conversion," Ph.D. Thesis, California Institute of Technology, 1977.

Thesis Appendix

A SECTIONAL APPROXIMATION TO THE DISCRETE GENERAL DYNAMIC EQUATION FOR AEROSOLS

1. INTRODUCTION

Understanding the dynamic behavior of aerosol growth by agglomeration is of major importance in atmospheric science. Thus much work has been devoted to solving the population balance equations which govern the aerosol agglomeration process. The population balance equations, often collectively called the discrete General Dynamic Equation (GDE), consist of an infinite set of nonlinear differential equations for the number densities of particles containing i monomers, where i = 1, 2,... . It is assumed that each particle consists of an integer multiple of monomers, which are usually taken to be molecules. Assuming that the agglomeration process conserves monomers, a particle formed by agglomeration will contain the sum of monomers contained in the two original particles. Given that agglomeration and homogeneous particle generation and removal are the only processes occurring, we are interested in determining the number of particles per unit volume of fluid containing i monomers, N_i as a function of time. The discrete GDE for N_i is,

$$\frac{dN_i}{dt} = \frac{1}{2} \sum_{j=1}^{i-1} \beta_{i-j,j} N_{i-j} N_j - N_i \sum_{j=1}^{\infty} \beta_{i,j} N_j + S_i \qquad [1]$$

where $\beta_{i,j}$ is the kinetic coefficient of agglomeration of two particles containing i and j monomers respectively, and S_i represents all homogeneous generation and removal processes of i-mers. To completely specify the problem, the initial number densities must also be known.

Previous work on the discrete GDE is given in Table 1. Exact solutions of Eq. [1] neglect S_i and require simplifying assumptions on the functional form of $\beta_{i,j}$. For $S_i = 0$ and a constant value of $\beta_{i,j}$, a closed form analytical solution to Eq. [1] has been reported (1). For the form of $\beta_{i,j}$ determined by Brownian coagulation and S_i=0, an exact recursion relation has also been reported (2). However to solve Eq. [1] for arbitrary $\beta_{i,j}$ and S_i, numerical computations must be resorted to. For numerical solution, an infinite set of differential equations is both impractical and unrealistic, thus one must truncate the discrete GDE at some convenient upper limit. If a molecule is considered to be the monomer, then the number of differential equations needed to simulate actual aerosols can be immense. As can be seen from Table 1 only several hundred particle sizes can be used, yet nearly all atmospheric aerosol particles contain orders of magnitude more monomers.

To circumvent this problem numerical solutions to the continuous approximation of the discrete GDE have been developed (7,8). Although these solutions seem to provide an acceptable alternative, the computational effort may still be too great for the desired

Table 1. Reported Solutions to the Discrete General Dynamic Equation

Investigator	Dynamics	Remarks
1. Smoluchowski (1)	Agglomeration ($\beta_{i,j}$=constant)	Exact Solution
2. Rice and Whitehead (2)	Agglomeration (Brownian)	Exact Solution
3. Hidy (3)	Agglomeration	400-600 particle sizes
4. Mockros, Quon, and Hjelmfelt (4)	Agglomeration and Generation	100 particle sizes
5. Takahashi and Kasahara (5)	Agglomeration and Removal	~100 particle sizes
6. Suzuki, Ho, and Higuchi (6)	Agglomeration	100 particle sizes

information. For example, if one were interested in determining the total concentration of particles in only a few particle size ranges, a large set of equations must first be solved for the details of the entire spectrum and then the detailed solution would be used to calculate the total concentration in each section. Clearly, one would like a technique to estimate the concentration in each section, without resorting to a detailed solution.

In this work a sectional model for aerosols with a broad spectrum in particle size is developed. By dividing the particle size domain into m sections, the model deals directly with the total number of particles in each section. Therefore, only one differential equation is required for each section. Although a sectional model (or lumped mode model as termed by the authors), has been recently presented in the literature (9), no rigorous derivation of the model was given. In order to clarify any misunderstandings about what approximations are involved, a rigorous derivation for a sectional model will be given.

2. GOVERNING EQUATIONS FOR A SECTIONAL MODEL

Let a $(k_{\ell-1}+1)$-mer and a (k_ℓ)-mer be the smallest and largest particle in the ℓ-th section respectively, where $k_0=0$ and $\ell=1,2,\ldots,m$. In order to span a large range in particle size, yet still retain an accurate description of the dynamics of the smallest particles, impose that $k_{\ell+1} \geq 2k_\ell$, where $\ell = 1, 2,\ldots m-1$.* Then the total number of agglomerations of particles within the ℓ-th section is given by

$$\frac{1}{2} \sum_{i=k_{\ell-1}+1}^{k_\ell} \sum_{j=k_{\ell-1}+1}^{k_\ell} \beta_{i,j} N_i N_j \qquad [2]$$

Since each agglomeration essentially removes a particle from the ℓ-th section, [2] also corresponds to the number of particles removed from section ℓ. Of the agglomerations given by [2]

$$\frac{1}{2} \sum_{i=k_\ell+1}^{2k_\ell} \sum_{j=i-k_\ell}^{k_\ell} \beta_{i-j,j} N_{i-j} N_j \qquad [3]$$

agglomerations result in the formation of particles in section $\ell + 1$, thus removing an additional particle from the ℓ-th section. The number of particles formed in section ℓ by agglomeration is

---

*This restriction hardly limits most applications of the model, yet greatly simplifies the mathematics.

$$\frac{1}{2}\sum_{i=k_{\ell-1}+1}^{2k_{\ell-1}}\ \sum_{j=i-k_{\ell-1}}^{k_{\ell-1}} \beta_{i-j,j}N_{i-j}N_j \qquad [4]$$

where $\ell \geq 2$.

Finally, the number of particles removed from section ℓ by scavenging is

$$\sum_{i=k_{\ell}+1}^{k_m}\ \sum_{j=k_{\ell-1}+1}^{k_{\ell}} \beta_{i,j}N_iN_j \qquad [5]$$

Combining Eqs. [2] - [5],

$$\frac{d\bar{N}_1}{dt} = -\frac{1}{2}\sum_{i=1}^{k_1}\ \sum_{j=1}^{k_1} \beta_{i,j}N_iN_j$$

$$-\frac{1}{2}\sum_{i=k_1+1}^{2k_1}\ \sum_{j=i-k_1}^{k_1} \beta_{i-j,j}N_{i-j}N_j \qquad [6]$$

$$-\sum_{i=k_1+1}^{k_m}\ \sum_{j=1}^{k_1} \beta_{i,j}N_iN_j + \bar{S}_1$$

and for $2 \leq \ell \leq m$,

$$\frac{d\bar{N}_\ell}{dt} = -\frac{1}{2}\sum_{i=k_{\ell-1}+1}^{k_\ell}\sum_{j=k_{\ell-1}+1}^{k_\ell}\beta_{i,j}N_iN_j$$

$$-\frac{1}{2}\sum_{i=k_\ell+1}^{2k_\ell}\sum_{j=i-k_\ell}^{k_\ell}\beta_{i-j,j}N_{i-j}N_j$$

$$+\frac{1}{2}\sum_{i=k_{\ell-1}+1}^{2k_{\ell-1}}\sum_{j=i-k_{\ell-1}}^{k_{\ell-1}}\beta_{i-j,j}N_{i-j}N_j \qquad [7]$$

$$-\sum_{i=k_\ell+1}^{k_m}\sum_{j=k_{\ell-1}+1}^{k_\ell}\beta_{i,j}N_iN_j \qquad 2 \leq \ell \leq m-1$$

where $\bar{N}_\ell$ and $\bar{S}_\ell$ are the total number and net generation rate of particles in section ℓ, respectively. It can be shown by induction that the following double summation transformation is valid for $k \geq 1$,

$$\sum_{i=k+1}^{2k}\sum_{j=i-k}^{k}\beta_{i-j,j}N_{i-j}N_j = \sum_{i=1}^{k}\sum_{j=k-i+1}^{k}\beta_{i,j}N_iN_j \qquad [8]$$

Hence Eqs. [6] and [7] become

$$\frac{d\bar{N}_1}{dt} = -\frac{1}{2}\sum_{i=1}^{k_1}\sum_{j=1}^{k_1}\beta_{i,j}N_iN_j \qquad [9]$$

$$- \frac{1}{2} \sum_{i=1}^{k_1} \sum_{j=k_1-i+1}^{k_1} \beta_{i,j} N_i N_j$$

$$- \sum_{i=k_1+1}^{k_m} \sum_{j=1}^{k_1} \beta_{i,j} N_i N_j + \bar{S}_1$$

$$\frac{d\bar{N}_\ell}{dt} = - \frac{1}{2} \sum_{i=k_{\ell-1}+1}^{k_\ell} \sum_{j=k_{\ell-1}+1}^{k_\ell} \beta_{i,j} N_i N_j$$

$$- \frac{1}{2} \sum_{i=1}^{k_\ell} \sum_{j=k_\ell-i+1}^{k_\ell} \beta_{i,j} N_i N_j \qquad [10]$$

$$+ \frac{1}{2} \sum_{i=1}^{k_{\ell-1}} \sum_{j=k_{\ell-1}-i+1}^{k_{\ell-1}} \beta_{i,j} N_i N_j$$

$$- \sum_{i=k_\ell+1}^{k_m} \sum_{j=k_{\ell-1}+1}^{k_\ell} \beta_{i,j} N_i N_j \qquad \ell \leq m-1$$

$$+ \bar{S}_\ell$$

In order to express $\frac{d\bar{N}_\ell}{dt}$ for $\ell = 1, 2, \ldots, m$, in terms of $\bar{N}_i$ for $i = 1, 2, \ldots, m$, we will make 2 approximations.

1) Within each section the number of particles of each multiplet is equal, that is,

$$N_i = \frac{\overline{N}_\ell}{(k_\ell - k_{\ell-1})} \qquad k_{\ell-1} + 1 \leq i \leq k_\ell \qquad [11]$$

Hence,

$$\sum_{i=k_{p-1}+1}^{k_p} \sum_{j=k_{\ell-1}+1}^{k_\ell} \beta_{i,j} N_i N_j = \overline{\beta}_{p,\ell} \overline{N}_p \overline{N}_\ell \qquad [12]$$

where $\overline{\beta}_{p,\ell}$ is a constant given by

$$\overline{\beta}_{p,\ell} = \frac{\sum_{i=k_{p-1}+1}^{k_p} \sum_{j=k_{\ell-1}+1}^{k_\ell} \beta_{i,j}}{(k_\ell - k_{\ell-1})(k_p - k_{p-1})} \; . \qquad [13]$$

Notice that $\overline{\beta}_{p,\ell}$ is the mean agglomeration coefficient between sections p and ℓ.

2) The variation in $\beta_{i,j}$ for particle i in section p and particle j in section ℓ is small enough such that the mean agglomeration coefficient, $\overline{\beta}_{p,\ell}$ resulting as a consequence of the first approximation

can be used for all agglomerations between particles in sections p and ℓ. As the number of multiplets within each section approaches unity, both approximations become exact. Thus for reasonably sized sections the approximations may not introduce significant errors into the exact equations, (i.e. Eqs. [9] and [10] for $\overline{N}_\ell$.)

Using Eqs. [11] and [13], Eq. [9] becomes

$$\frac{d\overline{N}_1}{dt} = -\overline{\beta}_{1,1}\overline{N}_1^2\left[\frac{3k_1+1}{4k_1}\right] - \overline{N}_1\sum_{i=2}^{m}\overline{\beta}_{1,i}\overline{N}_i + \overline{S}_1 \qquad [14]$$

By induction on k_ℓ and using Eqs. [11] and [13], it can be shown that for $\ell \geq 2$,

$$\sum_{i=1}^{k_\ell}\sum_{j=k_\ell-i+1}^{k_\ell}\beta_{i,j}N_iN_j = \frac{\overline{\beta}_{1,\ell}\overline{N}_1\overline{N}_\ell(k_1+1)}{(k_\ell-k_{\ell-1})} + \overline{\beta}_{\ell,\ell}\overline{N}_\ell^2\left\{\frac{k_\ell(k_\ell+1) - 2k_{\ell-1}(k_{\ell-1}+1)}{2(k_\ell-k_{\ell-1})^2}\right\} + \sum_{i=2}^{\ell-1}\overline{\beta}_{i,\ell}\overline{N}_i\overline{N}_\ell\frac{(k_i+k_{i-1}+1)}{(k_\ell-k_{\ell-1})} \qquad [15]$$

Hence

$$\frac{d\bar{N}_2}{dt} = \bar{\beta}_{1,1}\bar{N}_1^2\left[\frac{k_1+1}{4k_1}\right] - \bar{\beta}_{1,2}\bar{N}_1\bar{N}_2\,\frac{k_1+1}{2(k_1-k_2)}$$

$$+ \bar{\beta}_{2,2}\bar{N}_2^2\left[\frac{2k_1(2k_2+1) - k_2(3k_2+1)}{4(k_2-k_1)^2}\right] \qquad [16]$$

$$- \bar{N}_2 \sum_{i=3}^{m} \bar{\beta}_{2,i}\bar{N}_i + \bar{S}_2$$

and for $\ell \geq 3$

$$\frac{d\bar{N}_\ell}{dt} = \frac{\bar{\beta}_{1,\ell-1}\bar{N}_1\bar{N}_{\ell-1}(k_1+1)}{2(k_{\ell-1}-K_{\ell-2})}$$

$$- \frac{\bar{\beta}_{1,\ell}\bar{N}_1\bar{N}_\ell(k_1+1)}{2(k_\ell-k_{\ell-1})} \qquad [17]$$

$$+ \bar{\beta}_{\ell-1,\ell-1}\left\{\frac{k_{\ell-1}(k_{\ell-1}+1) - 2k_{\ell-2}(k_{\ell-2}+1)}{4(k_{\ell-1}-k_{\ell-2})^2}\right\}$$

$$+ \sum_{i=2}^{\ell-2} \frac{\bar{\beta}_{i,\ell-1}\bar{N}_i\bar{N}_{\ell-1}(k_i+k_{i-1}+1)}{2(k_{\ell-1}-k_{\ell-2})}$$

$$+ \bar{\beta}_{\ell,\ell}\bar{N}_\ell^2 \left\{ \frac{2k_{\ell-1}(2k_\ell+1) - k_\ell(3k_\ell+1)}{4(k_\ell-k_{\ell-1})^2} \right\}$$

$$- \bar{N}_\ell \sum_{i=2}^{\ell-1} \frac{\bar{\beta}_{i,\ell}\bar{N}_i(k_i+k_{i-1}+1)}{2(k_\ell-k_{\ell-1})} + \bar{S}_\ell$$

$$- \bar{N}_\ell \sum_{i=\ell+1}^{m} \bar{\beta}_{i,\ell}\bar{N}_\ell \qquad \ell \leq m-1$$

Combined with the initial values for $\bar{N}_\ell$, Eqs. [14], [16] and [17] constitute an approximate model for aerosol growth by agglomeration.

One attractive feature of the model is the flexibility in specifying the number and location of the sections. Although one can use as few sections as desired, the approximations may no longer be valid if too few sections are used. The most detailed application of the model can be obtained by specifying $k_1 = 1$ and $k_\ell = 2k_{\ell-1}$ for $2 \leq \ell \leq m$. Then for a domain extending to k_m, the maximum number of sections is

$$m = \frac{\log k_m}{\log 2} + 1 \qquad [18]$$

3. CONCLUSION

A sectional model for aerosol growth by agglomeration has been developed which can be used for estimating the total concentration of particles in a few arbitrarily located sections. Although the two approximations used to obtain the model become more inaccurate as the number of sections decreases, one might be able to obtain reasonable estimates with a relatively small number of differential equations. In order to determine the accuracy of the model, comparisons should be made with the detailed solution to the General Dynamic Equation. Based on this comparison, the number of sections required to compute a solution within a given domain and error tolerance should be determined.

REFERENCES

1. Smoluchowski, M. Von, Z., "Versuch Einer Mathematischen Theorie der Koagulationskinetik Kolloider Lösungen," Z. Physik. Chem. Leipzig 92, 129 (1917).

2. Rice, C. L. and Whitehead, R., "The Theory of the Coagulation of Emulsions," J. Colloid Interface Sci. 23, 174 (1967).

3. Hidy, G. M., "On the Theory of Non-interacting Particles in Brownian Motion," J. Colloid Interface Sci. 20, 123 (1965).

4. Mockros, L. F., Quon, J. E., and Hjelmfelt, A. T., "Coagulation of a Continuously Reinforced Aerosol," J. Colloid Interface Sci. 23, 90 (1967).

5. Takahashi, K. and Kasahara, M., "A Theoretical Study of the Equilibrium Particle Size Distribution of Aerosols," Atmos. Environ. 2, 441 (1968).

6. Suzuki, A., Ho, N.F.H., and Higuchi, W. I., "Prediction of the Particle Size Distribution Changes in Emulsions and Suspensions by Digital Computation," J. Colloid Interface Sci. 29, 552 (1969).

7. Berry, E. X., "Cloud Droplet Growth by Collection," J. Atmos. Sci. 24, 688 (1967).

8. Middleton, P. and Brock, J., "Simulation of Aerosol Kinetics," J. Colloid Interface Sci. 54, 249 (1976).

9. Whitby, K. T., Cantrell, B. K., and Kittelson, D. B., "Nuclei Formation Rates in a Coal-Fired Power Plant Plume," Atmos. Environ. 12, 313 (1978).